Universitat Autònoma de Barcelona

Quantum transport in Solid state devices for Terahertz frequency applications

Devashish Pandey

Quantum transport in Solid state devices for Terahertz frequency applications

Devashish Pandey
Department of Electronic Engineering
Universitat Autónoma de Barcelona (UAB)

Supervisor
Xavier Oriols Pladevall
and
Guillermo Albareda Piquer

In partial fulfillment of the requirements for the degree of
PhD in Electronic Engineering

December, 2020

Acknowledgements

I would like to thank all the people who directly or indirectly contributed to this PhD thesis. First and foremost I would like to thank Dr Xavier Oriols for giving me this opportunity to work under him and helping me in all accounts to settle comfortably after my arrival to Spain. Undoubtedly, I could not have expected a better guide and teacher as Xavier. Apart from a lot of quantum mechanics and quantum electron transport related issues he has taught me some crucial things that cannot be learned from a book like research ethics, rigour, the philosophy of physics and above all humility. He somehow taught me a very important thing that *the only limit is you.*

Then, I would like to thank Dr Guillermo Albareda for accepting to be my supervisor and providing his exceptional efforts in raising the quality of my work. He carries a gift of precision be it in conceptual arguments, in MATLAB coding or in research writing. I really learned a lot of this from him particularly, critical thinking and brainstorming. He has been always very kind and patient with my questions and problems.

I also want to express my gratitude to the faculty members of the electronic engineering department for their kindness and support. I specially want to thank Dr David Jiménez and Dr Jordi Bonache for their concern towards me. I want to thank Dr Ferran Martin for

creating a joyful and disciplined environment in the department. I am very thankful to Dr Arantxa for solving numerous issues of mine specially related to my PhD submission. I also thank Javier Hellín and Javier Gutierrez for solving many of my technical and bureaucracy related problems respectively.

Next I would like to thank my dear friends at UAB. Nikos and Ioanna have been like a family member to me and I thank them for their support and good wishes. I really enjoyed the company of Anibal and Noe and thank them for their warmth and support. A special thanks also to Carlos Couso, Marcos and Pau for going out of the way to help me during my initial time in Spain. I also thank Ertugrul, Laura, Matteo, Laura (Italy), Enrique, Zhen, Pedro, Ferney, Jan, Ana, Marti, Jonatan, Amilie, Marta, Li-Juan, Gerard, Ferran, Roushi for being kind to me.

And last but not the least I am very grateful to my wife for her unconditional love and support in everything I do, my parents my kind relatives, and my chuddie buddies in India.

Dedicated to all my teachers (gurus) in past and present

Abstract

The work presented in this thesis is dedicated to the understanding of practical and conceptual challenges in simulating dynamical properties beyond the quasi-static approximation, in solid-state quantum devices in scenarios where a full quantum mechanical treatment is necessary. The results of this thesis are particularly relevant for the computation of the fluctuations of the electric current in the THz regime which aids in determining the correlations, the evaluation of tunnelling times that define the cut-off frequency of high-frequency operated devices, or the assessment of thermodynamic work to realize quantum thermal engines.

The above mentioned dynamical properties involve multi-time measurements and hence are sensitive to quantum backaction. In the context of Orthodox quantum mechanics, the definition of these dynamical properties cannot be detached from the specification of the measurement apparatus. That is, defining *apparatus-independent* or *intrinsic* dynamical properties of quantum systems is incompatible with the postulates of Orthodox quantum mechanics.

All in all, a device engineer like me, working on practical problems related with the present and future solid-state devices, is forced to delve into the foundations of quantum mechanics if I really want to properly understand the high-frequency performance of solid-state devices. In this regard, I will show that the difficulties associated to the

understanding of dynamical properties can be solved by looking beyond Orthodox quantum mechanics. In particular, I have explored the modal interpretation of quantum mechanics, which is a mathematically precise quantum theory that reproduces all quantum mechanical phenomena. I will show that intrinsic properties can be easily defined in this new (non-orthodox) context. Importantly, I will prove that intrinsic properties can be identified with weak values and hence that they can be measured!

Focused on a particular modal theory, viz., Bohmian mechanics, an electron transport simulator will be discussed and applied to address both methodological and practical issues related to the simulation of quantum electron transport. The ontology of Bohmian mechanics naturally enables describing continuously monitored open quantum systems with a precise description of the conditional states for Markovian and non-Markovian regimes. This helps to provide an alternate to density matrix approach in the description of open quantum systems, which scales poorly computationally with the number of degrees of freedom.

Thus the Bohmian conditional state strategy, which has led to the development of an electron transport simulator, BITLLES will be shown to compute the dwell times for electrons in a two-terminal graphene barrier. It will be demonstrated that Bohmian trajectories are very appropriate to provide an unambiguous description of transit (tunneling) times and its relation to the cut-off frequencies in practical electron devices. Finally, a protocol incorporating collective-like measurements to evade the current measurement uncertainty in the classical and quantum computing electron devices will be discussed.

Contents

Publications related to this thesis

(Compendium of publications included in this thesis)

1. **Devashish Pandey**, Xavier Oriols, and Guillermo Albareda. From micro- to macrorealism: addressing experimental clumsiness with semi-weak measurements. *New Journal of Physics*, jun 2020

2. **Devashish Pandey**, Enrique Colomés, Guillermo Albareda, and Xavier Oriols. Stochastic Schrödinger Equations and Conditional States: A General Non-Markovian Quantum Electron Transport Simulator for THz Electronics. *Entropy*, 21(12), 2019

3. **Devashish Pandey**, Xavier Oriols, and Guillermo Albareda. Effective 1D Time-Dependent Schrödinger Equations for 3D Geometrically Correlated Systems. *Materials*, 13(13), 2020

4. **Devashish Pandey**, Matteo Villani, Enrique Colomés, Zhen Zhan, and Xavier Oriols. Implications of the Klein tunneling times on high frequency graphene devices using Bohmian trajectories. *Semiconductor Science and Technology*, 2018

5. **Devashish Pandey**, Laura Bellentani, Matteo Villani, Guillermo Albareda, Paolo Bordone, Andrea Bertoni, and Xavier Oriols. A Proposal for Evading the Measurement Uncertainty in Classical and Quantum Computing: Application to a Resonant Tunneling Diode and a Mach-Zehnder Interferometer. *Applied Sciences*, 9(11):2300, 2019

List of Figures

Part I

INTRODUCTION

Chapter 1

From steady state to time resolved quantum transport

Due to the miniaturization of electronic devices, semi-classical simulation techniques are no longer able to provide a correct description of electron devices. The majority of the device modelling community has thus migrated from semi-classical to steady state quantum simulation techniques. Today, a number of quantum electron transport simulators are available to the scientific community [1–5] where in almost all cases the framework of Orthodox quantum mechanics is utilized [1]. Most of these quantum transport simulators use time-independent equations. And yet, they can predict dynamical properties of devices such as AC, transients or noise. The adopted strategy is as follows: (i) first, simulate the DC characteristics which provides the dependence of the DC current and charge densities on the gate and drain voltages, (ii) second, obtain the transconductance and capacitances from these static properties, and (iii) finally, plug all this information into an analytical expression of the frequency response calculated by a small signal circuit model.

[1] An important exception to this rule is the BITLLES simulator that utilizes the framework of Bohmian Mechanics for quantum transport which is available here:

This strategy has been proven to be very successful in providing physical insights into the operation of electron devices and at the same time has been shown to be computationally very efficient [6, 7].

The success of time-independent (or steady-state) strategies relies in the fact that the transit time of electrons (which is usually of the orders of picosecond) is much less than the inverse of the operating frequency (of the orders of nanosecond) at which these devices are simulated. In such circumstances, the current can be reasonably computed under a steady-state approximation. By invoking ergodic arguments the ensemble value of the current measured in different experiments at different times can be said to be equivalent to the time average of the current in a single experiment. Therefore, steady-state properties require, in principle, only to deal with quantum computations that involve single-time measurement. The amount of information that time-independent simulators can provide is limited because they cannot offer information on multi-time correlations. Therefore, their predicting capabilities are still far from those of the traditional Monte Carlo solution of the semi-classical Boltzmann transport equation [8].

At moderately or very high frequencies, for example, the transit time of electrons starts to be comparable to the inverse of frequency of operation and the above time-independent (or steady-state) strategy starts to fail. Notably, computing current correlations at high frequencies not only requires to abandon the time-independent Schrödinger equation in favor of the time-dependent Schrödinger equation, but also needs a precise description of the collapse law, which is ultimately responsible for producing a particular output value of the current each time we measure. Whereas the Schrödinger equation is a unitary equation of motion, the collapse is a random non-unitary process. That is, when measured, quantum systems undergo a non-negligible perturbation that affects their future evolution. The perturbation caused in the system by the measure-

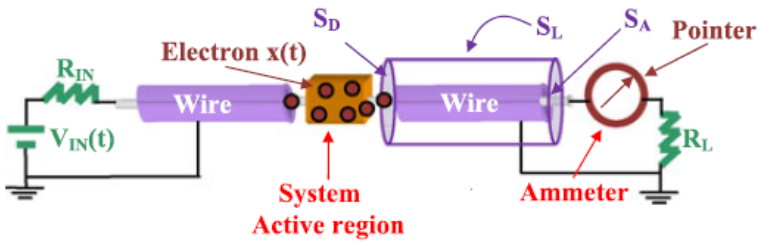

Figure 1.1: Figure depicting a typical scheme of an electronic device. The active region is shown by a brown region connected with wires (depicted by pink region) one end of which is connected to a battery (V_{IN}) and the other end (S_D) is connected to an ammeter (Pointer)

ment is usually referred to as quantum backaction. And this effect is responsible for making dynamical properties at high frequencies a complicated problem not only at the practical but also at the conceptual (or fundamental) level.

At this point it is important to understand the differences between classical and quantum backaction. For example, when measuring the electric current in a classical electronic circuit using an ammeter, the resistance of the ammeter affects the actual current flowing in the circuit and thus a value which is slightly less than the actual value of the current (without the ammeter) is measured. The crucial difference between the two (classical and quantum) system is that while the properties of a classical system are unambiguously defined even without the measuring apparatus, in quantum systems, described under the ontology of Orthodox quantum mechanics, these properties are undefined unless the measuring apparatus is explicitly considered. These peculiarity of Orthodox quantum mechanics introduces the following conceptual and practical difficulties in the modelling of quantum transport at high frequencies:

Difficulties in providing the total current operator: In an electron device the measurement of the current at the surface S_D in Figure 1.1 is done

through a long wire which is in-turn connected to the ammeter as shown in Figure 1.1. The ammeter measures the total current along with the noise of all the electrons in the wire. Furthermore, the measurement of this current by the ammeter does not significantly effect the current in the surface S_D. So, the measurement of the current in an electron device can be defined through a particular class of measurements referred to as weak or semi-weak measurements. The modelling of a weak measurement in Orthodox quantum mechanics requires to find a weak measurement operator of the total current, which includes particle and displacement components. The particle current is just related to the flux of electrons, while the displacement current is proportional to the time derivatives of the electrical field.

Importantly, at high frequencies one has to include both the displacement current and the particle current [9, 10]. Therefore the weak measurement operator must include the displacement currents (as no instantaneous current conservation at a particular time can be guaranteed without it and the quasi-static approximation is no longer applicable). Roughly speaking, the expectation value of the total current (I_t) has to be given as the sum of the averaged particle current (I_p) and the averaged displacement current (I_d), i.e.:

$$I_t(t) = I_p(t) + I_d(t) = \int_S \vec{j} \cdot d\vec{s} + \int_S \epsilon(\vec{r}) \frac{d\vec{E}(\vec{r}, t)}{dt} \cdot d\vec{s} \tag{1.1}$$

where $\vec{j}$ is the current density, $\epsilon(\vec{r})$ is the electric permitivity and $\vec{E}(\vec{r}, t)$ is the electric field [2]. The above discussed issue poses a problem even in the classical and semi-classical regimes, where utilizing the Ramo-Schokley theorem for defining the total current is necessary [11–13].

[2]The quantities in Eq. 1.1 are the ensemble mean values from the point of view of Orthodox theory. In Bohmian mechanics we have right to associate these properties to instantaneous values.

Therefore, finding a total current weak operator has to be described from a generalized measurement scheme (known as generalized Von-Neumann scheme), mathematically described by a POVM (Positive Operator Valued Measure) (we will discuss it in detail in subsequent sections). Orthodox theory only tells us that there is a hermitian operator associated with every observable, but it does not tell us which one. Therefore, we are left to answer the following questions in order to construct this operator: What is the POVM associated with the measurement of the total, particle plus displacement, current? Since the measurement has to be weak, how can one decide the weakness of the measurement? What should be the time lapse between measurements? These questions are certainly not easy to answer. But, even if defining such a POVM is a complicated task, Orthodox theory argues that such operator exists without providing any answer to the previous questions. Therefore, not being able to find a suitable operator is not a shortcoming of the Orthodox theory but a limitation of the physicist or engineer that is looking for it [3].

Difficulties in describing apparatus independent information: To quantify the speed of a field effect transistor (FET) the scientific community use some figure of merits (FoMs). The cut-off frequency (f_T) is considered to be an appropriate FoM to quantify the intrinsic speed of the FETs. The physical mechanism behind the origin of this frequency arises from the response time of electrons which gives rise to an intrinsic delay. This time is crucial in determining the response of the device to the change in applied voltage specially in the digital electronics applications, quantifying the intrinsic cut-off frequency. Now one can

[3]For example let us take a particle current operator which is defined as $\hat{j} = \frac{1}{2m}\left[|\vec{r}\rangle\langle\vec{r}|\hat{P} + \hat{P}|\vec{r}\rangle\langle\vec{r}|\right]$. One can, in principle, evaluate the eigenstates of this current operator apparently with a lot of mathematical difficulty associated to it. But these eigenstates even though mathematically correct are in form of functions which are too impractical to be associated with some physical system.

ask a straightforward question: if the estimation of cut-off frequency depends on the transit time of electrons in the active region how to calculate this time? From the perspective of Orthodox theory the most elementary answer would be: perform strong position measurement at the two extreme positions of the active region (the source and the drain). Though this answer is straightforward, the experimental realization of this proposition is simply useless as the first position measurement will project the initial state into a position eigenstate and hence it prevents the possibility of capturing any coherent evolution of the wavefunction. What I want is to know what is the time it takes for the electron to go from source to drain without including such measuring apparatus. Is it possible to get such information without measuring it?

The above problem is a direct consequence of the conceptual restriction in the ontology of the Orthodox theory, where properties of a quantum system does not exist until they are measured. Apart from the problematic descriptions of issues discussed above, the necessary inclusion of the measuring apparatus also leads to quantum contextuality, which means that the outcome of the measurement is dependent on the way the system is measured (or on the properties of the measuring apparatus). Thus one can have as many outcomes as there are number of measurement strategies which is very problematic in obtaining an unambiguous definition of a measured property [4]. This restriction imposes conceptual difficulties in defining the properties like the tunnelling time, thermodynamic work and the high frequency electrical current in a quantum system. These three paradigmatic examples will be discussed in the later part of the thesis where I

[4]I want to reiterate that just like backaction, contextuality is also not exclusively found in quantum mechanics, this also can takes place in a classical system which is measured with different apparatus. For example measuring current in a circuit using ammeter of different internal resistances will result in different value of electric current. But the different is that whereas in classical system a well defined distinct value of a property is possible independent of the measurement in Orthodox theory this is not possible and therefore contextuality becomes so crucial.

will propose a strategy derived from the ontology of Bohmian mechanics which will allow an unambiguous definition of these properties.

Difficulty in categorizing the system and the apparatus: In Orthodox theory we define an isolated quantum system (a microscopic closed system) which interacts with the classical (macroscopic) measuring apparatus. The difficulty with this proposition is, at what point will we place this distinction? Is there some well defined boundary between a quantum system and an apparatus? For example in an electron device is the definition of device region arbitrary or there is a strict boundary between the device and the measuring apparatus?

Though I have explained three particular difficulties that one finds when trying to explain the measurement of high frequency properties of quantum electron devices, I could have also described these issues under a single umbrella of the measurement problem in Orthodox theory as this is the origin of all the difficulties described above. The mentioned limitations in the Orthodox theory poses a serious problem in the near future as electron devices become even smaller and are foreseen to operate at the Terahertz (THz) regime. The solution to simulate such quantum electron devices necessitates one to enter into discussions pertaining to several non-trivial issues in quantum mechanics. Such discussions will need a very strict theoretical framework rather than engineering intuition. Typically the theoretical physicists provide a correct description of a theory to the engineers in order for them to apply those rigorously explored principles in engineering applications. But in this particular case, as discussed above, physicists have not been able to provide unequivocal recipe for computing some properties of interest to the engineers and therefore engineers are forced to enter into the discussions pertaining to the foundations of quantum mechanics. This thesis is therefore an

engineers perspective on the difficulties faced in the proper description of some properties that are very crucial in describing the future quantum devices.

An attempt to answer these questions will lead me to first understand these problems and their origin in the framework of Orthodox quantum mechanics and then provide an answer in the framework of a non-Orthodox theory which is discussed in the PART II of the thesis. Most of the difficulties that we encounter in the precise description of the dynamical information of a quantum system, in the Orthodox theory can be associated to the explicit inclusion of the measuring apparatus as discussed in chapter 2. These questions will then lead me to an alternate representation of quantum mechanics known as the modal interpretation as discussed in chapter 3. I will discuss how in this interpretation all the above discussed issues related to the backaction, quantum contextuality and the definition of generalized operators can be circumvented.

In PART III of the thesis I will discuss a quantum transport methodology derived from the ontology of Bohmian mechanics. The utility of this methodology in providing a precise description of the open quantum system in Markovian and non-Markovian regimes alike will be discussed in chapter 4. In chapter 5 I will discuss how the already discussed quantum transport methodology can be made computationally more efficient.

In PART IV of the thesis an application to the previously discussed methodology in the simulation of practical devices will be discussed. Particularly in chapter 6 the ability of the Bohmian intrinsic properties to compute tunneling time in a two terminal graphene based device will be demonstrated using the BITLLES simulator. In chapter 7 I will describe a proposal which will help to evade the current measurement uncertainty in the classical and quantum computing devices.

Finally, in PART V of the thesis I will provide a conclusion of all the work carried out in the thesis.

Part II

THEORETICAL OUTLOOK

Chapter 2

Are electrons there when nobody looks?

The predictions of quantum mechanics have been in many senses contrary to the intuition of the classical physics. Phenomena like quantum superposition, quantum entanglement, tunnelling, electron spin etc. has no parallel in classical physics. The word quantum mechanics is usually understood as a gigantic umbrella under which different interpretations of the quantum world exists e.g., the Copenhagen (Orthodox) interpretation [14–17], Ghirardi- Rimini-Weber (GRW) theory [18], Bohmian mechanics (or the pilot-wave) theory [16, 19–21] or many-worlds (or Everett) theory [22]. However, due to historical reasons the word quantum mechanics has been traditionally associated to the Orthodox theory [1]. Throughout this thesis, unless stated explicitly, any reference to quantum mechanics in general will imply implicitly a reference to the Orthodox theory.

In chapter 1 it was concluded that the description of certain properties would be greatly simplified if we could define an apparatus independent unperturbed

[1]For example, if one says that there are no well-defined trajectories in quantum mechanics, in fact, he/she wants to say there is no well-defined trajectories in the Orthodox interpretation of quantum mechanics.

dynamics of the system. I will refer to such properties as intrinsic properties. These properties can be defined as a pre-existing value of a beable [2] before the measurement. It is a property of a quantum system that is not connected to any experimental setup, and hence are properties that, by construction, belong only to the system. Orthodox quantum mechanics is, in general, incompatible with these type of properties. In modal interpretations of quantum mechanics (for eg. Bohmian mechanics) these properties are defined by simply disregarding the interaction of the system with the measuring apparatus. A well known example are the position of Bohmian particles of a quantum system without any position detector [19, 21, 26].

In the following sections I will discuss the implications of inclusion of the measuring apparatus which is a necessity in ontology of the Orthodox theory. I will also discuss how in the framework of Orthodox theory the information of a quantum system cannot be described without taking into account the backaction and quantum contextuality related to the measuring apparatus.

2.1 Wavefunction perturbation due to measurement and origin of backaction

In a classical system the properties are well defined regardless of whether these properties are being measured or not. Therefore, evaluating a property of such system at time t_1 and correlating the outcome with the value of the same (or another) property at a later time t_2 provides an unequivocal way of representing the dynamics of classical systems. In quantum mechanics, however, Bell [27] as well as Kochen and Specker [28], showed that measurements cannot be thought

[2] John S. Bell coined the word beable for all those properties of quantum systems that, in Bohmian mechanics, have a well-defined (pre-existing) values before any measurement is carried out [23–25]

of as simply revealing the underlying properties of the system in a way that is independent of the context in which the observable is measured. The result of correlating the outcome of measuring an observable at time t_1 with that at t_2 of the same (or another) observable depends, in general, upon the specification of the measuring apparatus. As I have already mentioned in chapter 1 this property of quantum mechanics is known as contextuality and the unavoidable perturbation that measurements induce on the subsequent evolution of quantum systems is commonly referred to as quantum backaction [29, 30].

To mathematically describe the measurement of a quantum system I make use of the generalized Von-Neumann measurement protocol [31]. To simplify the discussion of a generalized measurement of a property of a quantum system I consider a Hilbert space $\mathcal{H}$ that is decomposed into three different Hilbert spaces [32] corresponding to the system, ancilla and the pointer. First, the quantum system of interest from which we want to get information is described by the collective degree of freedom x. Second, the ancilla, which interacts with the system and is represented by the collective degree of freedom y. And third, the pointer, which interacts with the ancilla and is represented by the collective degree of freedom z. Then, the weak or indirect measurement of the properties of the system is, in fact, a strong measurement of the properties of the ancilla. That is, while the ancilla-pointer interaction must be strong, and hence a given position of the pointer z after a measurement is linked to a single position of the ancilla y (position eigenstate of y), the system-ancilla interaction can be more general and thus a given position of the ancilla y after the measurement cannot always be linked to a single eigenstate of the system. For the sake of clarity I will omit the reference to the pointer unless necessary.

I assume the full state of the system-ancilla-pointer to be initially described

by a separable state vector:

$$|\Psi(0)\rangle = \sum_i c_i(0)|s_i\rangle \otimes \int a(y,0)|y\rangle dy \otimes \int f(z,0)|z\rangle dz, \tag{2.1}$$

where the pure state system state vector [3] $|\psi(0)\rangle = \sum_i c_i(0)|s_i\rangle$ has been defined using the eigenstates $|s_i\rangle$ of the operator $\hat{S}$ of interest, with $\hat{S}|s_i\rangle = s_i|s_i\rangle$. Without the loss of generality, I choose here a discrete and nondegenerate spectrum $\{s_1, s_2, s_3....\}$ of the operator $\hat{S}$. The (ancilla) state vector $|\phi_W(0)\rangle = \int a(y,0)|y\rangle dy$ interacts with the system and also with the (pointer) state vector $|\phi_P(0)\rangle = \int f(z,0)|z\rangle dz$. The measurement process is a two step process classified as the pre-measurement and the read out explained as follows,

Pre-measurement: In this step a unitary evolution from $t = 0$ to t_1 entangles the ancilla with the system and the pointer with the ancilla as follows (a more detailed derivation can be found in Appendix A):

$$|\Psi(t_1)\rangle = \sum_i c_i|s_i\rangle \otimes \int a(y-\lambda s_i)|y\rangle dy \otimes \int f(z-y)|z\rangle dz. \tag{2.2}$$

The original ancilla wavefunction $a(y,0)$ splits into several wavefunctions $a(y - \lambda s_i)$ with $i = 1, 2, ..\infty$. Also, λ has been defined as a macroscopic parameter with dimensions of $[y]/[S]$ that relates y to s_i. The shape of $a(y_k - \lambda s_i)$ is arbitrary and includes, in particular, strong (direct measurement) interactions when $\int dy\ \ a(y - \lambda s_i)a(y - \lambda s_j) = \delta_{i,j}$ and weaker (indirect measurement) interactions when $\int dy\ a(y - \lambda s_i)a(y - \lambda s_j) \neq \delta_{i,j}$. I have defined $\delta_{i,j}$ as a Kronecker delta function. The only two conditions imposed on the ancilla wavefunctions $a(y - \lambda s_i)$ to be representative of an indirect or weak measurement are: (i) $\int y|a(y-\lambda s_i)|^2 dy = \lambda s_i\ \ \forall i$, which implies that the center of mass of $|a(y-\lambda s_i)|^2$

[3] I could have as well described the system in terms of a many body mixed state which even though rigorous would still not change the conclusions derived in this section. For the treatment of this section in terms of many body mixed state the reader is referred to Publication A

is λs_i, and (ii) $\int |a(y-\lambda s_i)|^2 dy = 1 \quad \forall i$, which simply states that the ancilla wavefunction is well normalized.

Read-out: The read-out process is described by the non-unitary operator $\hat{I}_S \otimes \hat{I}_W \otimes \hat{\mathbb{P}}_{z_k}$, where $\hat{I}_S$ is the identity operator defined in the system Hilbert space, $\hat{I}_W$ is the identity operator defined in the ancilla Hilbert space, and $\hat{\mathbb{P}}_{z_k} = |z_k\rangle\langle z_k|$ is a projector acting on the Hilbert space of the pointer. As mentioned previously, it becomes now evident that an indirect measurement of a system is just a direct measurement of an ancilla that is entangled with the system. The non-unitary operator $\hat{I}_S \otimes \hat{I}_W \otimes \hat{\mathbb{P}}_{z_k}$ causes the collapse of the pointer wavefunction providing the read-out value $z_k = y_k$ and the measured state becomes $|\Psi_k(t_1)\rangle = \sum_i c_i a(y_k - \lambda s_i)|s_i\rangle \otimes |y_k\rangle \otimes |z_k\rangle$. Therefore, the state of the system can be effectively represented by:

$$|\psi_k(t_1)\rangle = \sum_i a(y_k - \lambda s_i) c_i |s_i\rangle, \tag{2.3}$$

where the subscript k indicates the measurement of the pointer value $z_k = y_k$. Now the initial system state prior to the measurement was $|\psi(t_0)\rangle = \sum_i c_i |s_i\rangle$ and after the measurement the state can be given by Eq. 2.3. This state is what we call as the perturbed state. Also it can be clearly seen that this system state has been contaminated by the measuring apparatus, which is the effect of the backaction of the measuring apparatus on the system.

2.2 Ensemble expectation values in Orthodox theory

In contrast to classical mechanics Orthodox theory can only make statistical predictions about a system in a given state. Since in the most general cases the state

$|\psi(t)\rangle$ of the system is not an eigenstate of the operator $\hat{S}$ (representing an observable s, I am interested in), one obtains random measurement outcomes in a set of identically prepared experiments. Therefore to obtain a meaningful information of the observable it is useful to determine the ensemble expectation values. In this section I will discuss one time ensemble expectation values pertaining to single time measurements and two-time ensemble expectations for scenarios where the system state is measured consecutively at two different times

2.2.1 One-time expectation value

The expectation value of a property of a quantum system measured at time t_1, entangled with the ancilla giving the measurement outcomes y_k is given by:[4].

$$\langle y(t_1)\rangle = \int dy_k y_k P(y_k), \tag{2.4}$$

where $P(y_k)$ is the probability of reading out a particular value $y_k = z_k$. The probability of measuring a particular pointer position y_k can be then easily evaluated from Born's rule $P(y_k) = \langle \Psi_k(t_1)|\Psi_k(t_1)\rangle = \langle \psi_k(t_1)|\psi_k(t_1)\rangle$ applied to the non-normalized state in Eq. 2.3. While the probability distribution $P(y_k) = \sum_i |c_i|^2 |a(y_k - \lambda s_i)|^2$ clearly depends on the type of ancilla that I am considering, the expectation value in Eq. 2.4,

$$\langle y(t_1)\rangle = \int y_k \sum_i |c_i|^2 |a(y_k - \lambda s_i)|^2 dy_k = \sum_i |c_i|^2 \lambda s_i = \lambda \, \langle \hat{S}\rangle, \tag{2.5}$$

only depends on the system state $|\psi(t_1)\rangle = \sum_i c_i |s_i\rangle$.

It is apparent from Eq. 2.5 that the expectation values of static (one-time) properties provide information of the system that is not contaminated by the

[4]All integrals are definite integrals over all the possible values of the variables x, y and z $(-\infty, +\infty)$

measuring apparatus. Most of the quantum simulators working in steady state therefore do not have any problem related to the backaction of the measuring apparatus. In such situations it is enough to model the system correctly in terms of the wavefunction following a unitary equation of motion and one can safely avoid the complications associated to the non-unitary collapse law. This is the strategy followed in most of the time-independent simulators that I had mentioned in chapter 1.

2.2.2 Two-time expectation values

As discussed in chapter 1 there can be situations specially in the terahertz frequency applications that the steady state approximations fails because in such scenarios the dynamic characteristics will be influenced by the backaction of the measuring apparatus. In such regimes it is very important to model the multi-time correlations correctly. In the following discussion I will carefully compute the two-time correlation function from the above measurement scheme to account for a second measurement involving another observable $\hat{G}$ at time $t_2 > t_1$. By repeatedly reading-out the positions y_k (at t_1) and y_ω (at t_2) for a large number of identically prepared experiments, we can compute the corresponding two-time correlation function $\langle y(t_2)y(t_1)\rangle$ as:

$$\langle y(t_2)y(t_1)\rangle = \int dy_k \int dy_\omega \; y_k y_\omega P(y_\omega, y_k), \tag{2.6}$$

where $P(y_\omega, y_k)$ is the joint probability of subsequently reading-out the values y_k and y_ω at times t_1 and t_2, respectively. Primarily the state in Eq. 2.3 can be let to evolve freely from t_1 till t_2 according to the time-evolution operator $\hat{U} = \exp(i\hat{H}(t_2 - t_1)/\hbar)$, where $\hat{H}$ is the Hamiltonian that dictates the evolution of the system degrees of freedom x in the absence of any interaction with the

ancilla and pointer degrees of freedom. Therefore, the state of the system right before the second pre-measurement can be written as the (non-normalized) state:

$$|\psi_k(t_2)\rangle = \sum_{i,j} a(y_k - \lambda s_i) c_i c_{j,i} |g_j\rangle. \tag{2.7}$$

where $c_{j,i} = \langle g_j|\hat{U}|s_i\rangle$. Subsequently, under the assumption that there is no correlation between the ancilla degrees of freedom at times t_1 and t_2, the system state vector in (2.7) undergoes a second pre-measurement evolution by becoming entangled again with the ancilla and the pointer wavefunctions (see Appendix A):

$$|\Psi_k(t_2)\rangle = \sum_{i,j} a(y_k - \lambda s_i) c_i c_{j,i} |g_j\rangle \otimes \int a(y - \lambda g_j)|y\rangle dy \otimes \int f(z-y)|z\rangle dz, \tag{2.8}$$

where now $a(y - \lambda g_j)$ is the pointer wavefunction displaced by λg_j.

The read-out of the pointer position (for an output value y_ω) at time t_2 is described again by a non-unitary operator $\hat{I}_S \otimes \hat{I}_W \otimes \hat{\mathbb{P}}_{z_w}$ with $\hat{\mathbb{P}}_{z_w} = |z_w\rangle\langle z_w|$. This non-unitary operator causes the collapse of the state in Eq. 2.8 into $|\Psi_{k,\omega}(t_2)\rangle = \sum_{i,j} c_i c_{j,i} a(y_k - \lambda s_i) a(y_\omega - \lambda g_j)|g_j\rangle \otimes |y_\omega\rangle \otimes |z_w\rangle$, and so the state of the system can be effectively written as:

$$|\psi_{k,\omega}(t_2)\rangle = \sum_{i,j} c_i c_{j,i} a(y_k - \lambda s_i) a(y_\omega - \lambda g_j)|g_j\rangle. \tag{2.9}$$

Born's rule can be used again to write the probability:
$P(y_\omega, y_k) = \langle \Psi_{k,\omega}(t_2)|\Psi_{k,\omega}(t_2)\rangle = \langle \psi_{k,\omega}(t_2)|\psi_{k,\omega}(t_2)\rangle$ of subsequently measuring y_k and y_ω as:

$$P(y_\omega, y_k) = \sum_j \sum_{i,i'} c^*_{i'} c_i c^*_{j,i'} c_{j,i} a^*(y_k - \lambda s_{i'})\ a(y_k - \lambda s_i)|a(y_\omega - \lambda g_j)|^2. \tag{2.10}$$

By introducing the probability $P(y_\omega, y_k)$ in Eq. 2.10 into Eq. 2.6 we finally get:

$$\langle y(t_2)y(t_1)\rangle = \lambda \sum_{i,i'} \int dy_k y_k a(y_k - \lambda s_i) a^*(y_k - \lambda s_{i'}) \langle \psi(t_1)|s_{i'}\rangle ... \\ ... \langle s_{i'}|\hat{U}^\dagger \hat{G} \hat{U}|s_i\rangle \langle s_i|\psi(t_1)\rangle, \qquad (2.11)$$

where I have used $\int dy_\omega \; y_\omega \; |a(y_\omega - \lambda g_j)|^2 = \lambda g_j$ and $\hat{G} = \sum_j g_j |g_j\rangle\langle g_j|$ together with $c_i = \langle s_i|\psi(t_1)\rangle$ and $c_{j,i} = \langle g_j|U|s_i\rangle$. Expression (2.11) is completely general and describes the expectation value of the two-time correlation function of $\hat{S}$ and $\hat{G}$ at times t_1 and t_2. At this point what is significant is that in (2.11) I have not been able to eliminate the dependence of the ancilla degrees of freedom $a(y_k - \lambda s_i)$ and $a^*(y_k - \lambda s_{i'})$ in the evaluation of $\langle y(t_2)y(t_1)\rangle$. Therefore the backaction of the measuring apparatus cannot be removed in this case, contrarily to what happens to the one-time expectation values in Eq. 2.5. Also Eq. 2.11 suggest clearly that for different types of measurements (ancillas) one will get different time-correlation functions and hence the outcome is contextual since it depends on the type of measuring apparatus used. Therefore, when computing multi-time correlations, in the most general scenario in a quantum device, we have to consider the backaction of the measuring apparatus and the associated quantum contextuality which has as many different outcomes as the number of different proposed measurement strategies. A simple numerical demonstration of above discussion can be found in Appendix E (also see Figure E.1(a)).

Eq. 2.11 is a two-time correlation function in the most general scenario where one could witness an explicit backaction due to the measuring apparatus. But we can still try to find some particular regimes where one can totally avoid the backaction (perturbation) of the measuring apparatus on the system and obtain the intrinsic (unperturbed) properties that we are looking for. The most educated guess at this point could be to make the coupling between the system and the

measuring apparatus so weak that it measures the system with the least possible (negligible) perturbation. I refer to this regime as the ideally weak measurement regime which is explained as follows,

The case of ideally weak measurements: In principle, one can erroneously expect that by minimizing the interaction between system and ancilla, one can get a zero (or negligible) perturbation on the system. We will see here that intuitive definition of what a weak value can be is not actually correct. I define an ideally-weak measurement as the one where the system-ancilla coupling is minimized. This is mathematically equivalent to making the support of the ancilla wavefunction (in y) much larger than the support of system wavefunction (in λs) i.e. $y \gg \lambda s_k$. In this limit one can assume a first order Taylor approximation so that the ancilla wave packet can be written as $a(y_k - \lambda s_i) \approx a(y_k) - \lambda s_i \frac{\partial a(y_k)}{\partial y_k}$. As discussed in Appendix B, the general result in Eq. 2.11 reduces to $\langle y(t_2)y(t_1)\rangle = \lambda^2 \mathrm{Re}[\langle\psi(t_1)|\hat{U}^\dagger\hat{G}\hat{U}\hat{S}|\psi(t_1)\rangle]$. Defining the Heisenberg operators $\hat{G}(t_2) = \hat{U}^\dagger\hat{G}\hat{U}$ and $\hat{S}(t_1) = \hat{S}$, then in the ideally-weak measurement regime one can write the two-time correlation function as:

$$\langle y(t_2)y(t_1)\rangle = \lambda^2 \mathrm{Re}[\langle\psi(t_1)|\hat{G}(t_2)\hat{S}(t_1)|\psi(t_1)\rangle]. \tag{2.12}$$

At this point, one could naively think that in Eq. 2.12 we have finally arrived at the expression of two-time correlation function which provides an unperturbed dynamics of the system because the expression is independent of the measuring apparatus. I want to clarify this subtle aspect carefully where I will conclude that in-spite of obtaining the measurement independent outcome in Eq. 2.12 I still will not be able eradicate the backaction of the measuring apparatus. In order to show that I will demonstrate that the expectation value in Eq. 2.12 can be only understood as the result of a non-negligible perturbation of the measuring

apparatus on the state of the system. To see that, I first rewrite the general state in Eq. 2.9 using the above mentioned Taylor series expansion (more details can be found in Appendix C):

$$|\psi_{k,\omega}(t_2)\rangle = \Bigg(a(y_\omega)a(y_k)\hat{U} + \lambda^2\frac{\partial a(y_\omega)}{\partial y_\omega}\frac{\partial a(y_k)}{\partial y_k}\hat{G}\hat{U}\hat{S} - \lambda\frac{\partial a(y_\omega)}{\partial y_\omega}a(y_k)\hat{G}\hat{U} - ... \\ ...\lambda\frac{\partial a(y_k)}{\partial y_k}a(y_\omega)\hat{U}\hat{S}\Bigg)|\psi(t_1)\rangle. \tag{2.13}$$

For simplicity, I defined $\partial a/\partial y \equiv \partial a(y)/\partial y$. Erroneously assuming $\partial a(y)/\partial y = 0$, one could think that the state of the system after the two measurements can be approximated only by the first term in Eq. 2.13 as $|\tilde{\psi}_{k,\omega}(t_2)\rangle \approx a(y_\omega)a(y_k)\hat{U}|\psi(t_1)\rangle$. This approximation would indeed imply that the state of the system has not been perturbed during the two-time measurement. However, $|\tilde{\psi}_{k,\omega}(t_2)\rangle$ does not yield the result in Eq. 2.12 but a separable probability $P(y_\omega, y_k) = \langle\tilde{\psi}_{k,\omega}(t_2)|\tilde{\psi}_{k,\omega}(t_2)\rangle \approx |a(y_\omega)|^2|a(y_k)|^2 = P(y_\omega)P(y_k)$ that leads to $\langle y(t_2)y(t_1)\rangle \approx \lambda^2\langle\hat{G}\rangle\langle\hat{S}\rangle$. To understand why the approximation $|\psi_{k,\omega}(t_2)\rangle \approx |\tilde{\psi}_{k,\omega}(t_2)\rangle$ yields a wrong result, let us assume a system where either $\int y_\omega P(y_\omega)dy_\omega = 0$ or $\int y_k P(y_k)dy_k = 0$. If this is the case one will always get, $\langle y(t_2)y(t_1)\rangle \approx \lambda^2\langle\hat{G}\rangle\langle\hat{S}\rangle = 0$. Now, let us consider the very rare (non-zero) output results for, $y_k \to \infty$ and $y_\omega \to \infty$, corresponding to $a(y_\omega)a(y_k)\hat{U}|\psi(t_1)\rangle \to 0$ (because $a(y_\omega), a(y_k) \to 0$). Then, the other terms in Eq. 2.13 can no longer be neglected as they provide a non-zero contribution to $\langle y(t_2)y(t_1)\rangle$. The rare events associated to $y \to \infty$, and hence to a large perturbation of the system, provide physical non-zero correlations and are responsible for providing non-zero correlations in Eq. 2.12 [5]. Appendix D gives a simple

[5]Obviously, one can always redesign our experiment to have $\int y_\omega P(y_\omega)dy_\omega \neq 0$, $\int y_k P(y_k)dy_k \neq 0$, and both much more large (in absolute value) than the contributions from very large values of y mentioned above. Then, it will be true that the two-time correlations can be approximated by the uninteresting classical-like result $\langle y(t_2)y(t_1)\rangle \approx \langle y(t_2)\rangle\langle y(t_1)\rangle$. In this last case, since I have shown that $\langle y(t)\rangle$ is apparatus-independent, $\langle y(t_2)y(t_1)\rangle$ is also

numerical demonstration of Eq. 2.13 and the corresponding discussion above, where I have used the ground state of a harmonic oscillator as our system and a Gaussian Krauss operator as our ancilla.

The case of initial eigenstate of $\hat{S}$: The only scenario where the outcome of the second measurement does not depend on the first measurement is when the initial state of the system is an eigenstate of the operator $\hat{S}$, i.e., $|\psi(t_1)\rangle = |s_k\rangle$. In this case the first measurement always yields the same output result $y_k = \lambda s_k$ without having perturbed the state of the system, and hence the second measurement happens to be independent of the first measurement[6]. Mathematically this can be stated as:

$$\langle y(t_2)y(t_1)\rangle = \lambda^2 s_k \langle s_k|\hat{U}^\dagger \hat{G}\hat{U}|s_k\rangle = \lambda^2 \langle \hat{G}(t_2)\rangle\langle \hat{S}(t_1)\rangle, \tag{2.14}$$

where I have used that $\langle\psi(t_1)|s_{i'}\rangle\langle s_i|\psi(t_1)\rangle = \langle s_k|s_{i'}\rangle\langle s_i|s_k\rangle = \delta_{i,k'}\delta_{i',k'}$ and that $\int dy y|a(y-\lambda s)|^2 = \lambda s$. Equivalently, if $\langle s_{i'}|\hat{U}^\dagger\hat{G}\hat{U}|s_i\rangle = g_w\delta_{i',i}$ which means that the evolved state $\hat{U}|s_i\rangle$ is an eigenstate of $\hat{G}$, then Eq. 2.11 can be also written as $\langle y(t_2)y(t_1)\rangle = \lambda^2 g_w\langle\psi(t_1)|\hat{S}|\psi(t_1)\rangle = \lambda^2\langle\hat{G}(t_2)\rangle\langle\hat{S}(t_1)\rangle$. In these two scenarios, since the results $\langle\hat{G}(t_2)\rangle$ and $\langle\hat{S}(t_1)\rangle$ are apparatus-independent, the two-time correlation function in Eq. 2.14 also represents an apparatus-independent correlation function. Unfortunately, this result is not general enough and is invalid in many practical situations where the initial state is a coherent superposition of the observable eigenstates [7]. I can go even further to impose restrictions on the operator itself to try to obtain the intrinsic properties as I have demonstrated

apparatus-independent.

[6] In the later part of the thesis I will explain this scenario that has a very crucial ontological significance in the Orthodox theory and is referred to as the 'eigenvalue-eigenstate' link

[7] In quantum systems prepared by collapsing the system state into one eigenstate of the operator $\hat{S}$ at $t = 0$ and measuring the system by such operator $\hat{S}$ without time evolution, the trivial result $\langle y(t_2)y(0)\rangle = \lambda^2\langle\hat{G}(t_2)\rangle\langle\hat{S}(0)\rangle$ is obtained.

in the Appendix E where I conclude that Orthodox theory does not allow an unperturbed (intrinsic) dynamical information.

2.3 Why intrinsic dynamical properties can not be defined in Orthodox theory?

I started my discussion in the previous sections by asking a question if it is possible to get unperturbed dynamical information in the ontology of Orthodox theory and after a rigorous analysis I found out that the answer to that is not affirmative. As already said, the impossibility of obtaining an unperturbed information of a system complicates our description of systems that involves multi-time measurements because they will always be plagued by the backaction of the measuring apparatus and the quantum contextuality. But cannot one just ignore the measuring apparatus and describe the properties of the system alone? The answer provided by the Orthodox theory is a straight no ! In the following section I will explain that the reason for this is attributed to the ontology of the Orthodox theory.

In Orthodox theory there is defined a complex vector $|\Psi(t)\rangle$ defining the quantum system (which directly corresponds to a wavefunction) belonging to a Hilbert space $\mathcal{H}$. This complex vector $|\Psi(t)\rangle$ defines the state of the system the evolution of which follows a unitary Schrödinger equation. Further the Orthodox theory postulates that for any observable $\hat{S}$ there is a well defined value only if the state $|\Psi(t)\rangle$ is an eigenstate, $|\Psi_i(t)\rangle$ of the operator $\hat{S}$ which provides an outcome (eigenvalue) s_i. Now, Schrödinger equation being linear allows the possibility of the system to be in the linear superposition of the eigenstates $|\Psi_i(t)\rangle$ i.e. even the superposition state $|\Psi(t)\rangle = \sum_i c_i|\Psi_i(t)\rangle$ is a solution, which means that the system has two or more values of the observable simultaneously. The implications

of this are that one cannot give any definite eigenvalue value to these properties and hence they are undefined. To explain why only one value is obtained in the measurement outcome we need to define another dynamical law which unlike Schrödinger equation is not unitary and is called as collapse law. This law provides the dynamical effect of transforming the state $|\Psi(t)\rangle \rightarrow |\Psi_i(t)\rangle$ and in-turn provide the outcome s_i when a measurement is made which is referred to as the "eigenstate-eigenvalue link". The difficulty in this orthodox definition of what is a well-defined property of a system is now very evident. Before the measurement we cannot provide a well defined value of the system and therefore the ordinary view of reality which means that the properties of an object (like its position or velocity) have well defined values even when they are not measured is lost.

At this point I would like to mention that this difficulty of defining properties of systems has forced people to follow the "shut up and calculate" approach. But one cannot do much about it as it is just how the ontology of Orthodox theory is meant to be; very hard to digest but still able to provide good predictions. This predicament was faced by one of the best minds in the past. Since the Orthodox conception of the idea that only the measurement of a property gives reality to the property, there has been a lot of debate on the special status given to the *observer* in this theory. Physicists, over the years have often questioned this imposition in the Orthodox ontology. For example, Einstein wanted to discredit this assumption when he mentioned *"Do you think the moon is not there when nobody is looking?"* which is exemplified in Figure 2.1. Similarly, Feynman once mentioned that *"if a tree falls in a forest and there is nobody there to hear it, does it make noise"*. John Bell was one of the most outspoken physicist in this regard when he said [33]

"It would seem that the theory is exclusively concerned about 'results of measurement', and has nothing to say about anything else. What exactly qualifies

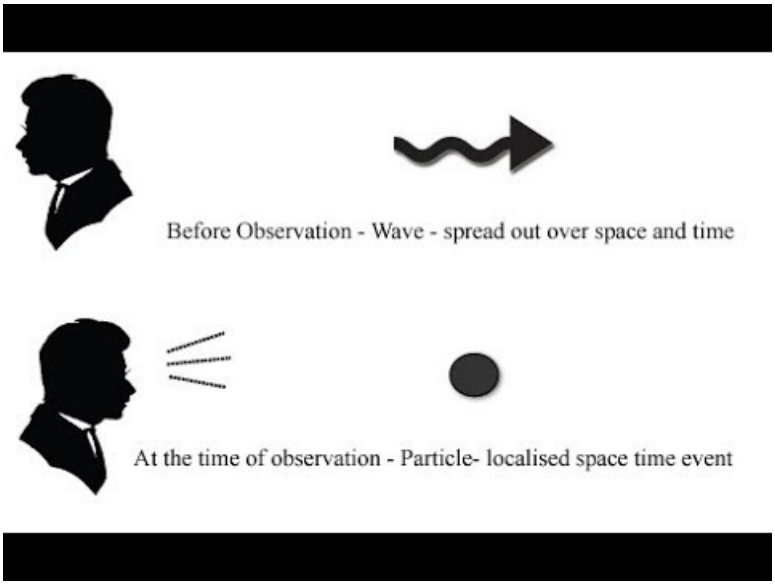

Figure 2.1: Figure depicting the predicament of Albert Einstein in relation to the special status of the observer given in the ontology of Orthodox theory. This figure shows that before observation the particle does not have a well defined position but once observed the particle instantaneously appears in a well defined position. (Courtesy: https://ponirevo.com/the-observer-effect-in-quantum-physics/)

some physical systems to play the role of 'measurer'? Was the wavefunction of the world waiting to jump for thousands of millions of years until a single-celled living creature appeared? Or did it have to wait a little longer, for some better qualified system . . . with a PhD?"(See Figure 2.2)

The problems that these physicists posed were related to the postulates of Orthodox quantum mechanics, which says that only when the observation is made is when the value of the property is *created*. Dirac supported this postulate and also clarified it in his textbook [34] where he says that a definite value cannot be ascribed to an observable measured in an arbitrary state. In his own words: *"The expression that an observable 'has a particular value' for a particular state is permissible in quantum mechanics in the special case when a measurement of the observable is certain to lead to the particular value, so that the state is an eigenstate of the observable"* [34].

Figure 2.2: Figure depicting the question raised by Bell when he asks, what qualifies some physical system to play the role of the observer? In the given figure the cat is responsible for giving reality to the poison trigger, but the reality of cat depends on the observation made by Schrödinger. Similarly the reality of Schrödinger is created by the omnipresent observer. But which observer gives reality to the omnipresent observer? (Courtesy: http://www.lls-ceilap.com/vi-jornadas—english.html)

As one can see from the above discussion the difficulties in defining *apparatus-independent* or *intrinsic* (unperturbed) information about the dynamics of quantum systems is rooted in the foundations of Orthodox quantum mechanics. More specifically, the so-called "eigenvalue-eigenstate link" establishes that quantum states cannot be associated to a well defined value of a given property unless such property is explicitly measured, the only exception being when the state itself is an eigensate of the measured property. There are, however, many situations where the conceptual understanding of a given phenomenon would be greatly simplified by the possibility of talking about well defined properties of quantum objects without the necessity of explicitly measuring them. Importantly, it is well known that the association of the definition of a property of a quantum system to the fact of being measured is a "deliberate theoretical choice" that is "not forced on us by experimental facts" [23]. In this respect, there are other quantum the-

ories, in empirical agreement with the Orthodox theory, where the definition of the properties of quantum objects is independent of the measurement [23]. These other theories allow, in particular, to define properties of quantum systems even when they are not measured (i.e., just as in classical mechanics). It is thus not surprising that there is a renewed interest in defining intrinsic properties within the so-called "quantum theories without observers" [35–37].

The definition of reality associated to the eigenstate-eigenvalue link exists only in the Copenhagen interpretation of quantum mechanics. For the Bohmian theory, for example, the trajectories of a quantum system are real independently of the fact of being measured or not. Therefore the definition of reality has different meaning in different quantum theories. One can hence say that the quantum reality is linked to the ontology of a theory and not to the experiments. Still this point of view is not very well understood in the scientific literature. There have been many attempts to provide a concrete definition of reality which does not need the support of any ontology i.e. the definition of reality that has a purely operationalistic point of view. In this regard Legett and Garg proposed a definition of reality constituting of two conditions that a property must meet in order to be classified as real [38]. Though these conditions do not require any ontology of a theory it indeed provides a check of the Orthodox reality associated to the eigenstate-eigenvalue link. These conditions are encapsulated in form of an inequality known as Legett-Garg inequality (LG inequality). They proposed that a property is a non-realistic property if (i) it is in the superposition of states (ii) if measuring these properties results in the perturbation of the system. Even though not explicitly, they wanted to provide a general test of realism (that they called macrorealism). However, as I have said, from the Bohmian point of view, the trajectories of a particle are real independently of whatever the Leggett and Garg define as real subjected to their inequality. What Leggett-Garg

tested was only the orthodox notion of reality. Once we accept that the Leggett-Garg inequality just deals with the concept of reality implicit in the Orthodox theory, we can discuss some of its aspects that are being debated in the literature. Though condition (i) is not very problematic there can always be an argument against condition (ii) since any classical system which is subjected to a clumsy measurement can be erroneously classified as non-realistic. This has led to what is referred to as the *clumsiness loophole*. A proposal to narrow it down has been discussed in Publication A.

Let us notice that macrorealism (as defined by Legett and Garg) cannot be proven true once and for all, viz., for any property at any time. If a test of macrorealism aims at evaluating our notion of classical realism, then a quantum object should satisfy the Leggett-Garg inequalities for any property at any time. However, even if an object were to pass a number of tests for different properties at different times, one never knows whether another property or lapse of time exists which the corresponding inequality would fail to pass. Therefore it is not a coincidence that most of experimental works testing Leggett and Garg inequalities in the laboratory are focused on ordinary quantum systems rather than on the type of "macroscopically distinct states" invoked by Leggett and Garg [39]. That is, existing tests only investigate a particular observable of interest $\mathcal{A}$ of a *microscopic* object (expected to behave quantum mechanically) at a given time [40–42]. Therefore it is more convenient to define what I refer to as microrealism which amounts to the relaxation of what Leggett and Garg called macrorealism into a definition of realism that is based on the so-called "eigenstate-eigenvalue link", i.e., the assumption that a system only has a determinate value for a particular observable when its state is an eigenstate of the corresponding operator [43, 44] at a particular instant.

After all the above discussions I conclude that the definition of reality is

different in different ontologies of quantum mechanics. Therefore the question: "Are electrons there when nobody looks?" has different answers depending on to which theory this question is asked. In the ontology of Orthodox theory the answer is "There are no electrons when nobody looks". On the contrary the same question in the Bohmian provides us the following answer: "Electrons always have a well defined position irrespective of whether one is looking or not". In the point of view of the author, for one working with electron devices, saying that electrons are not traversing the device when nobody is looking seems really hard to digest!

Chapter 3

Looking for intrinsic properties of quantum systems in non-Orthodox theory

In the previous discussion I established that adopting the Orthodox ontology, which implies the lack of *intrinsic properties* of general quantum systems, is just a deliberate choice that is not imposed by any experimental fact. Also I emphasised that there are other quantum theories empirically equivalent to the Orthodox theory that *can* indeed provide the unperturbed dynamics that we are looking for. Then, why should we disregard the possibility to define the intrinsic (back-action free) dynamics of quantum systems? Let me emphasise that there have been attempts in the past to define properties of the system beyond the eigenstate-eigenvalue link. For example the so-called Wigner function (or Wigner quasi-probability distribution function) was developed by Wigner himself as early as 1932 [45] with the aim to link the wavefunction to a probability distribution in phase space. This was one of the first attempts to look for additional intrinsic information of the behaviour of a quantum system beyond that provided by the

"eigenvalue-eigenstate link". Following the Orthodox postulates, the number of particles with a definite momentum at a given position is something that cannot be measured in a single-experiment measurement. Thus, this property (information of the system) cannot be a real value according to the Orthodox view. And nonetheless, the Wigner quasi-probability distribution function has been (and it is being) a very successful tool to gain insight into the dynamics of quantum systems. Somehow, the negative values of the probability is the price one has to pay when trying to go beyond the postulates of the Orthodox theory in looking simultaneously for well-defined positions and momentum.

A paradigmatic example of the difficulties of Orthodox quantum mechanics to provide intrinsic information is the tunneling time mentioned in previous sections. For an electronic engineer, the tunnelling time (understood as the time is takes an electron to traverse the device when no measuring apparatus is involved) is crucial in determining the cut-off frequency of an electronic device. Since such information is undefined in the Orthodox theory it must be provided by some non-Orthodox alternative. When one says to an electron device engineer that the time it takes an electron to traverse a barrier is undefined, the engineer will try to get such intrinsic information from other (less Orthodox) sources because he needs such information to anticipate what is the cut-off frequency of electron quantum devices. Presently, as discussed above, the same problem appears for the work distribution in the development of a quantum thermodynamic formalism of a system without linking the results to a particular type of measuring apparatus.

3.1 Defining intrinsic properties from modal theory

To alleviate the problems that arise in the Orthodox theory, which mandates defining properties linked to the measurement only, van Fraassen proposed to develop new quantum theories without imposing the "eigenstate-eigenvalue link" [46]. In addition to the *guiding state* associated to the wavefunction of the Orthodox theory, he introduced additional *property states* representing real valued properties not attached to any measurement. These theories are today known as modal quantum mechanics [46–48]. The essential feature of these approaches is that a quantum system has a well defined value of an observable even if the *guiding state* is not in an eigenstate of the corresponding operator. That is, in modal theories the *property states* are defined even if the quantum system is not interacting with a measuring apparatus. These *property states* can be thus understood as the *intrinsic properties* that we are looking for. Among a great variety of modal theories, Bohmian mechanics is probably the most prominent example where the *property state* of the position can be related to the so-called Bohmian trajectory [47].

Let me now start the discussion of modal quantum mechanics by defining intrinsic properties of a system. It will be very helpful to categorize the properties as static and dynamic properties which will help us to understand the utility of these properties more carefully.

Static intrinsic property: A static property G contains information of a system at a given time and for a given operator. When the system is decoupled from the measurement apparatus, the value of property G, $g(t)$, is an intrinsic property of the quantum system. Now, when a property G is measured at time t_0

it gives the value $g(t_0)$. This value coincides with an eigenvalue $g \equiv g(t_0)$ of the operator $\hat{G}$ in Orthodox theory. There is, however, a very important difference between the two theories that will become dramatic when discussing dynamical intrinsic properties. The Orthodox theory assumes that g is the (eigen) value of the quantum system after (not before) it is strongly measured. On the contrary, within the modal interpretation, $g(t_0)$ is the *intrinsic* value of the system even when no measurement is carried out. Thus, despite the fact that the eigenvalue g in the Orthodox theory coincides with the static intrinsic value $g(t_0)$ in the modal theory there are no static intrinsic properties defined in the Orthodox theory. In other words, before the strong measurement, the Orthodox theory states that the quantum system defined by the state $|\psi(t)\rangle$ has no property g (unless $|\psi(t)\rangle = |g(t)\rangle$) [49]. The well-known empirical uncertainty of quantum experiments is recovered in modal theories by assuming that identically prepared experiments are associated to the same *guiding state* $|\psi(t)\rangle$, but to a different *property state* $|g(t)\rangle$. To ensure that a modal theory is empirically equivalent to the Orthodox theory, the probability distribution of $g \equiv g(t)$ at time t has to be given by $|\psi(g,t)|^2$. Then, the ensemble value of G given by the modal theory $\langle G\rangle_M$ in different identically-prepared experiments is given by:

$$\langle G\rangle_M = \int dg\ |\psi(g,t)|^2 g = \langle\psi(t)|\hat{G}|\psi(t)\rangle = \langle G\rangle, \tag{3.1}$$

where for the case of a (partially) discrete spectrum the integral should be interpreted as a Stieltjes one.

Dynamic intrinsic property : A dynamical property bears information that is associated, at least, to one operator at two different times or two different (non-commuting) operators at the same time. Apart from the property $g(t)$ that is always well-defined within a modal theory, we can envision other intrinsic

properties $S_M(g(t))$ of the quantum system that is simultaneously defined by property S and G. By construction, such function $S_M(g(t))$ has to be linked to the *guiding state* $|\psi(t)\rangle$ and the *property state* $|g(t)\rangle$ [1]. The ensemble value of this property is given by:

$$\langle S\rangle_M = \int dg\ |\psi(g,t)|^2\ S_M(g), \tag{3.2}$$

I emphasize that, as it happens in Eq. 3.1, the modal interpretation allows to define $S_M(g(t))$ as an intrinsic (not-measured) property of the quantum system. An unavoidable requirement, however, is that the ensemble value reproduces the empirical (and Orthodox) value. It can be easily demonstrated [16, 21] that by defining $S_M(g(t))$ as:

$$S_M(g) = \int dg' \frac{\psi^*(g,t)S(g,g')\psi(g',t)}{|\psi(g,t)|^2}, \tag{3.3}$$

I get the desired identity:

$$\langle S\rangle_M = \int dg\ |\psi(g,t)|^2\ \left[\int dg' \frac{\psi^*(g,t)S(g,g')\psi(g',t)}{|\psi(g,t)|^2}\right] \equiv \langle\psi(t)|\hat{S}|\psi(t)\rangle = \langle S\rangle, \tag{3.4}$$

where I have defined $S(g,g') = \langle g|\hat{S}|g'\rangle$ and used the identities $\int dg\ |g\rangle\langle g| = 1$ and $\int dg'\ |g'\rangle\langle g'| = 1$. In the particular case when $\hat{S}$ and $\hat{G}$ commute, I get $\langle g|\hat{S}|g'\rangle = s_g\delta(g-g')$ which implies $S_M(g) = s_g$ with s_g the eigenvalue of $\hat{S}$ linked to the eigenvalue g. In other more general cases, the property $S_M(g)$ is a well-defined intrinsic property of the modal theory, without any counterpart in the Orthodox theory. For non-commuting operators $\hat{S}$ and $\hat{G}$, the eigenstate-

[1] Let us emphasize here that the physical soundness of $S_M(g(t))$ within a modal theory is not linked to the fact of whether $S_M(g(t))$ is measurable or not. In other words, the Bohmian velocity is a relevant intrinsic property of the Bohmian theory irrespective of its experimental accessibility.

eigenvalue link of the Orthodox theory does not allow to associate the value $S_M(g)$ with a real Orthodox property of the quantum system. Contrarily, according to the modal theory, $S_M(g)$ can be understood as a dynamical property that provides simultaneous information about the properties associated to the operators $\hat{G}$ and $\hat{S}$. Thus while the definition of intrinsic static properties do not entail any conceptual difficulty, in Orthodox quantum mechanics it is in not possible to define intrinsic dynamical properties for non-commuting operators. The dynamical intrinsic property $S_M(g)$ in Eq. 3.3 can be rewritten as:

$$S_M(g) = \int dg' \frac{\psi^*(g,t)S(g,g')\psi(g',t)}{|\psi(g,t)|^2} = \frac{\langle g|\hat{S}|\psi(t)\rangle}{\langle g|\psi(t)\rangle} \equiv {}_g\langle\hat{S}\rangle_{\psi(t)} \tag{3.5}$$

where I have used $\int dg' \; |g'\rangle\langle g'| = 1$. The identity Eq. 3.5 shows that the dynamical intrinsic property $S_M(g)$ coincides with the weak value ${}_g\langle\hat{S}\rangle_{\psi(t)}$ introduced by Aharonov, Albert and Vaidman (AAV) in 1988 [50]. This is a very important result since it provides a useful link between the intrinsic properties of the system derived from modal theories and the AAV weak values, which have been interpreted in many ways within the Orthodox theory. The possibility of obtaining the AAV weak value in the laboratory thus opens the possibility of measuring intrinsic properties. I will expand this discussion in section 3.3.

3.2 Bohmian mechanics as a special case to modal theory

Having established an unambiguous definition of intrinsic properties within modal quantum mechanics, I will now discuss the measurement of certain intrinsic properties in the context of Bohmian theory, which is a particular modal theory where the property state is the position eigenstate $|x(t)\rangle$. Before starting this discus-

sion, though, it is appropriate to provide a brief review of the ontology of this theory.

In Bohmian Mechanics, unlike in the Orthodox theory, a quantum particle has a well defined position (intrinsic property) at all times independent of the measurement. This position is then guided by the wavefunction, the evolution of which is given by the Schrödinger equation,

$$i\hbar\frac{\partial\Psi(\vec{x},t)}{\partial t} = \left[-\frac{\hbar^2}{2m}\nabla^2 + V(\vec{x},t)\right]\Psi(\vec{x},t) \tag{3.6}$$

where $V(\vec{x},t)$ is a scalar potential , m is the mass of the quantum particle, and $-\frac{\hbar^2}{2m}\nabla^2$ is the corresponding kinetic energy operator. Now Eq. 3.6 can be easily manipulated to arrive to a continuity equation that reads,

$$\frac{\partial|\Psi(\vec{x},t)|^2}{\partial t} + \vec{\nabla}\vec{j}(\vec{x},t) = 0 \tag{3.7}$$

where $|\Psi(\vec{x},t)|^2$ can be interpreted as the probability density of the particle and $\vec{j}(\vec{x},t) = |\Psi(\vec{x},t)|^2\frac{\hbar}{m}\,\mathrm{Im}\,\frac{\nabla\Psi}{\Psi}$ is the current density. At this point, one can invoke a natural assumption about the current density as the product of the charge density and velocity i.e. $\vec{j}(\vec{x},t) = \rho(\vec{x},t)\vec{v}(\vec{x},t)$ with $\rho(\vec{x},t) \equiv |\Psi(\vec{x},t)|^2$, and easily define the Bohmian velocity of a particle at position x and time t as as,

$$\vec{v}(\vec{x},t) = \frac{\vec{j}(\vec{x},t)}{|\Psi(\vec{x},t)|^2} = \frac{\hbar}{m}\,\mathrm{Im}\,\frac{\nabla\Psi(\vec{x},t)}{\Psi(\vec{x},t)}. \tag{3.8}$$

Eq. 3.8 is also known as the guidance equation. At this point, one can already notice the ontological differences between the Bohmain theory and the Orthodox theory. Whereas in the Bohmain theory the velocity is a well defined property independent of the measurement, in the Orthodox theory the concept of the velocity of a particle at a particular position does not exist due to the prohibition

of describing non-commuting observable at an instant, in this case the momentum and the position. Now integrating Eq. 3.8 I obtain the equation describing the evolution of the so-called Bohmian trajectories,

$$\vec{x}(t) = \vec{x}\,(t_0) + \int_{t_0}^{t} \vec{v}\,(\vec{x}, t')\,dt'. \tag{3.9}$$

One can derive similar equations for any number of degrees of freedom involved in a many-body wavefunction including the system as well as the measuring apparatus. So, in Bohmian mechanics there is no need to define an artificial boundary between apparatus and system nor to introduce a new physical law when the measurement is invoked (as it happens in the Orthodox theory). Accepting that the output of the measurement is indicated by a pointer and that this pointer is made of quantum particles too, then the measurement process can be simply understood in terms of (Bohmian) pointer positions.

Bohmian mechanics is thus a deterministic theory in the sense that if one knows the initial position of a particle one can then obtain the position at a later time. And yet, even though this theory is deterministic, there is still randomness involved in different experiments. This is because the exact initial positions of the particles cannot be known with certainty. We can only know its probability distribution, which is defined according to the quantum equilibrium condition [51]. It is very important to emphasize that, in the non-relativistic regime, Bohmian mechanics reproduces all empirical observations, just as Orthodox quantum mechanics does. This is a direct consequence of what is referred to as the equivariance principle, which assures that Bohmian trajectories reproduce the probability density at all times. Since the ontology of Bohmian mechanics allows to describe the properties of the system independently of the measurement, one can in principle exclude the degrees of freedom of the measuring apparatus and describe only the dynamics of the system alone. In the subsequent sections it will be shown

how this convenience helps us to define the intrinsic properties of the system.

As I have already mentioned in the beginning of this section, Bohmian mechanics can be understood as a modal theory where the *property state* $|g(t)\rangle \equiv |x(t)\rangle$ specifies the property as position of particles $g(t) \equiv x(t)$ at all times (with or without measuring apparatus)[47]. Once we understand that Bohmain mechanics is just a special case of the modal theory we can straightforwardly define (Bohmian) intrinsic properties as in Eq. 3.5. These Bohmian properties are referred to as *local-in-position* Bohmian properties and are considered as real numbers in the literature [16, 21]. Therefore we introduce an intrinsic Bohmian property S_B as a real function through,

$$S_B(x) = \mathrm{Re}\left[\int dx' \frac{\psi^*(x,t)S(x,x')\psi(x',t)}{|\psi(x,t)|^2}\right]. \tag{3.10}$$

Then, we can rewrite the Bohmian version of Eq. 3.5 including the above considerations as follows:

$$S_B(x) = \mathrm{Re}\left[{}_x\langle\hat{S}\rangle_{\psi(t)}\right], \tag{3.11}$$

where I have used $S(x,x') = \langle x|\hat{S}|x'\rangle$ and $\int dx'|x'\rangle\langle x'| = 1$. The right hand part of Eq. 3.11 is refereed to as local-in-position weak value [16, 21] (an AAV weak value with the postselected state as a position eigenstate) which is identical to intrinsic Bohmian properties (independent of the measuring apparatus).

The equivalence in (3.11) thus shows that local-in-position weak values are, by construction, free from the measurement back-action and hence provide intrinsic information of the system. The probability distribution of the different values of the intrinsic property is also independent of the measuring apparatus and is given by

$$P_B(s) = \lim_{M\to\infty} \frac{1}{M}\sum_{i=1}^{M} \delta[s - S_B(x^i(t))], \tag{3.12}$$

where $x^i(t)$ are the Bohmian trajectories corresponding to each i^{th} experiment defined through the so-called quantum equilibrium condition [21].

3.3 Interpretation of AAV weak values

In the previous section I have established a clear-cut equivalence between intrinsic Bohmian properties and local-in-position weak values. The importance of this connection is crucial because weak values can be experimentally determined in many circumstances. For instance, Howard Wiseman [52] showed that an operationalist definition of the velocity of a quantum particle involving weak and strong measurements separated by an infinitesimal time lapse ("using a technique that would make sense even to a physicist with no knowledge of quantum mechanics") yields a weak value defined in the sense of Aharonov, Albert and Vaidman (AAV) [50, 53]. This weak value is the Bohmian velocity [52, 54]. Following this theoretical achievement, a number of experiments have been carried out where the Bohmian velocity has been measured in the laboratory [55–59]. But, if the Bohmian velocity can be measured by means of weak values, why is this property not well-defined in Orthodox quantum mechanics?

The answer to the above apparent paradox is that the experimental procedure to get the weak value in the laboratory does not correspond to a single measurement of a unique system (but to the measurement of an ensemble of identical systems). Note that the definition of AAV weak value is defined through a single measurement (as demonstrated in Appendix F), and yet it cannot be accepted as an Orthodox property through the eingenvalue-eigenstate link. Thus there is a clear distinction between an experimental (or operationalist) weak value and AAV's weak value. Experimentally evaluated weak values deal with an ensemble of identically prepared quantum system. Each quantum system of the ensemble

suffers, first, a weak measurement of a property and, later, a strong measurement of a second property. Only those quantum systems for which the second strong measurement outcome is compatible with a desired value of the first property are (post-)selected. The experimental weak value is then proportional to the ensemble average value of the first weak measurement conditioned to some post-selected elements of the ensemble. We can describe the recipe of this procedure as follows,

1. Consider a large (infinite) ensemble of identically-prepared quantum systems at time t_0.

2. For each element of the ensemble:

   (a) A weak measurement of a property linked to the operator $\hat{S}$, giving the output y_s, is carried out at time t_1.

   (b) After the weak measurement, the quantum system undergoes a unitary time-evolution from t_1 till t_2.

   (c) At time t_2, a strong measurement of a second property linked to the operator $\hat{G}$ is carried out, giving the output y_g. Note that in the case of a strong measurement the output of the measuring apparatus y_g coincides with the eigenvalue of the system, g, linked to the operator $\hat{G}$.

3. From the ensemble of measured values y_s and y_g, only those quantum systems whose second strong measured output y_g is compatible with a given value of the second property $y_g = a$ are (post-)selected. This allows us to construct the joint probability of obtaining the ancilla outcomes y_s and $y_g = a$ as $P(y_g = a, y_s)$.

4. Finally, the experimental or operationalist weak value ${}_a\langle\hat{S}_{exp}\rangle_{\psi(t_2)}$ is ob-

tained as:

$$ {}_a\langle \hat{S}_{exp} \rangle_{\psi(t_2)} \equiv \frac{\int dy_s \; y_s P(y_g = a, y_s)}{\int dy_s P(y_g = a, y_s)}, \tag{3.13} $$

Notice that an experimental or operationalist definition of the weak value does not need to assume that wavefunctions and operators exist, and yet is still crystal clear what needs to be done in the laboratory to get ${}_a\langle \hat{S}_{exp} \rangle_{\psi(t_2)}$. This definition of weak value has no link with any ontology of any theory. However, once we have an operationalist definition that gives a value in the laboratory, one aims at looking for a physical interpretation within a given quantum theory.

AAV's weak value is inspired by a time-symmetric formulation of quantum mechanics [60, 61] to describe the system during the time interval between two strong (projective) measurements: an initial one pre-selecting the quantum system and a final one post-selecting it. The AAV's weak value is found from a single quantum system (not an ensemble) that interacts weakly and unitarily with an ancilla under the (post-selected) condition that a strong measurement provides the desired values of the property of the system (see Appendix F). There is no explicit weak measurement in the AAV's weak value because it is assumed that the weak measurement can be done without any back-action. Unfortunately, it is well known that this is not possible for general superposition states (as dicussed in section 2.2.2). Therefore, AAV's weak values (e.g., the Bohmian velocity) cannot be measured in a single measurement but only through an ensemble of measurements. That is, the back-action present in each weak measurement can only be eliminated in average, and therefore AAV's weak values can be experimentally accessed through ensemble averaging only. This is simply incompatible with the eigenvalue-eigenstate link, and hence an interpretation of experimentally accessible AAV's weak values in terms Orthodox quantum mechanics is not

possible.

Since its first introduction in 1988 [50], there have been many attempts in the literature to find an interpretation of weak values without abandoning the Orthodox quantum mechanics viewpoint, both in theory and experiments [55, 62–67]. Weak values have been given a number of different, often incompatible, interpretations [68–74]; see Ref. [75] for a recent review on the difficulties to accommodate the weak values within the Orthodox ontology. In my opinion, many of these attempts fail to properly distinguish between the AAV's and experimental weak values. Both can be numerically equivalent, but they are different at the ontological level, as I have discussed in the previous paragraph.

3.4 Computing quantum high frequency noise from intrinsic properties

Now, I should show that identifying local-in-position weak values with intrinsic Bohmian properties yields an extraordinarily useful tool to unveil the intrinsic dynamics of quantum systems. In particular, this will solve the conceptual and practical inconveniences that we encountered in the Orthodox theory when dealing with certain puzzling situations in defining the dwell time, the high frequency noise or any property associated to multi-time (or continuous) measurements. An unambiguous definition of these properties are of paramount importance in the development of future quantum technologies. Here, I will exemplify the importance of *intrinsic* properties in describing the quantum noise at high frequency, which is the most relevant example on the context of electron devices. The examples of the dwell time and thermodynamic work can be found in Appendix H.

As I have already discussed in chapter 1 the evolution of quantum transport

simulation strategies from steady state to time resolved regimes necessitates to describe electrons explicitly from the perspective of quantum mechanics. This results in various complications when computing the electric current within the framework of Orthodox theory. For the sake of continuity I will re-emphasize the discussion in chapter 1 and then provide a solution in terms of intrinsic properties.

The total current at high frequencies is the sum of the conduction (flux of particles) plus the displacement (time-derivative of the electric field) components [9, 10, 76, 77] as given in Eq. 1.1. It is a usual practice to partition an electron device into the active region, where all the relevant quantum phenomena takes place, for example tunnelling in the resonant tunnelling device, and the environment which collectively comprises of the metallic cables and the ammeter. The displacement current on a surface of an active region in an electron device is different from zero whenever electrons are able to modify the electric field on it (independently on how far the electrons are from that surface). Therefore, while in steady state this quantity is zero after time averaging, at high frequencies a proper solution of Maxwell's equations is needed to know the interplay between scalar potentials and electrical currents.

Typically I am interested in getting information of the total electrical current in a surface S_D of the electron device depicted in Figure 1.1 (this surface is also referred to as drain terminal of an electron device) of the active region. The pertinent point in the discussion is that in a realistic experimental scenario, there is no measuring apparatus on the surface S_D of the active device region where the dynamics of electrons is simulated. Instead, the ammeter is usually located at a macroscopic distance far from the active region of the nanoscale device and connected to it through macroscopic cables (wires) with an amount of electrons given by the Avogadro number as shown in Figure 1.1. Still, the current on surface S_D coincides with the current in the ammeter because of the conservation

of the total (particle plus displacement) current.

Now in order to simplify the discussion, I consider the *unperturbed* value of the total electrical current when only one electron is present in the active region. Once I am able to get the Bohmian trajectory $\vec{r}^i(t)$ of an electron moving through the device by solving a transport equation like the one in Eq. H.1, the total current generated by this electron (trajectory) in a surface S_D is given as follows,

$$I^i(t) = \int_{S_D} \vec{j}_c^i(\vec{r},t)\cdot \mathrm{d}\vec{s} + \int_{S_D} \epsilon(\vec{r})\frac{\mathrm{d}\vec{E}^i(\vec{r},t)}{\mathrm{d}t}\cdot \mathrm{d}\vec{s}, \tag{3.14}$$

where $\epsilon(\bar{r},t)$ is the (inhomogeneous) electric permittivity. The current (particle) density of the i^{th} experiment is given by $\vec{j}_c^i(\vec{r},t) = q\vec{v}(\vec{r}^i(t),t)\delta[\vec{r}-\vec{r}^i(t)]$ with q the electron charge[2]. The electric field $\vec{E}^i(\vec{r},t)$ is just the solution of the Gauss equation with the proper boundary conditions for a charge density given by $Q^i(\vec{r},t) = q\delta[\vec{r}-\vec{r}^i(t)]$. In principle, the integration of the density current in Eq. 3.14 on the surface S_D has a dependence on its position. However, such dependence disappears in practical two-terminal scenarios due to the total current and its conservation law.

Now, it can be proven that in a two terminal device of distance L with metallic contacts of surface $S_D = W\times H$, if $L \ll W, H$ (width and height) the total current can be written as [9, 10, 13]:

$$I^i(t) = \frac{q}{L}v_x^i(t), \tag{3.15}$$

where $v_x^i(t)$ is the velocity in the transport direction of the considered electron in the active region in the i^{th} experiment [3]. Outside the active region, the electron

[2]It is important to see the difference in the similar looking equations namely Eq. 1.1 and Eq. 3.14. Whereas the former is an Orthodox representation with the parameters defined as expectation values, in the later Bohmian case, which is defined for an i-th experiment, one is permitted to define an instantaneous value of the parameters involved.

[3]Typically, hundreds of electrons have to be considered in a realistic device and the total

is screened and its contribution to the total current can be neglected. Now using Eq. 3.15 I will try to arrive at the weak value of the current and see if it is equivalent to the unperturbed current $I^i(t)$.

The Bohmian velocity $v_x(t)$ is evaluated by the Bohmian guidance equation 3.8 as follows,

$$v_x(t) = \frac{\hbar}{m}\mathrm{Im}\left[\frac{\frac{\partial}{\partial x}\psi(\vec{r},t)}{\psi(\vec{r},t)}\right] = \frac{1}{m}\mathrm{Re}\left[\frac{\langle\vec{r}|\hat{P}_x|\psi(t)\rangle}{\langle\vec{r}|\psi(t)\rangle}\right], \tag{3.16}$$

where I have used $\langle\vec{r}|\hat{P}_x|\psi(t) = -i\hbar\frac{\partial}{\partial x}\psi(\vec{r},t)$. Now evaluating the velocity in Eq. 3.16 for a particular trajectory $\vec{r} = \vec{r}^i(t)$ we get the current for an i^{th} Bohmian experiment as in Eq. 3.15 which can be rewritten using Eq. 3.16 as,

$$I^i(t) = \frac{q}{L}v_x^i(t) = \frac{q}{mL}\mathrm{Re}\left[\frac{\langle\vec{r}^i(t)|\hat{P}_x|\psi(t)\rangle}{\langle\vec{r}^i(t)|\psi(t)\rangle}\right] = \frac{q}{mL}\mathrm{Re}\left[_{\vec{r}^i(t)}\langle\hat{P}_x\rangle_{\psi(t)}\right]. \tag{3.17}$$

Thus the unperturbed current is equivalent to the local-in-position weak measurement of the momentum operator $\hat{P}_x$ in the transport direction x, where $\langle\vec{r}|\psi(t)\rangle = \psi(\vec{r},t)$ is the wavefunction of the electron in the active region and $r^i(t)$ specifies the position where the local-in-position weak momentum is evaluated. From the information of $I^i(t)$ in Eq. 3.17, when $i = 1, ..., M$ experiments are considered, we can compute the ensemble value of the current as,

$$\langle I(t)\rangle = \lim_{M\to\infty}\frac{1}{M}\sum_{i=1}^{M}\frac{q}{mL}\mathrm{Re}\left[_{\vec{r}^i(t)}\langle\hat{P}_x\rangle_{\psi(t)}\right], \tag{3.18}$$

and also the autocorrelations of the total current.

The Fourier transform of the current correlations provides the power spectral

current in the i-th experiment can be computed by just adding the contribution of each electron $I^i(t) = \sum_{n=1}^{N_e} I_n^i(t)$ with N_e the number of electrons inside the volume $L \times W \times H$ at time t.

density of the fluctuations of the current at high frequencies.

$$\mathrm{PSD}(\omega) = \lim_{M\to\infty} \frac{1}{M} \sum_{i=1}^{M} \left(\frac{q}{mL}\right)^2 \int_{-\infty}^{\infty} d\tau e^{-i\omega\tau} \mathrm{Re}\left[\vec{r}^{i}(t_2)\langle \hat{P}_x \rangle_{\psi(t_2)}\right] ... \\ ...\mathrm{Re}\left[\vec{r}^{i}(t_1)\langle \hat{P}_x \rangle_{\psi(t_1)}\right], \qquad (3.19)$$

where I have assumed that we are dealing with a wide-sense stationary process where the correlation depends only on the time difference $\tau = t_2 - t_1$. Some of the authors of this paper have elaborated these ideas into the simulator named BITLLES which is an acronym for Bohmian interacting transport in non-equilibrium electronic structures [78–84].

Thus, I have successfully demonstrated that the unperturbed value of the total (particle + displacement) current in Eq. 3.15 can be computed by the help of the intrinsic property $v_x(t)$ which is called the Bohmian velocity. This property has a concrete definition in the ontology of Bohmian mechanics. The evaluation of intrinsic electrical currents helps us to safely avoid the complications involved in defining the POVM associated to the total current (particle + displacement). Furthermore, since the above definition of the electrical current is independent of the measuring apparatus, it is "universal" and non-contextual. Finally, is it easy to see from Eq. 3.17 that the intrinsic current is just the local-in-position weak value of the momentum and is indeed experimentally accessible [52].

Part III

METHODOLOGY DEVELOPMENT FOR DEVICE SIMULATION

Chapter 4

Conditional wavefunction approach to many-body correlations

In this chapter I outline some important ideas elaborated in the paper attached in Publication B. Open quantum systems serve as the starting point to solve the problem of dealing with a large number of degrees of freedom associated to a closed quantum system comprising not only the system but also the environment degrees of freedom (where environment includes everything but the system). Describing a closed system is conceptually very simple. The full wavefunction follows a unitary time dependent Schrödinger equation (TDSE) between measurements. As discussed in previous chapters, during measurements, some type of non-unitary collapse has to be included in the wavefunction. Solving this TDSE is, but, a formidable task and practically impossible in an exact level when more than very few degrees of freedom are involved. Thus it is a common practice to partition the full closed system into a quantum system and the environment and then address only the reduced density matrix of the quantum system by trac-

ing out the degrees of freedom of the environment. Such a strategy can be used in the description of the active region of an electron device as an open quantum system [85, 86]. Once this is made possible, one can then borrow any state-of-the-art mathematical tool developed to study open quantum systems [87, 88] for simulating a particular quantum system at hand.

A preferred technique in this regard has been the stochastic Schrödinger equation (SSE) approach [89–96]. Instead of directly solving equations of motion for the reduced density matrix, the SSE approach exploits the state vector nature of the so-called conditional states to alleviate some computational burden (and ensuring a complete positive map by construction [97]). Even if this technique allows to always reconstruct the full density matrix, a discussion on whether dynamical information can be directly extracted from such conditional states in non-Markovian scenarios has appeared recently in the literature [98, 99]. Somehow, the conditional states are more natural element in Bohmian mechanics than in Orthodox quantum mechanics. In other words, the Bohmian conditional wave function is a physical element of the Bohmian theory, while the conditional Orthodox wave function is just a mathematical representation.

In this regard Wiseman and Gambetta has acknowledged the Bohmian conditional wavefunction as a proper tool to describe general open quantum systems in non-Markovian scenarios [100, 101]. In this work I reinforce this idea by showing that the Bohmian conditional wavefunction is an exact decomposition and recasting of the time-evolution of a closed quantum system that yields a set of coupled, non-Hermitian, equations of motion that allows to describe the evolution of arbitrary subsets of the degrees of freedom on a formally exact level. Furthermore, since the measurement process is defined as a routine interaction between subsystems in Bohmian mechanics, conditional states can be used to describe either the measured or unmeasured dynamics of an open quantum system.

4.1 The Stochastic Schrödinger Equation (SSE)

Consider a typical electronic device as depicted in Figure 4.1, where the active region and the environment are distinguished for clarity. I can start with a closed quantum system (as the one shown in Figure 4.1a) comprising of all the degrees of freedom which is represented by a pure state, $|\Psi(t)\rangle$, evolving unitarily according to the time-dependent Schrödinger equation

$$i\hbar\frac{\partial|\Psi(t)\rangle}{\partial t} = \hat{H}|\Psi(t)\rangle. \tag{4.1}$$

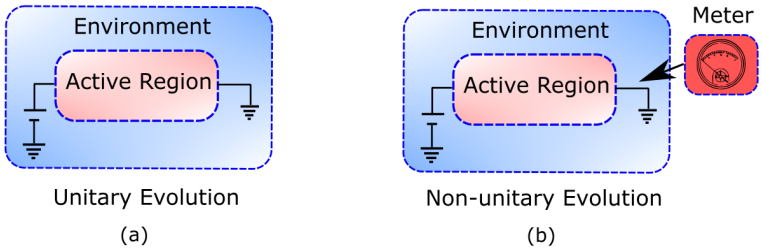

Figure 4.1: Panel (a): Schematic representation of an open quantum system, which can be partitioned into active region and environment. The evolution of the entire device is described by the state $|\Psi(t)\rangle$ that evolves unitarily according to the time-dependent Schrödinger equation. Panel (b): Schematic representation of a measured open quantum system, which can be partitioned into meter, active region and environment. The evolution of the device plus environment wavefunction is no longer unitary due to the (backaction) effect of the measuring apparatus.

Finding a solution to Equation (4.1) is inaccessible for most practical scenarios due to the large number of degrees of freedom involved and thus it is common to describe only the system (i.e., the active region) by a reduced density matrix,

$$\hat{\rho}_{\text{sys}}(t) = \text{Tr}_{\text{env}}\left[|\Psi(t)\rangle\langle\Psi(t)|\right], \tag{4.2}$$

where Tr_{env} denotes the trace over the environment degrees of freedom. If the time evolution of solution to Equation (4.2) is known, then the expectation value

of any observable $\hat{A}$ of the system can be evaluated as follows when the system is measured as depicted in Figure 4.1(b):

$$\langle \hat{A}(t) \rangle = \mathrm{Tr}_{\mathrm{sys}}[\hat{\rho}_{\mathrm{sys}}(t)\hat{A}], \tag{4.3}$$

We note that the Eq. 4.2 is evaluated without invoking the measuring apparatus as shown in Figure 4.1(a). Using the eigenstates $|q\rangle$ of the measuring apparatus as a mathematical base of our Hilbert space I can write the wavefunction of the closed system shown in Figure 4.1(a) as follows,

$$|\Psi(t)\rangle = \int dq \sqrt{P(q,t)} |q\rangle \otimes |\psi_q(t)\rangle, \tag{4.4}$$

Measuring the wavefunction above as shown in Figure 4.1(b) gives the measurement outcome q and the collapsed wavefunction can be written as,

$$|\Psi_q(t)\rangle = \sqrt{P(q,t)} |q\rangle \otimes |\psi_q(t)\rangle. \tag{4.5}$$

Then the wavefunction of the system alone can effectively be written as,

$$|\psi_q(t)\rangle = \frac{\left(\langle q| \otimes \hat{I}_{\mathrm{sys}}\right) |\Psi(t)\rangle}{\sqrt{P(q,t)}}, \tag{4.6}$$

The above wavefunction is conditioned on a particular environment value q which can be defined as the eigenvalue associated to the operator $\hat{Q}$. Initially the operator $\hat{Q}$ was considered only a mathematical construct (that is an element the eigenstates of which are used just to construct a basis). In more recent times, however, it has been generally accepted that the conditional states in Equation 4.6 can be interpreted as the states of the system conditioned on a type of sequential (sometimes referred to as continuous) measurement of the operator $\hat{Q}$ of the

environment now representing a physical measuring apparatus. The stochastic Schrödinger approach to open quantum systems consists on finding an equation of motion for the state in Eq. 4.6.

4.2 Markovian and non-Markovian regimes

For discussing the SSEs it is very important to invoke the concept of Markovianity. This is because the discussion will drastically differ depending on the regime of operation i.e. Markovian or non-Markovian. The Markovian regime, according to a pragmatic definition, is the regime where the entanglement between system and environment decays in a time scale $t_D \ll \tau$ where τ is defined as the time interval between measurements. In this regime the stochastic variables q_t and $q_{t+\tau}$ which are the environment eigen-values measured at times t and $t+\tau$ respectively are sampled, separately, from the probability distributions $P(q_t, t) = \langle \psi_q(t) | \psi_q(t) \rangle$ and $P(q_{t+\tau}, t+\tau) = \langle \psi_q(t+\tau) | \psi_q(t+\tau) \rangle$. Therefore no matter how the trajectories $\{q_t\}$ are connected in time, one always obtains the correct time-correlation function $\langle Q(t)Q(t+\tau) \rangle$. In this regime, the environment itself can be thought of as a type of measuring operator (as appears in generalized quantum measurement theory [102]) that keeps the open system in a pure state after the measurement (in fact after the system and environment correlation time t_D which is assumed to be very small). The open system can be then seen as an SSE in which the stochastic variable q_t (sampled from the distribution $P(q_t, t)$) is directly the output of a sequential measurement of the environment (see Publication B (Page 7)). The stochastic trajectory of this conditioned system state generated by the (Markovian) SSE is often referred to as a quantum trajectory [85, 91, 103] and can be used, for example, to evaluate time-correlation functions of the environment.

The above argument, however, cannot be applied to the situations where system-environment correlations are expected to decay on a time-scale comparable to the time-scale relevant for the system evolution, i.e., $t_D \sim \tau$. If one is aiming at computing multi-time correlations functions at high frequencies for example, then it is necessary to incorporate the effect (backaction) of the successive measurements on the evolution of the conditioned state. Even though these Orthodox conditional states are mathematically consistent to reproduce ensemble values, they suffers from interpretational issues when trying to connect the solutions of these conditioned states (trajectories) at different time.

This discussion can be simplified by saying that there is no wave function for a subsystem in the ontology of the Orthodox theory. A subsystem has to be defined from Orthodox theory by the reduced density matrix, not by a pure state. Although using Orthodox pure states can be a useful approximation for some (markovian) systems, in general, it is not possible to study quantum subsystems with Orthodox pure states. These ontological limitations are not true in Bohmian mechanics, where the conditional wave function can be used to study any (Markovian or non-Markovian) subsystem.

4.3 Bohmian conditional wavefunctions

A fundamental aspect of the Bohmian theory is that reality (of some properties) of quantum objects does not depend on the inclusion of the measuring apparatus. That is, the values of some observables, e.g., the value of the positions of the particles of the environment, exist independently of the measurement. In order to describe a measurement process with the explicit inclusion of the measuring apparatus one just have to introduce an additional degree of freedom of the apparatus into the equations of motion.

I explain now how the concept of conditional wave function for any subsystem appears naturally in Bohmian mechanics. Let me define a collective degree of freedom of the position of the particles of environment as q (also consisting the measuring apparatus) and x as the collective degree of freedom of the position of particles of the system, then, the Bohmian theory defines an experiment in the laboratory by means of two basic elements:

1. The wavefunction $\Psi(x, q, t)$, the evolution of which is governed by the time-dependent Schrödinger equation.

2. The trajetories $Q^i(t)$ and $X^i(t)$ of the environment and system respectively, which obey the guidance equation in Eq. 3.8.

The ensemble of trajectories reproduce the probability distribution of the Orthodox wavefunction (solution of Equation (4.1)) at all times due to the equivariance principle [21] and thus ensemble values computed from the Orthodox and Bohmian theory are empirically equivalent. From the full wavefunction $\langle x, q|\Psi(t)\rangle = \Psi(x, q, t)$ and the trajectories $Q^i(t), X^i(t)$, one can then easily construct the Bohmian conditional wavefunction of the system conditioned on the particular trajectory $Q^i(t)$ of the environment as follows,

$$\tilde{\psi}_{Q^i(t)}(x, t) = \Psi(x, Q^i(t), t) \tag{4.7}$$

The relevance of the Bohmian conditional wave function is that the trajectory of the system can be computed either from the velocity computed from Eq. 4.7 or from the velocity computed from the total wave function $\Psi(x, q, t)$ (when evaluated at the particular positions of the environment). The discussion about the ontological role of these conditional wave function has been discussed by Travis Norsen and co-authors [25, 104], but it is far from the scope of this paper.

Now once I impose $Q^i(t) \equiv q_t$, I obtain,

$$|\tilde{\psi}_{q_t}(t)\rangle = P(q_t, t)|\psi_{q_t}(t)\rangle. \tag{4.8}$$

The above equation is similar but not identical to Eq. 4.5. Whereas in Eq. 4.5 the wavefunction can be used only at the particular instant of time of measurement, the Bohmian trajectory $Q^i(t)$ and the conditional wavefunction $|\tilde{\psi}_{q_t}(t)\rangle$ are valid for any time (with or without measurement) for one experiment (labelled by the index i in the Bohmian language). Thus, Bohmian trajectory has a fundamental role in describing the history of the Bohmian conditional state for one particular experiment. I have mentioned at the beginning of this chapter, that the conditional wave functions has a physical role in Bohmian mechanics that is missing in Orthodox quantum mechanics. The conclusion of this chapter can thus be summarized as follows: The conditional wave function for Markovian or non-markovian system cannot be defined within the Orthodox quantum theory because, in general, an open quantum system cannot be described by a pure state. The same description is possible in the framework of Bohmian theory, because an open system can be described by an open system.

4.3.1 Application to electron transport

The Bohmian conditional wavefunction can be a very useful tool in the electron transport simulations in the quantum electron devices. Let me start the discussion by considering an arbitrary quantum system. The whole system, including the open system, the environment and the measuring apparatus, is described by a Hilbert space $\mathcal{H}$ that can be decomposed as $\mathcal{H} = \mathcal{H}_x \otimes \mathcal{H}_q$ where $\mathcal{H}_x$ is the Hilbert space of the open system and $\mathcal{H}_q$ the Hilbert space of the environment. If needed, the Hamiltonian $\mathcal{H}_q$ can include also the degrees of freedom of the

measuring apparatus. I define $x = \{x_1, x_2...x_n\}$ as the degrees of freedom of n electrons in the open system, while q collectively defines the degrees of freedom of the environment (and possibly the measuring apparatus). The open system plus environment Hamiltonian can then be written as:

$$\hat{H} = \hat{H}_q \otimes \hat{I}_{\mathrm{x}} + \hat{I}_q \otimes \hat{H}_{\mathrm{x}} + \hat{V} \tag{4.9}$$

where $\hat{H}_{\mathrm{x}}$ is the Hamiltonian of the system, $\hat{H}_q$ is the Hamiltonian of the environment (including the apparatus if required), and $\hat{V}$ is the interaction Hamiltonian between the system and the environment. We note at this point that the number of electrons n in the open system can change in time and so the size of the Hilbert spaces $\mathcal{H}_x$ and $\mathcal{H}_q$ can depend on time too.

The equation of motion for the Bohmian conditional wavefunction $\langle x|\tilde{\psi}_{q_t}(t)\rangle = \tilde{\psi}_{q_t}(x,t)$ in the position representation of the system can be derived by projecting the many-body (system-environment) Schrödinger equation into a particular trajectory of the environment $q_t \equiv Q(t)$, i.e. [105, 106]:

$$i\hbar\frac{d\tilde{\psi}_{q_t}(x,t)}{dt} = \langle q_t| \otimes \langle x|\hat{H}|\Psi(t)\rangle + i\hbar\nabla_q\langle q| \otimes \langle x|\Psi(t)\rangle\big|_{q=q_t}\frac{dq_t}{dt}. \tag{4.10}$$

Equation (4.10) can be rewritten as:

$$i\hbar\frac{d\tilde{\psi}_{q_t}(x,t)}{dt} = \left[-\frac{\hbar^2}{2m}\nabla_x^2 + U_{q_t}^{eff}(x,t)\right]\tilde{\psi}_{q_t}(x,t) \tag{4.11}$$

where

$$\tilde{U}_{q_t}^{eff}(x,t) = U(x,t) + V(x,q_t,t) + \mathcal{A}(x,q_t,t) + i\mathcal{B}(x,q_t,t). \tag{4.12}$$

In Equation 4.12, $U(x,t)$ is an external potential acting only on the system de-

grees of freedom, $V(x,q_t,t) = \langle q| \otimes \langle x|\hat{V}|\Psi\rangle/\Psi(x,q,t)\big|_{q=q_t}$ is the Coulomb potential between particles of the system and the environment evaluated at a given trajectory of the environment, $\mathcal{A}(x,q_t,t) = \frac{-\hbar^2}{2m}\nabla_q^2\Psi(x,q,t)/\Psi(x,q,t)\big|_{q=q_t}$ and $\mathcal{B}(x,q_t,t) = \hbar\nabla_q\Psi(x,q,t)/\Psi(x,q,t)\big|_{q=q_t}\dot{q}_t$ (with $\dot{q}_t = dq_t/dt$) are responsible for mediating the so-called kinetic and advective correlations between system and environment [105, 106]. Equation (4.11) is non-linear and describes a non-unitary evolution.

In an electron device, the number of electrons contributing to the electrical current are mainly those in the active region of the device. The number fluctuates as there are electrons entering and leaving the active region. Thus it is necessary to somehow model the addition and subtraction of the electrons in the active region. This creation and destruction of electrons leads to an abrupt change in the degrees of freedom of the many body wavefunction which cannot be treated with a Schrödinger-like equation for $\tilde{\psi}_{q_t}(x,t)$ with a fixed number of degrees of freedom. In the Bohmian conditional approach, this problem can be circumvented by decoupling the system conditional wavefunction $\tilde{\psi}_{q_t}(x,t)$ into a set of conditional wavefunctions for each electron. More specifically, for each electron x_i, we define a single particle conditional wavefunction $\tilde{\tilde{\psi}}_{q_t}(x_i,\bar{X}_i(t),t)$, where $\bar{X}_i(t) = \{X_1(t),..,x_{i-1}(t),x_{i+1},..,X_n(t)\}$ are the Bohmian positions of all electrons in the active region except x_i, and the second tilde denotes the single-electron conditional decomposition that we have considered on top of the conditional decomposition of the system-environment wavefunction. The set of equations of motion of the resulting $n(t)$ single-electron conditional wavefunctions

inside the active region can be written as:

$$i\hbar\frac{d\tilde{\bar{\psi}}_{q_t}(x_1,\bar{X}_1(t),t)}{dt} = \left[-\frac{\hbar^2}{2m}\nabla^2_{x_1}+\tilde{\bar{U}}^{eff}_{q_t}(x_1,\bar{X}_1(t),t)\right]\tilde{\bar{\psi}}_{q_t}(x_1,\bar{X}_1(t),t) \quad (4.13)$$

$$\vdots$$

$$i\hbar\frac{d\tilde{\bar{\psi}}_{q_t}(x_n,\bar{X}_n(t),t)}{dt} = \left[-\frac{\hbar^2}{2m}\nabla^2_{x_n}+\tilde{\bar{U}}^{eff}_{q_t}(x_n,\bar{X}_n(t),t)\right]\tilde{\bar{\psi}}_{q_t}(x_n,\bar{X}_n(t),t) \quad (4.14)$$

That is, the first conditional process is over the environment degrees of freedom and the second conditional process is over the rest of electrons on the (open) system.

The above ideas have lead to the development of an electron transport simulator based on the use of Bohmian conditional states. The resulting computational tool is called BITLLES [78–84, 107–109]. The ideas discussed in the chapter are elaborated in the published work which is attached in Publication B.

Chapter 5

GC-TDSE methodology for geometric correlations

In this chapter I discuss important aspects of the paper attached in Publication C, where I derive and discuss a method that is named "geometrically correlated 1D time dependent Schrödinger equation solver" (GC-TDSE). The GC-TDSE allows solving the 3D TDSE in terms of an ensemble of one-dimensional (1D) TDSEs. The technique is inspired by the so-called Born–Huang ansatz [110], which is a fundamental tool in the context of ab-initio molecular dynamics that allows separating fast and slow degrees of freedom in an effective way [111].

5.1 Motivation behind the method development

As an example of the practical utility of the SSE, a Monte Carlo simulation scheme to describe quantum electron transport in open systems that is valid both for Markovian or non-Markovian regimes guaranteeing a dynamical map that preserves complete positivity was proposed in Chapter 4. The resulting algorithm for quantum transport simulations reformulates the traditional "curse

of dimensionality" that plagues all state-of-the-art techniques for solving the time-dependent Schrödinger equation (TDSE). Specifically, the algorithm consists of the solution of an ensemble of single-particle SSEs that are coupled, one to each other, through effective Coulombic potentials [105, 112, 113]. Furthermore, the simulation technique accounts for dissipation [114] and guarantees charge and current conservation through the use of self-consistent time-dependent boundary conditions [84, 115, 116] that partially incorporate exchange correlation [83, 84]. However, even if we are able to treat each electron individually and still keep the correlations, through the conditional wave function, each electron still has to be defined in the three dimensional physical space. Solving a large number of three-dimensional (3D) single-particle TDSEs, may still be a very time-consuming task. Therefore, the above technique would greatly benefit from the possibility of further reducing the dimensionality of the associated numerical problem.

5.2 Methodology

Here, I consider an ansatz to separate transport and confinement directions. As it will be shown, the resulting technique allows to describe arbitrary geometric correlations in terms of a coupled set of 1D TDSEs. Therefore, while I have motivated the development of this method in the context of the simulation of (non-Markovian) quantum transport in open systems, the method presented here could be of great utility in many research fields where the reduction of the computational cost associated with the solution of an ensemble of SSEs may be advantageous. This includes, for example, the description of spin thermal transport [117, 118], thermal relaxation dynamics [85, 119], ionic motion [120, 121], or Bose–Einstein condensates [122–124] in terms of SSEs.

I start the discussion by considering a 3D-TDSE in position representation,

$$i\frac{\partial}{\partial t}\Psi(x,y,z,t) = H(x,y,z)\Psi(x,y,z,t), \tag{5.1}$$

where I have used atomic units, x, y, and z represent the three spatial coordinates, and $\Psi(x,y,z,t)$ is a well normalized wavefunction, i.e., $\iiint dx\ dy\ dz\ |\Psi(x,y,z,t)|^2 = 1\ \forall t$. In Eq. 5.1, $H(x,y,z)$ is the full Hamiltonian of the system:

$$H(x,y,z) \;=\; T_x + T_y + T_z + V(x) + W(x,y,z), \tag{5.2}$$

where $T_x = -\frac{1}{2}\frac{\partial^2}{\partial x^2}$, $T_y = -\frac{1}{2}\frac{\partial^2}{\partial y^2}$ and $T_z = -\frac{1}{2}\frac{\partial^2}{\partial z^2}$ are the kinetic energies associated with the degrees of freedom, x y and z respectively, while $V(x)$ is the potential associated to the x degree of freedom. The scalar potential $W(x,y,z)$ includes any other scalar potential that is not purely longitudinal, which is responsible for making the solution of Eq. 5.1 non-separable.

I can rewrite the Hamiltonian in Eq. 5.2 in terms of longitudinal and transverse components as:

$$H(x,y,z) = T_x + V(x) + H_x^{\perp}(y,z), \tag{5.3}$$

where $H_x^{\perp}(y,z)$ is the transverse Hamiltonian defined as:

$$H_x^{\perp}(y,z) = T_y + T_z + W(x,y,z). \tag{5.4}$$

The transverse Hamiltonian follows the eigenvalue equation as follows:

$$H_x^{\perp}(y,z)\phi_x^k(y,z) = \mathcal{E}_x^k\phi_x^k(y,z), \tag{5.5}$$

where $\mathcal{E}_x^k$ and $\phi_x^k(y,z)$ are the corresponding eigenvalues and eigenstates respec-

tively, and $k \in \mathbb{Z}$. Since the eigenstates $\phi_x^k(y,z)$ form a complete orthonormal basis in which to expand the Hilbert space spanned by the variables x, y, and z the 3D wavefunction in Eq. 5.1 can be expressed in terms of transverse eigenstates $\phi_x^k(y,z)$ as:

$$\Psi(x,y,z,t) = \sum_{k=1}^{\infty} \chi^k(x,t)\phi_x^k(y,z), \tag{5.6}$$

where $\chi^k(x,t) = \iint dydz\phi_x^k(y,z)\Psi(x,y,z,t)$ are complex longitudinal coefficients associated with the transverse eigenstate $\phi_x^k(y,z)$.

The wavefunction expansion in Eq. 5.6 can be introduced into Eq. 5.1 to obtain an equation of motion for the coefficients $\chi^k(x,t)$:

$$i\frac{\partial}{\partial t}\chi^k(x,t) = \left(T_x + \mathcal{E}_x^k + V(x)\right)\chi^k(x,t) - \sum_{l=1}^{\infty}\left(S^{kl}(x) + F^{kl}(x)\frac{\partial}{\partial x}\right)\chi^l(x,t), \tag{5.7}$$

where $\mathcal{E}_x^k$ are effective potential energies (that correspond to the eigenvalues in Eq. 5.5) and $F^{kl}(x)$ and $S^{kl}(x)$ are geometric (first and second order) coupling terms, which read:

$$F^{kl}(x) = \iint dydz\phi_x^{*l}(y,z)\frac{\partial}{\partial x}\phi_x^k(y,z), \tag{5.8a}$$

$$S^{kl}(x) = \frac{1}{2}\iint dydz\phi_x^{*l}(y,z)\frac{\partial^2}{\partial x^2}\phi_x^k(y,z). \tag{5.8b}$$

Let me emphasize that it is the main goal of the set of coupled equations in Eq. 5.7 to allow the evaluation of relevant observables in terms of 1D wavefunctions only. In this respect, let us take, for example, the case of the reduced probability density $\rho(x,t) = \iint dydz\Psi^*(x,y,z,t)\Psi(x,y,z,t)$. Using the basis expansion in

Equation (5.6), $\rho(x,t)$ can be written as:

$$\rho(x,t) = \sum_{k,l}^{\infty} \chi^{*l}(x,t)\chi^{k}(x,t) \iint dydz\phi_x^{*l}(y,z)\phi_x^{k}(y,z), \tag{5.9}$$

and using the normalization condition

$$\iint dydz\phi_x^{l}(y,z)\phi_x^{k}(y,z) = \delta_{lk}, \quad \forall x, \tag{5.10}$$

the above expression reduces to:

$$\rho(x,t) = \sum_{k=1}^{\infty} |\chi^{k}(x,t)|^2. \tag{5.11}$$

Therefore, according to Eq. 5.11, the reduced (longitudinal) density is simply the sum of the absolute squared value of the longitudinal coefficients $\chi^k(x,t)$. A numerical example to this methodology applied to a prototypical nanoconstriction can be found in published paper attached in Publication C

Part IV

APPLICATION TO DEVICE SIMULATION

Chapter 6

Tunneling time in Graphene devices operated at high-frequencies

In Chapter 3 I discussed how intrinsic properties allows us to provide an unambiguous definition of quantities involving multi time measurements for instance, tunnelling time which is explicitly discussed in Appendix H.2. These intrinsic properties are implicitly included in the simulator BITLLES to provide, for example, the information about the cut-off frequency of electron devices, which is a very important figure of merit to determine their speed. The following section provides a summary of the work included in Publication D

6.1 Motivation of the work

The trajectory-based Bohmian approach provides a very natural framework to quantify Klein tunneling times [125, 126] in linear band graphene devices (as shown in Figure 6.1). This is because Bohmian theory can provide the information

about the position of electrons even when they are not measured. Therefore, through the use of the intrinsic property of the position of the electron as a function of time, it is unproblematic to compute tunneling times. On the contrary, the Orthodox theory has a lot of problems to define the tunneling time because, in order to do that it has to look for an intrinsic property that is forbidden in its own ontological framework.

A careful analysis in the Bohmian framework allows to distinguish, not only between transmitted (N_T) and reflected electrons ($N_R{}^*$), but also allows to distinguish reflected electrons that spend a certain amount of time in the barrier (N_R). Without such a distinction, typical expressions found in the literature to compute dwell times derived from Orthodox ontology can give unphysical results when applied to predict cut-off frequencies. I explain this claim by the following arguments.

The typical expression for the Orthodox dwell time to quantify how much time a particle spends in a 2D spatial region limited by the boundaries $a < x < b$ and $-\infty < z < \infty$ is traditionally given by,

$$\tau_D = \int_0^\infty dt \int_a^b dx \int_{-\infty}^\infty dz |\psi(x, z, t)|^2 \tag{6.1}$$

The dwell time in Eq. 6.1 can be evaluated equivalently with Bohmian trajectories following the same procedure as detailed in Appendix H.2 to give the following expression:

$$\tau_D = \lim_{N\to\infty} \frac{1}{N} \sum_{i=1}^{N} \tau^i \tag{6.2}$$

With the definitions of the trajectories discussed above, the total number of trajectories can be given in their terms as $N = N_T + N_R + N_{R^*}$. Then, the dwell

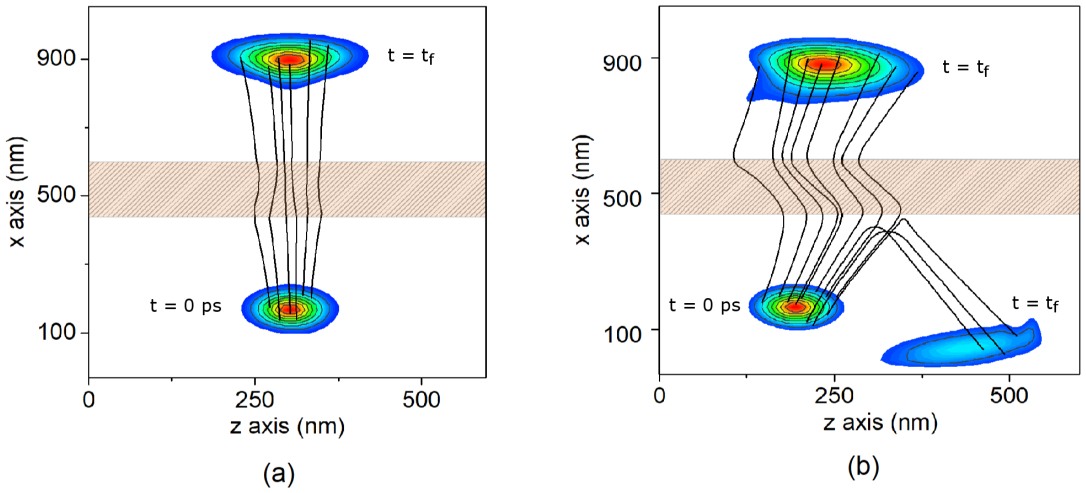

Figure 6.1: (a) Conditional wavefunction of the electron that impinges perpendicularly to a barrier in graphene (in the shaded orange region), along with the set of the associated Bohmian trajectories are plotted in the initial and final times computed from the BITLLES simulator. As it can be seen, from both the wave packet and the set of trajectories, the electron exhibits Klein tunneling and all trajectories traverse the barrier. (b) The same plot for an electron that impinge to the barrier at some angle. Now, there is no complete Klein tunneling and part of the wave packet and some trajectories are reflected. The transmitted part of the wave packet and transmitted trajectories suffered refraction according to Snell's law-like expression..

time τ_D in Eq. 6.2 can be rewritten as:

$$\tau_D = \lim_{N\to\infty} \frac{1}{N} \left(\sum_{l=1}^{N_T} \tau^l + \sum_{m=1}^{N_R} \tau^m \right), \tag{6.3}$$

since the trajectories N_{R^*} do not contribute to the dwell time. From the above equation I can define the transmission time, τ_T and the reflection time, τ_R as follows:

$$\tau_T = \frac{1}{N_T} \sum_{l=1}^{N_T} \tau^l \quad \text{and} \quad \tau_R = \frac{1}{N_R} \sum_{m=1}^{N_R} \tau^m \tag{6.4}$$

So the overall expression of the dwell time can be written as follows,

$$\tau_D = P_T \, \tau_T + P_R \, \tau_R \tag{6.5}$$

where I have defined the probabilities:

$$T \equiv P_T = \lim_{N\to\infty} \frac{N_T}{N} \tag{6.6}$$

The computation of the transmission coefficient T does not require a distinction between N_R and N_{R^*} trajectories since only the transmitted trajectories N_T are relevant here. Identically,

$$P_R = \lim_{N\to\infty} \frac{N_R}{N} \tag{6.7}$$

Notice that the reflected probability P_R is different from the reflection coefficient R, $P_R \neq R$, because the reflection coefficient requires including N_R and N_{R^*} in the numerator of Eq. 6.7.

Furthermore, because of these trajectories the previous probability definitions give $P_T + P_R \leq 1$ for which we would require to add the additional probability $P_{R^*} = N_{R^*}/N$ to satisfy $P_T + P_R + P_{R^*} = 1$. However, we know that the R^* trajectories have a transit time equal to zero, $\tau_i = 0$, then, the transit (tunneling)

time definition in expression Eq. 6.2 can be extremely misleading. If one get a scenario where $N_{R^*} \approx N$ then we get the unphysical result $\tau_D \approx 0$ in Eq. 6.3, that implies a cut-off frequency ($f_T = \frac{1}{\tau_D}$) is going to be infinite which is an unphysical result.

The mistake appears because we have to eliminate the trajectories N_{R^*} from the computations of the dwell times when such times have to be related to predict the high-frequency behavior of electron devices as discussed in chapter 1. The fundamental problem is that the identification of the particles N_T, N_R and N_{R^*} is not possible within the Orthodox theory. This is just a different way of realizing the controversy in defining the tunneling time in Orthodox quantum mechanics. On the contrary, the Bohmian theory provides a transparent procedure to eliminate N_{R^*} from the computations. Thus, the Bohmian dwell time (for deducing properly high-frequency performances) needs to be defined as:

$$\tau_{D_B} = \lim_{N_B \to \infty} \frac{1}{N_B} \left(\sum_{l=1}^{N_T} \tau^l + \sum_{m=1}^{N_R} \tau^m \right) \tag{6.8}$$

where $N_B = N_T + N_R$ are the number of trajectories entering into the barrier. Notice that now the scenario $N_{R^*} \approx N$ does not imply the unphysical result $\tau_{D_B} \approx 0$ in Eq. 6.8 because the particles N_{R^*} have no role.

6.2 Numerical calculation of tunnelling times

This discussion above related to the correction in the Orthodox dwell time is used in the numerical calculation of the dwell time in a Graphene based electron device. I consider a two terminal device whose band structure (energy of the Dirac point as a function of the x position) is plotted in Figure 6.2. The wave nature of the electrons is represented by a bispinor solution of the Dirac equation. In Figure

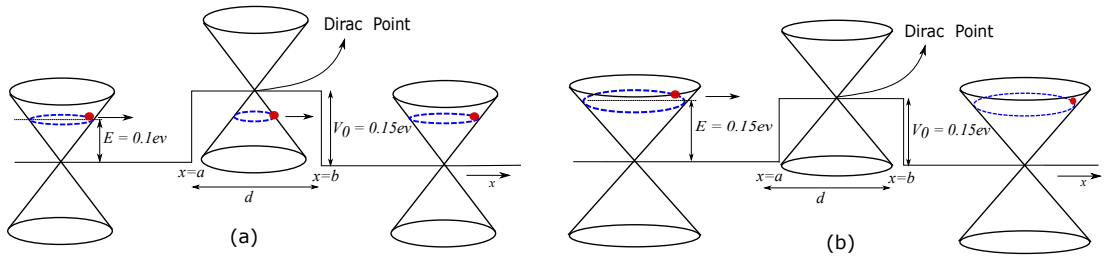

Figure 6.2: (a) Klein tunneling barrier region where the electron, which impinges perpendicularly to the barrier, has an energy E lower than the barrier height V_0. The cones represents the linear energy momentum dispersion at different positions. The electron has available states in the valence band of the barrier region which allows them to tunnel freely. The transmission coefficient in such cases is close to unity. (b) The same plot for an electron with energy similar to the barrier height $E = V_0$. In this case the electron has to occupy the Dirac point in the barrier region which has almost no available energy states. In these scenarios the transmission probability almost vanishes.

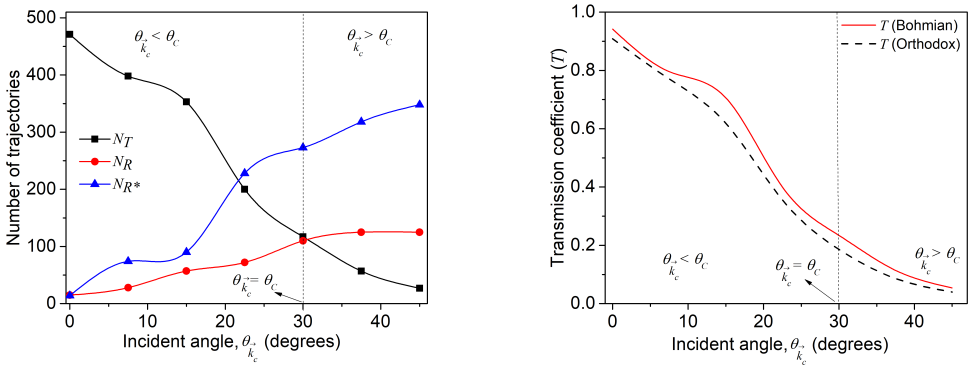

Figure 6.3: (a) Number of transmitted particles, N_T, particles entering into the barrier but eventually reflected, N_R and particles that are reflected before entering the barrier $N_R{}^*$ as a function of the incident angle. (b) Transmission coefficient as a function of the incident angle computed from the Orthodox quantum mechanics (dashed black line) and from Bohmian trajectories (solid red line)

6.3(a) I show how the number of transmitted trajectories vary with the angle of incidence ($\theta_{\vec{k}_c}$). The simulations show that for $\theta_{\vec{k}_c} = 0$, almost all the particles are transmitted. Increasing $\theta_{\vec{k}_c}$ leads to an increase in the reflected particles. By construction, the behavior of N_T in Figure 6.3(a) just reproduces the transmission coefficient T in Figure 6.3(b). The estimation of the current delay in an electron device takes into account only the particles entering in the barrier, either N_T or N_R. Thus for an unequivocal description of the tunnelling times it is very important to classify and discard the contribution by the trajectories ${N_R}^*$ which do not contribute to the electrical current and thus, to the tunnelling times. In the Orthodox computation, just with the bispinor (without trajectories), N_T, N_R and ${N_R}^*$ cannot be treated separately, and thus the above mentioned ambiguity appears.

In summary, the (Klein) tunneling times for electrons in a two-terminal graphene device made of a potential barrier between two metallic contacts has been studied. I show that for a zero incident angle (and positive or negative kinetic energy), the transmission coefficient is equal to one, and the dwell time is roughly equal to the barrier distance divided by the Fermi velocity. For electrons incident with a non-zero angle smaller than the critical angle, the transmission coefficient decreases and dwell time can still be easily predicted in the Bohmian framework. The main conclusion of this work is that, contrary to tunneling devices with parabolic bands, the very high mobility of graphene is roughly independent of the presence of Klein tunneling phenomena in the active device region.

Chapter 7

Evading measurement uncertainty in electron devices

The following chapter provides a summary of the published work included in Publication E. In this work a protocol has been proposed to alleviate the quantum uncertainty that arises due to a stochastic (collapse or state-reduction) law that unavoidably yields an uncertainty (variance) associated with the corresponding mean values.

7.1 Origin of Quantum measurement uncertainty in electronic devices

The process of measurement in a quantum system involves an uncertainty which is a consequence of the fact that each time a quantum measurement is done, the wave function collapses into an eigenstate of the operator $\hat{I}$ associated with the measuring apparatus. The observable output I_{out} is a random value equal to the eigenvalue associated with the mentioned eigenstate. In general, and this is true for the measurement of the electrical current, the state before measure-

ment $\psi_{out}(\vec{r},t)$ is not an eigenstate of the current $\psi_I(\vec{r},t) \neq \psi_{out}(\vec{r},t)$. In fact, the state before the measurement can be written as a superposition of many different current eigenstates. Thus, each time we repeat an experiment to obtain information about the output current, we get different values. This randomness in the output values can be quantified through the probability distribution $P(I) = |\langle\psi_I(\vec{r})|\psi_{out}(\vec{r},t)\rangle|^2$ given by Born's law. From a quantum engineering point of view, this quantum uncertainty (seen as noise in the current) is inconvenient for efficiently processing logical (either classical or quantum) information. Notice that here classical and quantum information is manipulated both by quantum electron devices. The difference appears if the information is a bit or a q-bit, but state-of-the art electronic devices are nowadays quantum electron devices as mentioned in the introductory chapter.

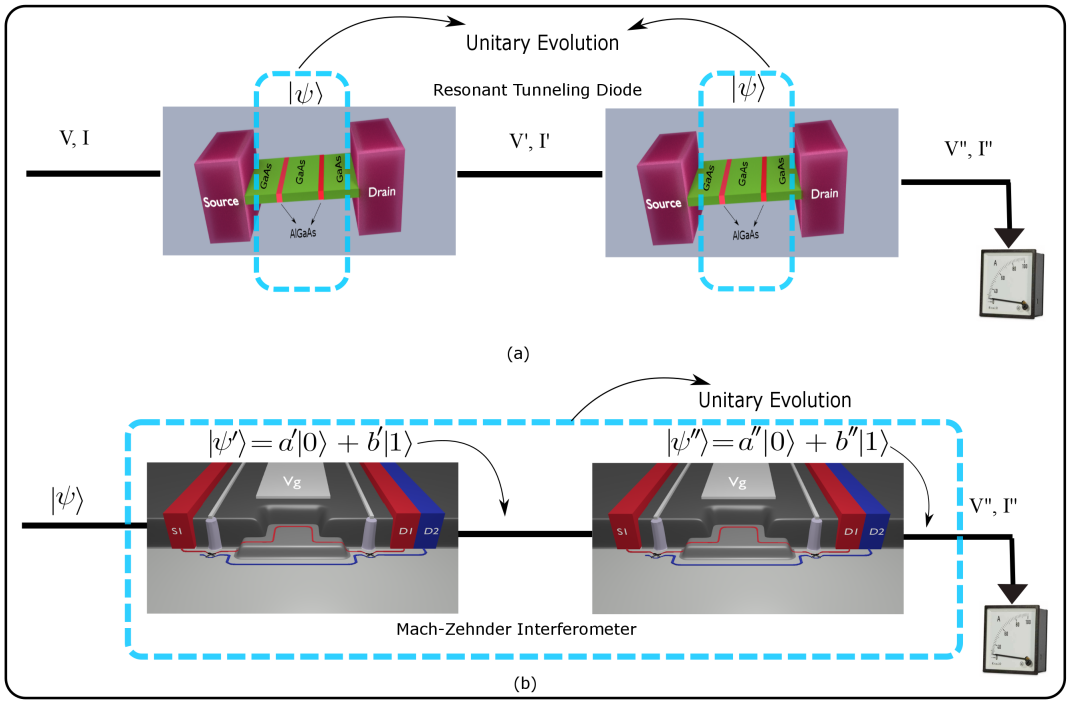

Figure 7.1: (a) Schematic of classical computing exemplified with RTD where only the active device is governed by unitary quantum evolutions (enclosed in the cyan color dashed line), while the contacts and the cable leads to quantum decoherence which provides a fixed value of the current obtained in the measuring apparatus (shown at the right end). (b) Schematic of quantum computing exemplified with an MZI where the quantum wholeness require that a coherent unitary evolution appears in all the gates (enclosed in the cyan color dashed line). Only at the end, when the wave function is measured, decoherence can be accepted.

In classical computations, the uncertainty on the electrical current can be eliminated by using the ensemble value of the current $\langle I \rangle$ computed from a large number of identical experiments, each one giving I^i, with the subindex i identifying the experiment. The ensemble value is defined as $\langle I \rangle = (\sum_{i=1}^{N_{exp}} I^i)/N_{exp}$, where $N_{exp} \to \infty$ is the number of experiments. In principle, this ensemble value would require repeating the same experiment for a large set of N_{exp} identical quantum electron devices. In practice, by invoking ergodic arguments, the repetition of the experiment is substituted by measuring at different times in the same quantum electron device as shown schematically in Figure 7.2 (represented by a

horizontal red arrow). Thus, instead of defining the signal of the output logical value as the instantaneous current I^1 (which has noise) one defines it as the DC value of the electrical current $\langle I \rangle$ computed during a large time interval (which has no noise). This solution is efficient for reducing the noise, but it requires a large measuring time. (In our simulation example with an RTD with a device active region length of 10 nm, the injection time of 0.05 ps and the velocity of electrons as 10^4 m/s, the time after which we get the non-fluctuating value of the current is around 50 ps. In any case, the measuring time is again a parameter that depends on many factors, like injection time, velocity of electrons, electron density, level of tolerable uncertainty. etc., and that can be enlarged or reduced as desired by manipulating these parameters.)

The quantum uncertainty described above represents also a problem for quantum computing. In fact, although the logical output information in quantum computing is encoded in the final wave function $\psi_{out}(\vec{r}, t)$ (not in an observable I^i), the quantum state $\psi_{out}(\vec{r}, t)$ is not itself an observable (i.e., it cannot be measured in a single shot measurement). Thus, the quantum state of the system needs to be deduced from the expectation value $\langle I \rangle$ constituting an infinite set of experiments, ideally as schematically shown in Figure 7.2 (represented by vertical red arrow). Carrying out these number of ensemble experiments consumes a lot of resources and time. For example an ion trap experiment [127] characterizing an 8 qubit state required 10 hours of measurements, despite collecting only 100 samples per observable and approximately a week for the postprocessing.

Therefore, the measurement process of such observable $\langle I \rangle$ has the same inconveniences mentioned above for classical computing, due to the quantum uncertainty. We notice that in a quantum computing algorithm, with many interconnected quantum gates, the measurement of the observable is done only at the last gate. In fact, trying to measure at an intermediate gate would be understood

as a type of decoherent phenomena that would dramatically perturb the unitary evolution required in typical quantum algorithms. In Figure 7.1 I encircle the regions of the connected gates where the dynamics of electrons are supposed to be governed by unitary quantum evolutions. From Figure 7.1, one can understand why decoherence is a serious problem for quantum computing, but not for classical computing. In an array of interconnected classical computing devices, the decoherence that can appear at the output of each particular device due to the measurement does not affect the performance of the algorithm because the interconnection between devices is done in terms of observables (not in terms of wave functions).

7.2 Collective-like measurement of current in electron devices

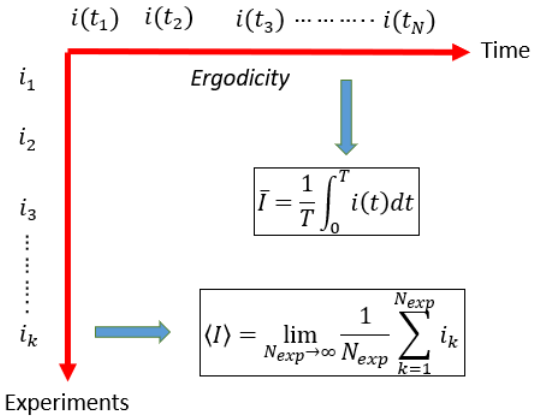

Figure 7.2: Figure depicting a scheme to represent the different aspects of obtaining a mean value in the classical and quantum computing devices. Whereas in the classical computing device the mean value is usually the time averaged value. The same in a quantum computing device is the ensemble value over an infinte number of experiments.

Certainly, the above problem could be alleviated if we were able to measure the ensemble value of the current or voltage in a single experiment. For that we foresaw a general strategy that is summarized bellow. Let us first discuss this strategy in the context of a classical computing device. This can be divided into two steps:

1. Modify the quantum device to accommodate a large number N of electrons defined by a many-particle wave function $\Psi_T(t_{in})$ at time t_{in} is:

$$|\Psi_T(t_{in})\rangle = |\psi^1(t_{in})\rangle \otimes |\psi^2(t_{in})\rangle \otimes .... \otimes |\psi^N(t_{in})\rangle, \tag{7.1}$$

   where the wave function $|\psi^i(t_{in})\rangle$ is the single-electron wavefunction corresponding to the i-th electron prepared under the same conditions that we have used to prepare the wave function $|\psi^1(t_{in})\rangle$ in the original quantum electron device.

2. We substitute the measuring apparatus described by the single-particle operator $\hat{I}^1$ with a new measuring apparatus whose associated many-body operator $\hat{I}_T$ is:

$$\hat{I}_T = \frac{\hat{I}^1 + \hat{I}^2 + ... + \hat{I}^N}{N}, \tag{7.2}$$

   where $\hat{I}^i = \hat{\mathbb{I}} \otimes .... \otimes \hat{I}^i \otimes ... \otimes \hat{\mathbb{I}}$ acts only on the quantum state $|\psi^i(t_{in})\rangle$ and $\hat{\mathbb{I}}$ is the identity operator in the small Hilbert space of each degree of freedom. Notice the presence of the factor $N \to \infty$ in the denominator of the operator $\hat{I}_T$.

How the above two steps can be accommodated using the present semiconductor technology has been discussed and numerically studied for a resonant tunneling diode and a Mach-Zehnder interferometer, for classical and quantum computations, respectively has been discussed in detail in Publication E. It is also

shown that the resulting protocol formally resembles the so-called collective measurements, although, its practical implementation is substantially different.

Part V

CONCLUSIONS

Conclusions derived from PART I : The need for smaller and faster solid state devices is pushing the technological and theoretical limits of device modelling community understanding. This has brought, in particular, the theoretical discussions which was once limited to classical (semi-classical) arguments to full quantum mechanical description. The classical mechanics has been a well established theory since centuries and therefore to develop devices based on classical mechanics one just need an accurate engineering perspective.

The regime where the present and future solid state devices are envisioned, classical mechanics fail to provide a proper description to the observed phenomena. These devices have to be explained from the principles of quantum mechanics which in the most general cases is the Orthodox theory. But the arguments that was used for the classical mechanics where the physicist provides the theoretical framework to the engineer, does not work since, Orthodox theory has difficulties to describe all the phenomena with the same comprehensibility as classical mechanics for classical electron devices. The primary reason for this is attributed to the necessity of defining the measurement dependent properties of a quantum system within the framework of the popular Orthodox theory as discussed in chapter 1 which leads to conceptual and practical difficulties. Therefore, presently a device engineer is forced to either "shut up and calculate" or to enter into the discussions related to the foundations of quantum mechanics (Orthodox theory).

Conclusions derived from PART II: Since Orthodox theory poses serious challenges in providing an accurate description of the present and future electronic devices it is important to understand the issues and an attempt has to be made to provide the solution. Therefore in chapter 2 (specially in section 2.1 and section 2.2) an attempt is made to first understand why is it not possible to obtain intrinsic properties (such as the position of electron inside an electron device)

in Orthodox theory. This already forces the author to enter into the discussions pertaining to the foundations of quantum mechanics. It can be thus realized that the very ontology of Orthodox theory prohibits in giving a definite value to any property of a system that is not measured. This difficulty in getting *apparatus-independent* or *intrinsic* information about the dynamics of quantum systems is actually rooted in the foundations of Orthodox theory as discussed in section 2.3. More specifically, the so-called "eigenvalue-eigenstate link" establishes that quantum states cannot be associated to a well defined value of a given property unless such property is explicitly measured, the only exception being when the state itself is an eigensate of the measured property.

Importantly, it is well known that the association of the reality (meaning that properties have well defined property even when they are not observed) with measurement is a "deliberate theoretical choice" that is "not forced on us by experimental facts" [23]. In this respect, there are other quantum theories, in empirical agreement with the Orthodox theory, where the reality of the properties of quantum objects is independent of the measurement [23]. These other theories allow, in particular, to define properties of quantum systems even when they are not measured (i.e., just as in classical mechanics). It is thus not surprising that there is a renewed interest in defining intrinsic properties within the so-called "quantum theories without observers"

In this respect the modal interpretation of quantum mechanics, which defines the properties of quantum systems without invoking the measuring apparatus are proven to be appropriate to describe the intrinsic properties of a quantum system as discussed in section 3.1 . A special case of this type of theories is, Bohmian mechanics, which is introduced in section 3.2. This theory is a mathematically precise quantum theory of particles that grounds the formalism and the predictions of Orthodox quantum mechanics. Bohmian mechanics introduces

the well defined position of particles in a quantum system at an ontological level independently of its measurement. That is, at every moment of time there exists not only a wavefunction but also a well-defined particle configuration. In particular, it is then straightforward to define a property of the system in terms of Bohmian trajectories [19, 21, 26]. Intrinsic properties in Bohmian mechanics are thus defined as the properties of the system when it does not interact with a measuring apparatus. That is, since the trajectories of the particles are defined at the ontological level, viz., irrespective of whether they are measured or not, defining the intrinsic dynamics of any property does not involve any ontological inconvenience.

Even though the intrinsic properties can be described without the need of a measuring apparatus it has been shown in section 3.1 that these unperturbed properties can be obtained in the laboratory through Aharonov, Albert and Vaidman (AAV) weak values. Likewise, in the framework of Bohmian mechanics as demonstrated in section 3.2, the local-in-position Bohmain intrinsic property can be obtained experimentally through the AAV weak values when the post-selected state is the position eigenstate, which is also referred to as local-in-position weak values [50]. Importantly, and contrarily to weak or indirect measurements of time-correlation functions (which was discussed in section 2.2.2), local-in-position weak values are free from quantum backaction effects. As a result, the intrinsic dynamics of quantum systems can be genuinely formulated in terms of unperturbed properties and experimentally assessed through weak values. This is a relevant statement, as the scientific community is persistently looking for dynamical properties whose expectation value is free from the contamination of measuring apparatuses [128]. Hence the intrinsic properties serves to be very useful in alleviating the conceptual and practical difficulties in defining the quantities that involves multi-time measurement.

In section 3.3 a very important discussion is provided pertaining to the interpretation of the AAV weak values. The conclusion that is drawn is that these intrinsic properties cannot be defined within the eigenvalue-eigenstate link of Orthodox quantum mechanics (unless the system is in an eigenstate of the associated property operator). Contrarily, intrinsic properties arise naturally in the context of modal quantum theories (e.g., Bohmian mechanics). It has been shown that intrinsic properties and AAV's weak values are the same precise thing (see Eq. 3.5 and Eq. 3.11). Thus, any attempt to give a physical meaning to AAV's weak values by means of a given ontology is, at the same time, an attempt to give physical meaning to the intrinsic properties described in thesis (and vice versa). In this respect, it has been shown that intrinsic properties and AAV's weak values have a clear-cut meaning within the ontology of modal quantum mechanics.

A simple byproduct of this result is that intrinsic properties and AAV's weak values cannot have a physical interpretation within the ontology of Orthodox quantum mechanics. Another important inference that is derived from the discussions is that the AAV weak value is in principle different from the operationalist definition of a weak value. The AAV weak value is found from a single quantum system where it is assumed that there is no explicit weak measurement. This is done by neglecting the perturbation induced by the weak measurement which as we have shown in section 2.2.2 is an incorrect assumption. The operationalist definition on the other hand implies an ensemble of experiments instead of a single measurement. So, only when the ensemble procedure is able to wash out the backaction present in each weak measurement due to ensemble averaging does the numerical value of AAV weak value and the operationalist weak value coincide.

Conclusion derived from PART III: The Bohmian mechanics ontology also leads to the development of robust methodologies for describing open quan-

tum systems as discussed in chapter 4 where the quantum system is an electron device. This methodology aids in defining a conditional state which can be interpreted as the state of the open quantum system evolving while its environment is under continuous monitoring. The ontological nature of the trajectories in Bohmian mechanics introduces the possibility of evaluating dynamic properties in terms of conditional wavefunctions for Markovian and non-Markovian dynamics, no matter whether the environment is actually being measured or not. The Bohmian conditional states thus lend themselves as a rigorous theoretical tool to evaluate static and dynamic properties of open quantum systems in terms of state vectors without the need of reconstructing a reduced density matrix which escalates the computational burden very quickly with the number of degrees of freedom.

The above technique would greatly benefit from the possibility of further reducing the dimensionality of a single particle 3D-TDSE by decoupling the transverse and the longitudinal components of the 3D wavefunction. In chapter 5 an efficient simulation scheme is provided inspired from the Born-Huang ansatz (GC-TDSE methodology). This methodology is applied to a prototypical 2D nanoconstriction having perfect agreement with the exact solution of the 2D wavefunction providing an appreciable computational advantage. For smooth time-independent constriction profiles under low applied bias, the GC-TDSE method implies up to three orders of magnitude less computational resources than solving the full 3D TDSE directly. For very high applied bias or time-dependent constriction profiles, the GC-TDSE may still be significantly less expensive than the solution of the full 3D TDSE, but would require introducing approximations to the solution of the potential-energies $\mathcal{E}_x^k$, ($F^{kl}(x,t)$ and $S^{kl}(x,t)$).

Conclusions derived from PART IV: The work presented in chapter 6

describes the dwell times for electrons in a two-terminal graphene barrier using the BITLLES simulator. It has been shown that Bohmian trajectories are well suited formalism to discuss transit (tunneling) times and its relation to the cut-off frequencies of electron devices. We have shown that Klein tunneling time (in gapless graphene with linear band structure) is not like the typical tunneling time (in materials with parabolic bands and with an energy gap). Such differences directly imply completely opposite features in the transit (tunneling) times of graphene structures in comparison to what is expected from traditional semiconductor structures with parabolic bands.

Because of the Klein paradox, for an incident angle equal to zero, $\theta_{\vec{k_c}} = 0$, the transmission coefficient is roughly equal to the unity, $T = 1$, with $N_R \approx 0$ and $N_{R^*} \approx 0$. Then, the velocity of particles in the barrier region and outside is roughly equal to the Fermi velocity, $v_f = 10^6$ m/s. This is true for all incident kinetic energy (with positive or negative kinetic energy). Then, the dwell time in the barrier region can be identically computed from the Orthodox expression τ_D or the Bohmian one τ_{D_B}, roughly estimated as $\tau_D \approx \tau_{D_B} \approx d/v_f$.

But for incident angles different from zero i.e. $\theta_{\vec{k_c}} > 0$, the transmission coefficient decreases because $N_{R^*} > 0$. Under these scenarios, the dwell time of the electrons has to be estimated only for the trajectories that spend some time in the barrier (what we name N_T and N_R in the text) but not by the trajectories N_{R^*} that do not spend time in the barrier. Then, the Orthodox expression τ_D in Eq. 6.1 is not adequate and it has to be substituted by the Bohmian dwell time expression τ_{D_B}.

In chapter 7 the problem of current uncertainty due to the intrinsic stochastic process of the quantum measurement of the electrical current is discussed. From an engineering point of view, this quantum uncertainty becomes an undesired quantum noise that makes the discrimination of the final state in classical or

quantum gates more difficult. I have therefore presented a protocol that modifies the original quantum electron device to accommodate a larger number of electrons inside, so that the total electrical current of the modified device (when normalized to the number of electrons inside) gives the value of the output current without quantum uncertainty. I provide numerical examples for classical and quantum computing, with an RTD and MZI, respectively. It has been demonstrated that the many-particle wavefunction associated with the modified device is, in fact, an eigenstate of the many-particle electrical current operator. The similitude and differences of this protocol with the collective measurements is mentioned in the text. The results of this protocol can be alternatively understood as a consequence of the central limit theorem. Although the assumption of non-interacting quasi-particles can seem reasonable in nanoscale electron devices, further work is needed to check whether or not the presence of strong Coulomb and exchange correlations among electrons located inside the device can affect the present predictions. In addition, the discussion on the advantages of the protocol presented here needs to be explored for the quantum measurements of transient currents and delay time of nanoscale quantum devices for classical and quantum gates.

Part VI

APPENDICES

Appendix A

The von-Neumann measurement protocol

In this Appendix I describe the Von-Neumann measurement protocol the results of which are utilized in chapter 2. In this protocol a measurement requires an entanglement between the system and the ancilla. Such entanglement can be obtained through a unitary interaction of the ancilla with the system given by the Von Neumann time-evolution operator $\exp(\frac{-i}{\hbar}\lambda\hat{S}\otimes\hat{P}_a)$ where $\hat{S}$ is the system operator (the observable we want to measure), $\hat{P}_a$ is the momentum operator for the ancilla and λ is the effective coupling constant quantifying the coupling strength between the system and ancilla. An additional unitary entanglement between the ancilla and the pointer will be required which is given by $\exp(\frac{-i}{\hbar}\gamma\hat{Y}\otimes\hat{P}_p)$ where $\hat{Y}$ is the ancilla operator (observable that we effectively measure), $\hat{P}_p$ is the momentum operator associated to the pointer and γ is the effective coupling constant quantifying the coupling between the ancilla and the pointer . I assume the full state of the system-ancilla-pointer to be initially described by a separable

state vector:

$$|\Psi(0)\rangle = \sum_i c_i(0)|s_i\rangle \otimes \int a(y,0)|y\rangle dy \otimes \int f(z,0)|z\rangle dz, \tag{A.1}$$

where the system state vector $|\psi(0)\rangle = \sum_i c_i(0)|s_i\rangle$ has been defined using the eigenstates $|s_i\rangle$ of the operator $\hat{S}$ of interest, with $\hat{S}|s_i\rangle = s_i|s_i\rangle$. Without the loss of generality, I chose here a discrete and nondegenerate spectrum $\{s_1, s_2, s_3....\}$ of the operator $\hat{S}$. The (ancilla) state vector $|\phi_W(0)\rangle = \int a(y,0)|y\rangle dy$ interacts with the system and also with the (pointer) state vector $|\phi_P(0)\rangle = \int f(z,0)|z\rangle dz$. Noticing that the ancilla and the pointer wave functions are represented in the position representation, the process of the pre-measurement described in the text can be mathematically described as follows,

$$|\Psi(t_1)\rangle = \exp\left(\frac{-i}{\hbar}\gamma \hat{Y} \otimes \hat{P}_p\right) \cdot \exp\left(\frac{-i}{\hbar}\lambda \hat{S} \otimes \hat{P}_a\right) |\Psi(0)\rangle. \tag{A.2}$$

when applying the first operator $\exp(\frac{-i}{\hbar}\lambda \hat{S} \otimes \hat{P}_a)$ on the initial state $|\Psi(0)\rangle$ given by Eq. A.1, we get:

$$|\Psi(t_1)\rangle \;=\; \exp\left(\frac{-i}{\hbar}\gamma \hat{Y} \otimes \hat{P}_p\right) \sum_i c_i|s_i\rangle \otimes \int a(y-\lambda s_i)|y\rangle dy \otimes \int f(z,0)|z\rangle dz, \tag{A.3}$$

where I have used,

$$\begin{aligned}
&\exp\left(\frac{-i}{\hbar}\lambda\hat{S}\otimes\hat{P}_a\right)\sum_i c_i|s_i\rangle\otimes\int a(y,0)|y\rangle dy \\
&=\sum_i c_i|s_i\rangle\otimes\int\int|y'\rangle\langle y'|\exp(-\lambda s_i\hat{P}_a)|y\rangle a(y,0)dy\;dy' \\
&=\sum_i c_i|s_i\rangle\otimes\int\exp\left(-\lambda s_i\frac{\partial}{\partial y}\right)a(y,0)|y\rangle dy \\
&=\sum_i c_i|s_i\rangle\otimes\int\left(1-\lambda s_i\frac{\partial}{\partial y}+\lambda^2 s_i^2\frac{\partial^2}{\partial y^2}-...\right)a(y,0)|y\rangle dy \\
&=\sum_i c_i|s_i\rangle\otimes\int a(y-\lambda s_i)|y\rangle dy. \qquad (A.4)
\end{aligned}$$

The second operator $\exp(\frac{-i}{\hbar}\gamma\hat{Y}\otimes\hat{P}_p)$ on the state given by Eq. A.3 can be finally written as:

$$\begin{aligned}
|\Psi(t_1)\rangle &= \exp\left(\frac{-i}{\hbar}\gamma\hat{Y}\otimes\hat{P}_p\right)\sum_i c_i|s_i\rangle\otimes\int a(y-\lambda s_i)|y\rangle dy\otimes\int f(z,0)|z\rangle dz \\
&= \sum_i c_i|s_i\rangle\otimes\int a(y-\lambda s_i)|y\rangle dy\otimes\int f(z-\gamma y)|z\rangle dz, \qquad (A.5)
\end{aligned}$$

where, as done in the previous step, I have used

$$\begin{aligned}
&\exp\left(\frac{-i}{\hbar}\gamma\hat{Y}\otimes\hat{P}_p\right)\int a(y-\lambda s_i)|y\rangle dy\otimes\int f(z,0)|z\rangle dz \\
&=\int a(y-\lambda s_i)|y\rangle dy\otimes\int\exp\left(-\gamma y\frac{\partial}{\partial z}\right)f(z,0)|z\rangle dz \\
&=\int a(y-\lambda s_i)|y\rangle dy\otimes\int\left(1-\gamma y\frac{\partial}{\partial z}+\gamma^2y^2\frac{\partial^2}{\partial z^2}-...\right)f(z,0)|z\rangle dz \qquad (A.6)
\end{aligned}$$

Since, the ancilla and pointer is supposed to have a strong coupling the coupling constant $\gamma = 1$. Therefore

$$\exp\left(\frac{-i}{\hbar}\hat{Y}\otimes\hat{P}_p\right)\int a(y-\lambda s_i)|y\rangle dy\otimes\int f(z,0)|z\rangle dz = \int a(y-\lambda s_i)|y\rangle dy\otimes\int f(z-y)|z\rangle dz. \tag{A.7}$$

That is what is used to arrive at Eq. 2.2.

Appendix B

Two-time correlation functions for an ideally-weak measurement

This Appendix provides a derivation to arrive to the result in Eq. 2.12 in the thesis. For scenarios where the ancilla wave packet has a support much more larger than support of the system wave packet, $y \gg \lambda s$, one can consider a first order Taylor's expansion of the ancilla wavefunction $a(y_k - \lambda s)$ around y giving,

$$a(y_k - \lambda s) \approx a(y_k) - \lambda \frac{\partial a(y_k)}{\partial y_k} s. \tag{B.1}$$

The evaluation of the main result in Eq. 2.11 for the ideal weak measurements used here, requires the evaluation of the integral $\int dy_k \; y_k a(y_k - \lambda s_i) a(y_k - \lambda s_{i'})^*$,

which can be evaluated when Eq. B.1 is considered as:

$$\begin{aligned}
\int dy_k \quad y_k \quad & a(y_k - \lambda s_i)a^*(y_k - \lambda s_{i'}) \\
&= \int dy_k\, y_k \left(a(y_k) - \lambda \frac{\partial a(y_k)}{\partial y_k} s_i\right)\left(a^*(y_k) - \lambda \frac{\partial a^*(y_k)}{\partial y_k} s_{i'}\right) \\
&= \int dy_k\, y_k a(y_k)a^*(y_k) - \lambda s_i \int_{-\infty}^{\infty} dy_k y_k a^*(y_k)\frac{\partial a(y_k)}{\partial y_k} \\
&- \lambda s_{i'} \int dy_k y_k a(y_k)\frac{\partial a^*(y_k)}{\partial y_k} + \lambda^2 s_i\, s_{i'} \int dy_k y_k \frac{\partial a^*(y_k)}{\partial y_k}\frac{\partial a(y_k)}{\partial y_k} \\
&= \lambda \frac{1}{2}(s_i + s_{i'}). \qquad \text{(B.2)}
\end{aligned}$$

In the evaluation of Eq. B.2 I have considered that ancilla wavefunction is real (not complex), $a(y_k - \lambda s_i) = a^*(y_k - \lambda s_i)$. I have also used the identity:

$$\int dy\; y\; a(y)\frac{\partial a(y)}{\partial y} = -1/2, \qquad \text{(B.3)}$$

because when integrating by parts, we get: $\int dy\; y\; a(y)\frac{\partial a(y)}{\partial y} = -\int dy a(y)a(y) - \int dy\; y\; \frac{\partial a(y)}{\partial y}a(y)$. Identically, in the evaluation of Eq. B.2, I have used:

$$\int dy\; y\; \frac{\partial a(y)}{\partial y}\frac{\partial a(y)}{\partial y} = 0, \text{ and } \int dy\; y\; a(y)a(y) = 0. \qquad \text{(B.4)}$$

Finally, putting Eq. B.2 into the integral Eq. 2.11, we get:

$$\begin{aligned}
\langle y(t_2)y(t_1)\rangle \quad &= \frac{\lambda^2}{2}\langle\Psi(t_1)|\hat{U}^\dagger\hat{G}\hat{U}\hat{S}|\psi(t_1)\rangle + \frac{\lambda^2}{2}\langle\Psi(t_1)|\hat{S}\hat{U}^\dagger\hat{G}\hat{U}|\psi(t_1)\rangle \\
&= \lambda^2 \mathrm{Re}[\langle\Psi(t_1)|\hat{U}^\dagger\hat{G}\hat{U}\hat{S}|\psi(t_1)\rangle], \qquad \text{(B.5)}
\end{aligned}$$

where I have used the identities $\hat{S} = \sum_i s_i|s_i\rangle\langle s_i|$ and $\hat{G} = \sum_j g_j|g_j\rangle\langle g_j|$, and $1 = \sum_i |s_i\rangle\langle s_i|$ and $\hat{G} = \sum_j |g_j\rangle\langle g_j|$. This last result reproduces Eq. 2.12 in the main text.

Appendix C

The perturbed state for an ideally weak measurement

This Appendix is dedicated to understand if the result Eq. 2.12 is contaminated by the measurement or not. For this it is relevant to first rewrite the general state in the system space in Eq. 2.9, according to the Taylor series used in Appendix B for the ancilla wavefunction in the ideally weak regime I get:

$$\begin{aligned}|\psi_{k,\omega}(t_2)\rangle &= \sum_{j,i} |g_j\rangle a(y_\omega - \lambda g_j)\langle g_j|\hat{U}|s_i\rangle a(y_k - \lambda s_i)\langle s_i|\psi(t_1)\rangle \\ &= \sum_{j,i} |g_j\rangle \left(a(y_\omega) - \lambda \frac{\partial a(y_\omega)}{\partial y_\omega} g_j\right) \langle g_j|\hat{U}|s_i\rangle \left(a(y_k) - \lambda \frac{\partial a(y_k)}{\partial y_k} s_i\right) \langle s_i|\psi(t_1)\rangle,\end{aligned} \tag{C.1}$$

which can be easily expanded to read:

$$\begin{aligned}
|\psi_{k,\omega}(t_2)\rangle &= a(y_\omega)a(y_k)\sum_{j,i}|g_j\rangle\langle g_j|\hat{U}|s_i\rangle\langle s_i|\psi(t_1)\rangle \\
&- \lambda\frac{\partial a(y_\omega)}{\partial y_\omega}a(y_k)\sum_{j,i}|g_j\rangle\langle g_j|\hat{U}|s_i\rangle s_i\langle s_i|\psi(t_1)\rangle \\
&- \lambda\frac{\partial a(y_k)}{\partial y_k}a(y_\omega)\sum_{j,i}|g_j\rangle g_j\langle g_j|\hat{U}|s_i\rangle\langle s_i|\psi(t_1)\rangle \\
&+ \lambda^2\frac{\partial a(y_\omega)}{\partial y_\omega}\frac{\partial a(y_k)}{\partial y_k}\sum_{j,i}|g_j\rangle g_j\langle g_j|\hat{U}|s_i\rangle s_i\langle s_i|\psi(t_1)\rangle. \qquad \text{(C.2)}
\end{aligned}$$

Using now $\hat{S} = \sum_i s_i|s_i\rangle\langle s_i|$ and $\hat{G} = \sum_i g_i|s_i\rangle\langle s_i|$ Eq. C.2 reduces to:

$$\begin{aligned}
|\psi_{k,\omega}(t_2)\rangle = \Bigg(a(y_\omega)a(y_k)\hat{U} + \lambda^2\frac{\partial a(y_\omega)}{\partial y_\omega}\frac{\partial a(y_k)}{\partial y_k}\hat{G}\hat{U}\hat{S} - \lambda\frac{\partial a(y_\omega)}{\partial y_\omega}a(y_k)\hat{G}\hat{U} - ... \\
...\lambda\frac{\partial a(y_k)}{\partial y_k}a(y_\omega)\hat{U}\hat{S}\Bigg)|\psi(t_1)\rangle. \qquad \text{(C.3)}
\end{aligned}$$

This is the result found in Eq. 2.13 in the main text.

Appendix D

The weak measurement as a displacement operator

In this Appendix I consider a quantum system defined by the wavefunction solution of the Schrödinger equation with a harmonic potential $V(x) = (1/2)\ m\ \Omega^2\ x^2$ with m the mass of the particle and Ω the oscillatory frequency of the oscillator [14, 16]. In particular, I consider that the initial state is the ground state at time $t_1 = 0$:

$$\psi(x, t_1) \equiv \langle x|\Psi(t_1)\rangle = \left(\frac{m\Omega}{\pi\hbar}\right)^{1/4} exp\left(\frac{-x^2}{2\sigma_S^2}\right) exp(-i\Omega t) \tag{D.1}$$

where the spatial dispersion of ground state σ_S is defined as:

$$\sigma_S = \sqrt{\frac{\hbar}{m\Omega}} \tag{D.2}$$

I am interested in the measurement of the position x. Therefore, the discrete eigenstates $|s_k\rangle$ described in chapter 2 are substituted here by a continuous set of eigenstates $|x\rangle$. For the Positive Operator Valued Measure describing the interaction of the ancilla with the system, I use a Gaussian Krauss operator,

whose representation in position is given by:

$$a(y-x) = \left(\frac{1}{\pi\sigma_M^2}\right)^{1/4} exp\left(\frac{-(x-y)^2}{2\sigma_M^2}\right) \tag{D.3}$$

where different types of measurements can be assigned to different values of σ_M defined as the spatial dispersion of ancilla wavepacket ($\sigma_M \to 0$ corresponds to a strong measurement, while $\sigma_M \to \infty$ to an ideal weak measurement). Trivially, the operator in Eq. D.3 accomplishes the conditions imposed on the ancilla wavepacket in section 2.1.

After the first measurement at time t_1 obtaining the measurement outcome y_k, the system wavepacket in Eq. D.1 is perturbed giving the new state as:

$$\psi_k(x,t_1) = a(y_k - x)\psi(x,t_1) = \left(\frac{1}{\pi\sigma_M^2}\right)^{1/4} exp\left(-\frac{(x-y_k)^2}{2\sigma_M^2}\right)\psi(x,t_1) \tag{D.4}$$

which is just the product of Eq. D.1 and Eq. D.3. The parameter λ is not needed here (we use $\lambda = 1$) because y and x are both position eigenvalues.

Let me consider the ideally weak measurement case as discussed theoretically in section 2.2.2. To realize that I assume $\sigma_M \gg \sigma_S$. Then, in the development of $(x-y_k)^2 = x^2 - 2xy_k + y_k^2$, we get $y_k \gg x$ so that $2xy_k \gg -x^2$ for positive x when $y_k > 0$, or for negative x when $y_k < 0$. Then, neglecting the term in x^2 we can rewrite Eq. D.4 as:

$$\psi_k(x,t_1) \approx \left(\frac{1}{\pi\sigma_M^2}\right)^{1/4} exp\left(-\frac{y_k^2 - 2xy_k}{2\sigma_M^2}\right)\psi(x,t_1) \tag{D.5}$$

The perturbed wavefunction $\psi_k(x,t_1)$ in Eq. D.5 can be related, in fact, to a coherent state of the harmonic oscillator $\psi_C^\alpha(x,t_1)$. Such state is defined at time

$t_1 = 0$ as [14, 15]:

$$\psi_C^{\alpha}(x,0) \equiv \langle x|\alpha\rangle = \left(\frac{m\Omega}{\pi\hbar}\right)^{1/4} exp\left(\frac{-m\Omega x^2}{2\hbar}\right) exp\left(-\alpha^2 + \sqrt{\frac{2m\Omega}{\hbar}}\alpha x\right) \quad \text{(D.6)}$$

where α is the eigenvalue associated to $\hat{a}|\alpha\rangle = \alpha|\alpha\rangle$ with $\hat{a}$ defined as the annihilation operator. Using Eq. D.1 and Eq. D.2, I can rewrite Eq. D.6 as:

$$\begin{aligned}\psi_C^{\alpha}(x,0) \quad &= \left(\frac{m\Omega}{\pi\hbar}\right)^{1/4} exp\left(-\frac{x^2}{2\sigma_S^2} - \frac{2(\sigma_S\alpha)^2}{2\sigma_S^2} + \frac{2\sqrt{2}(\alpha\sigma_S)x}{2\sigma_S^2}\right) \\ &= exp\left(-\frac{\alpha'^2 - 2\alpha' x}{2\sigma_S^2}\right)\psi(x,0) \end{aligned} \quad \text{(D.7)}$$

where α' is defined as:

$$\alpha' = \sqrt{2}\sigma_S\alpha \quad \text{(D.8)}$$

Apart from an irrelevant (position independent) normalization constant. The resemblance between the perturbed sate $\psi_k(x,0)$ in Eq. D.5 and the coherent state $\psi_C^{\alpha}(x,0)$ in Eq. D.7 just requires the definition of the measured value y_k as:

$$y_k = \frac{\alpha'\sigma_M^2}{\sigma_S^2} = \frac{\alpha\sigma_M^2}{\sigma_S} \quad \text{(D.9)}$$

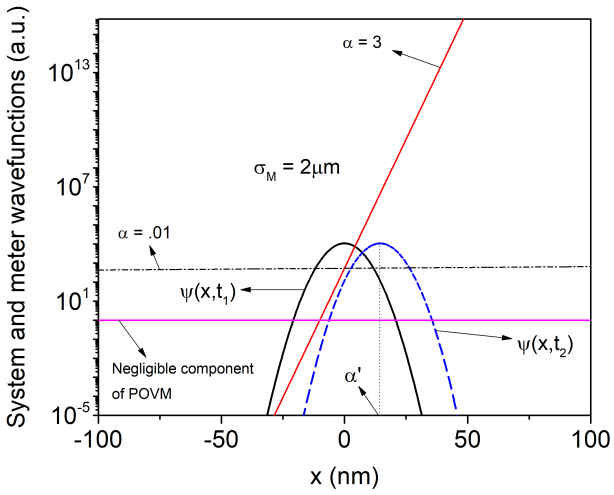

Figure D.1: Figure depicting the wavefunction perturbation in the ideally weak measurement regime. The figure shows a logarithmic plot of the x- dependence of ground state of the harmonic oscillator $\psi(x, t_1)$ (solid black line) and of the Gaussian Positive Operator Valued Measure $a(y)$ (ancilla) for different values of positive y related to different values of $\alpha = y\sigma_S/\sigma_M^2$ quantifying the range of eigenvalues of the ancilla. Black dahed-doted line corresponds to a $\alpha = 0.01$ (very less values of y) with a slope so small that the initial state has (almost) no variation after being multiplied by it. The solid red line corresponds to $\alpha = 3$ (very large values of y) where the slope induces a displacement of the initial ground state by an amount of $\alpha' = \sqrt{2}\sigma_S\alpha$ resulting in a $\psi(x, t_2)$ which demonstrates a very large perturbation shown in dashed blue line, which is now a coherent state (see Appendix D for details). The pink line corresponds to the irrelevant term $exp(-x^2/(2\sigma_M^2)) \approx 0$ in the ancilla. I have used $\sigma_S = \sqrt{\hbar/(m\Omega)} = 4.8106\ nm$ and $\sigma_M = 2\ \mu m$.

The previous demonstration that the Gaussian kraus operator in Eq. D.3 acting on the ground state produces a coherent state $\psi_C(x)$ can be alternatively demonstrated as follows. Let us define an operator $D(\alpha')$ such that $D(\alpha')\psi(x) =$

$\psi(x-\alpha')$. Using the taylor's expansion for the term on the right we get,

$$\begin{aligned}\psi(x-\alpha') &= \Psi(x) - \alpha'\frac{\partial}{\partial x}\psi(x) + \frac{(\alpha')^2}{2!}\left(\frac{\partial}{\partial x}\right)^2\psi(x) - .... \\ &= \left(1 - \alpha'\frac{\partial}{\partial x} + \frac{(\alpha')^2}{2!}\left(\frac{\partial}{\partial x}\right)^2 - ...\right)\psi(x) \\ &= exp\left(-\alpha'\frac{\partial}{\partial x}\right)\psi(x) \end{aligned} \tag{D.10}$$

On the other hand, from textbooks [129], the coherent state is alternatively defined as $\psi_C(x) = \langle x|D(\alpha)|0\rangle = \langle x|\alpha\rangle$ with:

$$D(\alpha) = exp\left(\frac{-\alpha^2}{2}\right)exp\left(\alpha\hat{a}^\dagger - \alpha^*\hat{a}\right) \tag{D.11}$$

now for real α where $\hat{a}^\dagger$ and $\hat{a}$ are creation and annihilation operator respectively, we get:

$$D(\alpha) = exp\left(\frac{-\alpha^2}{2}\right)exp\left(-\frac{2iP\alpha}{\sqrt{2\hbar m\omega}}\right) \tag{D.12}$$

where we have used $\frac{\hat{a}^\dagger - \hat{a}}{2i} = \frac{\hat{p}}{\sqrt{2\hbar m\omega}}$ with the momentum operator, in the position representation, is given by $\hat{p} = -i\hbar\partial/\partial x$. Finally, we get:

$$\psi_C(x) = \langle x|D(\alpha)|0\rangle \;\; = exp\left(\tfrac{-\alpha^2}{2}\right)exp\left(\tfrac{-2\alpha\hbar}{\sqrt{2\hbar m\omega}}\tfrac{\partial}{\partial x}\right)\langle x|0\rangle = D(\alpha)\psi_G(x) \tag{D.13}$$

Here we compare the Eq. (D.10) and Eq. (D.13) to see that, since the condition $\alpha = y\sigma_S/\sigma_M^2$ is met because it implies the previous identities $\alpha' = \frac{\alpha\sqrt{2\hbar}}{\sqrt{m\omega}} = \sqrt{2}\alpha\sigma_S$, both expressions are identical. This result demonstrate again that Gaussian Kraus operator acting on the ground state is like a translation operator which converts the ground state $\psi(x)$ into a coherent state $\psi_C(x)$. The reason why the ancilla wavepacket in Eq. D.4 with $\sigma_M \to \infty$ implies such a large perturbation on the ground state wavefunction, converting the measured state into a coherent

state, can be found in Eq. D.9 and in the logarithmic plot in Figure D.1. Most of the measured Figure D.1 values of y_k corresponds to small α (see $\alpha = 0.01$ in Figure D.1) where the measured and initial ground states are (almost) identical(solid black line in Figure D.1). However, because of $\sigma_M \to \infty$ we also have a small (but not zero) probability to get $y_k \to \infty$ which implies large α (see, for example, $\alpha = 3$ in Figure D.1). The slope of the line $\alpha = 3$ (solid red line) in the support of the ground state $\psi(x, t_1)$ is so large that the product of both terms leads to a non-negligible perturbation of the initial state, resulting in the displacement of the ground state (dashed red line) giving $\psi(x, t_2)$ which is a coherent state [15].

Appendix E

Two-time correlations for special operators

Since in general scenarios I was not able to find the unperturbed two-time correlation function in this Appendix I try to impose some restrictions on the operators and see if I can obtain some relevant result. Let me assume a particular operator and Hamiltonian that satisfy $\langle s_{i'}|\hat{U}^{\dagger}\hat{G}\hat{U}|s_i\rangle = g_o\frac{\partial^n\delta(s_{i'}-s_i)}{\partial s_i'^n}$ where g_o is a constant and I consider n as an arbitrary positive integer. Then, I can rewrite Eq. 2.11 as:

$$\langle y(t_2)y(t_1)\rangle = \lambda\sum_{i,i'}\int dy_k\; y_k\; a(y_k-\lambda s_i)a^*(y_k-\lambda s_{i'})\langle\psi(t_1)|s_{i'}\rangle... \\ ...g_o\frac{\partial^n\delta(s_{i'}-s_i)}{\partial s_i'^n}\langle s_i|\psi(t_1)\rangle \tag{E.1}$$

By properly applying the derivative of a delta function $\sum_{i'} \psi(s_i')a^*(y_k-\lambda s_{i'})\frac{\partial^n \delta(s_{i'}-s_i)}{\partial s_i'^n} = (-1)^n \frac{\partial^n(\psi(s_i)a^*(y_k-\lambda s_i))}{\partial s_i^n}$ with $\langle\ \psi|s_i\rangle = \psi^*(s_i)$ and $\langle\ s_i|\psi\rangle = \psi(s_i)$, I get:

$$\langle y(t_2)y(t_1)\rangle \quad = (-1)^n\lambda \sum_i g_o \int dy_k\ y_k\ a(y_k-\lambda s_i)\psi(s_i)\frac{\partial^n(\psi^*(s_i)a^*(y_k-\lambda s_i))}{\partial s_i^n} \tag{E.2}$$

As we can see, the multiple derivatives in the ancilla wavepacket gives rise to values of $\langle y(t_2)y(t_1)\rangle$ where the meter dependence persists on. There are, however, two particular values of n where such dependence disappears.

When $n = 0$, I find $\langle s_{i'}|\hat{U}^\dagger\hat{G}\hat{U}|s_i\rangle = g_o\delta(s_{i'}-s_i)$ which means that the evolved state $\hat{U}|s_i\rangle$ is an eigenstate of $\hat{G}$. So its easy to see from Eq. E.1 that,

$$\langle y(t_2)y(t_1)\rangle_{n=0} = \lambda g_o\langle\psi(t_1)|\hat{S}|\psi(t_1)\rangle = \lambda\langle\hat{G}(t_2)\rangle\langle\hat{S}(t_1)\rangle \tag{E.3}$$

This case is different from the condition in 2.14 that deals with an initial (not final) eigenstate even though the final result in both the cases are identical.

For $n = 1$ it would seem that since the state $|s_i\rangle$ is not the eigenstate of the operator, the meter dependence will persist, but when considering this case in Eq. E.2 one can see that the two conditions imposed on the ancilla wavepacket as introduced in the previous discussion will be required to compute the correlation which is given as,

$$\langle y(t_2)y(t_1)\rangle_{n=1} \quad = -\lambda\frac{g_o}{2}\left(1+\sum_i \psi(s_i)\frac{\partial\psi^*(s_i)}{\partial s_i}\right) \tag{E.4}$$

Clearly the dependence of $a(y-\lambda s)$ on the correlations $\langle y(t_2)y(t_1)\rangle$ has been eliminated and so the correlation is meter independent (see Figure E.1(b)). For an analytical result of this case in a harmonic oscillator see Appendix E.1. Only when $n > 1$ in the computation of Eq. E.2, the explicit meter dependence cannot

be removed as clearly demonstrated in the analytical result in Appendix E.2 where the case of $n = 2$ is used for demonstration (see Figure E.1).

E.1 Two-time correlation for position operator

This example represents the case $n = 1$ described above. Using Eq.(34) in the position basis with the operator $\hat{S} = \hat{X}$ I get;

$$\begin{aligned}\langle y(t_2)y(t_1)\rangle \quad &= \int dy_k \int dy_\omega \; y_k y_\omega P(y_\omega, y_k) \\ &= \lambda \int dx \int dx' \int dy_k \; y_k \; a(y_k - \lambda x)a^*(y_k - \lambda x')\langle\psi(t_1)|x'\rangle \times \\ &\langle x'|\hat{U}^\dagger \hat{X}\hat{U}|x\rangle\langle x|\psi(t_1)\rangle. \\ &= \lambda \int dx \int dx' \int dy_k \; y_k \; a(y_k - \lambda x)a^*(y_k - \lambda x')\psi^*(x') \\ &\langle x'|\hat{X}(t_1)\cos(\Omega t_2) + \frac{\hat{P}(t_1)}{m\Omega}\sin(\Omega t_2))|x\rangle\psi(x). \end{aligned} \tag{E.5}$$

Here I have used the time evolution operator of the position in harmonic oscillator as, $\hat{X(t_2)} = \hat{U}^\dagger \hat{X}(t_1)\hat{U} = \hat{X}(t_1)\cos(\Omega t_2) + \frac{\hat{P}(t_1)}{m\Omega}\sin(\Omega t_2))$. I decompose Eq. E.5 in two terms $\langle y(t_2)y(t_1)\rangle = I_1 + I_2$ defined below. The first term I_1 gives:

$$\begin{aligned} I_1 \quad &= \lambda \int dx \int dx' \int dy_k \; y_k \; a(y_k - \lambda x)a^*(y_k - \lambda x')\psi^*(x')\rangle\langle x'|\hat{X}(t_1)\cos(\Omega t_2)|x\rangle\psi(x). \\ &\text{Since } \langle x'|\hat{X}(t_1)|x\rangle = x\delta(x' - x) \\ &= \lambda \int dx \int dx' \int dy_k \; y_k \; a(y_k - \lambda x)a^*(y_k - \lambda x')\psi^*(x')x\cos(\Omega t)\delta(x' - x)\psi(x). \\ &= \lambda\cos(\Omega t_2) \int dx \int dy_k \; y_k \; |a(y_k - \lambda x)|^2 x|\psi(x)|^2 \end{aligned} \tag{E.6}$$

Using the identity $\int dy_k\ y_k\ |a(y_k - \lambda x)|^2 = \lambda x$, I arrive to,

$$I_1 \quad = \lambda^2 \cos(\Omega t_2) \int dx x^2 |\psi(x)|^2 = \lambda^2 \cos(\Omega t_2) \langle \hat{X}^2(t_1) \rangle \tag{E.7}$$

The second term I_2, using $\langle x'|\hat{P}(t_1)|x\rangle = -\hbar \frac{\partial \delta(x'-x)}{\partial x}$ gives:

$$\begin{aligned} I_2 \quad &= \lambda \int dx \int dx' \int dy_k\ y_k\ a(y_k - \lambda x) a^*(y_k - \lambda x') \psi^*(x') \rangle \langle x'| \frac{\hat{P}(t_1)}{m\Omega} \sin(\Omega t_2) |x\rangle \psi(x). \\ &= \frac{-i\hbar\lambda}{m\Omega} \sin(\Omega t_2) \int dx \int dx' \int dy_k\ y_k\ a(y_k - \lambda x) a^*(y_k - \lambda x') \times \\ &\psi^*(x') \frac{\partial}{\partial x'} \delta(x' - x) \psi(x). \\ &= \frac{-i\hbar\lambda}{m\Omega} \sin(\Omega t_2) \int dx \psi(x) \int dy_k\ y_k\ a(y_k - \lambda x) \int dx' a^*(y_k - \lambda x') \times \\ &\psi^*(x') \frac{\partial}{\partial x'} \delta(x' - x) \end{aligned} \tag{E.8}$$

Applying integration by parts to the last term of Eq. E.8 I get,

$$\begin{aligned} I_2 \quad &= \frac{i\hbar\lambda}{m\Omega} \sin(\Omega t_2) \int dx \psi(x) \int dy_k\ y_k\ a(y_k - \lambda x) \frac{\partial (a^*(y_k - \lambda x) \psi^*(x))}{\partial x} \\ &= \frac{i\hbar\lambda}{m\Omega} \sin(\Omega t_2) \int dx \psi(x) \frac{\partial \psi^*(x)}{\partial x} \int dy_k\ y_k\ |a(y_k - \lambda x)|^2 + \\ &\frac{i\hbar\lambda}{m\Omega} \sin(\Omega t_2) \int dx |\psi(x)|^2 \int dy_k\ y_k\ a(y_k - \lambda x) \frac{\partial a^*(y_k - \lambda x)}{\partial x} \end{aligned} \tag{E.9}$$

Now, to provide a compact expression I use the ground state of the harmonic oscillator in the position basis defined in Eq.(49). I decompose now $I_2 = I_2' + I_2''$

into the two terms present in last line of Eq. E.9.

$$\begin{aligned} I_2^{'} &= \frac{i\hbar\lambda}{m\Omega}\sin(\Omega t_2)\int dx\psi(x)\frac{\partial\psi^*(x)}{\partial x}\int dy_k\ y_k\ |a(y_k-\lambda x)|^2 \\ &= \frac{i\hbar\lambda^2}{m\Omega}\sin(\Omega t_2)\int dx x\psi(x)\frac{\partial\psi^*(x)}{\partial x} \\ &= -\frac{1}{\sigma_S^2}\frac{i\hbar\lambda^2}{m\Omega}\sin(\Omega t_2)\int dx x^2|\psi(x)|^2 \\ &= -\frac{1}{\sigma_S^2}\frac{i\hbar\lambda^2}{m\Omega}\sin(\Omega t_2)\langle\hat{X}^2\rangle = -\frac{i\hbar\lambda^2}{2m\Omega}\sin(\Omega t_2)\langle\hat{X}^2\rangle \end{aligned} \tag{E.10}$$

where I use $\langle\hat{X}^2(t_1)\rangle = \frac{\sigma_S^2}{2}$. For the term $I_2^{''}$ I have:

$$\begin{aligned} I_2^{''} &= \frac{i\hbar\lambda}{m\Omega}\sin(\Omega t_2)\int dx|\psi(x)|^2\int dy_k\ y_k\ a(y_k-\lambda x)\frac{\partial a^*(y_k-\lambda x)}{\partial x} \\ &= \frac{i\hbar\lambda^2}{2m\Omega}\sin(\Omega t_2) \end{aligned} \tag{E.11}$$

where I have used $\int dy_k\ y_k\ a(y_k-\lambda x)\frac{\partial a^*(y_k-\lambda x)}{\partial x} = \frac{\lambda}{2}$. Finally I get the real value:

$$\begin{aligned} \langle y(t_2)y(t_1)\rangle &= I_1 + I_2 = I_1 + I_2^{'} + I_2^{''} = \lambda^2\cos(\Omega t_2)\langle\hat{X}^2(t_1)\rangle \\ &= \cos(\Omega t_2)\langle\hat{X}^2(t_1)\rangle, \text{ when } \lambda = 1 \end{aligned} \tag{E.12}$$

E.2 Two-time correlation for position squared operator

This example is the representative of the case $n = 2$ described above. Rewriting a part of Eq.(34) in the position basis and using $\hat{S} = \hat{X}^2(t_1)$,

$$\begin{aligned}&\langle x'|\hat{U}^\dagger\hat{X}^2(t_1)\hat{U}|x\rangle = \langle x'|\hat{X}^2(t_2)|x\rangle \\ &= \langle x'|\hat{X}^2(t_1)\cos^2(\Omega t_2) + \frac{\hat{P}^2(t_1)}{(m\Omega)^2}\sin^2(\Omega t_2) + 2\frac{\hat{P}(t_1)}{m\Omega}.\hat{X}(t_1)\cos(\Omega t_2)\sin(\Omega t_2) \\ &+\frac{i\hbar}{m\Omega}\cos(\Omega t_2)\sin(\Omega t_2)|x\rangle\end{aligned} \tag{E.13}$$

where I have used $\hat{U}^\dagger\hat{X}^2(t_1)\hat{U} = (\hat{U}^\dagger\hat{X}(t_1)\hat{U})^2 = \hat{X}^2(t_2)$ and reminding ourselves that $\hat{U}^\dagger\hat{U} = \hat{I}$, where $\hat{I}$ is an identity matrix and finally using the commutation relation of position and momentum which lets us to write $\hat{X}\hat{P} = \hat{P}\hat{X} + i\hbar$

$$\begin{aligned}\langle x'|\hat{U}^\dagger\hat{X}^2(t_1)\hat{U}|x\rangle \quad &= x^2\cos^2(\Omega t_2)\delta(x'-x) - \frac{\hbar^2}{(m\Omega)^2}\sin^2(\Omega t_2)\frac{\partial^2\delta(x'-x)}{\partial x^2} - \\ &\frac{i\hbar}{m\Omega}\cos(\Omega t_2)\sin(\Omega t_2)\left(-2x\frac{\partial\delta(x'-x)}{\partial x} + \delta(x'-x)\right)\end{aligned} \tag{E.14}$$

Where I have used $\langle x'|\hat{X}(t_1)|x\rangle = x\delta(x'-x)$, $\langle x'|\hat{P}(t_1)|x\rangle = -i\hbar\frac{\partial\delta(x'-x)}{\partial x}$ and $\langle x'|\hat{P}^2(t_1)|x\rangle = -\hbar^2\frac{\partial^2\delta(x'-x)}{\partial x^2}$. At this point I would like to use a specific function for the ancilla, as a Gaussian kraus operator, which can be written as,

$$a(y_k - \lambda x^2) = \left(\frac{1}{\pi\sigma_M^2}\right)^{1/4} exp\left(\frac{-(y-\lambda x^2)^2}{2\sigma_M^2}\right) \tag{E.15}$$

Let $\langle y(t_2)y(t_1)\rangle = I_1 - I_2 - I_3$, where I_1, I_2, I_3 represents the first second

and the third term of the correlation obtained when introducing Eq. E.14 into Eq.(34). For the first term:

$$\begin{aligned} I_1 &= \lambda^2 \cos^2(\Omega t_2)\langle \hat{X}^4(t_1)\rangle \\ I_2 &= \lambda \frac{\hbar^2}{(m\Omega)^2}\sin^2(\Omega t_2)\int dx\psi(x)\int dy_k\ y_k\ a(y_k-\lambda x^2)\frac{\partial^2(a^*(y_k-\lambda x^2)\psi^*(x))}{\partial x^2} \end{aligned} \tag{E.16}$$

where I use the identity $\int dy_k\ y_k\ |a(y_k-\lambda x^2)|^2 = \lambda x^2$ where λ is just a constant for satisfying the dimensional arguments. I also use $\frac{\partial^2(a^*(y_k-\lambda x^2)\psi^*(x))}{\partial x^2} = \int dx'(a^*(y_k-\lambda x'^2)\psi^*(x'))\frac{\partial^2\delta(x'-x)}{\partial x^2}$. I develop

$$\begin{aligned} \frac{\partial^2(a^*(y_k-\lambda x^2)\psi^*(x))}{\partial x^2} &= \psi(x)\frac{\partial^2 a(y_k-\lambda x^2)}{\partial x^2} + a(y_k-\lambda x^2)\frac{\partial^2\psi(x)}{\partial x^2} + \\ & 2\frac{\partial a(y_k-\lambda x^2)}{\partial x}\frac{\partial\psi(x)}{\partial x} \end{aligned} \tag{E.17}$$

and

$$\begin{aligned} \frac{\partial^2 a(y_k-\lambda x^2)}{\partial x^2} &= \frac{4\lambda^2x^2(\lambda x^2-y_k)^2}{\sigma_M^4}a(y_k-\lambda x^2) - \frac{4\lambda^2x^2}{\sigma_M^2}a(y_k-\lambda x^2) + \\ & \frac{2\lambda(\lambda x^2-y_k)}{\sigma_M^2}a(y_k-\lambda x^2) \end{aligned} \tag{E.18}$$

I define $I_2 = I_2^{'} + I_2^{''} + I_2^{'''}$ as the first, second and third term of I_2 when using Eq. E.17 in Eq. E.16.

$$\begin{aligned} I_2^{'} &= \lambda\frac{\hbar^2}{(m\Omega)^2}\sin^2(\Omega t_2)\int dx\psi(x)\int dy_k\ y_k\ a(y_k-\lambda x^2)\psi(x)\frac{\partial^2 a(y_k-\lambda x^2)}{\partial x^2} \\ &= -\lambda\frac{\hbar^2}{(m\Omega)^2}\sin^2(\Omega t_2)\left(\frac{2\lambda^3}{\sigma_M^2}\langle\hat{X}^4(t_1)\rangle + \lambda\right) \end{aligned} \tag{E.19}$$

Using Eq. E.17 and Eq. E.18 in Eq. E.16 I get

$$I_2^{''} = \lambda \frac{\hbar^2}{(m\Omega)^2} \sin^2(\Omega t_2) \left(\frac{\lambda}{\sigma_S^4} \langle \hat{X}^4(t_1) \rangle - \frac{\lambda}{\sigma_S^2} \langle \hat{X}^2(t_1) \rangle \right)$$

$$I_2^{'''} = -\lambda \frac{\hbar^2}{(m\Omega)^2} \sin^2(\Omega t_2) \left(\frac{2\lambda}{\sigma_S^2} \langle \hat{X}^2(t_1) \rangle \right)$$

$$I_3 = \lambda \frac{i\hbar}{m\Omega} \cos(\Omega t_2) \sin(\Omega t_2) \left(\int dx \, (2x) \, \psi(x) \int dy_k \; y_k \; a(y_k - \lambda x^2) \frac{\partial f(x)}{\partial x} + \lambda \langle \hat{X}^2 \rangle \right)$$

$$= \lambda \frac{i\hbar}{m\Omega} \cos(\Omega t_2) \sin(\Omega t_2) \left(3\lambda \langle \hat{X}^2(t_1) \rangle - \frac{\lambda \langle \hat{X}^4(t_1) \rangle}{\sigma_S^2} \right) = 0 \tag{E.20}$$

where I use $\langle \hat{X}^2(t_1) \rangle = \frac{\sigma_S^2}{2}$ and $\langle \hat{X}^4(t_1) \rangle = \frac{3\sigma_S^4}{4}$. Finally I sum up the terms such that $\langle y(t_2) y(t_1) \rangle = I_1 - I_2 - I_3$

$$\langle y(t_2) y(t_1) \rangle \quad = \lambda^2 \cos^2(\Omega t_2) \langle \hat{X}^4(t_1) \rangle + \frac{\hbar^2 \lambda^2}{(m\Omega)^2} \sin^2(\Omega t_2) \left(\frac{3\lambda^2}{2\sigma_M^2} \sigma_S^4 + \frac{7}{4} \right) \tag{E.21}$$

When $t_1 = 0$ and $t_2 = T/2$ I get,

$$\langle y(t_2) y(t_1) \rangle \quad = \lambda^2 \cos^2(\Omega t) \langle \hat{X}^4 \rangle \tag{E.22}$$

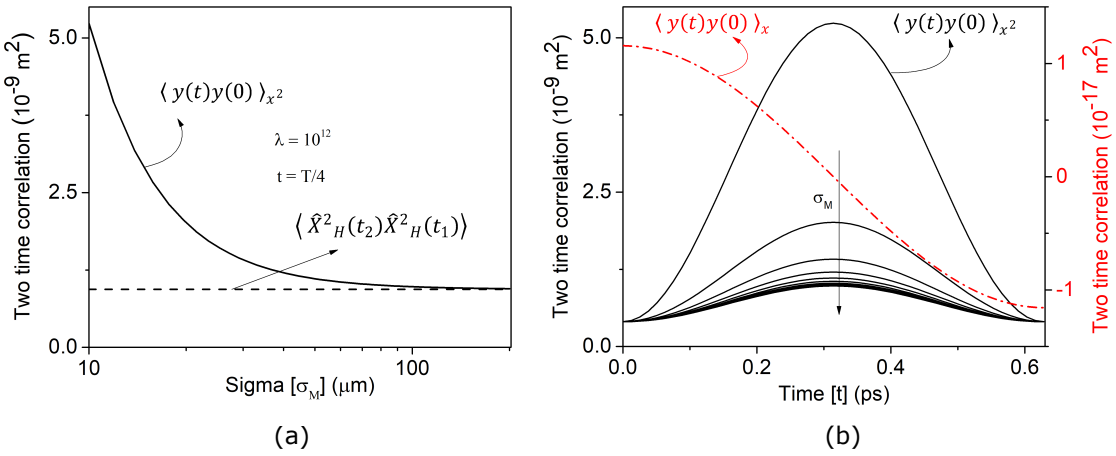

Figure E.1: (a) Ensemble values of the correlation between $y(t_1)$ and $y(t_2)$ for the observable x^2 in a harmonic oscillator (representative of case $n = 2$ given by Eq. E.21) at $t = T/4$ as a function of the apparatus dispersion σ_M, certifying that this observable (measured property) is not universal and depends on (is contaminated by) the measurement. For large σ_M the correlation approaches to the Heisenberg computation (dashed line) given by Eq. 2.12. I have used $\lambda = 10^{12}$ to get $y \approx 100\mu m$ (b) Plot of the correlations with respect to time, for observable x^2 using Eq. E.21 (black solid lines, left y-axis, with $\lambda = 10^{12}$) and x using Eq. E.12 (which is the representative of the case $n = 1$) in red dashed line (right y-axis, with $\lambda = 1$) for different values of σ_M. The correlations for observable x are meter independent, while for the observable x^2 a strong dependence on σ_M is obtained.

Appendix F

Derivation of AAV weak value

Let us assume that the coupling constant λ as described in Appendix A, is much smaller signifying a weak coupling of the system and the ancilla. In this case $\exp\left(\frac{-i}{\hbar}\lambda\hat{S}\otimes\hat{P}_a\right) \approx 1-\frac{i}{\hbar}\lambda\hat{S}\otimes\hat{P}_a$. Now the weak value implies a post-selection with respect to the state $|g_\omega\rangle$ which results in the final state after postselection as follows (assuming the instantaneous projection),

$$|\phi(t_1)\rangle = \exp\left(\frac{-i}{\hbar}\gamma\hat{Y}\otimes\hat{P}_p\right)\left(1-\frac{i}{\hbar}\lambda s_i\hat{P}_a\right)\langle g_\omega|\psi(t_1)\rangle\otimes\int a(y)|y\rangle dy\otimes\int f(z,0)|z\rangle dz$$

$$= \exp\left(\frac{-i}{\hbar}\gamma\hat{Y}\otimes\hat{P}_p\right)\langle g_\omega|\psi(t_1)\rangle\left(1-\frac{i}{\hbar}\lambda\frac{\langle g_\omega|\hat{S}|\psi(t_1)\rangle}{\langle g_\omega|\psi(t_1)\rangle}\hat{P}_a\right)\otimes ... \\ ...\int a(y)|y\rangle dy\otimes\int f(z,0)|z\rangle dz \qquad \text{(F.1)}$$

$$= \exp\left(\frac{-i}{\hbar}\gamma\hat{Y}\otimes\hat{P}_p\right)\langle g_\omega|\psi(t_1)\rangle\exp\left(\frac{-i}{\hbar}\lambda\ \ g_\omega\langle\hat{S}\rangle_{\psi(t_1)}\hat{P}_a\right)\otimes ... \\ ...\int a(y)|y\rangle dy\otimes\int f(z,0)|z\rangle dz \qquad \text{(F.2)}$$

where $g_\omega\langle\hat{S}\rangle_{\psi(t_1)} \equiv \frac{\langle g_\omega|\hat{S}|\psi(t_1)\rangle}{\langle g_\omega|\psi(t_1)\rangle}$ is the AAV weak value. Now, using the same arguments as used in the set of equations in Eq. A.6 I obtain,

$$|\phi(t_1)\rangle = \langle g_\omega|\psi(t_1)\rangle \int a\left(y - \lambda\ \ g_\omega\langle\hat{S}\rangle_{\psi(t_1)}\right)|y\rangle dy \otimes \int f(z-y)|z\rangle dz \qquad \text{(F.3)}$$

From Eq. F.3 it is clear that the AAV weak value is defined in a single experiment unlike the operationalist weak values that are defined from an ensemble of experiments.

Appendix G

Bohmian trajectories of a Harmonic Oscillator

In this Appendix I provide the intrinsic and measured Bohmian trajectories for a particle in the ground state of harmonic oscillator.

G.1 Intrinsic Bohmian trajectories

One can calculate the intrinsic Bohmian trajectory in the ground state of the harmonic oscillator by first computing the velocity of the trajectory of a particle when its not measured. The time dependent state of the ground state of the harmonic oscillator is given by Eq. D.1 as:

$$\psi(x,t) \equiv \langle x|\Psi(t)\rangle = \left(\frac{m\Omega}{\pi\hbar}\right)^{1/4} exp\left(-\frac{x^2}{2\sigma_S^2}\right) exp(-i\Omega t) \tag{G.1}$$

with Ω related to the eigenenergy of the ground state. The Bohmian velocity is given by $v_B(x,t) = \frac{\hbar}{m}\frac{\partial}{\partial x} arctan\left(\frac{\psi(x,t)_i}{\psi(x,t)_r}\right)$ where $\psi(x,t)_i$ and $\psi(x,t)_r$ are the real and imaginary parts in Eq. G.1 [21]. In our particular case, I get

$arctan\left(\frac{\psi(x,t)_i}{\psi(x,t)_r}\right) = -\Omega t$. Thus the resulting Bohmian velocity is, $v_B(x,t) = 0$. Since the velocity of the bohmian particle is zero, its position will be constant with time.

G.2 Measured Bohmian trajectories

In this section first I will try to describe the measured Bohmian trajectories and their ensemble value. The bohmian trajectories of the harmonic oscillator system measured at time t_1 with a Gaussian Kraus operator centred at y_k such that the measurement perturb the system strongly transform it into a coherent state as has already been discussed in Appendix D. Now, I will evaluate the Bohmian velocity in such a scenario where the trajectories are influenced by the measurement. To discuss the velocity I would need the time evolution of the coherent state which is given by $|\alpha(t)\rangle = |\alpha e^{-i\Omega t}\rangle$ where $|\alpha\rangle$ is the coherent state at time $t = 0$. So now in order to compute the measured Bohmian trajectories I will have to evaluate time dependent coherent state. But before that I must prove that the coherent state at time t given by $|\alpha(t)\rangle$ remains to be the eigen state of the annihilation operator which will facilitate the position representation of the time dependent coherent state. I start by writing the time development of the coherent state $|\alpha(t)\rangle = exp(-iHt/\hbar)|\alpha(0)\rangle$ and trying to simplify the eigen value equation

$$\hat{a}|\alpha(t)\rangle = \hat{a}exp(-iHt/\hbar)|\alpha(0)\rangle \tag{G.2}$$

multiplying the right side of the equation with $exp(-iHt/\hbar)exp(iHt/\hbar)$ and using the Heisenberg representation of the annihilation opeartor given by

$$\hat{a}(t) = exp(iHt/\hbar)\hat{a}exp(-iHt/\hbar) = \hat{a}exp(-i\Omega t) \tag{G.3}$$

I get,

$$\begin{aligned}\hat{a}|\alpha(t)\rangle &= exp(-iHt/\hbar)exp(-i\Omega t)\hat{a}|\alpha(0)\rangle \\ &= \alpha exp(-i\Omega t)exp(-iHt//\hbar)|\alpha(0)\rangle \\ &= \alpha(t)|\alpha(t)\rangle \end{aligned} \tag{G.4}$$

Now I proceed to deduce the time dependent coherent state, by starting with

$$\langle x|\hat{a}|\alpha(t)\rangle = \alpha(t)\langle x|\alpha(t)\rangle \tag{G.5}$$

Writing the annihilation operators in the standard form as follows

$$\hat{a} = \sqrt{\frac{m\Omega}{2\hbar}}\hat{X} + i\sqrt{\frac{1}{2\hbar m\Omega}}\hat{P} \tag{G.6}$$

Putting Eq. G.6 in Eq. G.5 and using $\langle x|\hat{X}|\alpha(t)\rangle = x\langle x|\alpha(t)$ and $\langle x|\hat{P}|\alpha(t)\rangle = -i\hbar\frac{\partial}{\partial x}\langle x|\alpha(t)\rangle$ I get

$$x\sqrt{\frac{m\Omega}{2\hbar}}\langle x|\alpha(t)\rangle + \hbar\sqrt{\frac{1}{2\hbar m\Omega}}\left(\frac{\partial}{\partial x}\right)\langle x|\alpha(t)\rangle = \alpha(t)\langle x|\alpha(t)\rangle \tag{G.7}$$

I know that $\langle x|\alpha(t)\rangle = \psi_C(x,t)$ I put this into Eq. G.7. Now I use the variable separable method to arrive at

$$\frac{\partial\psi_C(x,t)}{\psi_C(x,t)} = \left(\alpha(t)\sqrt{\frac{2m\Omega}{\hbar}} - x\frac{m\Omega}{\hbar}\right)\partial x \tag{G.8}$$

Intergrating both sides in Eq. G.8 its easy to see that,

$$\psi_C(x,t) = A_0 exp\left(\frac{-m\Omega x^2}{2\hbar}\right) exp\left(\sqrt{\frac{2m\Omega}{\hbar}}x\alpha(t)\right) \tag{G.9}$$

Subjecting this equation to the normalization condition $\int_{-\infty}^{\infty}|\psi_C(x,t)|^2dx = 1$ I get the time dependent coherent state given by

$$\psi_C(x,t) = \left(\frac{m\Omega}{\pi\hbar}\right)^{1/4} exp\left(\frac{-m\Omega x^2}{2\hbar}\right) exp\left(-\alpha^2(t) + \sqrt{\frac{2m\Omega}{\hbar}}x\alpha(t)\right) \quad \text{(G.10)}$$

Measuring the system state wavefunction giving the output y transform the ground state into a coherent state with $\alpha = y\sigma_S/\sigma_M^2$. Since $|\alpha(t)\rangle$ remains to be an eigen state of the annihilation operator for all times its easy to see that the time evolution of the coherent state in the position representation can be given as below. Writing the Eq. G.10 in the polar from $\psi_C(x,t) = R(x,t)exp\left(\frac{iS}{\hbar}\right)$ I find that

$$\psi_C(x,t) = \psi(x)exp\left(-\alpha^2\right) exp\left(\frac{\sqrt{2}\alpha x cos\Omega t}{\sigma_S}\right) exp\left[-i\left(\frac{\sqrt{2}\alpha x}{\sigma_S}sin\Omega t\right)\right] \quad \text{(G.11)}$$

where I have used the fact that $\alpha(t) = \alpha e^{-i\Omega t}$ and $\alpha(t)^2 = \alpha^2$ and $\psi(x) = \left(\frac{m\Omega}{\pi\hbar}\right)^{1/4} exp\left(\frac{-m\Omega x^2}{2\hbar}\right)$ is the ground state of harmonic oscillator. From Eq. G.11 I can find the argument of the complex wavefunction $\psi_C(x,t)$ as

$$S = -\hbar\left(\frac{\sqrt{2}\alpha x}{\sigma_S}sin\Omega t\right) \quad \text{(G.12)}$$

Now I can find the bohmian velocity [21] as follows,

$$v_B(x,t) = \frac{1}{m}\frac{\partial S}{\partial x} = -\frac{\hbar}{m}\frac{\sqrt{2}\alpha}{\sigma_S}sin\Omega t \quad \text{(G.13)}$$

It can be clearly seen that the Bohmian velocity depends linearly on the amount of perturbation quantified by α and it has a sinusoidal dependence on time. Now since I have the expression for the Bohmian velocity its easy to evaluate the

position of the bohmian particle at time t_1 perturbed by the measurement.

$$x(t_1) = \sqrt{2}\alpha\sigma_S cos\Omega t_1 + C = \sqrt{2}\alpha\sigma_S cos\Omega t_1 + C \tag{G.14}$$

By using the initial condition I find the constant $C = x(0) - \sqrt{2}\alpha\sigma_S$. Using this value in the above equation and using $\alpha' = \sqrt{2}\alpha\sigma_S$ in Eq. D.8 I get

$$x(t_1)_k = \alpha' cos\Omega t_1 + x(0) - \alpha' = \frac{y_k\sigma_S^2}{\sigma_M^2} cos\Omega t_1 + x(0) + \frac{y_k\sigma_S^2}{\sigma_M^2} \tag{G.15}$$

Where Eq. G.15 is the Bohmian trajectory of the harmonic oscillator system measured at time t_1 with a Gaussian Kraus operator centred at y_k. Computing the ensemble of Bohmian trajectories over all initial positions, with $\langle x(0)\rangle_{B,k} = \alpha'$, I get

$$\begin{aligned} \langle x(t_1)\rangle_{B,k} \quad &= \langle \alpha' cos\Omega t_1 + x(0) - \alpha' \rangle \\ &= \alpha' cos\Omega t - \alpha' + \langle x(0)\rangle = \alpha' cos\Omega t - \alpha' + \alpha' \end{aligned} \tag{G.16}$$

$$\langle x(t_1)\rangle_{B,k} = \alpha' cos\Omega t_1 = \frac{y_k\sigma_S^2}{\sigma_M^2} cos\Omega t_1 \tag{G.17}$$

Appendix H

Examples of utility of intrinsic properties

In this Appendix apart from the high frequency quantum noise, I discuss the other two paradigmatic examples of utility of intrinsic properties viz. the quantum thermodynamic work and the dwell time.

H.1 The quantum work distribution

Quantum work is the basic ingredient in the development of quantum thermodynamics which is one of the most important topics in the field of open quantum systems. Quantum thermodynamics is essential in developing new quantum technologies such as quantum heat engines. It also plays a fundamental role in the consistency of the second law of thermodynamics in the quantum regime. However, there are many issues that are still being investigated, most notably related to the definition of work and heat. The problem is that these thermodynamic variables are not observables related to Hermitian (super)operators, but are trajectory (history) dependent [130–132]. This has culminated in the so-called

"no-go" theorem that states that in fact there cannot exist a (super)operator for work that simultaneously satisfies all the physical properties required from it [133]. This conclusion is based on three requirements to be fulfilled by what Acin *et al.* [133] define to be a properly defined positive definite work distribution. Namely:

1. The work distribution is described by a positive operator valued measurement (POVM).

2. For initial states that commute with the initial Hamiltonian the work distribution reduces to the two-point measurement (TPM) work distribution.

3. The work distribution respects the change in the Hamiltonian expectation value.

Now, evaluating quantum work by means of a TMP measurement protocol of the energy will imply that the first measurement projects the initial state into an energy eigenstate, hence preventing the possibility of capturing any coherent evolution of the state. The alternative Orthodox protocols for the evaluation of the quantum work such as Gaussian measurements [134, 135], weak measurements [136, 137], collective measurements [133], etc. all suffer from quantum contextuality, which provides as many different work definitions as measurement schemes exist. The problem appears due to the requirement of the Orthodox theory to include a measuring apparatus that in practice does not exist which I have already discussed at length in the main text of the thesis. Now by using the intrinsic properties we are not interested in the explicit measurement of work, but on using dynamical information of the quantum (sub)system in conjunction with quantum thermodynamic equations to compute, e.g., the temperature variation of a larger system involving a macroscopic thermodynamic environment.We are thus seeking for an *unperturbed* value of work.

To define an unperturbed work distribution, I here follow similar steps as in Refs. [138, 139], where a detailed derivation of quantum work based on Bohmian mechanics can be found. Here, I will quickly move to the definition of intrinsic work to discuss in detail how this definition solves the above described puzzling situation. I thus start by defining a single particle[1] wavefunction solution of the following Schrödinger equation:

$$i\hbar\frac{\partial\psi(\vec{r},t)}{\partial t}=\left(\frac{(-i\hbar\vec{\nabla}-q\vec{A}(\vec{r},t))^2}{2m}+qV(\vec{r},t)\right)\psi(\vec{r},t). \tag{H.1}$$

where $\vec{r}$ is defined as a vector in the ordinary three dimensional space, $\vec{\nabla}$ is the gradient operator and $-i\hbar\vec{\nabla}-q\vec{A}(\vec{r},t)$ is the canonical momentum with $A(\vec{r},t)$ the electromagnetic vector potential. When the wavefunction is written in polar form as $\psi(\vec{r},t)=R(\vec{r},t)\exp\left(\frac{i\mathcal{S}(\vec{r},t)}{\hbar}\right)$ where $R(\vec{r},t)$ and $\mathcal{S}(\vec{r},t)$ are the modulus and phase, respectively, the real part of Eq. H.1 evaluated along the Bohmian trajectory $\vec{r}=\vec{r}^{\,i}(t)$ for the i^{th} experiment, gives us the following equation for the unperturbed power:

$$\begin{aligned}\frac{d\mathcal{E}(\vec{r}^{\,i}(t))}{dt} &= \frac{d}{dt}\left(\frac{1}{2}m\vec{v}^2(\vec{r}^{\,i}(t),t)+Q(\vec{r}^{\,i}(t),t)\right)\\ &= q\vec{v}(\vec{r}^{\,i}(t),t)\vec{E}(\vec{r}^{\,i}(t),t)+\frac{\partial Q(\vec{r}^{\,i}(t),t)}{\partial t}.\end{aligned} \tag{H.2}$$

Here $\mathcal{E}(\vec{r}^{\,i}(t),t)$ is the unperturbed energy of the system, $v(\vec{r}^{\,i}(t),t)$ is the Bohmian velocity, $Q(\vec{r}^{\,i}(t),t)$ is the quantum potential and $\vec{E}(\vec{r}^{\,i}(t),t)$ is the electric field [2]. While I have considered an external electromagnetic field interacting with the

[1] A many-body treatment will not add any new insight on the discussion.

[2] Notice that this electric field $\vec{E}(\vec{r},t)$ in Eq. H.2 is different from the electric field $\vec{E}^i(\vec{r},t)$ in Eq. 3.14 used in the section 3.4. There, the electron located at $\vec{r}=\vec{r}^{\,i}(t)$ generates an electric field $\vec{E}^i(\vec{r},t)$ which leads to a density current everywhere inside the device. In Eq. H.2, on the other hand, $\vec{E}(\vec{r},t)$ is an external electric field without self-consistency with the electric charge of the electron considered.

quantum system, no measuring apparatus is accounted for in Eq. H.2. Thus, from Eq. H.2, I can describe the unperturbed work represented by the wavefunction $\psi(\vec{r},t)$ and the trajectory $\vec{r}^{i}(t)$, during the time interval $t_2 - t_1$ by just subtracting the initial energy $\mathcal{E}(\vec{r}^{i}(t_1),t_1)$ from the final one $\mathcal{E}(\vec{r}^{i}(t_2),t_2)$. As I have already mentioned, this result corresponds to the single experiment labelled by the superscript i. Getting ensemble values of the work just requires repeating the previous procedure for different initial positions of the particles, according to the quantum equilibrium hypothesis [21].

As stressed along the thesis, the very crucial aspect of this unperturbed work is its measurability in the laboratory using the local-in-position weak values. So subsequently it will be demonstrated how does the intrinsic value of the work is equivalent to the local-in-position weak value of the energy operator. The local-in-position weak value of the work can be given as follows,,

$$\mathrm{Re}\left({}_{\vec{r}^{i}(t)}\langle\hat{\mathcal{E}}\rangle_{\psi(t)}\right) = \mathrm{Re}\left(\frac{\langle\vec{r}^{i}(t)|\hat{H}|\psi(t)\rangle}{\langle\vec{r}^{i}(t)|\psi(t)\rangle}\right). \tag{H.3}$$

Now using the Hamiltonian from Eq. H.1 in Eq. H.3 and writing the wavefunction in the polar form to evaluate $\langle\vec{r}^{i}(t)|\hat{H}|\psi(t)\rangle$, I can rewrite Eq. H.3 as:

$$\begin{aligned}\mathrm{Re}\left({}_{\vec{r}^{i}(t)}\langle\hat{\mathcal{E}}\rangle_{\psi(t)}\right) &= \left[\frac{-\hbar^2}{2m}\frac{\nabla^2 R(\vec{r},t)}{R(\vec{r},t)} + \frac{(\vec{\nabla}S(\vec{r},t))^2}{2m}\right]_{r=r^{i}(t)} \\ &= Q(\vec{r}^{i}(t),t) + \frac{1}{2}m\vec{v}(\vec{r}^{i}(t),t)^2,\end{aligned} \tag{H.4}$$

where ∇^2 is the Laplacian operator and R and $\mathcal{S}$ are the modulus and phase of the wavefunction. Now comparing, Eq. H.2 and Eq. H.4 , it is straightforward to see that,

$$\mathrm{Re}\left({}_{\vec{r}^{i}(t)}\langle\hat{\mathcal{E}}\rangle_{\psi(t)}\right) = \mathcal{E}(\vec{r}^{i}(t),t). \tag{H.5}$$

I thus conclude that the intrinsic Bohmian energy is equal to the local-in-position weak value of the energy and hence that it can be, in principle, measured experimentally. Given a collection of weak values of the energy at times t_1 and t_2, one can then easily evaluate the quantum work in the i^{th} experiment as,

$$W^i(t_2, t_1) = \text{Re}\left(_{\vec{r}^i(t_2)}\langle\hat{\mathcal{E}}\rangle_{\psi(t_2)}\right) - \text{Re}\left(_{\vec{r}^i(t_1)}\langle\hat{\mathcal{E}}\rangle_{\psi(t_1)}\right). \tag{H.6}$$

The work distribution on the other hand can be given as follows,

$$\mathcal{P}(w, t_2, t_1) = \lim_{M\to\infty} \frac{1}{M} \sum_{i=1}^{M} \delta(w - W^i(t_2, t_1)). \tag{H.7}$$

From the work distribution in Eq. H.7 I can now evaluate the corresponding expectation value:

$$\langle W(t_2, t_1)\rangle = \int dw\; w\; \mathcal{P}(w, t_2, t_1) = \lim_{M\to\infty} \frac{1}{M} \sum_{i=1}^{M} W^i(t_2, t_1). \tag{H.8}$$

where M is the total number of experiments considered $i = 1, 2, .., M$.

The above Bohmian approach circumvents the conceptual problem of the unavoidable contextuality of quantum work in the Orthodox theory. The unperturbed "Bohmian work" fulfills the aforementioned last two requirements (ii and iii) for a properly defined work distribution and reduces to the known definitions in the appropriate limits. Furthermore, it also circumvents the no-go theorem in [133] because it cannot be associated with a POVM and hence also alleviates the practical problem of mandating to define a POVM in the Orthodox theory. In Bohmian approach on the other hand work is always defined as a positive value for the work probability distribution and, moreover, describes a property that is non-contextual (as it does not depend on the back-action of the measuring apparatus). These are new conditions that should, in our opinion substitute (i)

in [133], i.e.:

(i.1) The work definition must always lead to a positive-valued probability distribution

(i.2) The work distribution should not be contextual, i.e., it should not depend on the back-action of the measurement.

H.2 The quantum dwell time

Measuring the time spent by a particle within a particular region $\vec{a} < \vec{r} < \vec{b}$ requires measuring the time t_1 at which the particle enters that region and later, the time t_2 at which the particle leaves it. As we have already seen, the measurement of the position of the particle implies the perturbation of the state of the system in most general circumstances. Thus, any subsequent measurement of the position is generally influenced by the first measurement. In spite of its controversial definition in Orthodox quantum theory, the concept of dwell time is necessary, for example, to evaluate the maximum working frequency of state-of-the-art transistors and hence the performance of modern computers [76] as I had already discussed in chapter 1. In this respect, it is important to notice that when using the information of the dwell time in the evaluation of the performance of computers, there are no position detectors at the two ends ($\vec{a}$ and $\vec{b}$) of the active region of the transistors. A valid question is then which of the two dwell times, the measured or the unperturbed one, provide a better estimation of the maximum working frequency of transistors. Anyhow, what is definitely true is that to estimate the maximum working frequency of transistors nobody evaluates dwell times by means of projective measurements [128, 140].

The *unperturbed* value of the dwell time can be easily computed from *intrinsic* Bohmian trajectories $\vec{r}^{\,i}(t)$. Again, for simplicity, I only consider one electron

inside the active region in each experiment. The expectation value of the unperturbed dwell time can be defined as:

$$\tau_D = \lim_{M\to\infty} \frac{1}{M} \sum_{i=1}^{M} \tau^i, \tag{H.9}$$

where τ^i is defined as the time spent by the (intrinsic) i^{th} Bohmian trajectory inside the region $\vec{a} < \vec{r} < \vec{b}$, i.e.:

$$\tau^i = \int_0^\infty dt \Theta[\vec{r}^{\,i}(t) - \vec{a}]\Theta[\vec{b} - \vec{r}^{\,i}(t)], \tag{H.10}$$

where Θ is the unit step function. The above expression can be rewritten as

$$\tau_D = \lim_{M\to\infty} \frac{1}{M} \sum_{i=1}^{M} \int_0^\infty dt \int_{\vec{a}}^{\vec{b}} \delta[\vec{r} - \vec{r}^{\,i}(t)] d\vec{r}. \tag{H.11}$$

Using (3.16) and Eq. 3.17, $\vec{r}^{\,i}(t)$ can be defined in terms of weak values as:

$$\vec{r}^{\,i}(t) = \vec{r}^{\,i}(0) + \frac{1}{m} \int_0^t dt' \text{Re}\left[{}_{\vec{r}^{\,i}(t')}\langle \hat{P}_x \rangle_{\psi(t')} \right], \tag{H.12}$$

with $\vec{r}^{\,i}(0)$ as the initial position of the trajectory in i-th experiment. Making use of the quantum equilibrium condition [21] in Eq. H.11, I get the well-know expression

$$\tau_D = \int_0^\infty dt \int_{\vec{a}}^{\vec{b}} |\psi(\vec{r}, t)|^2 d\vec{r}, \tag{H.13}$$

which is certainly an unperturbed property of the quantum system as there is no contamination from the measuring apparatus. Notice that the experimental validation of the above arguments requires the intrinsic Bohmian trajectories that can be reconstructed from the intrinsic Bohmian velocity field understood as a local-in-position weak value of the momentum [52]. Eq. H.12 gives a way to

compute the intrinsic value of dwell time from the local-in-position weak value of the momentum operator, $\hat{P}$ but I can alternatively compute this time from a definition of the dwell time operator $\hat{D}$ as follows,

$$\tau_D = \int_0^\infty dt \int_{\vec{a}}^{\vec{b}} |\psi(\vec{r},t)|^2 d\vec{r} = \int_0^\infty dt \int_{\vec{a}}^{\vec{b}} \langle\psi(t) \mid \vec{r}\rangle\langle\vec{r} \mid \psi(t)\rangle d\vec{r} \tag{H.14}$$

Defining the operator $\hat{A} = \int_{\vec{a}}^{\vec{b}} |\vec{r}\rangle\langle\vec{r}|$, Eq. H.14 can be written as

$$\tau_D = \int_0^\infty dt \langle\psi(t)|\hat{A}|\psi(t)\rangle = \left\langle \psi(0) \left| \int_0^\infty dt \hat{U}^\dagger \hat{A} \hat{U} \right| \psi(0) \right\rangle \tag{H.15}$$

where I have defined $|\psi(t)\rangle = \hat{U}|\psi(0)\rangle$. Now I define the tunnelling time operator $\hat{D} = \int_0^\infty dt \hat{U}^\dagger \hat{A} \hat{U}$ which allows us to write Eq. H.15 as follows,

$$\tau_D = \left\langle \psi(0)|\hat{D}|\psi(0) \right\rangle \tag{H.16}$$

Subsequently I can easily represent the above expression in terms of weak value of the tunnelling time operator $\hat{D}$ with post-selected state $|\vec{r}\rangle$ and the initial state $|\psi(0)\rangle$ by a simple transformation as follows,

$$\begin{aligned} \tau_D &= \int d\vec{r} \langle\psi(0) \mid \vec{r}\rangle \langle\vec{r} \,|\hat{D}|\psi(0)\rangle = \int d\vec{r} \;|\psi(\vec{r},0))|^2 \;{}_{\vec{r}}\langle\hat{D}\rangle_{\psi(\vec{r},0)} \\ &= \lim_{M\to\infty} \frac{1}{M} \sum_{i=1}^{M} {}_{\vec{r}^i(0)}\langle\hat{D}\rangle_{\psi(\vec{r},0)} \end{aligned} \tag{H.17}$$

where I have used the quantum equilibrium expression
$|\psi(\vec{r},0)|^2 = \lim_{M\to\infty} \frac{1}{M} \sum_{i=1}^{M} \delta(\vec{r} - \vec{r}^i(0))$ in the last identity of Eq. H.17. By comparing Eq. H.9 and Eq. H.17, it is easy to obtain the relation between the Bohmian intrinsic tunnelling time and the weak value of the tunnelling time as follows,

$$\tau^i = {}_{\vec{r}^i(0)}\langle\hat{D}\rangle_{\psi(\vec{r},0)} \tag{H.18}$$

which says that the Bohmian dwell time of the i-th particle is exactly equal to the weak value of the dwell time operator associated to the i-th particle defined as the one whose initial position is $\vec{r}^{\,i}(0)$. Once more, Eq. H.18 shows a deep connection between weak values and intrinsic dynamic properties.

Certainly, there exist many Orthodox protocols to compute either the dwell time or the tunneling [141–146]. For example, one can make use of a physical clock to measure the time elapsed during the tunneling [143–146]. Larmor precession was precisely introduced to measure the time associated with scattering events [144, 146]. Anyhow, what is essential here is that the scientific community has been persistent in looking for observables of dynamical properties whose expectation value is free from any contamination from the (physically nonexistent) measuring apparatus. This is exactly what *intrinsic* properties discussed in this thesis are meant for.

Part VII

COMPENDIUM OF PUBLICATIONS

Publication A

Devashish Pandey, Xavier Oriols, and Guillermo Albareda. From micro- to macrorealism: addressing experimental clumsiness with semi-weak measurements. *New Journal of Physics*, jun 2020

New Journal of Physics
The open access journal at the forefront of physics

Deutsche Physikalische Gesellschaft DPG
IOP Institute of Physics

Published in partnership with: Deutsche Physikalische Gesellschaft and the Institute of Physics

OPEN ACCESS

RECEIVED
30 December 2019

REVISED
21 May 2020

ACCEPTED FOR PUBLICATION
9 June 2020

PUBLISHED
27 July 2020

PAPER

From micro- to macrorealism: addressing experimental clumsiness with semi-weak measurements

Devashish Pandey[1], **Xavier Oriols**[1] **and Guillermo Albareda**[1,2,3]

[1] Departament d'Enginyeria Electrònica, Universitat Autònoma de Barcelona, 08193 Bellaterra, Spain
[2] Max Planck Institute for the Structure and Dynamics of Matter, 22761 Hamburg, Germany
[3] Institute of Theoretical and Computational Chemistry, Universitat de Barcelona, 08028 Barcelona, Spain

E-mail: guillermo.albareda@mpsd.mpg.de and xavier.oriols@uab.cat

Keywords: Leggett–Garg inequalities, no-signaling in time, macrorealism, generalized von Neumann measurements, quantum-to-classical transition, weak measurement, semi-weak measurements

Abstract

We propose a protocol that allows to assess the precise correspondence between thought and practical experiments, a critical point for addressing experimental clumsiness in a test of macro- or micro-realism. Two-time generalized von Neumann measurements of properties $\mathcal{A}$ and $\mathcal{B}$ are shown to obey the so-called no-signaling in time condition for initial states defined as an incoherent sum of eigenstates of $\mathcal{A}$. An experiment for witnessing the use of this type of measurements in the laboratory is then devised by proving the existence of five conditions that have to be fulfilled by any generalized von Neumann measurement. Ensuring the use of this type of measurements and then testing the no-signaling in time condition for a range of system-meter coupling strengths allows to test realism in a highly reproducible manner and to critically narrow the so-called clumsiness loophole. The resulting protocol is applicable to general (not only dichotomic) variables, and it is employed to show, both analytically for general systems and numerically for a collection of harmonic oscillators, that quantum systems made of a large number of uncorrelated particles are genuinely macrorealist, i.e., realistic with respect to all intensive properties at any time.

1. Introduction

The concept of realism, viz, objects have well defined properties independently of whether they are measured, has been an unquestioned pillar in the development of many physical theories. The advent of quantum mechanics, however, shook up those foundations from the bottom up [1, 2]. Today, despite the overwhelming success of the quantum theory to reproduce many types of experiments, the reality of quantum objects is still a lively topic of debate [3, 4].

Based on the measurements of a property $\mathcal{A}$ of a quantum object at a spatial position and of another property $\mathcal{B}$ of another quantum object (entangled with the first one) at another distant location, John Bell derived an inequality for the probabilities of the measurements of $\mathcal{A}$ and $\mathcal{B}$ assuming spatial independence between the two measurements [5–7]. Such spatial independence is named locality in the literature. Inspired on Bell's test of locality, Leggett and Garg [8] derived an inequality for the probabilities of the consecutive measurement of properties $\mathcal{A}$ and $\mathcal{B}$ of a quantum object when temporal independence between the two measurements is assumed. Such temporal independence is understood as the non-invasiveness of the first measurement. In the literature, historically, the invasiveness of a measurement has been linked to the definition of quantum reality. The orthodox eigenstate–eigenvalue link ensures that whenever a quantum object is described by an eigensate of the property $\mathcal{A}$, it can be measured in a non-invasive way, and thus, one can assume that the property $\mathcal{A}$ 'was there' before the measurement (and hence that it is a 'real' property) [9–11].

Notwithstanding the recent surge of interest in the Leggett–Garg inequalities [12–15], controversy remains on what precise reality is shown by its violation [16, 17]. The confusion arises because while general definitions of locality or non-invasiveness are applicable to any ontic model, a general definition of reality, valid for all ontic models, does not exist. For example, the reality in orthodox quantum mechanics is different from the reality in Bohmian mechanics, and both are different from the reality invoked by stochastic collapse theories. The controversy disappears when it is recognized that either Leggett–Garg inequalities can be used only as a test of non-invasive measurability (valid for any ontic model), or as a test of the reality of orthodox quantum mechanics [16, 17]. In this paper, as mostly assumed in the literature, we will adopt this second viewpoint.

It is the goal of this work to address the so-called clumsiness loophole in a test of realism. Before we get to that point, however, and to avoid any possible semantics conflict, let us carefully introduce the concept of microrealism in contrast to the concept of macrorealism[4].

1.1. Macrorealism versus microrealism

First of all let us notice that macrorealism cannot be proven true once and for all, viz, for any property at any time. If a test of macrorealism aims at evaluating our notion of classical realism, then a quantum object should satisfy the Leggett–Garg inequalities for any property at any time. However, even if an object were to pass a number of tests for different properties at different times, one never knows whether another property or lapse of time exists which the corresponding inequality would fail to pass. It is thus not a coincidence that most of experimental works testing Leggett and Garg inequalities in the laboratory are focused on ordinary quantum systems rather than on the type of 'macroscopically distinct states' invoked by Leggett and Garg [19]. That is, existing tests only investigate a particular observable of interest $\mathcal{A}$ of a *microscopic* object (expected to behave quantum mechanically) at a given time [12, 20, 21]. All this amounts to the relaxation of what Leggett and Garg called macrorealism into a definition of realism that is based on the so-called 'eigenstate–eigenvalue link', i.e., the assumption that a system only has a determinate value for a particular observable when its state is an eigenstate of the corresponding operator [17, 22].

We define *microrealism* or realism with respect to a property $\mathcal{A}$ when the following two conditions are fulfilled:

- (R1) *Realism of an object with respect to a property $\mathcal{A}$ at a given time*: given a property $\mathcal{A}$ associated to an operator $\hat{A}$ which has available to it two or more distinct eigenvalues (and eigenstates), a realistic object with respect to property $\mathcal{A}$ is, at a given time, in a definite one of these eigenstates.
- (R2) *Discernibility between coherent and incoherent sums of eigenstates of $\hat{A}$*: it is possible, *in principle*, to determine experimentally whether an object is a coherent sum of eigenstates of $\hat{A}$ or it is an incoherent sum of eigenstates of $\hat{A}$.

Condition (R1) defines the reality of a property of an object according to orthodox quantum mechanics. Alternatively, (R2) forces the ontological definition of realism to be, *in principle*, empirically testable. The correspondence between thought (i.e., *in principle*) and practical experiments is at the heart of the so-called 'clumsiness loophole' and will be the subject of discussion in section 1.2.

In this paper, we will use the term "incoherent sum of eigenstates" to refer to proper mixtures [59], i.e., those mixed states for which it can be given an ignorance interpretation and hence that obey a unitary evolution[5]. In this respect, the need of condition (R2) can be justified as follows. One may think that by simply comparing the outcome of an ensemble of projective measurements of $\mathcal{A}$, microrealism could be already confirmed or ruled out. That is, the system is in an eigenstate of $\hat{A}$ if the same outcome is obtained over and over again and it is in a superposition state of $\hat{A}$ otherwise. Unfortunately, in the presence of a certain degree of uncertainty in the preparation of the system due to technological limitations, this procedure might lead to erroneously concluding that property $\mathcal{A}$ of such system is non-microrealistic when it is actually microrealistic. Another reason why condition (R2) is better formulated in terms of an incoherent sum of eigenstates because we could be explicitly interested in testing the reality of a property of a system that is naturally defined as a proper mixture of eigenstates of $\hat{A}$.

Following the original idea of Leggett and Garg, and with the same spirit of Bell's theorem without inequalities [23, 24], two recent works by Kofler and Brukner [16] and independently by Li *et al* [25] have proposed an alternative to the Leggett–Garg inequalities. Solely based on comparing the probability distribution for a property at some time for the cases where previously a measurement has or has not been performed, the conditions derived in references [16, 25], commonly called 'no-signaling in time' (NSIT),

[4] Note that the concept of microrealism was introduced much before the word macrorealism was coined by Leggett and Garg. See, for example, the work by Maxwell [18].

[5] Note that this is in contrast to improper mixtures, for which the density operator arises from tracing out a certain number of degrees of freedom and hence its evolution is generally nonunitary.

can be violated according to quantum mechanical predictions. As it will be shown later, in this work we will adopt the NSIT condition as a statistical realization of (R2).

1.2. The clumsiness loophole

Either tests of microrealism, based on the Leggett–Garg inequalities or on the NSIT condition, suffer from a serious vulnerability. While Leggett–Garg inequalities and the NSIT conditions may serve well conceptually to define (R2), they do not assert that it is impossible to affect a realistic object by a *clumsy* measurement. Take a classical system for example. If the first measurement of $\mathcal{A}$ at time t induces a strong enough perturbation on the system, then both Leggett–Garg inequalities and the NSIT condition could be easily violated and one would erroneously conclude that the classical system is not realistic. In other words, the violation of Leggett–Garg inequalities or the NSIT condition can only be a proof that the property $\mathcal{A}$ of the system is either (i) non-realistic or (ii) realistic but subjected to a *clumsy* measurement technique [26].

This problem can be summarized as the impossibility of assessing the fulfillment of the following condition:

- (R3) *Correspondence between thought (in principle) and practical (implemented) measuring apparatus*: it is possible to ensure that the measurement scheme that has been designed at the theoretical level to test realism corresponds exactly to the experimental set-up that has been implemented in the laboratory.

That is, an hypothesis such as (R3) can be easily falsified but cannot be proven true once and for all. Even if the measurement set-up were to pass a number of tests for non-invasiveness, one never knows whether some test exists which the measurement scheme would fail. This problem is known as the 'clumsiness loophole' [26], and such loophole can always be exploited to refute the implications of a Leggett–Garg or NSIT test of realism.

There are experiments, however, where it is more difficult to accept that a bad-functioning apparatus yielded erroneous conclusions. Leggett and Garg themselves [8] acknowledged the existence of such a loophole, but maintained that clever measurement schemes might be designed to minimize it. A number of works have thus addressed the clumsiness loophole by relying on the so called ideal negative measurements, where information is obtained from the lack of response of a detector [12–15]. However, even this type of measurements should pass a number of tests to address a possible lack of correspondence between thought and practical experiment. Since the apparatuses for measuring properties $\mathcal{A}$ and $\mathcal{B}$ are located in the same lab, as part of the same experimental setup, it is not obvious how to discard (uncontrolled) variables with spurious effects on the measurement of $\mathcal{A}$ that may imply a non-negligible effect on the measurement of $\mathcal{B}$. Thus the clumsiness loophole remains a topic of debate[6].

1.3. The objective of this paper

In the above context, the best one can do is to address the clumsiness loophole by making the 'violation' of (R3) so contrived as to be doubtful. Following this consideration, the notion of 'adroit measurement' has been introduced in reference [26]. By witnessing first the use of adroit measurements in the laboratory using projective measurements, the authors were able to conclude that a system violating the Leggett–Garg inequalities was either (i) non-realistic or (ii) realistic but with the property that two adroit measurements can somehow collude to cheat the experimentalists. In the same line of thought but using a different strategy, in this work we propose a protocol that allows to address the precise correspondence between thought and practical experiments and hence to cope with the clumsiness loophole.

In section 2 we will first frame the notion of 'two-time generalized von Neumann' measurements as a sub-class of positive-operator valued measure. The von Neumann model, originally developed for projective measurements, is generalized by introducing an ancilla that interacts with the system. The ancilla is then strongly measured and provides more or less precise information of the system depending on the their mutual coupling strength. According to recent literature [19, 32], we will define strong, semi-weak and weak measurements depending on the system-meter coupling strength, while we will use the notion of generalized von Neumann measurements to refer indistinctly to these three measurement regimes.

Generalized von Neumann measurements are not the focus of our work, but in section 3 will be proven to be good candidates for testing microrealism as they fulfill the NSIT condition for quantum objects with well defined properties. Therefore, an experiment for witnessing the use of this type of measurements in the

[6] In a Bell test of local realism, special relativity can be used to close the so-called 'communication loophole' between *bad* measuring apparatus at both labs separated by a large distance [27–30]. One could still argue, however, the existence of two 'conspiratorial demons' inside the measuring apparatus of such labs that, without communicating among them, have decided, in advance, what type of output data will be provided to cheat the experimentalists [31]. It is generally accepted that such type of hypothesis are 'too conspiratorial' to be taken seriously, so that recent tests of Bell inequalities are, for most of the scientific community, considered to be free from this type of 'loophole'. Unfortunately, no such clear defense exists for the clumsiness loophole affecting a test of realism.

laboratory will be devised by proving the existence of five conditions that have to be fulfilled by these type of measurements. Explaining the violation of NSIT under the fulfillment of these five conditions in terms of experimental clumsiness, while possible, will be ruled out as wildly implausible (or too conspiratorial). The clumsiness loophole will be thus critically narrowed, and only a considerably smaller conspiracy loophole remains because the use of generalized von Neumann measurements can be highly promoted but not completely ensured.

In section 4, we will address the question of whether microrealism can help to understand the quantum-to-classical transition. We will define *genuine macrorealism* as the status of a quantum object that is microrealistic *with respect to all intensive (non-additive) properties at any time*. In this respect, we will show (both analytically and numerically for a case example) that weakly-correlated quantum systems with a large number of particles satisfy (R1) for any intensive property at any time. These results suggest the viewpoint where what we call classical objects are, in fact, quantum objects that are realistic at the macroscopic level with respect to some (not all) properties[7]. We will conclude in section 5.

2. Two-time generalized von Neumann weak measurements

Consider that we want to test the reality of an object with respect to a property $\mathcal{A}$ (associated to an operator $\hat{A}$). Consider also that the object of interest is a quantum many-body system described by a (non-separable) pure state at time t,

$$|\psi(t)\rangle = \sum_i c_i(t)|a_i\rangle, \tag{1}$$

where $c_i(t) = \langle a_i|\psi(t)\rangle$, and $|a_i\rangle$ are the eigenstates of the operator $\hat{A}$, i.e., $\hat{A}|a_i\rangle = a_i|a_i\rangle$ with a_i the corresponding eigenvalues. Note that, without the loss of generality, we have assumed that the spectral decomposition of $\hat{A}$ is non-degenerate and hence that it can be written using Dirac's bra-ket formalism.

The expectation value of $\mathcal{A}$ can be then evaluated by repeatedly reading-out the pointer position of the corresponding measuring apparatus over a large ensemble of identically prepared experiments. In a generalized von Neumann measurement [33–35], each experiment in the ensemble can be described as follows. The read-out of the property $\mathcal{A}$ is obtained through the pointer position $y_{\mathcal{A}}(t)$ of the measuring apparatus, which we consider to be initially described by the state $|\phi(t)\rangle = \int \Omega_y(t)|y\rangle \mathrm{d}y$. A pre-measurement first entangles the ancilla and the system and yields:

$$|\Psi(t)\rangle = \sum_i c_i(t)|a_i\rangle \otimes \int \Omega_{y-a_i}(t)|y\rangle \,\mathrm{d}y, \tag{2}$$

where $\Omega_{y-a_i}(t)$ is the displaced wavefunction of the ancilla by an amount a_i. Subsequently, the read-out process consists on strongly measuring the ancilla, which provides a definite value of the meter position $y_{\mathcal{A}}$.[8] This step is described by the action of the non-unitary operator $\hat{\mathbb{I}}_S \otimes \hat{\mathbb{P}}_{y_{\mathcal{A}}}$ on the wavefunction in equation (2), where $\hat{\mathbb{I}}_S$ is the many-body identity operator and $\hat{\mathbb{P}}_{y_{\mathcal{A}}} = |y_{\mathcal{A}}\rangle\langle y_{\mathcal{A}}|$ causes the collapse of the ancilla wavefunction into a given read-out value $y_{\mathcal{A}}$, i.e.:

$$|\Psi_{\mathcal{A}}(t)\rangle = \sum_i c_i(t)|a_i\rangle \otimes \Omega_{y_{\mathcal{A}}-a_i}(t)|y_{\mathcal{A}}\rangle. \tag{3}$$

According to equation (3), the above (two-step) measurement process can be effectively described in the subspace of the system by introducing the (non-normalized) state:

$$|\psi_{\mathcal{A}}(t)\rangle = \sum_i \Omega_{y_{\mathcal{A}}-a_i}(t)c_i(t)|a_i\rangle, \tag{4}$$

where the ability of the generalized von Neumann measurement to provide the information y_A without collapsing the system state is highlighted. To avoid unnecessary complexity, hereafter we will refer to both the ancilla interacting with the system and the pointer measuring the ancilla as the meter or measuring apparatus.

[7] For example, the center-of-mass of the Sun follows a classical trajectory, but this well-defined (center-of-mass) position is fully compatible with a pure quantum nuclear fusion of hydrogen nuclei into helium inside it. In this respect, what we call genuine macrorealism could be also referred to as *anthropomorphic macrorealism*.

[8] For simplicity, we assume along the paper that the variables y and a_i are both microscopic variables. If this were not the case, then an irrelevant multiplicative (macroscopic) factor would be needed.

2.1. One-time probabilities

Following Born's rule, the probability of finding a value $y_{\mathcal{A}}$ of the pointer position at time t can be equivalently expressed either as $P(y_{\mathcal{A}}) = \langle \Psi_{\mathcal{A}}(t)|\Psi_{\mathcal{A}}(t)\rangle$ or as $P(y_{\mathcal{A}}) = \langle \psi_{\mathcal{A}}(t)|\psi_{\mathcal{A}}(t)\rangle$:

$$P(y_{\mathcal{A}}) = \sum_i |\Omega_{y_{\mathcal{A}}-a_i}(t)|^2 |c_i(t)|^2. \tag{5}$$

At this point, a degree of mixedness on the definition of the initial state in equation (1) can be easily introduced through a (proper) density matrix,

$$\hat{\rho} = \sum_s p_s |\psi_s\rangle\langle\psi_s|, \tag{6}$$

where p_s is the fraction of the ensemble that is represented by the pure state $|\psi_s\rangle$. Each state $|\psi_s\rangle$ corresponds to one possible s-definition of the initial state $|\psi\rangle$ in equation (1). Note that we are considering proper mixtures of pure states that are only due to our ignorance about the initial conditions.

A mixed initial state can be thus accounted for in the probability distribution of equation (5) by simply summing over p_s as:

$$P(y_{\mathcal{A}}) = \sum_s p_s P_s(y_{\mathcal{A}}), \tag{7}$$

where we have identified $P_s(y_{\mathcal{A}}) = \sum_i |\Omega_{y_{\mathcal{A}}-a_i}(t)|^2 |c_i^s(t)|^2$ and $c_i^s(t) = \langle a_i|\psi_s\rangle$. The above result tells us that, for generalized von Neumann measurements, one time probabilities do always depend on the measuring apparatus. In particular, the probability distribution in equation (7) depends on the wavefunction of the measuring apparatus, and it is so even if the system happens to be defined as an incoherent sum of eigenstates of $\hat{A}$. In such a case, $|\psi_s\rangle = |a_s\rangle$ in equation (6) and hence $P_s(y_{\mathcal{A}}) = |\Omega_{y_{\mathcal{A}}-a_s}(t)|^2$, which still depends on the meter wavefunction.

The unavoidable dependence of the probability distribution in equation (7) on the measuring apparatus is a trivial but significant result that can be used to define a first condition to be fulfilled by any generalized von Neumann measurement, i.e.:

$$\text{C1: } \frac{\mathrm{d}}{\mathrm{d}\sigma_{\mathcal{A}}} P(y_{\mathcal{A}}) \neq 0 \quad \forall t, \tag{8}$$

where we have introduced $\sigma_{\mathcal{A}}$ as the inverse of the system-meter coupling strength or, equivalently, the support (or dispersion) of the meter wavefunction $\Omega_{y_{\mathcal{A}}-a_s}(t)$. Note that $\sigma_{\mathcal{A}}$ is directly related to the resolution of the measuring apparatus [36–39]. In reference [14], for example, the coupling of the system to an auxiliary qubit essentially provides the measurement with an adjustable strength $\sigma_{\mathcal{A}}$ that can be experimentally modified. While not necessary, the meter wavefunction could be approximated to have a Gaussian form with a standard deviation $\sigma_{\mathcal{A}}$ [40–43]. This type of meter wavepackets are known as Gaussian (Kraus) operators [36, 44].

Hereafter we will distinguish between three measurements regimes, viz, strong, weak and semi-weak. For that, we define the *effective dimension of the system with respect to a property* $\mathcal{A}$ as $d_{\text{eff}} := \max(\{\Delta\mathcal{A}\})$, where $\{\Delta\mathcal{A}\}$ is a list of distances between occupied eigenvalues of $\hat{A}$, and thus $\max(\{\Delta\mathcal{A}\})$ refers to the distance between the two eigenvalues that correspond to the highest and lowest occupied eigenstates of $\hat{A}$. Note that the effective dimension of the system is only zero, i.e., $d_{\text{eff}} = 0$, for microrealistic properties of pure states as only one eigenstate of $\hat{A}$ is occupied. Either for incoherent sums of eigenstates or coherent states $d_{\text{eff}} \neq 0$. Accordingly, we can define the following three measurement regimes:

- Projective (or strong) measurement: it is the regime where $\sigma_{\mathcal{A}} \ll d_{\text{eff}}$. In this regime each output value $y_{\mathcal{A}}$ is linked to a single eigenvalue a_i, and hence it is a precise measurement.
- Semi-weak measurements: it is the regime where $\sigma_{\mathcal{A}} \sim d_{\text{eff}}$. In this regime each output values $y_{\mathcal{A}}$ can be linked to a number of eigenvalues a_i of $\hat{A}$, and hence it is an imprecise measurement.
- Weak measurement: it is the regime where $\sigma_{\mathcal{A}} \gg d_{\text{eff}}$. In this regime each output values $y_{\mathcal{A}}$ is linked to all occupied eigenvalues a_i of $\hat{A}$, and hence it is the least precise measurement.

Interestingly, we will see that certain relevant quantities that involve two-time measurements become independent of $\sigma_{\mathcal{A}}$ in the weak measurement regime. Hereafter, we will use the acronym WM to refer only to the *weak measurement* regime defined above.

2.2. One-time expectation values

In order to ensure that the probability distribution in equation (7) provides the correct expectation value of $\hat{A}$ at any time t, i.e.:

$$\langle y_{\mathcal{A}}(t)\rangle = \sum_s p_s \int \mathrm{d}y_{\mathcal{A}} y_{\mathcal{A}} P_s(y_{\mathcal{A}}) = \sum_s p_s \langle\psi_s|\hat{A}|\psi_s\rangle = \langle\hat{A}(t)\rangle, \tag{9}$$

it is enough to make the pointer wavefunction to be well normalized, viz, $\int \mathrm{d}y_{\mathcal{A}}|\Omega_{y_{\mathcal{A}}}|^2 = 1$, and obeying:

$$\int \mathrm{d}y_{\mathcal{A}} y_{\mathcal{A}}|\Omega_{y_{\mathcal{A}}-a_i}|^2 = a_i \quad \forall t. \tag{10}$$

This property is again consistent with the idea that it is more probable that an actual eigenvalue of $\hat{A}$ lies close to the measured value $y_{\mathcal{A}}$ and that the probability to be the actual value then decreases smoothly by growth of $|y_{\mathcal{A}} - a_i|$.

Note that while each outcome probability distribution $P_s(y_{\mathcal{A}})$ depends on the meter wavefunction through $|\Omega_{y_{\mathcal{A}}-a_i}|^2$, the expectation value in equation (9) does not. Therefore, provided that the condition in equation (10) is fulfilled, one should always obtain the same expectation value in equation (9) independently of the specific system-meter interaction strength $\sigma_{\mathcal{A}}$, i.e.:

$$\text{C2: } \frac{\mathrm{d}}{\mathrm{d}\sigma_{\mathcal{A}}}\langle y_{\mathcal{A}}(t)\rangle = 0, \quad \forall t. \tag{11}$$

This result should be understood as a second, unarguable, condition to be fulfilled by a generalized von Neumann measurement.

2.3. Two-time (joint) probabilities

A subsequent measurement of a second property $\mathcal{B}$, associated to the operator $\hat{B} = \sum_i b_i|b_i\rangle\langle b_i|$, with b_i and $|b_i\rangle$ the corresponding eigenvalues and eigenstates, can be easily introduced in the above scheme by simply reading-out the pointer position of a second measuring apparatus at time $\tau \geqslant t$. For that, we first let the state in equation (4) to evolve freely from t until τ. Using the identity operator $\mathbb{I} = \sum_j|b_j\rangle\langle b_j|$, the state of the system right before the second pre-measurement can be written as:

$$|\psi_{\mathcal{A}}(\tau)\rangle = \sum_{i,j}\Omega_{y_{\mathcal{A}}-a_i}(t)c_i(t)c_{i,j}(\tau)|b_j\rangle, \tag{12}$$

where we have defined the coefficients $c_{i,j}(\tau) = \langle b_j|\hat{U}_\tau|a_i\rangle$, and $\hat{U}_\tau = \exp(\mathrm{i}\hat{H}\tau/\hbar)$ is the (free) time-evolution operator of the system between t and τ. We then let the system and the measuring apparatus to get entangled, so that at time τ the full system-meter wavefunction reads:

$$|\Psi_{\mathcal{A}}(\tau)\rangle = \sum_{i,j}\Omega_{y_{\mathcal{A}}-a_i}(t)c_i(t)c_{i,j}(\tau)|b_j\rangle \otimes \int \Omega_{y-b_j}(\tau)|y\rangle\,\mathrm{d}y. \tag{13}$$

Reading-out the pointer position $y_{\mathcal{B}}$ at time τ yields:

$$|\Psi_{\mathcal{A},\mathcal{B}}(\tau)\rangle = \sum_{i,j}\Omega_{y_{\mathcal{A}}-a_i}(t)c_i(t)c_{i,j}(\tau)|b_j\rangle \otimes \Omega_{y_{\mathcal{B}}-b_j}(\tau)|y_{\mathcal{B}}\rangle. \tag{14}$$

Again, the state of the system after the two-time measurement process can be effectively written in the Hilbert space of the system as:

$$|\psi_{\mathcal{A},\mathcal{B}}(\tau)\rangle = \sum_{i,j}\Omega_{y_{\mathcal{B}}-b_j}(\tau)\Omega_{y_{\mathcal{A}}-a_i}(t)c_i(t)c_{i,j}(\tau)|b_j\rangle, \tag{15}$$

and therefore, according to Born's law, the joint probability of measuring $y_{\mathcal{A}}$ at time t and $y_{\mathcal{B}}$ at time τ can be written either as $P(y_{\mathcal{A}}, y_{\mathcal{B}}) = \langle\Psi_{\mathcal{A},\mathcal{B}}(\tau)|\Psi_{\mathcal{A},\mathcal{B}}(\tau)\rangle$ or as $P(y_{\mathcal{A}}, y_{\mathcal{B}}) = \langle\psi_{\mathcal{A},\mathcal{B}}(\tau)|\psi_{\mathcal{A},\mathcal{B}}(\tau)\rangle$, i.e.:

$$P(y_{\mathcal{A}}, y_{\mathcal{B}}) = \sum_j|\Omega_{y_{\mathcal{B}}-b_j}(\tau)|^2\sum_{i,i'}\mathcal{C}^j_{i,i'}(\tau,t)\mathcal{L}_{i,i'}(\Omega_{y_{\mathcal{A}}}(t)), \tag{16}$$

where we have defined the coefficients $\mathcal{C}^j_{i,i'} = c^*_{i'}(t)c^*_{i',j}(\tau)c_{i,j}(\tau)c_i(t)$, and a function of the first meter wavefunction $\mathcal{L}_{i,i'} = \Omega^*_{y_{\mathcal{A}}-a_{i'}}(t)\Omega_{y_{\mathcal{A}}-a_i}(t)$.

A (proper) mixedness can be added to the result in equation (16) through the density matrix in equation (6). This yields:

$$P(y_{\mathcal{A}}, y_{\mathcal{B}}) = \sum_s p_s\sum_j|\Omega_{y_{\mathcal{B}}-b_j}(\tau)|^2\sum_{i,i'}\mathcal{C}^{j,s}_{i,i'}(t,\tau)\mathcal{L}_{i,i'}(\Omega_{y_{\mathcal{A}}}(t)), \tag{17}$$

where now $\mathcal{C}^{j,s}_{i,i'} = c^{s,*}_{i'}(t)c^{s,*}_{i',j}(\tau)c^{s}_{i,j}(\tau)c^{s}_{i}(t)$.

The explicit dependence of equation (17) on the wavefunction of the first measuring apparatus tells us that the joint probability of subsequently reading-out the values $y_{\mathcal{A}}$ and $y_{\mathcal{B}}$ will be, in most general conditions, a function of the system-meter coupling strength of the first measurement. As it will be evident later, the fact that equation (17) depends on the second measuring apparatus is irrelevant for the purposes of this work.

Note that, when the state of the system prior to the measurement of $\mathcal{A}$ can be defined as an incoherent sum of eigenstates of $\hat{A}$, equation (17) reduces to (see appendix A),

$$P(y_{\mathcal{A}}, y_{\mathcal{B}}) = \sum_s p_s |\Omega_{y_{\mathcal{A}}-a_s}(t)|^2 \sum_j |\Omega_{y_{\mathcal{B}}-b_j}(\tau)|^2 |c^s_j(\tau)|^2, \tag{18}$$

where $c^s_j(\tau) = \langle b_j|\hat{U}_\tau|a_s\rangle$. Equation (18) can be equivalently written as,

$$P(y_{\mathcal{A}}, y_{\mathcal{B}}) = \sum_s p_s P_s(y_{\mathcal{A}}) P_s(y_{\mathcal{B}}), \tag{19}$$

where we have identified $P_s(y_{\mathcal{A}}) = |\Omega_{y_{\mathcal{A}}-a_s}(t)|^2$ and $P_s(y_{\mathcal{B}}) = \sum_j |\Omega_{y_{\mathcal{B}}-b_j}(\tau)|^2 |c^s_j(\tau)|^2$. Therefore, even if the two-time measurement process becomes two independent (single-time) measurement processes, the result in equation (19) still depends on the wavefunction of the first measuring apparatus through $P_s(y_{\mathcal{A}})$. This can be expressed more succinctly as:

$$\text{C3: } \frac{\mathrm{d}}{\mathrm{d}\sigma_{\mathcal{A}}} P(y_{\mathcal{A}}, y_{\mathcal{B}}) \neq 0, \tag{20}$$

which represents a third condition for witnessing the use of generalized von Neumann measurements in the laboratory.

As the reader may have noticed, there is only one escape to the condition in equation (20), viz, that the classical distribution of pure states p_s in equation (6) is such that the sum in equations (17) or (19) leads to $\frac{\mathrm{d}}{\mathrm{d}\sigma_{\mathcal{A}}} P(y_{\mathcal{A}}, y_{\mathcal{B}}) = 0$. This situation, however, could be understood only under a 'conspiratorial' action. To see that, note that the classical distribution p_s that makes $\frac{\mathrm{d}}{\mathrm{d}\sigma_{\mathcal{A}}} P(y_{\mathcal{A}}, y_{\mathcal{B}}) = 0$ depends on the number of different $\sigma_{\mathcal{A}}$ considered to experimentally evaluate equation (20). That is, the violation of equation (20) requires the design of p_s as well as the number of pure states involved in the initial mixed state of equation (6) to be in accordance with the specific experimental receipt that is later used to evaluate the derivative $\mathrm{d}/\mathrm{d}\sigma_{\mathcal{A}}$.

Let us finally note that there is some confusion in the literature with respect to the WM regime. It is not uncommon to find works where it is stated that a WM is one for which it is always possible to extract information of a system and at the same time reduce the backaction on the system to an arbitrary small amount by adjusting the strength of the coupling between system and measuring apparatus. Such a conclusion is wrong. Even the so-called 'ideal negative result measurements' [12–15] may not change the properties of objects themselves, but they alter their subsequent time evolution due to an instant (nonlocal) change of the quantum wave function, thus violating the result in equation (19) [16]. This consideration will bring us later in section 3.2 to introduce one of the main results of our work: even if the quantum backaction of the measuring apparatus cannot be eliminated, and hence two-time probabilities depend on $\sigma_{\mathcal{A}}$, this backaction can be minimized to the level where marginal probabilities are independent of the coupling strength between system and measuring apparatus.

2.4. Two-time expectation values

Starting from the general result in equation (17) it is easy to evaluate the expectation value of the two-time correlation function $\langle y_{\mathcal{A}}(t)y_{\mathcal{B}}(\tau)\rangle = \iint \mathrm{d}y_{\mathcal{A}}\,\mathrm{d}y_{\mathcal{B}} y_{\mathcal{B}} y_{\mathcal{A}} y_{\mathcal{B}} P(y_{\mathcal{A}}, y_{\mathcal{B}})$ as:

$$\langle y_{\mathcal{A}}(t)y_{\mathcal{B}}(\tau)\rangle = \sum_s p_s \int \mathrm{d}y_{\mathcal{B}} y_{\mathcal{B}} \sum_j |\Omega_{y_{\mathcal{B}}-b_j}(\tau)|^2 \sum_{i,i'} \mathcal{C}^{j,s}_{i,i'}(t,\tau) \int \mathrm{d}y_{\mathcal{A}} y_{\mathcal{A}} \mathcal{L}_{i,i'}(\Omega_{y_{\mathcal{A}}}(t)). \tag{21}$$

Using the center-of-mass property of the meter wavefunction, $\int \mathrm{d}y_{\mathcal{B}} y_{\mathcal{B}} |\Omega_{y_{\mathcal{B}}-b_j}(\tau)|^2 = b_j$, the above equation reduces to:

$$\langle y_{\mathcal{A}}(t)y_{\mathcal{B}}(\tau)\rangle = \sum_s p_s \sum_j b_j \sum_{i,i'} \mathcal{C}^{j,s}_{i,i'}(t,\tau) \int \mathrm{d}y_{\mathcal{A}} y_{\mathcal{A}} \mathcal{L}_{i,i'}(\Omega_{y_{\mathcal{A}}}(t)). \tag{22}$$

In general equation (22) depends on the wavefunction of the measuring apparatus of the property $\mathcal{A}$. However, the result in equation (22) can be simplified when the initial state is an incoherent sum of

eigenstates of $\hat{A}$. Specifically, the joint probability can be then written as in equation (19) and consequently the two-time correlation function in equation (22) reduces to:

$$\langle y_{\mathcal{A}}(t) y_{\mathcal{B}}(\tau)\rangle = \sum_s p_s \int \mathrm{d}y_{\mathcal{A}} y_{\mathcal{A}} P_s(y_{\mathcal{A}}) \int \mathrm{d}y_{\mathcal{B}} y_{\mathcal{B}} P_s(y_{\mathcal{B}}) = \sum_s p_s \langle\psi_s|\hat{A}(t)|\psi_s\rangle\langle\psi_s|\hat{B}(\tau)|\psi_s\rangle, \tag{23}$$

where we have introduced the definition of the Heisenberg operators, $\hat{B}(\tau) = \hat{U}_\tau^\dagger \hat{B} \hat{U}_\tau$ and $\hat{A}(t) = \hat{A}$. Therefore, for incoherent sums of eigenstates of $\hat{A}$, two-time expectation values do not depend on the measuring apparatus of the first measurement of $\mathcal{A}$.

Note that, except for initial pure states, the equality in equation (23) cannot be assessed experimentally because the terms $\langle\psi_s|\hat{A}(t)|\psi_s\rangle$ and $\langle\psi_s|\hat{B}(\tau)|\psi_s\rangle$ cannot be practically evaluated (since p_s expresses our ignorance about the initial state).

3. Testing realism with generalized von Neumann measurements

We now want to show that the two-time generalized von Neumann measurements described above are good candidates for testing microrealism. As it will be shown in section 3.1, two-time generalized von Neumann measurements fulfill the so-called NSIT condition for systems with a property $\mathcal{A}$ fulfilling (R1). Therefore testing the NSIT condition using two-time generalized von Neumann measurements can be used to accomplish (R2) and hence to design a thought experiment to distinguish between coherent and incoherent sum of eigenstates of a property $\mathcal{A}$. Later in section 3.2 we will conceive a protocol that allows to address (R3) by witnessing the proper implementation of generalized von Neumann measurements in the lab.

3.1. No-signaling in time

To see that generalized von Neumann measurements fulfill the NSIT condition for realistic properties we simply need to evaluate the marginal probability of the joint probability $P(y_{\mathcal{A}}, y_{\mathcal{B}})$ for mixed states of the form $\hat{\rho} = \sum_s p_s |a_s\rangle\langle a_s|$. Using the joint probability in equation (19) we can already write,

$$\text{NSIT}: \int \mathrm{d}y_{\mathcal{A}} P(y_{\mathcal{A}}, y_{\mathcal{B}}) = \int \mathrm{d}y_{\mathcal{A}} \sum_s p_s P_s(y_{\mathcal{A}}) P_s(y_{\mathcal{B}}) = \sum_s p_s P_s(y_{\mathcal{B}}) = P(y_{\mathcal{B}}), \tag{24}$$

where we have used $\int \mathrm{d}y_{\mathcal{A}} P_s(y_{\mathcal{A}}) = 1$. For initial states described by an incoherent sum of eigenstates of $\hat{A}$, we have thus trivially recovered the NSIT condition of references [16, 25, 45]. On the contrary, for initial states where $|\psi_s\rangle = \sum_i c_i^s(t)|a_i\rangle$ are not eigenstates of $\hat{A}$, equation (17) does not simplify to equation (19) and thus the NSIT condition in equation (24) cannot be reached except for a very particular system-meter coupling regime (as it will be shown below). Therefore two-time generalized von Neumann measurements in combination with the NSIT condition are hereby proven to be 'good' measurements for testing the realism of a quantum object with respect to a property $\mathcal{A}$ and hence can be thought of as a realization of (R2).

3.2. The weak measurement regime: addressing (R3)

If one could witness the proper implementation of generalized von Neumann measurements in the laboratory, and thus ensure (R3), then the fulfillment of the NSIT condition in equation (24) would readily imply that the property $\mathcal{A}$ is microrealistic (and that it is non-microrealistic otherwise). If, on the contrary, we cannot assert the use of generalized von Neumann measurements in the laboratory, then, based on the violation of equation (24) one can only conclude that the property $\mathcal{A}$ of a system is either (i) non-microrealistic or (ii) microrealistic but subjected to a measurement technique that happens to be invasive.

We thus need to conceive an experiment that allows us to enforce the correspondence between thought and practical experiments. In other words, we need to make sure that the implementation of the two-time generalized von Neumann measurements in the lab has been done correctly. In this respect, in section 2 we have already derived three preliminary conditions (C1)–(C3), viz equations (8), (11) and (20), that have to be fulfilled by any generalized von Neumann measurement. Unfortunately, these conditions have been proven to be necessary but not sufficient for an experimental setup to be representative of a two-time generalized von Neumann measurement. In order to make the validation of the use of this type of measurements in the laboratory more convincing and hence minimize a hypothetical experimental clumsiness, we here introduce two more necessary conditions. These two additional conditions will be based on the WM regime defined in section 2.1, under which two-time correlation functions and marginal probabilities will be proven to be independent of the system-meter coupling strength of first measurement

apparatus. As it will be evident later, the existence of the WM regime will also facilitate the reproducibility of tests of realism based on generalized von Neumann measurements.

In the WM regime, where $\sigma_{\mathcal{A}} \gg \mathrm{d}_{\mathrm{eff}}$, the meter wavefunction of the measuring apparatus of $\mathcal{A}$ can be approximated using a Taylor series up to first order around $y_{\mathcal{A}}$ and thus the last addend in equation (17) can be written as:

$$\mathcal{C}^{j,s}_{i,i'}(t,\tau)\mathcal{L}_{i,i'}(\Omega_{y_{\mathcal{A}}}(t)) = \mathcal{C}^{j,s}_{i,i'}(t,\tau)\left(\Omega_{y_{\mathcal{A}}}(t) - \frac{\partial\Omega_{y_{\mathcal{A}}}(t)}{\partial y_{\mathcal{A}}}a_i\right)\left(\Omega_{y_{\mathcal{A}}}(t) - \frac{\partial\Omega_{y_{\mathcal{A}}}(t)}{\partial y_{\mathcal{A}}}a_{i'}\right). \tag{25}$$

Introducing the above expansion in equation (17) and integrating over $y_{\mathcal{A}}$, the marginal of the joint probability $P(y_{\mathcal{A}}, y_{\mathcal{B}})$ can be written as:

$$\int \mathrm{d}y_{\mathcal{A}} P(y_{\mathcal{A}}, y_{\mathcal{B}}) = \sum_s p_s \sum_j |\Omega_{y_{\mathcal{B}}-b_j}(\tau)|^2 \sum_{i,i'} \mathcal{C}^{j,s}_{i,i'}(t,\tau)\left(1 + a_{i'}a_i \int \mathrm{d}y_{\mathcal{A}}\left(\frac{\partial\Omega_{y_{\mathcal{A}}}(t)}{\partial y_{\mathcal{A}}}\right)^2\right), \tag{26}$$

where we have used the normalization condition $\int \mathrm{d}y_{\mathcal{A}}|\Omega_{y_{\mathcal{A}}}|^2 = 1$ and also that (integrating by parts) $\int \mathrm{d}y_{\mathcal{A}}\Omega_{y_{\mathcal{A}}}\frac{\partial\Omega_{y_{\mathcal{A}}}}{\partial y_{\mathcal{A}}} = |\Omega_{y_{\mathcal{A}}}|^2|_{-\infty}^{+\infty} - \int \mathrm{d}y_{\mathcal{A}}\frac{\partial\Omega_{y_{\mathcal{A}}}}{\partial y_{\mathcal{A}}}\Omega_{y_{\mathcal{A}}} = 0$ for well normalized wavefunctions that fulfill $|\Omega_{y_{\mathcal{A}}}|^2 \to 0$ when $y_{\mathcal{A}} \to -\infty, \infty$.

Next we evaluate the integral in equation (26) by parts, i.e.:

$$\int \mathrm{d}y_{\mathcal{A}}\left(\frac{\partial\Omega_{y_{\mathcal{A}}}(t)}{\partial y_{\mathcal{A}}}\right)^2 = \frac{\partial\Omega_{y_{\mathcal{A}}}(t)}{\partial y_{\mathcal{A}}}\Omega_{y_{\mathcal{A}}}(t)|_{-\infty}^{\infty} - \int \mathrm{d}y_{\mathcal{A}}\frac{\partial^2\Omega_{y_{\mathcal{A}}}(t)}{\partial y_{\mathcal{A}}^2}\Omega_{y_{\mathcal{A}}}(t). \tag{27}$$

The first term on the r.h.s of Equation (27) is zero because $\Omega_{y_{\mathcal{A}}} \to 0$ when $y_{\mathcal{A}} \to -\infty, \infty$. The second term in Equation (27) can also be equated to zero when multiplied by $a_{i'}a_i$ and the corresponding coefficients $C^{j,s}_{i,i'}$ if we notice that in Equation (25) we already considered terms containing higher order derivatives to be negligible under the WM regime. We then conclude that:

$$\int \mathrm{d}y_{\mathcal{A}} P(y_{\mathcal{A}}, y_{\mathcal{B}}) = \sum_s p_s \sum_j |\Omega_{y_{\mathcal{B}}-b_j}(\tau)|^2 \sum_{i,i'} \mathcal{C}^{j,s}_{i,i'}(t,\tau) = P(y_{\mathcal{B}}), \tag{28}$$

where we have used that $\sum_{i,i'}\mathcal{C}^{j,s}_{i,i'}(t,\tau) = |c^s_j(\tau)|^2$ and that $P(y_{\mathcal{B}}) = \sum_s p_s P_s(y_{\mathcal{B}}) = \sum_s p_s \sum_j |\Omega_{y_{\mathcal{B}}-b_j}(\tau)|^2 |c^s_j(\tau)|^2$.

The result in (28) has a clear cut meaning. In the WM regime where $\sigma_{\mathcal{A}} \gg d_{\mathrm{eff}}$ the NSIT condition in (24) is fulfilled either for initial states described by a coherent or an incoherent sum of eigenstates of $\mathcal{A}$. In other words:

$$\text{C4:} \quad \int \mathrm{d}y_{\mathcal{A}} P(y_{\mathcal{A}}, y_{\mathcal{B}}) = P(y_{\mathcal{B}}) \quad \forall\sigma_{\mathcal{A}} \gg \mathrm{d}_{\mathrm{eff}}. \tag{29}$$

Note that the above result can be equivalently stated as $\mathrm{d}\int \mathrm{d}y_{\mathcal{A}} P(y_{\mathcal{A}}, y_{\mathcal{B}})/\mathrm{d}\sigma_{\mathcal{A}} = 0$ for any $\sigma_{\mathcal{A}} \gg \mathrm{d}_{\mathrm{eff}}$, as $P(y_{\mathcal{B}})$ is independent of $\sigma_{\mathcal{A}}$. That is, in the WM regime the marginal probability of the joint probability describing a two-time generalized von Neumann measurement is independent of the system-meter coupling of the first measurement.

The WM regime has also implications on the two-time correlation function $\langle y_{\mathcal{A}}(t)y_{\mathcal{B}}(\tau)\rangle$ of equation (22). Specifically, it can be shown (see appendix B) that two-time correlation functions are also independent of the coupling parameter $\sigma_{\mathcal{A}}$ when this parameter is much larger than the effective dimension of the system, i.e.:

$$\text{C5:} \quad \frac{\mathrm{d}}{\mathrm{d}\sigma_{\mathcal{A}}}\langle y_{\mathcal{A}}(t)y_{\mathcal{B}}(\tau)\rangle = \sum_s p_s \frac{\mathrm{d}}{\mathrm{d}\sigma_{\mathcal{A}}}\mathrm{Re}\langle\psi_s(t)|\hat{B}(\tau)\hat{A}(t)|\psi_s(t)\rangle = 0 \quad \forall\sigma_{\mathcal{A}} \gg \mathrm{d}_{\mathrm{eff}}, \tag{30}$$

where we have used again the definition of the Heisenberg operators, $\hat{B}(\tau) = \hat{U}^{\dagger}_{\tau}\hat{B}\hat{U}_{\tau}$ and $\hat{A}(t) = \hat{A}$.

Note that since d_{eff} is not known in practice, assessing the WM regime (by evaluating equations (29) and (30)) requires the design of a number of measurement set-ups with different system-meter coupling strengths $\sigma_{\mathcal{A}}$. The larger the number of measurement set-ups that are compared one against each other the more trustworthy the assessment of the WM regime will be. Put differently, the probability that (C4) and (C5) are fulfilled simultaneously by a number of measurement apparatuses different from the generalized von Neumann measurements described here is expected to decrease with the number of experimental set-ups used to validate these two conditions.

3.3. Proposal for a test of realism

We are now in a position to propose a test of microrealism. This test is based on the following two steps:

(S1) Make sure that the measurement of $\mathcal{A}$ at time t is carried out using a generalized von Neumann measurement. This can be done by assessing conditions (C1)–(C5).

(S2) Test the NSIT condition for a range of system-meter couplings ($0 \lesssim \sigma_{\mathcal{A}} \lesssim \infty$). A property $\mathcal{A}$ is realistic if the NSIT condition is satisfied for all $\sigma_{\mathcal{A}}$ and non-realistic otherwise.

Note that for a system consisting of a coherent sum of eigenstates of $\hat{A}$ at time t, the NSIT condition is fulfilled only for a certain range of $\sigma_{\mathcal{A}}$, which defines the WM regime. Therefore, whenever the NSIT condition is violated, having proven the validity of conditions (C1)–(C5) will be the only guarantee that the actual experimental set-up represents a generalized von Neumann measurement. Alternatively, for a system consisting of an incoherent sum of eigenstates at time t, the NSIT condition is fulfilled independently of $\sigma_{\mathcal{A}}$, which means that any generalized von Neumann measurement is, by construction, carried out in the WM regime.

Also important is the fact that the proposed test in (S1) and (S2) is highly reproducible. Reproducibility is certainly a delicate issue in quantum mechanics. Measuring an observable $\mathcal{A}$ at time t and correlating the outcome, $y_{\mathcal{A}}(t)$, with the measured value of $\mathcal{B}$, $y_{\mathcal{B}}(\tau)$, at a later time $\tau \geqslant t$, represents an unequivocal way of representing the dynamics of classical systems in terms of joint probabilities, i.e., $P(y_{\mathcal{A}}, y_{\mathcal{B}}) \leftrightarrow$ system dynamics. In quantum mechanics, however, the unavoidable backaction of the measurement process [46, 47] precludes such a clear-cut connection. Even using the best technological means, different measurement schemes, can yield different probability distributions, i.e., $P(y_{\mathcal{A}}, y_{\mathcal{B}}) \leftrightarrow$ system + apparatus dynamics. Potentially, this property of quantum mechanics could result in contradictions among different tests of realism that are based on different experimental set-ups. In this respect, testing the NSIT condition for a previously validated, through conditions (C1)–(C5), experimental set-up makes the results of different experiments easy to compare one to each other.

Let us note that the use of two operators $\hat{A}$ and $\hat{B}$ that commute with the Hamiltonian has to be excluded from our test. This is because for this type of properties the time order of the measurements is irrelevant and the two-time measurements can be understood as a single measurement at a particular time with two different ancillas. In this circumstance, it is impossible to discern between a coherent and incoherent sum of states by simply analysing the statistics of a single measurement, and hence our test would not work. However, since we are only interested in knowing the nature of a property with respect to the initial state (prior to the first measurement), it is enough to ensure that the second measured property $\mathcal{B}$ does not commute with the Hamiltonian. Therefore, the property $\mathcal{B}$ must be always chosen such that its corresponding operator $\hat{B}$ does not commute with $\hat{A}$. This makes our test robust against any type of property.

Let us finally mention that the test defined by steps (S1) and (S2) is based on the NSIT condition and hence it allows to witness the nature of very general type of properties, i.e., not only of (bounded) dichotomic variables as it happens in tests based on the Leggett–Garg inequalities.

3.4. Collusion loopholes

The reader can still mention an unavoidable loophole the existence of which is sustained on the ability of, for example, classical simulations to reproduce any quantum measurement statistics. Certainly, classical simulations of quantum measurement statistics can be always thought of as alternative descriptions of Leggett–Garg's (but also Bell's) inequalities that are simply *possible* at the conceptual level. Following this line of thought, a sufficiently adroit 'demon' could always introduce a classical computer within our measuring instruments to falsify the output statistics. This type of loophole is indeed inherent to the consideration of any no-go theorem from the conceptual point of view, and hence it could invalidate not only any existing test of micro- or macrorealism (e.g., [12, 48] or [49]), but achingly, also any test of local realism reported to date (e.g., [50, 51], or [52]). In the practical context, however, while *possible*, loopholes based on, e.g., superluminal causes, super-determinism or acyclic retro-causation are commonly ruled out as wildly *implausible*. Examples of thorough philosophical accounts on conspiratorial loopholes can be found in references [31, 53, 54].

But, moreover, let us notice that one of the main virtues of the proposed protocol, (S1) and (S2), is that, due to its intrinsic (possibly collaborative) nature involving a number of different experimental set-ups for assessing the WM regime, it can be also utilized to unveil a hypothetical conspiracy. Testing the WM conditions (C4) and (C5) as well as conditions (C1)–(C3) should allow us to confine the type of measurements used in the lab to the class of generalized von Neumann measurements described in section 2.

4. When to expect genuine macrorealism?

The protocol described in (S1) and (S2) only assesses realism for a quantum object at a given time t and with respect to a property $\mathcal{A}$. As we indicated in the introduction, in a test of macrorealism where our classical intuition about physical objects is at stake, the validity of the NSIT condition in equation (24) should be proven for all observables at any time. In this respect, it is well-known that the Bell–Kochen–Specker theorems [7, 55] puts important restrictions on how such macrorealism can be made compatible with quantum mechanics. Here we argue that what Leggett and Garg called macrorealism should be expected only with respect to observables representing intensive (non-additive) properties of systems with a (very) large number of particles. More precisely, we define *genuine macrorealism* as follows:

- A quantum object is *genuinely macrorealistic* when it is microrealistic with respect to all intensive (non-additive) properties at any time.

For pure states, the concept of genuine macrorealism can be understood as follows. Let us consider an intensive property $\mathcal{A}$ associated to the N-particle operator:

$$\hat{A} = \frac{1}{N}\sum_{\xi=1}^{N} \hat{A}_\xi, \tag{31}$$

where $\hat{A}_\xi = \hat{I} \otimes \cdots \otimes \hat{a} \otimes \cdots \otimes \hat{I}$, and the index ξ denotes the degree of freedom that the single-particle operator, $\hat{a}$, acts on. We then define the states $|a_{i_1}, \ldots, a_{i_N}\rangle = |a_{i_1}\rangle \otimes \cdots \otimes |a_{i_N}\rangle$ to be the eigenstates of $\hat{A}$, i.e., $\hat{A}|a_{i_1}, \ldots, a_{i_N}\rangle = \bar{a}_i |a_{i_1}, \ldots, a_{i_N}\rangle$, where

$$\bar{a}_i = \frac{1}{N}\sum_{\xi=1}^{N} a_{i_\xi}, \tag{32}$$

are the corresponding eigenvalues, with $\hat{a}|a_{i_\xi}\rangle = a_{i_\xi}|a_{i_\xi}\rangle$.

Given the above definition, we now want to determine in what circumstances the general state in equation (1) becomes an eigenstate of the intensive operator $\hat{A}$ in equation (31), i.e., $\hat{A}|\psi(t)\rangle \approx \langle\hat{A}(t)\rangle|\psi(t)\rangle$. For that, we will look for the identity $\langle\hat{A}^2(t)\rangle = \langle\hat{A}(t)\rangle^2$ which is satisfied only for quantum systems whose property $\mathcal{A}$ is at any time t coincident with the expectation value $\langle\hat{A}(t)\rangle$. At this point we will consider only pure many-particle states, as the addition of a classical degree of uncertainty in the form of a mixed state will only require a post-processing (without any conceptual implication).

We start by writing the expectation value $\langle\hat{A}(t)\rangle$ as:

$$\langle\hat{A}(t)\rangle = \sum_{i_1,\ldots,i_N} \bar{a}_i |c_{i_1,\ldots,i_N}(t)|^2 = \frac{1}{N}\sum_{i_1,\ldots,i_N}\sum_{\xi=1}^{N} |c_{i_1,\ldots,i_N}(t)|^2 a_{i_\xi}, \tag{33}$$

where we have introduced the coefficients $c_{i_1,\ldots,i_N}(t) = \langle a_{i_1}| \otimes \cdots \otimes \langle a_{i_N}|\psi(t)\rangle$ and we have used that $\langle a_{i_1}, \ldots, a_{i_N}|\hat{A}_\xi|a_{i'_1}, \ldots, a_{i'_N}\rangle = a_{i'_\xi}\delta_{i_1,i'_1}\cdots\delta_{i_N,i'_N}$. Thus,

$$\langle\hat{A}(t)\rangle^2 = \frac{1}{N^2}\sum_{\substack{i_1,\ldots,i_N \\ i'_1,\ldots,i'_N}}\sum_{\xi,\nu}^{N} |c_{i_1,\ldots,i_N}(t)|^2 |c_{i'_1,\ldots,i'_N}(t)|^2 a_{i_\xi} a_{i'_\nu}. \tag{34}$$

On the other hand, by writing

$$\hat{A}^2 = \frac{1}{N^2}\left(\sum_{\xi=1}^{N}\hat{A}_\xi^2 + \sum_{\xi=1}^{N}\sum_{\nu\neq\xi}^{N}\hat{A}_\xi\hat{A}_\nu\right), \tag{35}$$

we can easily evaluate $\langle\hat{A}^2(t)\rangle$ as:

$$\langle\hat{A}^2(t)\rangle = \frac{1}{N^2}\left(\sum_{i_1,\ldots,i_N}\sum_{\xi=1}^{N} |c_{i_1,\ldots,i_N}(t)|^2 a_{i_\xi}^2 + \sum_{i_1,\ldots,i_N}\sum_{\xi=1}^{N}\sum_{\nu\neq\xi}^{N} |c_{i_1,\ldots,i_N}(t)|^2 a_{i_\xi} a_{i_\nu}\right). \tag{36}$$

To make the comparison between equations (34) and (36) simpler, we rewrite the above expression as:

$$\langle\hat{A}^2(t)\rangle = \frac{1}{N^2}\sum_{\substack{i_1,\ldots,i_N \\ i'_1,\ldots,i'_N}}\sum_{\xi,\nu}^{N} |c_{i_1,\ldots,i_N}(t)|^2 |c_{i'_1,\ldots,i'_N}(t)|^2 a_{i_\xi} a_{i_\nu}, \tag{37}$$

where we have introduced the identity $\sum_{i'_1,\ldots,i'_N}|c_{i'_1,\ldots,i'_N}(t)|^2=1$. The dispersion of the intensive property $\mathcal{A}$, defined as $\mathrm{Var}(\mathcal{A}(t))=\langle\hat{A}(t)\rangle^2-\langle\hat{A}^2(t)\rangle$, can be finally written as:

$$\mathrm{Var}(\mathcal{A}(t))=\frac{1}{N^2}\sum_{\substack{i_1,\ldots,i_N\\ i'_1,\ldots,i'_N}}\sum_{\xi,\nu}^{N}|c_{i_1,\ldots,i_N}(t)|^2|c_{i'_1,\ldots,i'_N}(t)|^2a_{i_\xi}\left(a_{i'_\nu}-a_{i_\nu}\right), \tag{38}$$

which is in general different from zero.

4.1. Genuine macrorealistic many-particle systems

Examples of genuine macrorealism, far from being atypical, can be common for large systems made of weakly-correlated particles. Assume that a many particle quantum system can be well approximated by a separable state:

$$|\psi(t)\rangle=|\psi_1(t)\rangle\otimes\cdots\otimes|\psi_N(t)\rangle, \tag{39}$$

where $|\psi_i(t)\rangle$ are arbitrary time-dependent single-particle states. Introducing equation (39) into equation (34) one gets:

$$\langle\hat{A}(t)\rangle^2=\frac{1}{N^2}\sum_{\xi=1}^{N}\langle a_\xi(t)\rangle^2+\frac{1}{N^2}\sum_{\xi=1}^{N}\langle a_\xi(t)\rangle\sum_{\nu\neq\xi}^{N}\langle a_\nu(t)\rangle \tag{40}$$

where $\langle a_\xi(t)\rangle=\sum_i|c_{i_\xi}(t)|^2a_{i_\xi}$ and we have used that $c_{i_1,\ldots,i_N}(t)=c_{i_1}(t)\cdots c_{i_N}(t)$ and that $\sum_i|c_{i_\xi}(t)|^2=1$ for any ξ. On the other hand, introducing equation (39) into equation (36) we get:

$$\langle\hat{A}^2(t)\rangle=\frac{1}{N^2}\sum_{\xi=1}^{N}\langle a_\xi^2(t)\rangle+\frac{1}{N^2}\sum_{\xi=1}^{N}\langle a_\xi(t)\rangle\sum_{\nu\neq\xi}^{N}\langle a_\nu(t)\rangle, \tag{41}$$

where $\langle a_\xi^2(t)\rangle=\sum_i|c_{i_\xi}(t)|^2a_{i_\xi}^2$. We can now write $\mathrm{Var}(\mathcal{A}(t))=\langle\hat{A}(t)^2\rangle-\langle\hat{A}(t)\rangle^2$ using equations (40) and (41) as:

$$\mathrm{Var}(\mathcal{A}(t))=\frac{1}{N^2}\sum_{\xi=1}^{N}\left(\langle a_\xi^2(t)\rangle-\langle a_\xi(t)\rangle^2\right)=\frac{1}{N^2}\sum_{\xi=1}^{N}\mathrm{Var}(a_\xi(t)). \tag{42}$$

In view of equation (42), the identity $\langle\hat{A}^2\rangle=\langle\hat{A}\rangle^2$ is not valid in general because $\mathrm{Var}(a_\xi(t))=\langle a_\xi^2(t)\rangle-\langle a_\xi(t)\rangle^2\neq0$, which means that the state in (39) is not an eigenstate of the operator $\hat{A}$ in equation (31). However, as $N\to\infty$, $\mathrm{Var}(\mathcal{A}(t))\to0$ because, even though equation (42) involves N finite addends, it is divided by N^2. Then, the many particle quantum state in equation (39) meets the condition $\langle\hat{A}^2\rangle=\langle\hat{A}\rangle^2$, and hence we conclude that $\hat{A}|\psi(t)\rangle=\langle\hat{A}\rangle|\psi(t)\rangle$ in the limit $N\to\infty$.

This result means that, even if individually $|\psi_\xi(t)\rangle$ are not eigenstates of $\hat{a}$, in the limit $N\to\infty$ the many particle quantum state in (39) is an eigenstate of $\hat{A}$. We emphasize that the reason why the many-particle state in (39) becomes an eigenstate of $\hat{A}$ is not because of the specific nature of the single particle states $|\psi_\xi(t)\rangle$ or the operator $\hat{a}$, but because of the limit $N\to\infty$ that we have taken into account to evaluate equation (42). Note that this result might have been explained also using the central limit theorem. For the type of state in equation (39) we know that there is no correlation between the distribution of single-particle eigenvalues $\{a_\xi\}$ and $\{a_\nu\}$ that define the distribution of many-particle eigenvalues $\{\bar{a}\}$ in (32). Then, $\{\bar{a}\}$ can be understood as a normalized sum of independent random variables whose distribution tends towards a normal distribution with a standard deviation given in (42) that goes to zero when $N\to\infty$. This is true for any initial probability distributions of $\{a_\xi\}$ and $\{a_\nu\}$, as far as they are uncorrelated. Thus, according to our previous definitions, we could argue that the many particle quantum state in (39) satisfies genuine macrorealism. This is in contrast with the quantumness of each individual degree of freedom of the quantum system itself, which, being preserved, would prevent us to talk about realism at the microscopic level.

This result can be understood in the context of the quantum-to-classical transition, as it indicates that what we call classical objects are in fact quantum objects with many degrees of freedom that, obeying the laws of quantum mechanics at the microscopic level, do not show quantum uncertainty for non-additive properties. According to the Ehrenfest theorem, an intensive property $\mathcal{A}$ that fulfills $\mathrm{Var}(\mathcal{A}(t))=0$ at any time t seems to imply that its dynamics is compatible with Newton dynamics. This conclusion, which is in accordance with previous works [56–58], can be understood from a pure operational point of view and hence it does not depend on the different interpretations of quantum mechanics.

Finally, let us note that the above exercise based on the evaluation of Var($\mathcal{A}$), while valid for pure states, cannot be used in practice for general mixed states. Alternatively, the test in (S1) and (S2), based on the NSIT condition and the use of generalized von Neumann measurements, should be applied.

4.2. Non-macrorealistic many-particle systems

We now seek for quantum systems with a large number N of particles that do not satisfy genuine macrorealism because of the strong correlations among different particles. One can think, for example, of a non-separable quantum state with probabilities $|c_{i_1,\ldots,i_N}(t)|^2 = 0.5$ when $a_\xi = \alpha, \forall\xi$ and $|c_{i_1,\ldots,i_N}(t)|^2 = 0.5$ when $a_\xi = \beta, \forall\xi$. The resulting state,

$$|\psi(t)\rangle = \sqrt{0.5}|\alpha,\ldots,\alpha\rangle + \sqrt{0.5}|\beta,\ldots,\beta\rangle, \tag{43}$$

is the superposition of two states with different values of the property linked to the single-particle operator $\hat{a}$, so that the mean value of $\hat{A}$ in (33) can be written as:

$$\langle\hat{A}(t)\rangle = \frac{1}{2N}\sum_{\xi=1}^{N}\alpha + \frac{1}{2N}\sum_{\xi=1}^{N}\beta = \frac{1}{2}(\alpha+\beta), \tag{44}$$

which tells that there is a 50% probability of measuring all N particles with a well-defined value α of the property a, and another 50% probability of measuring all N particles with a well-defined value β of the property a. Introducing the state in equation (43) into (36) we also get:

$$\langle\hat{A}^2(t)\rangle = \frac{1}{2N^2}\sum_{\xi,\nu}^{N}\alpha^2 + \frac{1}{2N^2}\sum_{\xi,\nu}^{N}\beta^2 = \frac{1}{2}(\alpha^2+\beta^2). \tag{45}$$

We can now write $\mathrm{Var}(\mathcal{A}(t)) = \langle\hat{A}(t)\rangle^2 - \langle\hat{A}^2(t)\rangle = (\alpha-\beta)^2/4$. Clearly, $\langle\hat{A}^2(t)\rangle \neq \langle\hat{A}(t)\rangle^2$ even when $N\to\infty$. This means that the state defined in (43) will never be an eigensate of $\hat{A}$, and hence the interference effects between the state $|\alpha,\ldots,\alpha\rangle$ and the state $|\beta,\ldots,\beta\rangle$ will prevail at the macroscopic ($N\to\infty$) level[9].

4.3. Numerical example: center-of-mass position of N uncoupled harmonic oscillators

To illustrate the proposed test of microrealism, we consider a simple numerical experiment. For a simple analytical example, the reader can take a look at the results in appendix C for a spin qubit. Alternatively, here we will evaluate the autocorrelation function of the center-of-mass position operator, $\hat{X} = \sum_{\xi=1}^{N}\hat{X}_\xi/N$ (where the index ξ denotes the degree of freedom that the single-particle operator $\hat{X}_\xi$ acts on for a number N of uncoupled one-dimensional double-well oscillator (see figure 1). Hereafter we use atomic units, $\hbar = m = 1$, and define the single-particle oscillator Hamiltonian as:

$$\hat{H} = \sum_{\xi=1}^{N}\hat{P}_\xi^2/2 + \omega_0^2\hat{X}_\xi^2/2 + \cosh^{-2}(\alpha\hat{X}_\xi), \tag{46}$$

where $\hat{P}_\xi$ is the ξth momentum operator and the natural frequency of the underlying harmonic oscillator is $\omega_0 = 4.3\times10^{-3}$ a.u. The characteristic width of the barrier between the two wells is set to $\alpha = 5\times10^{-2}$ a.u and we choose $t = 0$ such that the only relevant time in the discussion is $\tau \geqslant 0$.

We consider an initial pure state which consists of all the oscillators being prepared in the ground state, i.e., $|\psi(t)\rangle = |\psi_1^{(\mathrm{g})}(t)\rangle\otimes\cdots\otimes|\psi_N^{(\mathrm{g})}(t)\rangle$, where $|\psi_i^{(\mathrm{g})}(t)\rangle$ represents the ground state of the i-th harmonic oscillator. For pure states, assessing the NSIT condition is equivalent to checking equation (23), i.e.:

$$\mathrm{NSIT} \Leftrightarrow \langle y_\mathcal{A}(t)y_\mathcal{B}(\tau)\rangle = \langle y_\mathcal{A}(t)\rangle\langle y_\mathcal{B}(\tau)\rangle \quad \forall\,\text{pure state}. \tag{47}$$

Note that for initial mixed states the equivalence in equation (47) cannot be attained due to the (classical) ignorance associated to the result in equation (23), i.e., $\langle y_\mathcal{A}(t)y_\mathcal{B}(\tau)\rangle = \sum_s p_s\langle\psi_s|\hat{A}|\psi_s\rangle\langle\psi_s|\hat{B}|\psi_s\rangle \neq \langle y_\mathcal{A}(t)\rangle\langle y_\mathcal{B}(\tau)\rangle$. This explains why, for general mixed states, a test of realism must be based on the NSIT condition in equation (24) instead.

By assuming at this point a Gaussian-type meter wavefunction of the form $\Omega_{y-a_j} = \frac{1}{2\sigma\sqrt{\pi}}\exp\left[-(y-a_j)^2/4\sigma^2\right]$, and taking the non-interacting limit of equation (22) we obtain (see appendix D):

[9] A relevant question is which type of state, equation (39) or equation (43), is more common in nature as $N\to\infty$. Although such discussion is far from the scope of this work, we believe that entropic arguments can be invoked to justify that genuine macrorealism is more and more common as the number of particles grows. By far, the state (43) requires much more order than the state in (39).

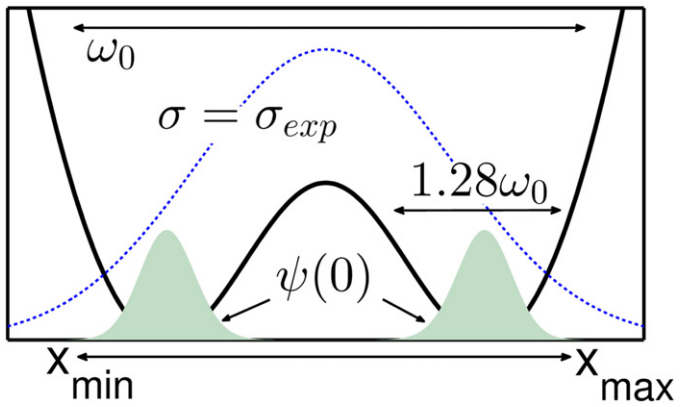

Figure 1. Schematic picture of the double-well oscillator. The potential energy curve is plot in solid black line. The initial state of the system (area in green) is taken to be the ground state of the system. Two main frequencies are involved in the dynamics of the system, viz, ω_0 and $1.28\omega_0$, related respectively with the inter-well and intra-well dynamics. The relevant upper and lower bounds of the spectrum of $\hat{X}$ are denoted by $x_{\max}$ and $x_{\min}$ respectively, and the exponential function defined in equation (49b) is depicted for a particular value of σ_X in dashed blue line.

$$\langle y_{\mathcal{A}}(t) y_{\mathcal{B}}(\tau)\rangle = \frac{1}{2N}\sum_{i,j}^{\infty} \mathcal{E}_{j,i}\mathfrak{B}_{j,i}\left(a_i + (N-1)\langle \hat{A}(t)\rangle\right) + \text{c.c.}, \tag{48}$$

where we have defined the coefficients:

$$\mathfrak{B}_{\substack{i_1,\ldots,i_N \\ j_1,\ldots,j_N}} = \langle a_{j_1},\ldots,a_{j_N}|\hat{B}(\tau)|a_{i_1},\ldots,a_{i_N}\rangle, \tag{49a}$$

$$\mathcal{E}_{\substack{i_1,\ldots,i_N \\ j_1,\ldots,j_N}} = c^*_{j_1,\ldots,j_N}\ \exp\left[-\frac{\left(\sum_{\nu}^{N} a_{i_\nu} - a_{j_\nu}\right)^2}{8\sigma_{\mathcal{A}}^2 N^2}\right] c_{i_1,\ldots,i_N}. \tag{49b}$$

Note that in the limit of $N \to \infty$ equation (48) trivially reduces to $\langle y_{\mathcal{A}}(t)\rangle\langle y_{\mathcal{B}}(\tau)\rangle$. The result in equation (48) generally depends on the system-meter coupling $\sigma_{\mathcal{A}}$, and only in the limit where the measuring apparatus for measuring the property $\mathcal{A}$ has a dispersion $\sigma_{\mathcal{A}}$ much larger than the effective dimension of the system $d_{\text{eff}} := \sum_{\nu=1}^{N} \max(\{\Delta\mathcal{A}_\nu\})/N$, where $\max(\{\Delta\mathcal{A}_\nu\})$ is the distance between the highest and lowest occupied eigenstates of the spectrum of $\hat{A}_\nu$, then equation (48) reduces to:

$$\text{WM} \Leftrightarrow \langle y_{\mathcal{A}}(t) y_{\mathcal{B}}(\tau)\rangle = \text{Re}\left(\langle\psi(t)|\hat{B}(\tau)\hat{A}(t)|\psi(t)\rangle\right) \quad \forall \text{ pure state}. \tag{50}$$

The dynamics of a single oscillator for different values of σ_X is shown in figure 2. For a projective measurement, i.e., $\sigma_X \to 0$, the dynamics presents a central resonance peak at ω_0 (in dashed red line). This is due to the strong perturbation induced by the projective measurement at $t = 0$, which yields a subsequent dynamics characterized by a large amplitude (over-the-barrier) oscillation. Contrarily, in the limit $\sigma_X \to \infty$ the measurement produces only a small perturbation to the initial state and yields an ensuing dynamics confined in the wells with a characteristic frequency $\omega = 1.28\omega_0$ (in dashed blue line). In between these two regimes, an infinite number of dynamics can be inferred depending on the system-meter coupling σ_X (in black solid lines).

To conclude whether the position of a single oscillator is microrealistic in a reproducible manner, we need to ensure that the measurement of X is carried out using a generalized von Neumann measurement, and then compare the expectation values $\langle y(0)y(\tau)\rangle$ and $\langle y(0)\rangle\langle y(\tau)\rangle$. Steps (S1) and (S2), or equivalently equations (47) and (50), can be assessed in a compact way through the quantity:

$$\Delta(\sigma_X, N) = \frac{\mathrm{d}\langle y_X(0)y_X(\tau)\rangle}{\mathrm{d}\sigma_X}\mathrm{d}\sigma_X - \Delta_{\text{QC}} \tag{51}$$

where $\Delta_{\text{QC}} = \langle y_X(0)y_X(\tau)\rangle - \langle y_X(0)\rangle\langle y_X(\tau)\rangle$. This can be seen as follows. Consider first the WM regime where (C4) and (C5) are fulfilled. Then equation (51) reduces to $\Delta(\sigma_X, N) = -\Delta_{\text{QC}} = f(N)$, where $f(N)$ is a function only of N (not of σ_X). This can be seen by noticing that equation (50) does not depend on σ_X (see also the condition (C5) in equation (30)) and thus the first term in equation (51) is zero. Also, according to (C2) in equation (11) the term Δ_{QC} does not depend on σ_X and thus $\Delta(\sigma_X, N)$ is a function

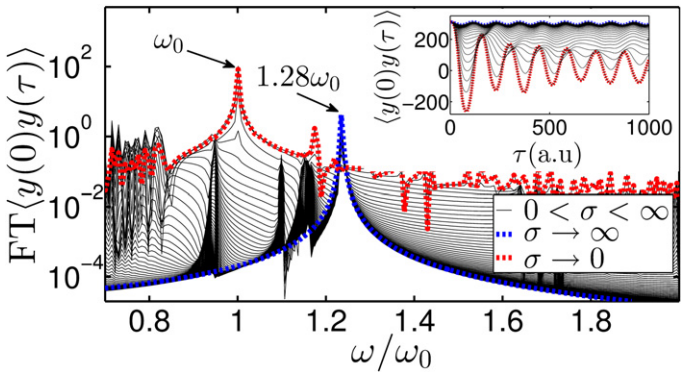

Figure 2. Semi-log plot of the Fourier transform of the autocorrelation function in equation (48) as a function of σ_X and τ (solid black lines). The limits of $\sigma_X \to 0$ and $\sigma_X \to \infty$ are shown respectively in dashed red and blue lines. In the inset: the same results but for the autocorrelation function.

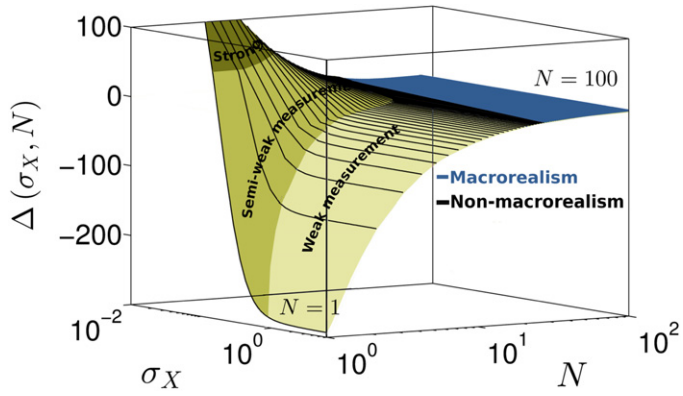

Figure 3. $\Delta(\sigma_X, N)$ as a function of σ_X and the number N of oscillators for $\tau = 33.3\pi$. Results for the strong, semi-weak and weak measurement regimes, depending on the system-meter coupling parameter σ_X, have different underlying colors associated. Non-realistic and realistic results are shown in black and blue respectively.

only of N. Thus, the fulfillment of (S1) implies, in particular, the existence of a plateau of $\Delta(\sigma_X, N)$ for large enough $\sigma_{\mathcal{A}}$.

Step (S2) is as follows. If the NSIT condition in equation (47) is fulfilled then $\langle y_X(0)y_X(\tau)\rangle = \langle y_X(0)\rangle\langle y_X(\tau)\rangle$ and hence $\Delta_{\mathrm{QC}} = 0$. If this holds for any $\sigma_{\mathcal{A}}$ and not only in the WM regime, then the property is realist. Alternatively, if the NSIT condition in equation (47) is not fulfilled or fulfilled only in the WM regime, then the property is non-realist.

In figure 3 we plot the quantity $\Delta(\sigma_X, N)$ as a function of σ_X and the number N of oscillators. Whenever $\Delta(\sigma_X, N)$ becomes constant, equation (50) is fulfilled, and whether the center-of-mass position is realistic or not can be checked by simply evaluating $\Delta(\sigma_X, N)$ in the asymptotic region, i.e., X is realistic if $\Delta(\sigma_X, N)$ vanishes in the asymptotic region and non-realistic otherwise. A single oscillator is non-microrealistic with respect to X because $\Delta(\sigma_X, 1)$ changes with $\sigma_{\mathcal{A}}$ and furthermore it converges to a non-zero value in the WM regime (i.e., for $\sigma_{\mathcal{A}} \to \infty$). For $N > 1$, the N oscillators become entangled right after the first measurement process. This yields a smooth transition (exponential decay with N) between the non-microrealistic (in black) and macrorealistic (in blue) results (for $N \lesssim 30$ and $N \gtrsim 30$ respectively). That is, for a large enough number of double well oscillators, the dynamics of $\hat{X}$ becomes entirely independent of σ_X, which is a clear-cut signature of genuine macrorealism.

5. Conclusions

Testing the reality of an object according to orthodox quantum mechanics requires a strict control of the correspondence between thought and real (implemented) experiments. This is crucial, e.g., to avoid the so-called 'clumsiness loophole'. In this work we have proposed a test of realism that is based on witnessing the use of generalized von Neumann measurements in the lab. Assessing conditions (C1)–(C3), respectively in equations (8), (11) and (20), and conditions (C4) and (C5), in equations (29) and (30), allows to

critically narrow experimental clumsiness and thereafter testing the NSIT condition in equation (24) for a range of system-meter couplings $\sigma_{\mathcal{A}}$ allows to determine, unequivocally, whether a property $\mathcal{A}$ is realistic or not.

Importantly, the resulting protocol, i.e., (S1) and (S2), is robust for any type of property. This includes tests in situations where Leggett–Garg inequalities and ideal negative measurement cannot be used at all, e.g., unbounded and non-dichotomic properties. Furthermore, the fact that the proposed test involves the validation of the measurement apparatus in the WM regime makes its conclusions independent of the system-meter coupling of the first measurement and thus also highly reproducible.

We have also showed that any intensive property $\mathcal{A}$ of a quantum system made of a large enough number of weakly-correlated particles is microrealistic at any time. Only rather exotic quantum systems, with a very high degree of order, do not satisfy this property. This result has been used to define genuine macrorealistic objects as quantum objects that are microrealistic with respect to all intensive properties at any time. Noticeably, genuine macrorealism is compatible with the existence of non-microrealistic properties of the quantum object at the microscopic level (when, for example, only a fraction of the total number of the degrees of freedom is considered).

The above conclusions have been numerically exemplified by testing the nature of the center-of-mass position of a number N of one-dimensional double-well oscillators. In general, the N oscillators become entangled right after the first measurement and this allows a smooth transition between the non-microrealistic and microrealistic results. For a large enough number N of oscillators, the dynamics of the center-of-mass position becomes completely independent of the system-meter coupling strength of the first measurement, a clear signature of genuine macrorealism.

Our results, in accordance with previous works, indicate that what we call classical objects are in fact quantum objects with many degrees of freedom that, obeying the laws of quantum mechanics, satisfy microrealism for all intensive properties at any time.

Acknowledgments

DP and XO acknowledge financial support from Spain's Ministerio de Ciencia, Innovación y Universidades under Grant No. RTI2018-097876-B-C21 (MCIU/AEI/FEDER, UE), the Generalitat de Catalunya under Grant No 001-P-001644 (QUANTUM CAT). The European Union's Horizon 2020 research and innovation programme under grant agreement No Graphene Core2 785219 and under the Marie Skodowska-Curie Grant agreement No 765426 (TeraApps). GA also acknowledge financial support from the European Union's Horizon 2020 research and innovation programme under the Marie Sklodowska–Curie Grant agreement No 752822, the Spanish Ministerio de Economía y Competitividad (CTQ2016-76423-P), and the Generalitat de Catalunya (2017 SGR 348).

Appendix A. Derivation of joint probability in equation (18)

We start with the general expression for the two-time joint probability in equation (17),

$$P(y_{\mathcal{A}}, y_{\mathcal{B}}) = \sum_s p_s \sum_j |\Omega_{y_{\mathcal{B}}-b_j}(\tau)|^2 \sum_{i,i'} \mathcal{C}^{j,s}_{i,i'}(t,\tau)\mathcal{L}_{i,i'}(\Omega_{y_{\mathcal{A}}}(t)). \tag{A.1}$$

By rewriting the coefficients $\mathcal{C}^{j,s}_{i,i'}(t,\tau)$ as:

$$\mathcal{C}^{j,s}_{i,i'}(t,\tau) = c^{s,*}_{i'}(t)c^{s,*}_{i',j}(\tau)c^{s}_{i,j}(\tau)c^{s}_{i}(t) = \langle\psi_s(t)|a_{i'}\rangle\langle a_{i'}|\hat{U}^{\dagger}_{\tau}|b_j\rangle\langle b_j|\hat{U}_{\tau}|a_i\rangle\langle a_i|\psi_s(t)\rangle, \tag{A.2}$$

and using $|\psi_s\rangle = |a_s\rangle$ we get,

$$\mathcal{C}^{j,s}_{i,i'} = \delta_{s,i'}\langle a_{i'}|\hat{U}^{\dagger}_{\tau}|b_j\rangle\langle b_j|\hat{U}_{\tau}|a_i\rangle\delta_{i,s}. \tag{A.3}$$

Introducing equation (A.3) back into equation (A.1) we already get equation (18) of the main text:

$$P(y_{\mathcal{A}}, y_{\mathcal{B}}) = \sum_s p_s |\Omega_{y_{\mathcal{A}}-a_s}(t)|^2 \sum_j |c^{s}_{j}(\tau)|^2 |\Omega_{y_{\mathcal{B}}-b_j}(\tau)|^2, \tag{A.4}$$

where $c^{s}_{j}(\tau) = \langle b_j|\hat{U}_{\tau}|a_s\rangle$. By identifying $P_s(y_{\mathcal{A}}) = |\Omega_{y_{\mathcal{A}}-a_s}(t)|^2$ and $P_s(y_{\mathcal{B}}) = \sum_j |c^{s}_{j}(\tau)|^2 |\Omega_{y_{\mathcal{B}}-b_j}(\tau)|^2$, equation (A.4) can be finally written as in equation (19), i.e.:

$$P(y_{\mathcal{A}}, y_{\mathcal{B}}) = \sum_s p_s P_s(y_{\mathcal{A}}) P_s(y_{\mathcal{B}}). \tag{A.5}$$

Appendix B. Derivation of equation (30)

Using equation (25) and the center-of-mass property of the meter wavefunction $\int \mathrm{d}y_{\mathcal{B}}|\Omega_{y_{\mathcal{B}}-b_j}|^2 = b_j$, equation (22) reads:

$$\langle y_{\mathcal{A}}(t)y_{\mathcal{B}}(\tau)\rangle = \int \mathrm{d}y_{\mathcal{A}}y_{\mathcal{A}}\sum_s p_s\sum_j b_j\sum_{i,i'}\mathcal{C}^{j,s}_{i,i'}(t,\tau)\left(\Omega_{y_{\mathcal{A}}}(t)-\frac{\partial\Omega_{y_{\mathcal{A}}}(t)}{\partial y_{\mathcal{A}}}a_i\right)\left(\Omega_{y_{\mathcal{A}}}(t)-\frac{\partial\Omega_{y_{\mathcal{A}}}(t)}{\partial y_{\mathcal{A}}}a_{i'}\right). \quad \text{(B.1)}$$

Now, using the following three equalities, $\int \mathrm{d}y_{\mathcal{A}}y_{\mathcal{A}}\Omega_{y_{\mathcal{A}}}\frac{\partial\Omega_{y_{\mathcal{A}}}}{\partial y_{\mathcal{A}}} = -1/2$, $\int \mathrm{d}y_{\mathcal{A}}y_{\mathcal{A}}\left(\frac{\partial\Omega_{y_{\mathcal{A}}}}{\partial y_{\mathcal{A}}}\right)^2 = 0$, and $\int \mathrm{d}y_{\mathcal{A}}y_{\mathcal{A}}\Omega^2_{y_{\mathcal{A}}} = 0$, equation (B.1) can be written as:

$$\langle y_{\mathcal{A}}(t)y_{\mathcal{B}}(\tau)\rangle = \sum_s p_s\sum_j b_j\sum_{i,i'}\mathcal{C}^{j,s}_{i,i'}(t,\tau)\frac{(a_i+a'_i)}{2}. \quad \text{(B.2)}$$

Using then the explicit form of the coefficients,

$$\mathcal{C}^{j,s}_{i,i'}(t,\tau) = \langle\psi_s(t)|a_{i'}\rangle\langle a_{i'}|\hat{U}^\dagger_\tau|b_j\rangle\langle b_j|\hat{U}_\tau|a_i\rangle\langle a_i|\psi_s(t)\rangle, \quad \text{(B.3)}$$

and the spectral decomposition of the operators $\hat{A}$ and $\hat{B}$, equation (B.2) finally simplifies to:

$$\langle y_{\mathcal{A}}(t)y_{\mathcal{B}}(\tau)\rangle = \sum_s p_s\ \mathrm{Re}\left(\langle\psi_s(t)|\hat{B}(\tau)\hat{A}(t)|\psi_s(t)\rangle\right), \quad \text{(B.4)}$$

where we have introduced the definition of the Heisenberg operators, $\hat{B}(\tau) = \hat{U}^\dagger_\tau\hat{B}\hat{U}_\tau$ and $\hat{A}(t) = \hat{A}$. The above result is independent of the wavefunction of the meter of $\mathcal{A}$, and hence we conclude that in the WM regime the following equation must be fulfilled:

$$\text{C5}: \ \frac{\mathrm{d}}{\mathrm{d}\sigma_{\mathcal{A}}}\langle y_{\mathcal{A}}(t)y_{\mathcal{B}}(\tau)\rangle = 0 \quad \forall\sigma_{\mathcal{A}} \gg \mathrm{d}_{\mathrm{eff}}. \quad \text{(B.5)}$$

Appendix C. Test of microrealism for a single qubit state

Consider a spin qubit represented by the state:

$$|\psi(t)\rangle = c_0|s_{x0}\rangle + c_1|s_{x1}\rangle \quad \text{(C.1)}$$

where $|c_0|^2 + |c_1|^2 = 1$, and $|s_{x0}\rangle = \frac{1}{\sqrt{2}}\begin{pmatrix}1\\1\end{pmatrix}$ and $|s_{x1}\rangle = \frac{1}{\sqrt{2}}\begin{pmatrix}1\\-1\end{pmatrix}$ are the eigenstates of the Pauli matrix $\hat{\sigma}_x$. The evolution of the state in equation (C.1) is dictated by the following Hamiltonian,

$$\hat{H} = \hat{S}_z = \frac{\hbar}{2}\hat{\sigma}_z, \quad \text{(C.2)}$$

where $\hat{S}_z$ is the spin operator in the z direction and $\hat{\sigma}_z$ is the z Pauli matrix.

Whether the initial state in equation (C.1) is an eigenstate of the spin operator $\hat{S}_x = \frac{\hbar}{2}\hat{\sigma}_x$ can be tested using our protocol in (S1) and (S2). In a real experiment we should first address (S1), however, in this thought experiment we can presuppose (S1) and move directly to step (S2). For that, we only need to test the NSIT condition in equation (24). This can be done by comparing the probability distribution of measuring $\hat{S}_x$ only at time τ, i.e., $P(y_{s_\tau}) = \sum_{j=1}^2|\Omega_{y_{s_\tau}-s_j}(\tau)|^2|c_j(\tau)|^2$, with the result in equation (16), which here reads:

$$\int \mathrm{d}y_{s_t}P(y_{s_t},y_{s_\tau}) = \sum_{j=1}^2|\Omega_{y_{s_\tau}-s_j}(\tau)|^2\sum_{i,i'=1}^2\mathcal{C}^j_{i,i'}(\tau,t)\int \mathrm{d}y_{s_t}\Omega^*_{y_{s_t}-s_{i'}}(t)\Omega_{y_{s_t}-s_i}(t), \quad \text{(C.3)}$$

where y_{s_t} and y_{s_τ} are the outcomes of the first (at time t) and second (at time τ) measurement of $\hat{S}_x$ respectively. Now, for superposition states where both c_0 and c_1 are different from zero, it is easy to realize that:

$$\int \mathrm{d}y_{s_t}P(y_{s_t},y_{s_\tau}) \neq P(y_{s_\tau}), \quad \text{(C.4)}$$

except for the case where the measurement of $\hat{S}_x$ is carried out in the WM regime, where $\int \mathrm{d}y_{s_t}\Omega^*_{y_{s_t}-s_{i'}}(t)\Omega_{y_{s_t}-s_i}(t) = 1$ and thus we can use $\sum_{i,i'=1}^2\mathcal{C}^j_{i,i'}(\tau,t) = |\langle s_{xj}|U_\tau|\psi(t)\rangle|^2 = |c_j(\tau)|^2$. Therefore, for general system-meter coupling strengths the NSIT condition (see equation (24)) is not fulfilled, and thus

the property $\hat{S}_x$ of the system is non-microrealistic. Alternatively, if the initial state in equation (C.1) is an eigenstate of $\hat{S}_x$, then either c_0 or c_1 is zero, and according to the definition of the coefficients $C^j_{i,i'}$ it is easy to see that (C.3) always reduces to:

$$\int \mathrm{d}y_{s_t} P(y_{s_t}, y_{s_\tau}) = P(y_{s_\tau}), \tag{C.5}$$

independently of the system-meter coupling strength. Therefore, we can conclude that the system is microrealistic with respect to $\hat{S}_x$.

C.1. Alternative test based on two-time time-correlation functions

Since in our example we considered a pure initial state, we also could have used two-time correlation functions instead of joint probabilities to arrive to the same conclusions. To see that, let us first consider equation (22), which here reads:

$$\langle y_{s_t} y_{s_\tau}\rangle = \sum_{i',i=1}^{2} c^*_{i'} \langle s_{x_{i'}}|\hat{S}_x(\tau)|s_{x_i}\rangle c_i \int \mathrm{d}y_{s_t} y_{s_t} \Omega^*_{y_{s_t}-s_{i'}}(t)\Omega_{y_{s_t}-s_i}(t), \tag{C.6}$$

where we have defined $\hat{S}_x(\tau) = \hat{U}^\dagger_\tau \hat{S}_x(t)\hat{U}_\tau$. In our particular example the operator $\hat{S}_x(t) = |s_{x0}\rangle s_0 \langle s_{x0}| + |s_{x1}\rangle s_1 \langle s_{x1}|$ where $s_0 = +1$ and $s_1 = -1$ are the eigenvalues corresponding to the eigenstates $|s_{x0}\rangle$ and $|s_{x1}\rangle$ respectively. We can alternately define $\hat{S}_x(t) = |s_{z0}\rangle s_0 \langle s_{z1}| - |s_{z1}\rangle s_1 \langle s_{z0}|$ in the basis of our Hamiltonian $\hat{S}_z$ just to facilitate the derivation. The evolution of $\hat{S}_x(t)$ in the Heisenberg picture can be then written as:

$$\hat{S}_x(\tau) = \mathrm{e}^{\mathrm{i}\tau\omega}|s_{z0}\rangle s_0 \langle s_{z1}| - \mathrm{e}^{-\mathrm{i}\tau\omega}|s_{z1}\rangle s_1 \langle s_{z0}|, \tag{C.7}$$

where we have defined $\omega = (E_0 - E_1)/\hbar$. Introducing equation (C.7) into equation (C.6) we obtain,

$$\langle y_{s_t} y_{s_\tau}\rangle = \sum_{i',i=1}^{2} c^*_{i'} c_i \left(\mathrm{e}^{\mathrm{i}\tau\omega}\langle s_{x_{i'}}|s_{z0}\rangle s_0 \langle s_{z1}|s_{x_i}\rangle - \mathrm{e}^{-\mathrm{i}\tau\omega}\langle s_{x_{i'}}|s_{z1}\rangle s_1 \langle s_{z0}|s_{x_i}\rangle\right) \int \mathrm{d}y_{s_t} y_{s_t} \Omega^*_{y_{s_t}-s_{i'}}(t)\Omega_{y_{s_t}-s_i}(t). \tag{C.8}$$

We now switch back to the $\hat{S}_x$ basis, i.e., $|s_{z0}\rangle = \frac{1}{\sqrt{2}}|s_{x0}\rangle + \frac{1}{\sqrt{2}}|s_{x1}\rangle$ and $|s_{z1}\rangle = \frac{1}{\sqrt{2}}|s_{x0}\rangle - \frac{1}{\sqrt{2}}|s_{x1}\rangle$, and note that for a real ancilla wavepacket $\int \mathrm{d}y_{s_t} y_{s_t} \Omega^*_{y_{s_t}-s_0}(t)\Omega_{y_{s_t}-s_1}(t) = \int \mathrm{d}y_{s_t} y_{s_t} \Omega^*_{y_{s_t}-s_1}(t)\Omega_{y_{s_t}-s_0}(t)$. Furthermore since $s_0 = -s_1$, then equation (C.8) can be finally written as:

$$\langle y_{s_t} y_{s_\tau}\rangle = \left(s_0^2|c_0|^2 + s_1^2|c_1|^2\right)\cos(\omega\tau) + \left(2s_1\ \mathrm{Im}\left(c_0 c_1^*\right)\int \mathrm{d}y_{s(t)} y_{s(t)} \Omega^*_{y_{s(t)}-s_0}(t)\Omega_{y_{s(t)}-s_1}(t)\right)\sin(\omega\tau). \tag{C.9}$$

Arrived at this point, it is easy to test whether our initial state is an eigenstate of $\hat{S}_x$ or not. We only need to compare the result in equation (C.9) with the product of single-time expectation values $\langle\hat{S}_x(t)\rangle\langle\hat{S}_x(\tau)\rangle$. When the initial state in equation (C.1) is an eigenstate of $\hat{S}_x$, then either c_1 or c_0 is zero and thus equation (C.9) reduces to:

$$\langle y_{s_t} y_{s_\tau}\rangle = s_0^2\ \cos\ \omega\tau, \tag{C.10}$$

in the case where $|c_0|^2 = 1$ or to $\langle y_{s_t} y_{s_\tau}\rangle = s_1^2\ \cos\ \omega\tau$ in the case where $|c_1|^2 = 1$. For the particular case where $|c_0|^2 = 1$, we also know that $\langle\hat{S}_x(t)\rangle = \langle y_{s_t}\rangle = s_0$ and that $\langle\hat{S}_x(\tau)\rangle = \langle y_{s_\tau}\rangle = \langle s_{x0}|\hat{S}_x(\tau)|s_{x0}\rangle$ which using equation (C.7) yields $\langle\hat{S}_x(\tau)\rangle = s_0\cos\omega\tau$. Therefore, we can write:

$$\langle y_{s_t} y_{s_\tau}\rangle = \langle y_{s_t}\rangle\langle y_{s_\tau}\rangle, \tag{C.11}$$

and hence conclude that the system is microrealistic with respect to $\hat{S}_x$. Note that the same conclusion is reached if we consider $|c_1|^2 = 1$ and $c_0 = 0$. Alternatively, for general superposition states where c_0 and c_1 are both different from zero, equation (C.9) cannot be written as the product of two single-time mean values, i.e.:

$$\langle y_{s_t} y_{s_\tau}\rangle \neq \langle y_{s_t}\rangle\langle y_{s_\tau}\rangle, \tag{C.12}$$

and hence we have to conclude that the system is non-microrealistic with respect to $\hat{S}_x$.

Appendix D. Two-time correlation function for Gaussian meters and separable many-body states: derivation of expression equation (48)

For pure initial states and, equation (22) reduces to:

$$\langle y_{\mathcal{A}}(t) y_{\mathcal{B}}(\tau)\rangle = \sum_j b_j \sum_{i,i'} C^j_{i,i'}(t,\tau)\int \mathrm{d}y_{\mathcal{A}} y_{\mathcal{A}} \mathcal{L}_{i,i'}(\Omega_{y_{\mathcal{A}}}(t)). \tag{D.1}$$

Assuming at this point a Gaussian-type meter wavefunction of the form $\Omega_{y-a_j} = \frac{1}{2\sigma\sqrt{\pi}} \exp\left[-(y-a_j)^2/4\sigma_{\mathcal{A}}^2\right]$, then we can use the property:

$$\int \mathrm{d}y_{\mathcal{A}} y_{\mathcal{A}} \Omega^*_{y_{\mathcal{A}}-a_{i'}}(t)\Omega_{y_{\mathcal{A}}-a_i}(t) = \frac{1}{2}(a_i + a_{i'})\mathrm{e}^{-\frac{(a_i-a_{i'})^2}{8\sigma_{\mathcal{A}}^2}} \tag{D.2}$$

to rewrite (D.1) as:

$$\langle y_{\mathcal{A}}(t) y_{\mathcal{B}}(\tau)\rangle = \frac{1}{2}\sum_j b_j \sum_{i,i'} \mathcal{C}^j_{i,i'}(t,\tau)(a_i + a_{i'})\mathrm{e}^{-\frac{(a_i-a_{i'})^2}{8\sigma_{\mathcal{A}}^2}}, \tag{D.3}$$

where $\mathcal{C}^j_{i,i'}(t,\tau) = c^*_{i'}(t)c^*_{i',j}(\tau)c_{i,j}(\tau)c_i(t)$.

Now, for $\mathcal{A}$ being an intensive property as defined in equation (31), the coefficients $c_i(t)$ and $c_{i,j}(\tau)$ read $c_i(t) \equiv \langle a_{j_1}, \ldots, a_{j_N}|\psi(t)\rangle$ and $c_{i,j}(\tau) \equiv \langle b_{j_1}, \ldots, b_{j_N}|\hat{U}_\tau|a_{i_1}, \ldots, a_{i_N}\rangle$, where $|a_{i_1}, \ldots, a_{i_N}\rangle = |a_{i_1}\rangle \otimes \cdots \otimes |a_{i_N}\rangle$ and $|b_{j_1}, \ldots, b_{j_N}\rangle = |b_{j_1}\rangle \otimes \cdots \otimes |b_{j_N}\rangle$. Considering a separable state $|\psi(t)\rangle = |\psi_1(t)\rangle \otimes \cdots \otimes |\psi_N(t)\rangle$ and the definition of the eigenvalues in equation (32), then equation (D.3) can be rewritten as:

$$\begin{aligned}\langle y_{\mathcal{A}}(t) y_{\mathcal{B}}(\tau)\rangle = \frac{1}{2N^2}\sum_{\xi,\xi'}^{N}\sum_{j_1,\ldots,j_N} b_{j_\xi} \sum_{\substack{i_1,\ldots,i_N \\ i'_1,\ldots,i'_N}} (a_{i_{\xi'}} + a_{i'_{\xi'}})\mathrm{e}^{-\frac{(\sum_{\xi''}^{N} a_{i_{\xi''}} - a_{i'_{\xi''}})^2}{8\sigma_{\mathcal{A}}^2 N^2}} \\ \times \Big(\langle\psi_1(t)|a_{i'_1}\rangle\langle a_{i'_1}|\hat{U}^\dagger_\tau|b_{j_1}\rangle\langle b_{j_1}|\hat{U}_\tau|a_{i_1}\rangle\langle a_{i_1}|\psi_1(t)\rangle \\ \times \langle\psi_N(t)|a_{i'_N}\rangle\langle a_{i'_N}|\hat{U}^\dagger_\tau|b_{j_N}\rangle\langle b_{j_N}|\hat{U}_\tau|a_{i_N}\rangle\langle a_{i_N}|\psi_N(t)\rangle\Big).\end{aligned} \tag{D.4}$$

Now, by separating equation (D.4) into $\xi = \xi'$ and $\xi \neq \xi'$ terms we can write:

$$\begin{aligned}\langle y_{\mathcal{A}}(t) y_{\mathcal{B}}(\tau)\rangle = \frac{1}{2N^2}\sum_{\xi}^{N}\Bigg[\sum_{i_\xi,i'_\xi}(a_{i_\xi} + a_{i'_\xi})\mathrm{e}^{-\frac{(a_{i_\xi}-a_{i'_\xi})^2}{8\sigma_{\mathcal{A}}^2 N^2}}\langle\psi_{\mathcal{A}}|a_{i'_\xi}\rangle\langle a_{i'_\xi}|\hat{U}^\dagger_\tau\hat{B}\hat{U}_\tau|a_{i_\xi}\rangle\langle a_{i_\xi}|\psi_\xi\rangle \\ + \sum_{\xi'\neq\xi}\sum_{\substack{i_1,\ldots,i_N \\ i'_1,\ldots,i'_N}}(a_{i_{\xi'}} + a_{i'_{\xi'}})\mathrm{e}^{-\frac{(\sum_{\xi''}^{N} a_{i_{\xi''}} - a_{i'_{\xi''}})^2}{8\sigma_{\mathcal{A}}^2 N^2}}\Big(\langle\psi_1(t)|a_{i'_1}\rangle\langle a_{i'_1}|a_{i_1}\rangle\langle a_{i_1}|\psi_1(t)\rangle\langle\psi_\xi(t)|a_{i'_\xi}\rangle \\ \times \langle a_{i'_\xi}|\hat{U}^\dagger_\tau\hat{B}\hat{U}_\tau|a_{i_\xi}\rangle\langle a_{i_\xi}|\psi_\xi(t)\rangle\langle\psi_{\xi'}(t)|a_{i'_{\xi'}}\rangle\langle a_{i'_{\xi'}}|a_{i_{\xi'}}\rangle\langle a_{i_{\xi'}}|\psi_{\xi'}(t)\rangle\langle\psi_N(t)|a_{i'_N}\rangle\langle a_{i'_N}|a_{i_N}\rangle \\ \times \langle a_{i_N}|\psi_N(t)\rangle\Big)\Bigg],\end{aligned} \tag{D.5}$$

which, in turn, by using $\langle a_{i'_{\xi'}}|a_{i_{\xi'}}\rangle = \delta_{i',i} \quad \forall k$ can be simplified as:

$$\begin{aligned}\langle y_{\mathcal{A}}(t) y_{\mathcal{B}}(\tau)\rangle = \frac{1}{N^2}\sum_{\xi}^{N}\sum_{i_\xi,i'_\xi} a_{i_\xi}\mathrm{e}^{-\frac{(a_{i_\xi}-a_{i'_\xi})^2}{8\sigma_{\mathcal{A}}^2 N^2}}\langle\psi_\xi|a_{i'_\xi}\rangle\langle a_{i'_\xi}|\hat{U}^\dagger_\tau\hat{B}\hat{U}_\tau|a_{i_\xi}\rangle\langle a_{i_\xi}|\psi_\xi\rangle \\ + \sum_{\xi'\neq\xi}^{N}\sum_{i_\xi,i'_\xi}\mathrm{e}^{-\frac{(a_{i_\xi}-a_{i'_k})^2}{8\sigma_{\mathcal{A}}^2 N^2}}\langle\psi_\xi(t)|a_{i'_\xi}\rangle\langle a_{i'_\xi}|\hat{U}^\dagger_\tau\hat{B}\hat{U}_\tau|a_{i_\xi}\rangle\langle a_{i_\xi}|\psi_\xi(t)\rangle\langle\psi_{\xi'}(t)|\hat{A}|\psi_{\xi'}(t)\rangle + \text{c.c.}\end{aligned} \tag{D.6}$$

By rearranging terms we can re-express (D.6) as:

$$\langle y_{\mathcal{A}}(t) y_{\mathcal{B}}(\tau)\rangle = \frac{1}{2N^2}\sum_{\xi}^{N}\sum_{i_\xi,i'_\xi}\mathrm{e}^{-\frac{(a_{i_\xi}-a_{i'_\xi})^2}{8\sigma_{\mathcal{A}}^2 N^2}}\langle\psi_\xi|a_{i'_\xi}\rangle\langle a_{i'_\xi}|\hat{B}(\tau)|a_{i_\xi}\rangle\langle a_{i_\xi}|\psi_\xi\rangle\left(a_{i_\xi} + \sum_{k\neq\xi'}^{N}\langle\psi_{\xi'}(t)|\hat{A}(t)|\psi_{\xi'}(t)\rangle\right) + \text{c.c.} \tag{D.7}$$

Finally, by assuming $|\psi_\xi(t)\rangle = |\psi(t)\rangle \quad \forall k$ we obtain:

$$\langle y_{\mathcal{A}}(t) y_{\mathcal{B}}(\tau)\rangle = \frac{1}{2N}\sum_{i,i'} e^{-\frac{(a_i - a_{i'})^2}{8\sigma_{\mathcal{A}}^2 N^2}} \langle\psi|a_{i'}\rangle\langle a_{i'}|\hat{B}(\tau)|a_i\rangle\langle a_i|\psi\rangle \left(a_i + (N-1)\langle\hat{A}(t)\rangle\right) + \text{c.c.}, \tag{D.8}$$

which, using the definitions in equations (49a) and (49b), can be rewritten as in equation (48) of the main text:

$$\langle y_{\mathcal{A}}(t) y_{\mathcal{B}}(\tau)\rangle = \frac{1}{2N}\sum_{i,j} \mathcal{E}_{j,i}\mathfrak{B}_{j,i}\left(a_i + (N-1)\langle\hat{A}(t)\rangle\right) + \text{c.c.} \tag{D.9}$$

ORCID iDs

Devashish Pandey https://orcid.org/0000-0003-0349-6913

References

[1] Fine A and Brown H R 1988 *The Shaky Game: Einstein, Realism and the Quantum Theory* (Chicago, IL: University of Chicago Press)
[2] Zeilinger A 2005 *Nature* **438** 743
[3] Kovachy T, Asenbaum P, Overstreet C, Donnelly C, Dickerson S, Sugarbaker A, Hogan J and Kasevich M 2015 *Nature* **528** 530
[4] Ockeloen-Korppi C, Damskägg E, Pirkkalainen J M, Asjad M, Clerk A, Massel F, Woolley M and Sillanpää M 2018 *Nature* **556** 478
[5] Einstein A, Podolsky B and Rosen N 1935 *Phys. Rev.* **47** 777
[6] Bell J S 1964 *Phys. Phys. Fiz.* **1** 195
[7] Bell J S 2004 *Speakable and Unspeakable in Quantum Mechanics: Collected Papers on Quantum Philosophy* (Cambridge: Cambridge University Press)
[8] Leggett A J and Garg A 1985 *Phys. Rev. Lett.* **54** 857
[9] Leggett A J 1988 *Found. Phys.* **18** 939–52
[10] Leggett A J 2008 *Rep. Prog. Phys.* **71** 022001
[11] Leggett A J 2002 *J. Phys.: Condens. Matter.* **14** R415
[12] Knee G C *et al* 2012 *Nat. Commun.* **3** 606
[13] Robens C, Alt W, Meschede D, Emary C and Alberti A 2015 *Phys. Rev.* X **5** 011003
[14] Katiyar H, Brodutch A, Lu D and Laflamme R 2017 *New J. Phys.* **19** 023033
[15] Bose S, Home D and Mal S 2018 *Phys. Rev. Lett.* **120** 210402
[16] Kofler J and Brukner Č 2013 *Phys. Rev.* A **87** 052115
[17] Maroney O and Timpson C 2014 Quantum-vs. macro-realism: What does the Leggett-Garg inequality actually test? arXiv:1412.6139
[18] Maxwell N 1976 *Found. Phys.* **6** 275–92
[19] Emary C, Lambert N and Nori F 2013 *Rep. Prog. Phys.* **77** 016001
[20] Palacios-Laloy A, Mallet F, Nguyen F, Bertet P, Vion D, Esteve D and Korotkov A N 2010 *Nat. Phys.* **6** 442
[21] Goggin M, Almeida M, Barbieri M, Lanyon B, O'brien J, White A and Pryde G 2011 *Proc. Natl Acad. Sci.* **108** 1256–61
[22] Benatti F, Ghirardi G and Grassi R 1994 *Found. Phys. Lett.* **7** 105–26
[23] Greenberger D M, Horne M A, Shimony A and Zeilinger A 1990 *Am. J. Phys.* **58** 1131–43
[24] Mermin N D 1993 *Rev. Mod. Phys.* **65** 803
[25] Li C M, Lambert N, Chen Y N, Chen G Y and Nori F 2012 *Sci. Rep.* **2** 885
[26] Wilde M M and Mizel A 2012 *Found. Phys.* **42** 256–65
[27] Clauser J F and Shimony A 1978 *Rep. Prog. Phys.* **41** 1881
[28] Kwiat P G, Eberhard P H, Steinberg A M and Chiao R Y 1994 *Phys. Rev.* A **49** 3209
[29] Huelga S F, Ferrero M and Santos E 1995 *Phys. Rev.* A **51** 5008
[30] Rosenfeld W, Weber M, Volz J, Henkel F, Krug M, Cabello A, Zukowski M and Weinfurter H 2009 *Adv. Sci. Lett.* **2** 469–74
[31] Cuffaro M E 2017 *Br. J. Phil. Sci.* **69** 633–55
[32] Dressel J, Broadbent C, Howell J and Jordan A N 2011 *Phys. Rev. Lett.* **106** 040402
[33] von Neumann J 2018 *Mathematical Foundations of Quantum Mechanics: New Edition* (Princeton, NJ: Princeton University Press)
[34] Jacobs K 2014 *Quantum Measurement Theory and its Applications* (Cambridge: Cambridge University Press)
[35] Jacobs K and Steck D A 2006 *Contemp. Phys.* **47** 279–303
[36] Wiseman H M and Milburn G J 2009 *Quantum Measurement and Control* (Cambridge: Cambridge University Press)
[37] Bednorz A, Belzig W and Nitzan A 2012 *New J. Phys.* **14** 013009
[38] Bednorz A, Franke K and Belzig W 2013 *New J. Phys.* **15** 023043
[39] Moreira S V, Keller A, Coudreau T and Milman P 2015 *Phys. Rev.* A **92** 062132
[40] Novelli A, Belzig W and Nitzan A 2015 *New J. Phys.* **17** 013001
[41] Barchielli A, Lanz L and Prosperi G 1982 *Il Nuovo Cimento* B **72** 79–121
[42] Bednorz A and Belzig W 2008 *Phys. Rev. Lett.* **101** 206803
[43] Ochoa M A, Belzig W and Nitzan A 2018 *Sci. Rep.* **8** 15781
[44] Kraus K 1983 *States, Effects and Operations: Fundamental Notions of Quantum Theory* (Berlin: Springer)
[45] Kofler J and Brukner Č 2008 *Phys. Rev. Lett.* **101** 090403
[46] Braginsky V B, Braginsky V B and Khalili F Y 1995 *Quantum Measurement* (Cambridge: Cambridge University Press)
[47] Dicke R H 1981 *Am. J. Phys.* **49** 925–30
[48] Knee G C, Kakuyanagi K, Yeh M C, Matsuzaki Y, Toida H, Yamaguchi H, Saito S, Leggett A J and Munro W J 2016 *Nat. Commun.* **7** 1–5

[49] Formaggio J, Kaiser D, Murskyj M and Weiss T 2016 *Phys. Rev. Lett.* **117** 050402
[50] Weihs G, Jennewein T, Simon C, Weinfurter H and Zeilinger A 1998 *Phys. Rev. Lett.* **81** 5039
[51] Hensen B *et al* 2015 *Nature* **526** 682
[52] Shalm L K *et al* 2015 *Phys. Rev. Lett.* **115** 250402
[53] Palmer T 2015 *Phil. Trans. R. Soc.* A **373** 20140246
[54] Lewis P J 2006 *Br. J. Phil. Sci.* **57** 359–81
[55] Kochen S and Specker E P 1975 *The Problem of Hidden Variables in Quantum Mechanics* (*The Logico-Algebraic Approach to Quantum Mechanics*) (Berlin: Springer) pp 293–328
[56] Kochen S 2015 *Found. Phys.* **45** 557–90
[57] Oriols X and Benseny A 2017 *New J. Phys.* **19** 063031
[58] Kofler J and Brukner Č 2007 *Phys. Rev. Lett.* **99** 180403
[59] d'Espagnat B 2018 *Conceptual Foundations of Quantum Mechanics* (Boca Raton, FL: CRC Press)

Publication B

Devashish Pandey, Enrique Colomés, Guillermo Albareda, and Xavier Oriols. Stochastic Schrödinger Equations and Conditional States: A General Non-Markovian Quantum Electron Transport Simulator for THz Electronics. *Entropy*, 21(12), 2019

entropy

MDPI

Article

Stochastic Schrödinger Equations and Conditional States: A General Non-Markovian Quantum Electron Transport Simulator for THz Electronics

Devashish Pandey [1], Enrique Colomés [1], Guillermo Albareda [1,2,3,*] and Xavier Oriols [1,*]

[1] Departament d'Enginyeria Electrònica, Universitat Autònoma de Barcelona, 08193 Bellaterra (Barcelona), Spain; devashishpandey21@gmail.com (D.P.); e.colomescapon@gmail.com (E.C.)
[2] Max Planck Institute for the Structure and Dynamics of Matter, 22761 Hamburg, Germany
[3] Institute of Theoretical and Computational Chemistry, Universitat de Barcelona, 08028 Barcelona, Spain
* Correspondence: guillermo.albareda@mpsd.mpg.de (G.A.); xavier.oriols@uab.cat (X.O.)

Received: 25 October 2019; Accepted: 21 November 2019; Published: 25 November 2019

Abstract: A prominent tool to study the dynamics of open quantum systems is the reduced density matrix. Yet, approaching open quantum systems by means of state vectors has well known computational advantages. In this respect, the physical meaning of the so-called conditional states in Markovian and non-Markovian scenarios has been a topic of recent debate in the construction of stochastic Schrödinger equations. We shed light on this discussion by acknowledging the Bohmian conditional wavefunction (linked to the corresponding Bohmian trajectory) as the proper mathematical object to represent, in terms of state vectors, an arbitrary subset of degrees of freedom. As an example of the practical utility of these states, we present a time-dependent quantum Monte Carlo algorithm to describe electron transport in open quantum systems under general (Markovian or non-Markovian) conditions. By making the most of trajectory-based and wavefunction methods, the resulting simulation technique extends to the quantum regime, the computational capabilities that the Monte Carlo solution of the Boltzmann transport equation offers for semi-classical electron devices.

Keywords: conditional states; conditional wavefunction; Markovian and Non-Markovian dynamics; stochastic Schrödinger equation; quantum electron transport

1. Introduction

Thanks to its accuracy and versatility, the Monte Carlo solution of the Boltzmann transport equation has been, for decades, the preferred computational tool to predict the DC, AC, transient, and noise performances of semi-classical electron devices [1]. In the past decade, however, due to the miniaturization of electronic devices (with active regions approaching the de Broglie wavelength of the transport electrons), a majority of the device modeling community has migrated from semi-classical to fully quantum simulation tools, marking the onset of a revolution in the community devoted to semiconductor device simulation. Today, a number of quantum electron transport simulators are available to the scientific community [2–4]. The amount of information that these simulators can provide, however, is mainly restricted to the stationary regime and therefore their predicting capabilities are still far from those of the traditional Monte Carlo solution of the semi-classical Boltzmann transport equation [1]. This limitation poses a serious problem in the near future as electron devices are foreseen to operate at the Terahertz (THz) regime. At these frequencies, the discrete nature of electrons in the active region is expected to generate unavoidable fluctuations of the current that could interfere with the correct operation of such devices both for analog and digital applications [5].

A formally correct approach to electron transport beyond the quasi-stationary regime lies on the description of the active region of an electron device as an open quantum system [6,7]. As such, one can

then borrow any state-of-the-art mathematical tool developed to study open quantum systems [8,9]. A preferred technique has been the stochastic Schrödinger equation (SSE) approach [10–17]. Instead of directly solving equations of motion for the reduced density matrix, the SSE approach exploits the state vector nature of the so-called conditional states to alleviate some computational burden (and ensure a complete positive map by construction [18]). Even if this technique allows to always reconstruct the full density matrix, a discussion on whether dynamical information can be directly extracted from such conditional states in non-Markovian scenarios has appeared recently in the literature [19,20]. This debate is very relevant to us as we are interested in computing not only one-time expectation values (i.e., DC performance) but also dynamical properties (i.e., AC, transient, and noise), such as multi-time correlation functions, at THz frequencies. At these frequencies the environment correlations are expected to decay on a time-scale comparable to the time-scale relevant for the system evolution [21]. Furthermore, the displacement current becomes important at very high frequencies and a self-consistent solution of the Maxwell equations and the Schrödinger equation is necessary [21,22].

Some light on how to utilize the SSE technique to access dynamical information without the need of reconstructing the reduced density matrix has already been shed by Wiseman and Gambetta by acknowledging the Bohmian conditional wavefunction as the proper mathematical tool to describe general open quantum systems in non-Markovian scenarios [23,24]. In this work we reinforce this idea by showing that the Bohmian conditional wavefunction, together with the corresponding Bohmian trajectory, is an exact decomposition and recasting of the unitary time-evolution of a closed quantum system that yields a set of coupled, non-Hermitian, equations of motion that allows to describe the evolution of arbitrary subsets of the degrees of freedom on a formally exact level. Furthermore, since the measurement process is defined as a routine interaction between subsystems in Bohmian mechanics, conditional states can be used to describe either the measured or unmeasured dynamics of an open quantum system. As an example of the practical utility of the conditional wavefunctions, we present here a Monte Carlo simulation scheme to describe quantum electron transport in open systems that is valid both for Markovian or non-Markovian regimes and that guarantees a dynamical map that preserves complete positivity [25–29].

This paper is structured as follows. In Section 2 we provide a brief account on the SSE approach and on how nanoscale electron devices can be understood as open quantum systems. Section 3 focuses on the physical interpretation of the conditional states (i.e., system states conditioned on a particular value of the environment) in the contexts of the orthodox and Bohmian quantum mechanical theories. Section 4 provides an overall perspective on the points raised in the previous sections and puts into practice the conditional wavefunction concept to build a general purpose electron transport simulator, called BITLLES, beyond the steady state (Markovian) regime. As an example of the use of conditional states, numerical simulations of the THz current in a graphene electron device are presented in Section 5. Final comments and conclusions can be found in Section 6.

2. Electron Devices as Open Quantum Systems

In this section we introduce the SSE approach to open quantum systems and discuss how it can be used to reconstruct the reduced density matrix. We then explain how a nanoscale electron device can be understood as an open quantum system and how the SSE approach can be applied to predict its performance.

2.1. Open Quantum Systems

As usual, we start with a closed quantum system (see Figure 1a). This system is represented by a pure state, $|\Psi(t)\rangle$, which evolves unitarily according to the time-dependent Schrödinger equation:

$$i\hbar\frac{\partial|\Psi(t)\rangle}{\partial t} = \hat{H}|\Psi(t)\rangle. \tag{1}$$

Finding a solution to Equation (1) is inaccessible for most practical scenarios due to the large number of degrees of freedom involved. Therefore, it is a common practice to partition the system into two subsets of degrees of freedom, viz., open system and environment [6]. The open system can be described by a reduced density matrix:

$$\hat{\rho}_{\text{sys}}(t) = \text{Tr}_{\text{env}}\left[|\Psi(t)\rangle\langle\Psi(t)|\right], \tag{2}$$

where Tr_{env} denotes the trace over the environment degrees of freedom. The reduced density matrix $\hat{\rho}_{\text{sys}}$ can be shown to obey, in most general circumstances, a non-Markovian master equation [30,31]:

$$\frac{\partial\hat{\rho}_{\text{sys}}(t)}{\partial t} = -i\left[\hat{H}_{\text{int}}(t), \hat{\rho}_{\text{sys}}(t)\right] + \int_{t_0}^{t}\hat{\mathcal{K}}(t,t')\hat{\rho}_{\text{sys}}(t')dt', \tag{3}$$

where $\hat{H}_{\text{int}}(t)$ is a system Hamiltonian operator in some interaction picture and $\hat{\mathcal{K}}(t,s)$ is the "memory kernel" superoperator, which operates on the reduced state $\hat{\rho}_{\text{sys}}(t)$ and represents how the environment affects the system. If the solution to Equation (3) is known then the expectation value of any observable $\hat{A}$ of the system can be evaluated as:

$$\langle\hat{A}(t)\rangle = \text{Tr}_{\text{sys}}[\hat{\rho}_{\text{sys}}(t)\hat{A}]. \tag{4}$$

Unfortunately, solving Equation (3) is not an easy task. The effect of $\hat{\mathcal{K}}(t,s)$ on $\hat{\rho}_{\text{sys}}(t)$ cannot be explicitly evaluated in general circumstances. Moreover, even if the explicit form of $\hat{\mathcal{K}}(t,s)$ is known, the solution to Equation (3) is very demanding as the density matrix $\hat{\rho}_{\text{sys}}(t)$ scales very poorly with the number of degrees of freedom of the open system. Finally, if one is aiming at computing multi-time correlations functions, then it is necessary to incorporate the effect (backaction) of the successive measurements on the evolution of the reduced density matrix, which is, in general non-Markovian regimes, a very complicated task both from the practical and conceptual points of view.

2.2. Stochastic Schrodinger Equations

A breakthrough in the computation of the reduced density matrix in Equation (2) came from the advent of the SSE approach [32]. The main advantage behind the SSE approach is that the unknown to be evaluated is in the form of a state vector (of N_{sys} degrees of freedom) rather than a matrix (of size N_{sys}^2) and thus there is an important reduction of the associated computational cost. In addition, it provides equations of motion that, by construction, ensure a complete positive map [18] so that the SSE approach guarantees that the density matrix always yields a positive probability density, a requirement that is not generally satisfied by other approaches that are based on directly solving Equation (3) [33].

The central mathematical object in the SSE approach to open quantum systems is the conditional state of the system:

$$|\psi_q(t)\rangle = \frac{\left(\langle q|\otimes\hat{I}_{\text{sys}}\right)|\Psi(t)\rangle}{\sqrt{P(q,t)}}, \tag{5}$$

where $P(q,t) = \langle\psi_q(t)|\psi_q(t)\rangle = \langle\Psi(t)|\hat{I}_{\text{sys}}\otimes|q\rangle\langle q|\otimes\hat{I}_{\text{sys}}|\Psi(t)\rangle$ and $|q\rangle$ are the eigenstates of the so-called unraveling observable $\hat{Q}$ belonging to the Hilbert space of the environment. To simplify the discussion, and unless indicated, q represents the collection of degrees of freedom of the environment. Using the eigenstates $|q\rangle$ as a basis for the environment degrees of freedom, it is then easy to rewrite the full state $|\Psi(t)\rangle$ as:

$$|\Psi(t)\rangle = \int dq\sqrt{P(q,t)}|q\rangle\otimes|\psi_q(t)\rangle, \tag{6}$$

which can be simply understood as a Schmidt decomposition of a bipartite (open system plus environment) state. Thus, a complete set of conditional states can be always used to reproduce the reduced density matrix at any time as:

$$\hat{\rho}_{\mathrm{sys}}(t) = \int dq P(q,t) |\psi_q(t)\rangle\langle\psi_q(t)|. \tag{7}$$

Let us note that no specific (Markovian or non-Markovian) assumption was required to write Equation (7). In fact, the above definition of the reduced density matrix simply responds to the global unitary evolution in Equation (1), which (as depicted in Figure 1a) does not include the effect of any measuring apparatus.

2.3. Nanoscale Electron Devices as Open Quantum Systems

At first sight, one could be inclined to say that a nanoscale electron device perfectly fits into the above definition of open quantum system. The open system would then be the device's active region and the environment (including the contacts, the cables, ammeter, etc.) the so called reservoirs or contacts (see Figure 1a). In addition, the observable of interest $\hat{A}$ in Equation (4) would be, most probably, the current operator $\hat{I}$. As long as we are interested only in single-time expectation values, i.e., static or stationary properties, this picture (and the picture in Figure 1a) is perfectly valid. Therefore, the SSE approach introduced in Equations (5)–(7) can be easily adopted to simulate electron devices and hence to predict their static performance.

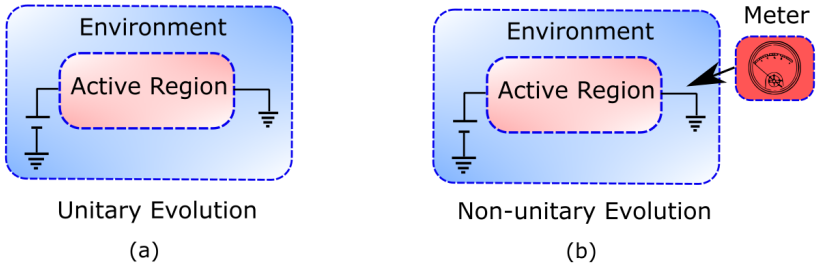

Figure 1. Panel (**a**): Schematic representation of an open quantum system, which can be partitioned into active region and environment. The evolution of the entire device is described by the state $|\Psi(t)\rangle$ that evolves unitarily according to the time-dependent Schrödinger equation. Panel (**b**): Schematic representation of a measured open quantum system, which can be partitioned into meter, active region, and environment. The evolution of the device plus environment wavefunction is no longer unitary due to the (backaction) effect of the measuring apparatus.

However, if one aims at computing dynamical properties such as time-correlation functions, e.g., $\langle I(t+\tau)I(t)\rangle$, then a valid question is whether such an expectation value is expected to be measurable at the laboratory. If so, what would then be the effect of the measurement of I at time t on the measurement of I at a later time $t+\tau$?. Figure 1b schematically depicts this question by drawing explicitly the measuring apparatus (or meter). As it is well known, the action of measuring in quantum mechanics is not innocuous. It is quite the opposite: in many relevant situations, extracting information from a system at time t has a non-negligible effect on the subsequent evolution of the system and hence also on what is measured at a later time $t+\tau$. Therefore, as soon as we are concerned about dynamic information (i.e., time-correlation functions), we need to ask ourselves whether an approach to open quantum systems such as the SSE approach can be of any help. In the next section we will answer this question and understand whether the conditional states $|\psi_q(t)\rangle$ defined in Equation (5) do include the backaction of the measuring apparatus depicted in Figure 1b.

3. Interpretation of Conditional States in Open Quantum Systems

The conditional states in Equation (5) were first interpreted as a simple numerical tool [32], that is, exploiting the result in Equation (7) as a numerical recipe to evaluate any expectation value of interest. This interpretation is linked to the assumption that the operator $\hat{A}$ in Equation (4) is the physically relevant operator (associated to a real measuring apparatus), while the operator $\hat{Q}$ associated to the definition of the conditional state in Equation (5) is only a mathematical object with no attached

physical reality, i.e., it merely represents a basis. In more recent times, however, it has been generally accepted that the conditional states in Equation (5) can be interpreted as the states of the system conditioned on a type of sequential (sometimes referred to as continuous) measurement [34] of the operator $\hat{Q}$ of the environment (now representing a physical measuring apparatus that substitutes the no longer needed operator $\hat{A}$) [6,12,35]. From a practical point of view, this last interpretation is very attractive as it would allow to link the conditional states, $|\psi_q(t)\rangle$, at different times and thus compute time-correlation functions without the need of introducing the measuring apparatus or of reconstructing the full density matrix. Whether or not this later interpretation is physically sound in general circumstances is the focus of our discussion in the next subsections.

3.1. The Orthodox Interpretation of Conditional States

Let us start by discussing, in the orthodox quantum mechanics theory, what is the physical meaning of the conditional states that appear in Equation (5). When the full closed system follows the unitary evolution of Figure 1a, the conditional state $|\psi_q(t)\rangle$ can be understood as the (renormalized) state that the system is left in after projectively measuring the property Q of the environment (with outcome q). This can be easily seen by noting that the superposition in Equation (6) is, after a projective measurement of Q, reduced (or collapsed) to the product state

$$|\Psi_q(t)\rangle = \sqrt{P(q,t)}|q\rangle \otimes |\psi_q(t)\rangle. \tag{8}$$

It is important to notice that the conditional state $|\psi_{q'}(t')\rangle$ at a later time, $t' > t$, can be equivalently defined as the state of the system when the superposition in Equation (6) is measured at time t' and yields the outcome q'. This interpretation, however, is only valid if no previous measurement (in particular at t) has been performed, as depicted in Figure 2a. Otherwise, the collapse of the wavefunction at time t, yielding the state $\sqrt{P(q,t)}|q\rangle \otimes |\psi_q(t)\rangle$, should be taken into account in the future evolution of the system, which would not be the same as if the measurement had not been performed at the previous time. Therefore, the equation of motion of the conditional states, as defined in Equation (5), cannot be, in general, the result of a sequential measurement protocol such as the one depicted in Figures 1b or 2b. This conclusion seems obvious if one recalls that our starting point was Figure 1a, where there is no measurement.

3.1.1. Orthodox Conditional States in Markovian Scenarios

Even if the conditional states solution of the SSE cannot be generally interpreted as the result of a sequential measurement, such an interpretation has been proven to be very useful in practice for scenarios that fulfill some specific type of Markovian conditions. We are aware that there is still some controversy on how to properly define Markovianity in the quantum regime (see, e.g., Ref. [18]), so it is our goal here only to acknowledge the existence of some regimes (i.e., particular observation time intervals) of interest where the role of the measurement of the environment has no observable effects. In this regime, Figure 1a,b as well as Figure 2a,b can be thought to be equivalent.

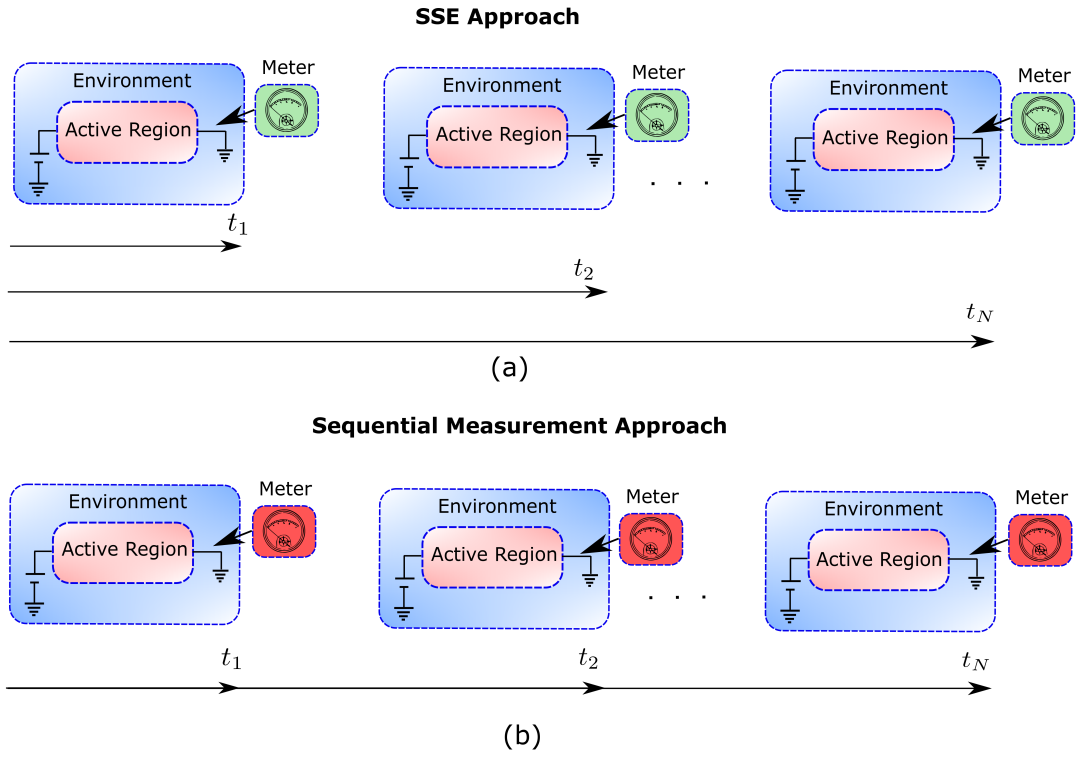

Figure 2. Panel (**a**): Schematic representation of the SSE approach. The states of the system conditioned on a particular value of the environment at time t, $|\psi_q(t)\rangle$, can be given a physical meaning only if no measurement has been performed at a previous time $t' < t$. This approach can be always used to reconstruct the correct reduced density matrix of the system at any time but cannot be used to link in time the conditional states for non-Markovian scenarios. Panel (**b**): Schematic representation of a sequential measurement. The wavefunction of the system plus environment is measured sequentially. In this picture, the link between the states of the full system plus environment at different times is physically motivated.

In our pragmatical definition of Markovianity the entanglement between system and environment decays in a time scale t_D that is much smaller than the observation time interval τ, i.e., $t_D \ll \tau$. In this regime, the environment itself can be thought of as a type of measuring operator (as appears in generalized quantum measurement theory [36]) that keeps the open system in a pure state after the measurement. The open system can be then seen as an SSE in which the stochastic variable q_t (sampled from the distribution $P(q_t, t)$) is directly the output of a sequential measurement of the environment. The stochastic trajectory of this conditioned system state generated by the (Markovian) SSE is often referred to as a quantum trajectory [6,12,35] and can be used, for example, to evaluate time-correlation functions of the environment as:

$$\langle Q(t)Q(t+\tau)\rangle \overset{t_D \ll \tau}{=} \int\int P(q_t,t)P(q_{t+\tau},t+\tau)q_t q_{t+\tau}dq_t dq_{t+\tau} = \langle Q(t)\rangle\langle Q(t+\tau)\rangle. \tag{9}$$

Let us emphasize that the stochastic variables q_t and $q_{t+\tau}$ in Equation (9) are sampled, separately, from the probability distributions $P(q_t,t) = \langle\psi_q(t)|\psi_q(t)\rangle$ and $P(q_{t+\tau},t+\tau) = \langle\psi_q(t+\tau)|\psi_q(t+\tau)\rangle$. Therefore, as we have schematically depicted in Figure 3, no matter how the trajectories $\{q_t\}$ are connected in time, one always obtains the correct time-correlation function $\langle Q(t)Q(t+\tau)\rangle$.

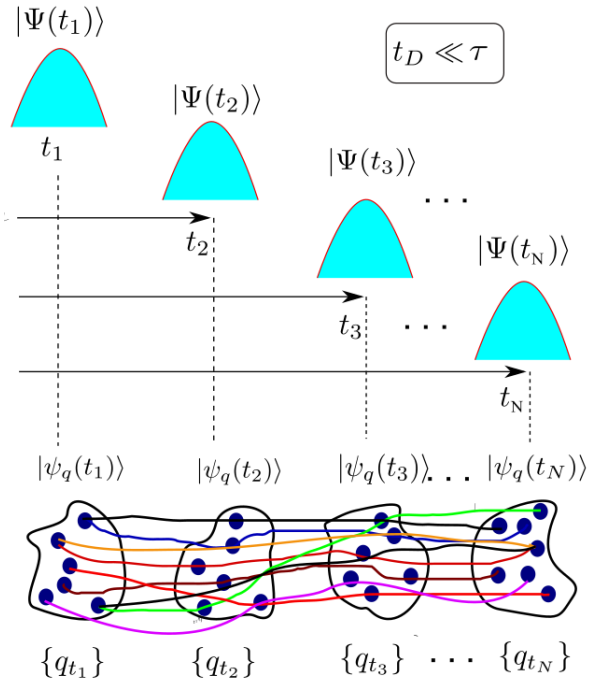

Figure 3. Schematic representation of the combined system plus environment wavefunction (blue Gaussians) measured at different times that result in a state of the system $|\psi_q(t)\rangle$ conditioned to the set of environment values $\{q_t\}$ shown in dark blue circles. In the Markovian regime there exists no specific recipe about how the different q_t's must be connected in time (colored solid lines). No matter how these points are connected in time, one always gets the right expectation value in Equation (9).

It is important to realize that we started our discussion on the physical meaning of the Markovian SSE with an open system whose environment is not being measured (see Figures 1a and 2a). Noticeably, we have ended up discussing an environment that is being measured at every time interval τ (see Figure 2b). How is that possible? Well, the reason is that measuring the environment at time t does not affect the system conditional states at a later time τ when the built-in correlations in the environment due to the measurement at time t decay in a time interval t_D much smaller than the time interval between measurements τ. In other words, Figure 1a,b as well as Figure 2a,b are not distinguishable when $t_D \ll \tau$. In this sense, the Markovian regime has some similarities with a classical system, where it is accepted that information can be extracted without perturbation.

3.1.2. Orthodox Conditional States in Non-Markovian Scenarios

For nanoscale devices operating at very high (THz) frequencies, the relevant dynamics and hence the observation time interval τ are both below the picoseconds time-scale and the previous assumption of Markovianity, i.e., $t_D \ll \tau$, starts to break down. Under the condition $t_D \sim \tau$, non-Markovian SSE have been proposed which allow an alternative procedure for solving the reduced state $|\psi_q(t)\rangle$ [17,33,37–41]. However, non-Markovian SSEs constructed from Equation (5), unlike the Markovian SSEs, suffer from interpretation issues [17]. In the non-Markovian regime, the perturbation of the environment due to the quantum backaction of a measurement at time t would not be washed out in the time lapse $\tau \sim t_D$ and hence the joint probability distribution would not become separable, i.e., $P(q_t, q_{t+\tau})) \neq P(q_t)P(q_{t+\tau})$. As a direct consequence, connecting in time the different solutions q_t and $q_{t+\tau}$ (sampled independently from the probability distributions $P(q_t, t)$ and $P(q_{t+\tau}, t+\tau)$ as in Figure 3 to make a trajectory "would be a fiction" [17,19,20]. Here, the word "fiction" means that the time-correlations computed in Equation (9) are wrong, i.e., the expectation value in Equation (9) would simply be different from the experimental result.

According to D'Espagnat the above discussion can be rephrased in terms of the so-called proper and improper mixtures [42]. Following D'Espagnat arguments, the reduced density matrix in Equation (7) is an improper mixture because it has been constructed by tracing out the degrees of freedom of the environment. On the contrary, a proper mixture is a density matrix constructed to simultaneously define several experiments where a closed system is described, at each experiment, by different pure states. Due to our ignorance, we do not know which pure state corresponds to which experiment, so we only know the probabilities of finding a given pure state. D'Espagnat argues that the ignorance interpretation of the proper density matrix, cannot be applied in the improper density matrix discussed here (See Appendix A). To understand why under a Markovian regime open systems can be described by pure states (using a proper mixture), we remind that Markovianity implies conditions on the observation time. For a given correlation time t_D, a given open system can be in the Markovian or non-Markovian regimes depending on the time of observation τ. That is, for small enough observation times all open systems are non-Markovian and hence must be understood as an improper mixture. On the contrary, for large enough observation times, open systems can behave as closed systems (with a negligible entanglement with the environment) and be effectively represented by pure states.

3.2. The Bohmian Interpretation of Conditional States

So, under non-Markovian (i.e., the most general) conditions, the conditional states $|\psi_q(t)\rangle$ can be used to reconstruct the reduced density matrix as in Equation (7) but cannot be used to provide further information on its own. This interpretation problem is rooted in the fact that orthodox quantum mechanics only provides reality to objects whose properties (such as q) are being directly measured. However, as explained in the previous subsection, it is precisely the fact of introducing the measurement of q (without including the pertinent backaction on the system evolution) which prevents the conditional states $|\psi_q(t)\rangle$ of the non-Markovian SSE from being connected in time for $t_D \sim \tau$. In this context, a valid question regarding the interpretation of $|\psi_q(t)\rangle$ is whether or not we can obtain information of, e.g., the observable Q without perturbing the state of the system. The answer given by orthodox quantum mechanics is crystal clear: this is not possible (except for Markovian conditions) because information requires a measurement, and the measurement induces a perturbation. Notice, however, that the assumption that only measured properties are real is not something forced on us by experimental facts, but it is a deliberate choice of the orthodox quantum theory. Therefore, we here turn to a nonorthodox approach: the Bohmian interpretation of quantum mechanics [43–48].

A fundamental aspect of the Bohmian theory is that reality (of the properties) of quantum objects does not depend on the measurement. That is, the values of some observables, e.g., the value of the positions of the particles of the environment, exist independently of the measurement. If q is the collective degree of freedom of the position of the particles of the environment and x is the collective degree of freedom of the position of particles of the system; then, the Bohmian theory defines an experiment in the laboratory by means of two basic elements: (i) the wavefunction $\langle q, x|\Psi(t)\rangle = \Psi(x, q, t)$ and (ii) an ensemble of trajectories $Q^i(t), X^i(t)$ of the environment and of the system. We use a superindex i to denote that each time an experiment is repeated, with the same preparation for the wavefunction $\Psi(x, q, t)$, the initial positions of the environment and system particles can be different. They are selected according to the probability distribution $|\Psi(X^i, Q^i, 0)|^2$ [44]. The equation of motion for the wavefunction $\Psi(x, q, t)$ is the time-dependent Schrödinger equation in Equation (1), while the equations of motion for the environment and system trajectories $Q^i(t), X^i(t)$ are obtained by time-integrating the velocity fields $v_q(x, q, t) = J_q(x, q, t)/|\Psi(x, q, t)|^2$ and $v_x(x, q, t) = J_x(x, q, t)/|\Psi(x, q, t)|^2$ respectively. Here, $J_q(x, q, t)$ and $J_x(x, q, t)$ are the standard current densities of the environment and the system respectively. We highlight the (nonlocal) dependence of the Bohmian velocities of the particles of the environment on the particles of the system, and vice-versa. This shows

just the entanglement between environment and system at the level of the Bohmian trajectories. According to the continuity equation

$$\frac{d|\Psi(x,q,t)|^2}{dt} + \nabla_x(v_x(x,q,t)|\Psi(x,q,t)|^2) + \nabla_q(v_q(x,q,t)|\Psi(x,q,t)|^2) = 0, \tag{10}$$

the ensemble of trajectories $\{Q(t), X(t)\} = \{Q^1(t), X^1(t), Q^2(t), X^2(t)....Q^M(t), X^M(t)\}$ with $M \to \infty$ can be used to reproduce the probability distribution $|\Psi(x,q,t)|^2$ at any time. Thus, by construction, the computation of ensemble values from the orthodox and Bohmian theories are fully equivalent, at the empirical level.

From the full wavefunction $\langle x,q|\Psi(t)\rangle = \Psi(x,q,t)$ (solution of Equation (1)) and the trajectories $Q^i(t), X^i(t)$, one can then easily construct the Bohmian conditional wavefunction of the system and environment as $\tilde{\psi}_{Q^i(t)}(x,t) = \Psi(x,Q^i(t),t)$, and $\tilde{\psi}_{X^i(t)}(q,t) = \Psi(X^i(t),q,t)$ respectively. Notice that this Bohmian definition of conditional states does not require to specify if the system is measured or not because the ontological nature of the trajectories $\{Q(t), X(t)\}$ does not depend on the measurement. Consequently, the conditional wavefunctions $\tilde{\psi}_{Q^i(t)}(x,t)$, with the corresponding Bohmian trajectories, contain all the required information to evaluate dynamical properties of the system no matter whether Markovian or non-Markovian conditions are being considered. This can be seen by noticing that the velocity of the trajectory $X^i(t)$ given by $v_q(X^i(t), Q^i(t))$ can be equivalently computed either from (the $x-$spatial derivatives of) the global wavefunction $\Psi(x,Q,t)$ evaluated at $X^i(t)$ and $Q^i(t)$ or from (the x-spatial derivative of) the conditional wavefunction $\tilde{\psi}_{Q^i(t)}(x,t)$ evaluated at $X^i(t)$. In other words, the Bohmian velocities computed from $\Psi(x,Q,t)$ or $\tilde{\psi}_{Q^i(t)}(x,t)$ are identical. Thus, in a particular experiment i and for a given time t, the dynamics of the Bohmian trajectory $X^i(t)$ can be computed either from $\tilde{\psi}_{Q^i(t)}(x,t)$ or from $\Psi(x,q,t)$.

The Bohmian conditional wavefunction of the system can now be connected to the orthodox conditional wavefunction in Equation (5) by imposing $Q^i(t) \equiv q_t$. Then one can readily write:

$$|\tilde{\psi}_{q_t}(t)\rangle = P(q_t,t)|\psi_{q_t}(t)\rangle. \tag{11}$$

At first sight, one can think that the difference between the Bohmian and orthodox conditional states is just a simple renormalization constant $P(q_t,t)$ (see Appendix B for a more detailed explanation of the role of this renormalization constant). However, the identity in Equation (11) has to be understood as to be satisfied at any time t, which implies that the following identity should prevail:

$$Q^i(t) \equiv q_t, \qquad \forall\, t \tag{12}$$

We emphasize the importance of Equation (12) in ensuring the accomplishment of Equation (11). If we consider another experiment $Q^j(t) \equiv q'_t$, we have to define another conditional state $|\tilde{\psi}_{q'_t}(t)\rangle$. It can happen that, at a particular time $t \equiv t_1$, both conditional states become identical i.e., $|\tilde{\psi}_{q_{t_1}}(t_1)\rangle = |\tilde{\psi}_{q'_{t_1}}(t_1)\rangle$. However, this does not imply that both conditional wavefunctions can identically be used in the computation of time-correlations. This is because every Bohmian trajectory has a fundamental role in describing the history of the Bohmian conditional state for one particular experiment. Therefore, the trajectory $Q^i(t)$ uniquely describes the evolution of the conditional wavefunction $|\tilde{\psi}_{q_t}(t)\rangle$ for one experiment (labeled by the index i in the Bohmian language) the same way as the trajectory $Q^j(t)$ and the conditional wave function $|\tilde{\psi}_{q'_t}(t)\rangle$ describes the experiment labeled by j. As we said, $|\tilde{\psi}_{q_{t_1}}(t_1)\rangle = |\tilde{\psi}_{q'_{t_1}}(t_1)\rangle$ are the same orthodox conditional states, but do not necessarily represent the same Bohmian conditional wavefunction. This subtle difference explains why SSEs cannot be connected in time and used to study the time-correlation of non-Markovian open system whereas the same can be done through the Bohmian conditional states, without any ambiguity.

The mathematical definition of the measurement process in Bohmian mechanics and in the orthodox quantum mechanics differs substantially [44]. In the orthodox theory a collapse (or reduction)

law, different from the Schrödinger equation, is necessary to describe the measurement process [45]. Contrarily, in Bohmian mechanics the measurement is treated as any other interaction as far as the degrees of freedom of the measuring apparatus are taken into account [44]. Therefore, while in the orthodox theory the conditional states $|\psi_{q_t}(t)\rangle$ cannot be understood without the perturbation of the full wavefunction $\Psi(x,q,t)$, in Bohmian mechanics the states $|\tilde{\psi}_{q_t}(t)\rangle$ do have a physical meaning even when the full wavefunction $\Psi(x,q,t)$ is unaffected by the measurement of the environment [23]. Interestingly, this introduces the possibility of defining what we call "unmeasured (Bohmian) conditional states" when it is assumed that there is no measurement or that the measurement of q_t at time t has a negligible influence on the subsequent evolution of the conditional state.

Importantly, the Bohmian conditional states and the corresponding Bohmian trajectories can be used not only to reconstruct the reduced density matrix in Equation (7) at any time but the environment trajectories $\{Q(t)\}$ allow us to correctly predict any dynamic property of interest including time-correlation functions, e.g.,

$$\langle Q(t)Q(t+\tau)\rangle = \frac{1}{M}\sum_{i=1}^{M} Q^i(t)Q^i(t+\tau) = \int\int P(q_t,q_{t+\tau})q_t q_{t+\tau}dq_t dq_{t+\tau}, \tag{13}$$

where $M\to\infty$ is the number of experiments (Bohmian trajectories) considered in the ensemble and we have defined $P(q_t,q_{t+\tau}) = \frac{1}{M}\sum_{i=1}^{M}\delta(q_t - Q^i(t))\delta(q_{t+\tau} - Q^i(t+\tau))$. As it is shown in Figure 4, the evaluation of Equation (13) and any other dynamic property when $t_D \sim \tau$ can be done only by connecting the (Bohmian) trajectories at different times in accordance with the continuity equation in Equation (10). This is in contrast with the evaluation of the dynamics in the Markovian regime where any position of the environment at time t_1 can be connected to another position of the environment at time t_2 (see Figure 3) and hence we can write $\langle Q(t)Q(t+\tau)\rangle \overset{t_D\ll\tau}{=} \frac{1}{M^2}\sum_{i,j}^{M} Q^i(t)Q^j(t+\tau)$. This very relevant point was first explained by Gambetta and Wiseman [23,24].

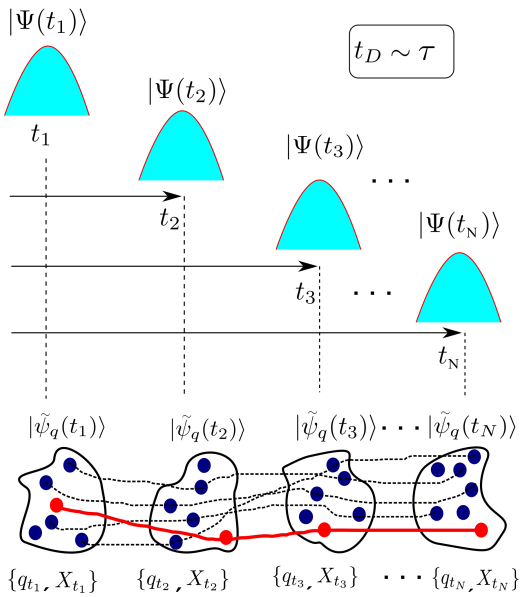

Figure 4. Schematic representation of the combined system+environment wavefunction (blue Gaussians) that is measured at different times and results in a Bohmian conditional state $|\tilde{\psi}_q(t)\rangle$ conditioned to the set of environment values $\{q_t\}$ shown in dark blue circles. In the non-Markovian regime only those values from the set of values satisfying the continuity equation in Equation (10) can be linked in time to form a trajectory (shown as connected red circles). Dashed lines represent connections that do not follow the continuity equation and hence cannot be used to evaluate any dynamic property.

Although the Bohmian theory can also provide measured properties of the system that coincide with the orthodox results in Figure 2b, let us emphasize once more the merit of the unmeasured properties provided by the Bohmian theory, which remains mainly unnoticed in the literature. As it has been already explained, in the orthodox theory, measuring a particular value of the environment property q at time t cannot be conceived without the accompanying perturbation of the wavefunction $\Psi(x,q,t)$. Under non-Markovian conditions, it is precisely this perturbation that prevents the conditional states of the system $|\psi_{q_t}(t)\rangle$ from being connected in time to form a trajectory. Contrarily, in Bohmian mechanics, the existence of the environment trajectories $\{Q(t)\}$, even in the absence of any measurement, allows the possibility of connecting in time the conditional states $|\tilde{\psi}_{q_t}(t)\rangle$ even when $t_D \sim \tau$.

Note that in the Bohmian framework, where the measurement apparatus is simply represented by an additional number of degrees of freedom interacting with the system (i.e., without requiring any additional collapse law), a discussion about measured and unmeasured properties of quantum systems is pertinent [49]. At a practical level, the measurement of many classical systems implies non-negligible perturbations. In particular, electronic devices at high frequencies are paradigmatic examples where such perturbations occur. It is well-known that the experimental setup (for e.g., a coaxial cable) connecting the electronic device to the meter induces dramatic perturbations in high-frequency measurements. An important task for device engineers is to determine what part of the measured signal is due to the intrinsic behaviour of the electron device and what part is due to rest of the experimental setup. When trying to predict the "intrinsic" behaviour of the electronic devices, the coaxial cables are modelled by "parasitic" capacitors or inductors to account for their "spurious" effect. Even the measurement of the whole experimental setup is repeated twice, with and without the "intrinsic" device under test (DUT), to subtract the results and determine experimentally the "intrinsic" properties of the electronic device alone. Such "intrinsic" properties of the electronic devices are what we define in this manuscript as the unmeasured properties of quantum systems.

4. Bohmian Conditional Wavefunction Approach to Quantum Electron Transport

The different notions of reality invoked by the orthodox quantum theory and Bohmian mechanics lead to practical differences in the abilities that these theories can offer to provide information about quantum dynamics. Specifically, we have shown that contrarily to orthodox quantum mechanics, Bohmian mechanics allows to physically interpret (i.e., link in time) the conditional states of the SSE approach in general non-Markovian scenarios. The reason is that whereas in the Bohmian theory the reality of the current is independent of any measurement, the orthodox theory gives reality to the electrical current only when it is being measured (this is the so-called eigenstate–eigenvalue link). From the practical point of view, this has a remarkable consequence. In the Bohmain approach the total current can be defined in terms of the dynamics of the electrons (Bohmian) trajectories without the need to define a measurement operator. As it will be shown in this section, the possibility of computing the total current at high frequencies without specifying the measurement operator is certainly a great advantage of the Bohmian approach in front of the orthodox one [44]. In particular, one can then avoid cumbersome questions like, is the measurement operator of the electrical current strong or weak? If weak, how weak? How often do such operator acts on the system? Every picosecond, every femtosecond? At high frequencies, how we introduce the contribution of the displacement current in the electrical current operator?

In this section we provide a brief summary of the path that the authors of this work followed for developing an electron transport simulator based on the use of Bohmian conditional states. The resulting computational tool is called BITLLES [28,29,50–56]. Let us start by considering an arbitrary quantum system. The whole system, including the open system, the environment, and the measuring apparatus, is described by a Hilbert space $\mathcal{H}$ that can be decomposed as $\mathcal{H} = \mathcal{H}_x \otimes \mathcal{H}_q$ where $\mathcal{H}_x$ is the Hilbert space of the open system and $\mathcal{H}_q$ the Hilbert space of the environment. If needed, the Hamiltonian $\mathcal{H}_q$ can include also the degrees of freedom of the measuring apparatus as

explained in Section 3.2. We define $x = \{x_1, x_2 ... x_n\}$ as the degrees of freedom of n electrons in the open system, while q collectively defines the degrees of freedom of the environment (and possibly the measuring apparatus). The open system plus environment Hamiltonian can then be written as:

$$\hat{H} = \hat{H}_q \otimes \hat{I}_x + \hat{I}_q \otimes \hat{H}_x + \hat{V} \tag{14}$$

where $\hat{H}_x$ is the Hamiltonian of the system, $\hat{H}_q$ is the Hamiltonian of the environment (including the apparatus if required), and $\hat{V}$ is the interaction Hamiltonian between the system and the environment. We note at this point that the number of electrons n in the open system can change in time and so the size of the Hilbert spaces $\mathcal{H}_x$ and $\mathcal{H}_q$ can depend on time too.

The equation of motion for the Bohmian conditional states $\langle x|\tilde{\psi}_{q_t}(t)\rangle = \tilde{\psi}_{q_t}(x,t)$ in the position representation of the system can be derived by projecting the many-body (system-environment) Schrödinger equation into a particular trajectory of the environment $q_t \equiv Q(t)$, i.e., [26,57]:

$$i\hbar \frac{d\tilde{\psi}_{q_t}(x,t)}{dt} = \langle q_t| \otimes \langle x|\hat{H}|\Psi(t)\rangle + i\hbar \nabla_q \langle q| \otimes \langle x|\Psi(t)\rangle\big|_{q=q_t} \frac{dq_t}{dt}. \tag{15}$$

Equation (15) can be rewritten as:

$$i\hbar \frac{d\tilde{\psi}_{q_t}(x,t)}{dt} = \left[-\frac{\hbar^2}{2m}\nabla_x^2 + U_{q_t}^{eff}(x,t) \right] \tilde{\psi}_{q_t}(x,t), \tag{16}$$

where

$$\tilde{U}_{q_t}^{eff}(x,t) = U(x,t) + V(x,q_t,t) + \mathcal{A}(x,q_t,t) + i\mathcal{B}(x,q_t,t). \tag{17}$$

In Equation (17), $U(x,t)$ is an external potential acting only on the system degrees of freedom, $V(x,q_t,t)$ is the Coulomb potential between particles of the system and the environment evaluated at a given trajectory of the environment, $\mathcal{A}(x,q_t,t) = \frac{-\hbar^2}{2m}\nabla_q^2 \Psi(x,q,t)/\Psi(x,q,t)\big|_{q=q_t}$ and $\mathcal{B}(x,q_t,t) = \hbar \nabla_q \Psi(x,q,t)/\Psi(x,q,t)\big|_{q=q_t} \dot{q}_t$ (with $\dot{q}_t = dq_t/dt$) are responsible for mediating the so-called kinetic and advective correlations between system and environment [26,57]. Equation (16) is non-linear and describes a non-unitary evolution.

In summary, Bohmian conditional states can be used to exactly decompose the unitary time-evolution of a closed quantum system in terms of a set of coupled, non-Hermitian, equations of motion [26,57–59]. An approximate solution of Equation (16) can always be achieved by making an educated guess for the terms $\mathcal{A}$ and $\mathcal{B}$ according to the problem at hand. Specifically, in the BITLLES simulator the first and second terms in Equation (17) are evaluated through the solution of the Poisson equation [29]. The third and fourth terms are modeled by a proper injection model [60] as well as proper boundary conditions [56,61] that include the correlations between active region and reservoirs. Electron-phonon decoherence effects can be also effectively included in Equation (16) [25].

In an electron device, the number of electrons contributing to the electrical current are mainly those in the active region of the device. This number fluctuates as there are electrons entering and leaving the active region. This creation and destruction of electrons leads to an abrupt change in the degrees of freedom of the many body wavefunction which cannot be treated with a Schrödinger-like equation for $\tilde{\psi}_{q_t}(x,t)$ with a fixed number of degrees of freedom. In the Bohmian conditional approach, this problem can be circumvented by decomposing the system conditional wavefunction $\tilde{\psi}_{q_t}(x,t)$ into a set of conditional wavefunctions for each electron. More specifically, for each electron x_i, we define a single particle conditional wavefunction $\tilde{\tilde{\psi}}_{q_t}(x_i, \bar{X}_i(t), t)$, where $\bar{X}_i(t) = \{X_1(t), .., x_{i-1}(t), x_{i+1}, .., X_n(t)\}$ are the Bohmian positions of all electrons in the active region except x_i, and the second tilde denotes the single-electron conditional decomposition that we have considered on top of the conditional

decomposition of the system-environment wavefunction. The set of equations of motion of the resulting $n(t)$ single-electron conditional wavefunctions inside the active region can be written as:

$$i\hbar \frac{d\tilde{\bar{\psi}}_{q_t}(x_1, \bar{X}_1(t), t)}{dt} = \left[-\frac{\hbar^2}{2m} \nabla^2_{x_1} + \tilde{\bar{U}}^{eff}_{q_t}(x_1, \bar{X}_1(t), t) \right] \tilde{\bar{\psi}}_{q_t}(x_1, \bar{X}_1(t), t) \tag{18}$$

$$\vdots$$

$$i\hbar \frac{d\tilde{\bar{\psi}}_{q_t}(x_n, \bar{X}_n(t), t)}{dt} = \left[-\frac{\hbar^2}{2m} \nabla^2_{x_n} + \tilde{\bar{U}}^{eff}_{q_t}(x_n, \bar{X}_n(t), t) \right] \tilde{\bar{\psi}}_{q_t}(x_n, \bar{X}_n(t), t). \tag{19}$$

That is, the first conditional process is over the environment degrees of freedom and the second conditional process is over the rest of electrons within the (open) system.

We remind here that, as shown in Figure 2b, the active region of an electron device (acting as the open system) is connected to the ammeter (that acts as the measuring apparatus) by a macroscopic cable (that represents the environment). The electrical current provided by the ammeter is then the relevant observable that we are interested in. Thus, the evaluation of the electrical current seems to require keeping track of all the degrees of freedom, i.e., of the system and the environment, which is of course a formidable computational task (see (d) Table 1). At THz frequencies, however, the electrical current is not only the particle current but also the displacement current. It is well-known that the total current defined as the particle current plus the displacement current is a divergence-less vector [21,22]. Consequently, the total current evaluated at the end of the active region is equal to the total current evaluated at the cables. So the variable of the environment associated to the total current, $q_t \equiv I(t)$, can be equivalently computed at the borders of the open system. The reader is referred to Ref. [62] for a discussion on how $I(t)$ can be defined in terms of Bohmian trajectories with the help of a quantum version of the Ramo–Schokley–Pellegrini theorem [63]. In particular, it can be shown that the total (particle plus displacement) current in a two-terminal devices can be written as [63]:

$$I(t) = \frac{e}{L} \sum_{i=1}^{n(t)} v_{x_i}(X_i(t), \bar{X}_i(t), t) = \frac{e}{L} \sum_{i=1}^{n(t)} \mathrm{Im} \left(\frac{\nabla_{x_i} \tilde{\bar{\psi}}_{q_t}(x_i, \bar{X}_i(t), t)}{\tilde{\bar{\psi}}_{q_t}(x_i, \bar{X}_i(t), t)} \right) \Bigg|_{x_i = X_i(t)}, \tag{20}$$

where L is the distance between the two (metallic) contacts, e is the electron charge, and $v_{x_i}(X_i(t), \bar{X}_i(t), t)$ is the Bohmian velocity of the i-th electron inside the active region. Let us note that $I(t)$ is the electrical current given by the ammeter (although computed by the electrons inside the open system). Since the cable has macroscopic dimensions, it can be shown that the measured current at the cables is just equal to the unmeasured current (taking into account only the simulation of electrons inside the active region) plus a source of (nearly white) noise which is only relevant at very high frequencies [62]. The basic argument is that the (non-simulated) electrons in the metallic cables have a very short screening time. In other words, the electric field generated by an electron in the cable spatially decreases very rapidly due to the presence of many other mobile charge carriers in the cable that screen it out. Thus, the contribution of this outer electron to the displacement current at the border of the active region is negligible [64].

Summarizing, for the computation of the current at THz frequencies, the degrees of freedom of the environment can be neglected without any appreciable deviation from the correct current value [62]. This introduces an enormous computational simplification as shown (e) in Table 1. This is, for the specific scenarios that we are interested in, the computation cost of the Bohmian conditional wavefunction approach has the same computational cost as the orthodox SSE approach (see Table 1). Yet, in contrast to the orthodox conditional states, which can be used only to evaluate the dynamics of quantum systems in the Markovian regime, the Bohmian conditional states provide direct information on the dynamics of both Markovian or non-Markovian systems.

Table 1. An estimation of the computational cost (in memory) of different approaches mentioned in the text. Here N_{sys} and N_{env} are the number of degrees of freedom of the system and the environment while M denotes the number of elements required.

		Computational Element	N° of Trajectories	N° of Degrees of Freedom	Computational Cost
(a)	**Full wave function**	$\Psi(x,q,t)$	–	N_{sys} ; N_{env}	$N_{sys} \times N_{env}$
(b)	**Density Matrix**	$\rho(x,x')$	–	N_{sys}	N_{sys}^2
(c)	**Orthodox Conditional state (SSE)**	$\psi_{q_t}(x,t)$; q_t	M	N_{sys}	$M(N_{sys}+1)$
(d)	**Bohmian Conditonal state**	$\tilde{\psi}_{q_t}(x,t)$; $\tilde{\psi}_{x_t}(q,t)$; q_t ; x_t	M	N_{sys} ; N_{env}	$M(N_{sys}+N_{env}+2)$
(e)	**Bohmian Conditonal state (used in Section 5)**	$\tilde{\psi}_{q_t}(x,t)$; x_t	M	N_{sys}	$M(N_{sys}+1)$

5. Numerical Results

In this section we present numerical results obtained with the BITLLES simulator (see Section 4) that demonstrate the ability of the Bohmian conditional wavefunction approach to provide dynamics information for both Markovian and non-Markovian scenarios. We simulate a two-terminal electron device whose active region is a graphene sheet contacted to the outer by two (ohmic) contacts. Graphene is a $2D$ material that has attracted a lot of attention recently because of its high electron mobility. It is a gapless material with linear energy band, which differs from the parabolic energy bands of traditional semiconductors. In graphene, the conduction and valence bands coincide at an energy point known as the Dirac point. Thus, the dynamics of electrons is no longer governed by an (effective mass) Schrödinger equation but by the Dirac equation, allowing transport from the valence to the conduction band (and vice versa) through Klein tunneling. A Bohmian conditional bispinor (instead of a conditional scalar wavefunction) is used to describe electrons inside the device. The change from a wavefunction to a bispinor does not imply any conceptual difficulty but just a mere increment of the computational cost. More details can be found in Appendix C.

In particular, we want to simulate electron transport in graphene at very high frequencies (THz) taking into account the electromagnetic environment of the electron device. Typically, nanoscale devices are small enough to assume that, even at THz frequencies, the electric field is much more relevant than the magnetic field. Therefore, only the Gauss law (first Maxwell's equations) is enforced to be fulfilled in a self-consistent way (i.e., taking into account the actual charge distribution in the active region). However, the environment of nanoscale devices is commonly a metallic element of macroscopic dimensions. In there, the magnetic and electric fields become both relevant, acting as active (detecting or emitting) THz antennas. For the typical electromagnetic modes propagating in the metals, the magnetic and electric fields are translated into the language of currents and voltages and the whole antenna is modeled as a part of an electric circuit. In this work, the graphene device interacts with an environment that is modeled by a Resistor (R) and a capacitor (C) connected in series through ideal cables (see the schematic plots in Figure 5a–c).

The active region of the graphene device is simulated with the Bohmian conditional wavefunction approach explained in the previous section, while the RC circuit is simulated using a time-dependent finite-difference method. We consider the system plus environment to be in equilibrium. Specifically, the self-consistent procedure to get the current is as follows: an initial (at time $t = 0$) zero voltage is applied at the source ($V_S(0) = 0$) and drain ($V_D(0) = 0$) contacts of the graphene active region. At room temperature this situation yields a non-zero current from Equation (20) (i.e., $I(0) \neq 0$) because of thermal noise. Such current $I(0)$ enters the RC circuit and leads to a new voltage $V_S(dt) \neq 0$ at the next time step dt (where dt represents the time step that defines the interaction between the RC circuit

and the quantum device which was set to $dt = 0.5$fs). The new source $V_S(dt) \neq 0$ and fixed drain $V_D(dt) = 0$ voltages now lead to a new value of the current $I(dt) \neq 0$ in (20) which is different from zero not only because of thermal noise but also because there is now a net bias $(V_D(dt) - V_S(dt) \neq 0)$. This new current $I(dt)$ is used (in the RC circuit) to get a new $V_S(2dt)$ that is introduced back in the device to obtain $I(2dt)$ and so on. Importantly, as the system and environment are in equilibrium, the expectation value of $I(t)$ is zero at any time, i.e., $\langle I(t) \rangle = 0 \ \ \forall t$.

We consider three different environments (with different values of the capacitance). In Figure 5a we plot the total (particle plus displacement) electrical current at the end of the active region when $R = 0$ and $C = \infty$. The same information is shown in Figure 5b,c for two different values of the capacitance $C = 2.6 \times 10^{-17}$ F and $C = 1.3 \times 10^{-17}$ F. In all cases the value of the resistance is $R = 187\ \Omega$, and we assumed the current $I(t)$ to be positive when it goes from drain to source.

The effect of the RC circuit is, mainly, to attenuate the current fluctuations, which are originated due to thermal noise. This can be seen by comparing Figure 5a with Figure 5b,c. The smaller the capacitance the smaller the current fluctuations. This can be explained as follows: when the net current is positive, the capacitor in the source starts to be charged and so the voltage at the source increases trying to counteract the initially positive current. Therefore, the smaller the capacitance the faster the RC circuit reacts to a charge imbalance.

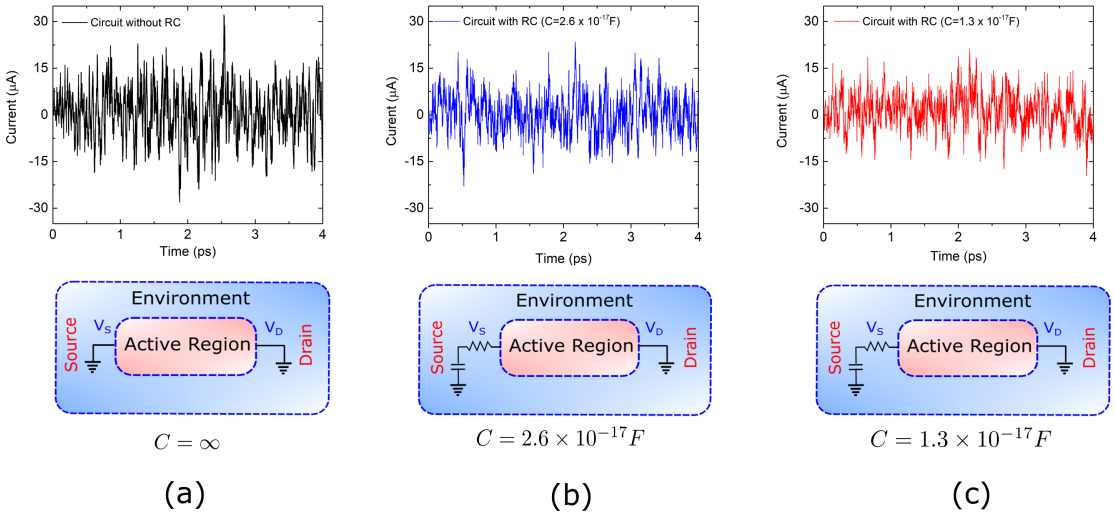

Figure 5. Total (particle plus displacement) electrical current $I(t)$ evaluated at the ammeter as a function of time for a graphene device connected to three different RC circuits with $R = 187\ \Omega$. The values of the capacitances are: (**a**) $C = \infty$, (**b**) $C = 2.6 \times 10^{-17}$ F and (**c**) $C = 1.3 \times 10^{-17}$ F.

In Figure 6 we plot the total (particle plus displacement) current–current correlations as a function of the observation time τ for the three scenarios in Figure 5. Correlations at very small observation times provide information of the variance of the current, which, as explained above, is reduced as the value of the capacitance is increased. Numerical simulations (not shown here) exhibit that the role of the resistor R is less evident because the active region itself has a much larger (than $R = 187\ \Omega$) associated resistance. Numerically the distinction between Markovian and non-Markovian dynamics boils down to the comparison of time correlations as defined in Equations (9) and (13). Since there is no net bias applied to the graphene device (i.e., it is in equilibrium), an ensemble average of the current (over an infinite set of trajectories like the one depicted in Figure 5) yields $\langle I(t) \rangle = 0 \ \ \forall t$. Time correlation functions computed in Equation (9) are thus zero by construction, i.e., $\langle I(t) \rangle \langle I(t+\tau) \rangle = 0 \ \ \forall t, \tau$. Therefore, the non-Markovian dynamics occurring at very high-frequencies (below the ps time-scale in Figure 6 expressly shows) fixes the correlation time of the environment at $t_D \sim$ ps. Although all three

values of the capacitance C in Figure 6 yield the same order of magnitude for $t_D \sim$ ps, it seems also true that the smaller the value of the capacitance, the smaller t_D.

Current–current correlations shown in Figure 6 can be better understood by assessing the transit time of electrons. For a velocity of roughly 10^6 m/s inside an active region of $L = 40$ nm length is roughly $\tau_T = L/v_x = 0.04$ ps. Positive correlations correspond to transmitted electrons traveling from drain to source (as well as electrons traversing the device from source to drain). While $0 < t < \tau_T$ electrons are transiting inside the active region, such electrons provide always a positive (or negative) current as seen in expression (20). In other words, if we have a positive current at time t because electrons are traveling from drain to source, we can expect also a positive current at times t' satisfying $t < t' < t + \tau_T$. The negative correlations belong to electrons that are being reflected. They enter in the active region with a positive (negative) velocity and, after some time τ_R inside the device, they are reflected and have negative (positive) velocities until they leave the device after spending roughly $2\tau_R$ in the active region. Thus, during the time $\tau_R < t < 2\tau_R$ which will be different for each electron depending on the time when they are reflected, we can expect negative correlations. Interestingly, during the 4 ps simulation the number of Bohmian trajectories reflected are double in the black ($C = \infty$) simulation than in the red one ($C = 1.3 \times 10^{17}$ F). This can be explained in a similar way as we explained the reduction of the current fluctuations. The fluctuations of the electrical current imply also fluctuations of the charge inside the active region, which are translated (through the Gauss law) into fluctuations of the potential profile. Thus, the larger the noisy current, the larger the noisy internal potential profile. This implies a larger probability of being reflected by the Klein tunneling phenomenon. Therefore, if one aims at describing the dynamics of nanoscale devices with a time-resolution τ that is comparable to (or goes beyond) the electron transit time τ_T, a non-Markovian approach is necessary. This is so because the total current $I(t)$ (which has contributions from the displacement and the particle currents) shows correlations at times that are smaller than the electron transit time.

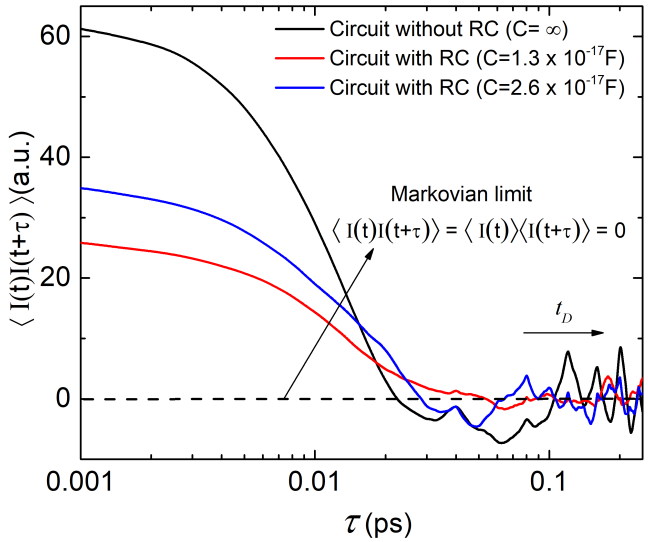

Figure 6. Total current–current correlation as a function of time for the three different experiments in Figure 5. The zero is indicated by a dashed line to show the tendency of the total current, understood as a property of the environment, to vanish at long times τ. Zero autocorrrelation implies an independence between $I(t)$ and $I(t + \tau)$ which is typical for Markovian scenarios. This is not true for the short τ considered here which are the representatives of the non-Markovian dynamics.

6. Conclusions and Final Remarks

Theoretical approaches to open quantum systems that rely on the manipulation of state vectors instead of a reduced density matrix have well known computational advantages. Two major benefits are the substantial reduction of the dimensionality of the involved mathematical objects and the preservation of complete positivity [18]. However, substituting density matrices by state vectors constitutes also an attempt to achieve a more detailed description of the dynamics of open quantum systems [6,19]. It is well recognized, for example, that the continuous measurement of an open quantum system with associated Markovian dynamics can be described by means of a SSE (see Table 2 O4). The conditional state solution to such an equation over some time interval can be linked to a "quantum trajectory" [12,19] of one property of the environment. Thus, the conditional state can be interpreted as the state of the open system evolving while its environment is under continuous monitoring. This is true in general for Markovian systems, no matter whether or not the environment is being actually measured (i.e., it is valid for both Figure 1a,b). This fact is of great importance for designing and experimentally implementing feedback control in open quantum systems [35]. If this interpretation could also be applied to non-Markovian SSEs [33,37], then this would be very significant for quantum technologies, especially in condensed matter environments (e.g., electron devices), which are typically non-Markovian [6].

Table 2. Validity of Bohmian vs. orthodox conditional states to provide dynamic information of open quantum system depending on the relation between the environment decoherence time t_D and the observation period τ. Here (un)measured refers to unmeasured and measured indistinctively.

Validity of Conditional States to Provide Dynamic Information	**Non-Markovian -Measured-** $t_D > \tau = 0$	**Non-Markovian -Unmeasured-** $t_D > \tau = 0$	**Non-Markovian -(Un)measured-** $t_D \sim \tau > 0$	**Markovian -(Un)measured-** $t_D \ll \tau$
Orthodox	(O1) ✓	(O2) ✗	(O3) ✗	(O4) ✓
Bohmian	(B1) ✓	(B2) ✓	(B3) ✓	(B4) ✓

Unfortunately, for non-Markovian conditions, the above interpretation is only possible for the rather exotic scenario where the environment is being continuously monitored and the system is strongly coupled to it. As no correlation between the system and the environment can build up, the evolved system is kept in a pure state. This is the well-known quantum Zeno regime [65,66], under which conditional states can be trivially used to describe the frozen properties of the system (see Table 2 O1). Without the explicit consideration of the measurement process (as in Figure 1a), however, the postulates of the orthodox theory restrict the amount of dynamical information that can be extracted from state vectors (see Table 2 O2). In most general conditions, for $\tau > 0$ and non-Markovian dynamics, while conditional states can be used to reconstruct the reduced density matrix, they cannot be used to evaluate time-correlations (see Table 2 O3) [20,23]. This is not only true when the environment is being measured (as in Figure 1b), but also when it is not measured (as in Figure 1a).

Therefore, we turned to a nonorthodox approach: the Bohmian interpretation of quantum mechanics. The basic element of the Bohmian theory (as in other quantum theories without observers) is that the intrinsic properties of quantum systems do not depend on whether the system is being measured or not. Such ontological change is, nevertheless, fully compatible with the predictions of orthodox quantum mechanics because a measurement-independent reality of quantum objects is not in contradiction with non-local and contextual quantum phenomena. Yet, the ontological nature of the trajectories in Bohmian mechanics introduces the possibility of evaluating dynamic properties in terms of conditional wavefunctions for Markovian and non-Markovian dynamics, no matter whether the environment is being actually measured or not (see Table 2, B1–B4 and Figure 7a,b).

In summary, the Bohmian conditional states lend themselves as a rigorous theoretical tool to evaluate static and dynamic properties of open quantum systems in terms of state vectors without the need of reconstructing a reduced density matrix. Formally, the price to be paid is that for developing a SSE-like approach based on Bohmian mechanics one needs to evaluate both the trajectories of the environment and of the system see (d) Table 1. Nonetheless, we have seen that this additional computational cost can be substantially reduced in practical situations. For THz electron devices (see Section 5), for example, we showed that invoking current and charge conservation one can easily get rid of the evaluation of the environment trajectories. This reduces substantially the computational cost associated to the Bohmian conditional wave function approach (as shown (e) in Table 1). Let us also notice that here we have always assumed that the positions of the environment are the variables that the states of the system are conditioned to. However, it can be shown that the mathematical equivalence of the SSEs with state vectors conditioned to other "beables" of the environment (different from the positions) is also possible. It requires using a generalized modal interpretation of quantum phenomena, instead of the Bohmian theory. A review on the modal interpretation can be found in [67,68].

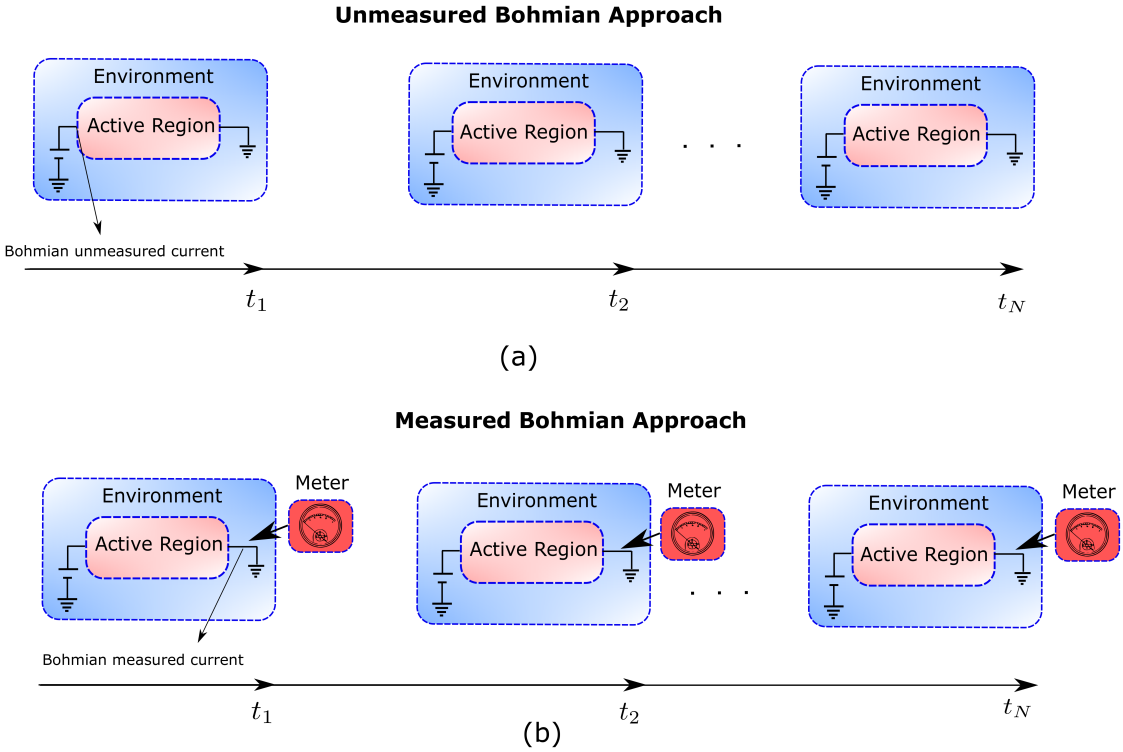

Figure 7. (**a**) Figure depicting the Unmeasured Bohmian approach in which the computation of any property (electric current in an electron device) is independent of the measuring apparatus. (**b**) The continuous measurement of the electric current through an ammeter (measuring apparatus) can be also described in Bohmian mechanics by including the degrees of freedom of the measuring apparatus.

As an example of the practical utility of the Bohmian conditional states, we have introduced a time-dependent quantum Monte Carlo algorithm, called BITLLES, to describe electron transport in open quantum systems. We have simulated a graphene electron device coupled to an RC circuit and computed its current–current correlations up to the THz regime where non-Markovian effects are relevant. The resulting simulation technique allows to describe not only DC and AC device's characteristics but also noise and fluctuations. Therefore, BITLLES extends to the quantum regime the computational capabilities that the Monte Carlo solution of the Boltzmann transport equation has been offering for decades for semi-classical devices.

Author Contributions: Conceptualization, D.P., G.A. and X.O. ; methodology, D.P., G.A. and X.O.; software, E.C. and X.O.; validation, D.P., G.A., E.C.and X.O.; formal analysis, D.P., G.A. and X.O.; investigation, D.P., G.A. and X.O.; resources, D.P., G.A. and X.O.; data curation, D.P., E.C., G.A., and X.O.; writing–original draft preparation, D.P., G.A. and X.O.; writing–review and editing, D.P., E.C., G.A. and X.O.; visualization, D.P., E.C., G.A. and X.O.; supervision, G.A. and X.O.; project administration, G.A. and X.O.; funding acquisition, X.O and G.A.

Funding: We acknowledge financial support from Spain's Ministerio de Ciencia, Innovación y Universidades under Grant No. RTI2018-097876-B-C21 (MCIU/AEI/FEDER, UE), the European Union's Horizon 2020 research and innovation programme under grant agreement No Graphene Core2 785219 and under the Marie Skodowska-Curie grant agreement No 765426 (TeraApps). G.A. also acknowledges financial support from the European Unions Horizon 2020 research and innovation programme under the Marie Skodowska-Curie Grant Agreement No. 752822, the Spanish Ministerio de Economa y Competitividad (Project No. CTQ2016-76423-P), and the Generalitat de Catalunya (Project No. 2017 SGR 348).

Acknowledgments: The authors are grateful to Howard Wiseman and Bassano Vacchini for enlightening comments.

Conflicts of Interest: The authors declare no conflict of interest.

Appendix A. D'Espagnat Distinction between "Proper" and "Improper" Mixtures

An alternative explanation on the difficulties of state vectors in describing open quantum system comes from the distinction between "proper" and "improper" mixtures by D'Espagnat.

- The "proper" mixture is simply a mixture of different pure states of a closed system. We define such pure states as $|\psi_q\rangle$ with $q = 1, .., N$. We know that each of these states represent the closed system in one of the repeated experiments, but we ignore which state corresponds to each experiment. We only know the probability $P(q)$ that one experiment is represented by the pure state $|\psi_q\rangle$. Then, if we are interested in computing some ensemble value of the system, over all experiments, von Neumann introduced the mixture $\rho = \int P(q)|\psi_q\rangle\langle\psi_q|dq$. It is important to notice that we are discussing here human ignorance (not quantum uncertainty). The system is always in a well-defined state (for all physical computations), but we (the humans) ignore what the state is in each experiment.
- The "improper" mixture refers to the density matrix that results from a trace reduction of a pure sate (or statistical operator) of a whole system that includes the system and the environment. The reduced density of the system alone is given by tracing out the degrees of freedom of the environment, giving the result in Equation (7), which is mathematically (but not physically) equivalent to the results of the "proper" mixture constructed from our "ignorance" of which state represents the system.

D'Espagnat claims that the ignorance interpretation of the "proper" mixture cannot be given to the "improper" mixture. The D'Espagnat's argument is as follows. Let us assume a pure global system (inclding the open system and the environment) described by Equation (1). Then, if we accept that the physical state of the system is given by $|\psi_q(t)\rangle$, we have to accept that the system-plus-environment is in the physical state $|q\rangle \otimes |\psi_q(t)\rangle$ with probability $P(q)$. The ignorance interpretation will then erroneously conclude that the the global system is in a mixed state, not in a pure state as assumed in Equation (1). The error is assuming that the system is in a well-defined state that we (the humans) ignore it. This is simply not true. D'Espagnat results shows that a conditional state cannot be a description of an open system with all the static and dynamic information that we can get from the open system.

In addition, let us notice that the conclusion of D'Espagnat applies to any open quantum system without distinguishing between Markovian or non-Markovian scenarios. However, indeed, there is no contradiction between the D'Espagnat conclusion and the attempt of the SSE of using pure states to describe Markovian open quantum systems for static and dynamic properties. Both are right. D'Espagnat discussion is a formal (fundamental) discussion about conditional states, while the discussion about Markovian scenarios is a practical discussion about simplifying approximation when extracting information of the system at large τ.

Finally, let us notice that the D'Espagnat conclusions do not apply to Bohmian mechanics because the Bohmian definition of a quantum system involves a wave function plus trajectories. The conditional state $\tilde{\psi}_{Q^i(t)}(x,t) = \Psi(x,Q^i(t),t)$, together with the environment and system trajectory $Q^i(t)$ and $X^i(t)$, contains all the (static and dynamic) information of the open system in this i-th experiment. An ensemble over all experiments prepared with the same global wavefunction $\Psi(x,q,t)$ requires an ensemble of different environment and system trajectories $Q^i(t)$ and $X^i(t)$ for $i = 1,2,...,M$ with $M \to \infty$.

Appendix B. Orthodox and Bohmian Reduced Density Matrices

The orthodox and Bohmian definitions of a quantum state are different. The first uses only a wave function, while the second uses the same wave function plus trajectories. It is well known that both reproduce the same ensemble values by construction. Here, we want to discuss how the orthodox density matrix (without trajectories) can be described by the Bohmian theory with trajectories.

We consider a system plus environment defined by a Hilbert space $\mathcal{H}$ that can be decomposed as $\mathcal{H} = \mathcal{H}_x \otimes \mathcal{H}_q$ where x is the collective positions of particles of the system while q are the collective positions of the particles of the environment.The expectation value of any observable O_x of the system can be computed as $\langle O_x \rangle = \langle \Psi | \hat{O}_x \otimes \hat{I}_q | \Psi \rangle$ with $\hat{I}_q$ the identity operator for the environment. We describe the typical orthodox procedure to define the orthodox reduced density matrix by tracing out all degrees of freedom of the environment:

$$\rho(x,x',t) = \int dq \Psi^*(x',q,t)\Psi(x,q,t) \tag{A1}$$

From Equation (A1) the mean value of the observable O_x can be computed as,

$$\langle O_x \rangle = \int dx \left(O_x \rho(x,x',t)|_{x'=x} \right) \tag{A2}$$

In this appendix, we want to describe Equations (A1) and (A2) in terms of the Bohmian conditional wavefunctions and trajectories described in the text. The conditonal wavefunction associated to the system during the i-th experiment conditioned on a particular value of the environment $Q^i(t)$ is defined as $\psi_{Q^i(t)}(x,t) = \Psi(x,Q^i(t),t)$, being $\Psi(x,q,t) = \langle x,q|\Psi\rangle$ the position representation of the global state. We start from the general expression for the ensemble value in the position representation as,

$$\langle O_x \rangle = \int dx \int dq \; \Psi^*(x,q,t) O_x \Psi(x,q,t) \tag{A3}$$

Multiplying and dividing by $\Psi^*(x,q,t)$ we get,

$$\begin{aligned} \langle O_x \rangle &= \int dx \int dq \; \frac{|\Psi(x,q,t)|^2 O_x \Psi(x,q,t)}{\Psi^*(x,q,t)} \\ &= \frac{1}{M} \sum_{i=1}^{M} \int dx \int dq \frac{\delta[(x-X^i(t)]\delta[(q-Q^i(t)]O_x\Psi(x,q,t)}{\Psi^*(x,q,t)} \\ &= \frac{1}{M} \sum_{i=1}^{M} \int dx \frac{O_x \Psi(x,Q^i(t),t)}{\Psi^*(x,Q^i(t),t)} \delta(x-X^i(t)) \end{aligned} \tag{A4}$$

where we have used the quantum equilibrium condition $|\Psi(x,q,t)|^2 = \frac{1}{M}\sum_{i=1}^{M}\delta[(x-X^i(t)]\delta[(q-Q^i(t)]$ with $M\to\infty$. Now, we multiply and divide by $\Psi^*(x,Q^i(t),t)$ to get,

$$\begin{aligned}\langle O_x\rangle &= \frac{1}{M}\sum_{i=1}^{M}\int dx \frac{O_x\Psi^*(x,Q^i(t),t)\Psi(x,Q^i(t),t)}{|\Psi(x,Q^i(t),t)|^2}\delta(x-X^i(t)) \\ &= \int dx\left[O_x\sum_{i=1}^{M}P_i\tilde{\psi}^{i*}(x',t)\tilde{\psi}^i(x,t)\right]_{x'=x=X^i(t)} \end{aligned} \tag{A5}$$

where $P_i = 1/M$ can be interpreted as the probability associated to each $i = 1,2,...,M$ experiment and we have defined:

$$\tilde{\psi}^i(x,t) \equiv \frac{\Psi(x,Q^i(t),t)}{\Psi(X^i(t),Q^i(t),t)}. \tag{A6}$$

Now, once we arrive at Equation (A5), one can be tempted to define a type of Bohmian reduced density matrix in terms of the conditional wavefunctions for $i = 1,2,...,M$ experiments as,

$$\rho_w(x',x,t) = \sum_{i=1}^{M}P_i\,\tilde{\psi}^{i*}(x',t)\tilde{\psi}^i(x,t) = \sum_{i=1}^{M}P_i\,\frac{\Psi^*(x',Q^i(t),t)}{\Psi^*(X^i(t),Q^i(t),t)}\frac{\Psi(x,Q^i(t),t)}{\Psi(X^i(t),Q^i(t),t)}, \tag{A7}$$

where we have arbitrarily eliminated the role of the trajectories. However, strictly speaking Equation (A1) is not equal to Equation (A7). If we include all $i = 1,2,...,M$ experiments in the computation of (A7), there are trajectories $Q^i(t)$ and $Q^j(t)$ that at the particular time t can be represented by the same conditional wavefunction $\tilde{\psi}^i(x,t) = \tilde{\psi}^j(x,t)$ if $Q^i(t) = Q^j(t)$. Such over-summation due to the repetition of the same trajectories is not present in (A1).

To simplify the subsequent discussion, let us assume that q is one degree of freedom in a 1D space. Let us cut such 1D space into small intervals of length Δq. Each interval is defined as $j\,\Delta q < q < (j+1)\,\Delta q$ and it is labelled by the index j. Then, we can define $G^j(t)$ as the number of positions $Q^i(t)$ that are inside the j-interval at time t as:

$$G^j(t) = \sum_{i=1}^{M}\int_{j\,\Delta q}^{(j+1)\,\Delta q}\delta[q-Q^i(t)]dq \tag{A8}$$

With this definition, assuming that Δq is so small that all $Q^i(t)$ inside the interval and all the corresponding Bohmian conditional wave functions $\Psi(x,Q^j(t),t)$, system positions $X^i(t)$, and probabilities P_i are almost equivalent, and given by q^j, $\Psi(x,q^j,t)$, x^j and P_j respectively, we can change the sum over $i = 1,...,M$ experiments into a sum over $j = ...,-1,0,1,...$ spatial intervals to rewrite Equation (A7) as:

$$\rho_w(x',x,t) = \sum_{j=-\infty}^{j=+\infty}G^j(t)P_j\,\frac{\Psi^*(x',q^j,t)}{\Psi^*(x^j,q^j,t)}\frac{\Psi(x,q^j,t)}{\Psi(x^j,q^j,t)} \approx \int dq^j N^j(t)\Psi^*(x',q^j,t)\Psi(x,q^j,t) \tag{A9}$$

where $N^j(t) = G^j(t)P_j\,/\,\left(\Psi^*(x^j,q^j,t)\Psi(x^j,q^j,t)\right)$. So, finally, a proper normalization of the Bohmian conditional states allows us to arrive to Equation (A1) from Equation (A7). Such normalization is already discussed in quation (11) in the text. The moral of the mathematical developments of this appendix is that open systems are more naturally described in terms of density matrix than in terms of conditional states when using the orthodox theory, while the contrary happens when using the Bohmian theory. Because of the additional variables of the Bohmian theory, the conditional states are a natural Bohmian tool to describe open systems.

Appendix C. Equations of Motion for Single-Electron Conditional States in Graphene

As said in the text, graphene dynamics are given by the Dirac equation and not by the usual Schrödinger one. The presence of the Dirac equation on the description of the dynamics of electrons in graphene is not due to any relativistic correction but to the presence of a linear energy-momentum dispersion (in fact, the graphene Fermi velocity $v_f = 10^6\ m/s$ is faster than the electron velocity in typical parabolic band materials but still some orders of magnitude slower than the speed of light). Thus, the conditional wavefunction associated to the electron is no longer a scalar but a bispinor. In particular, the initial bispinor is defined (located outside of the active region) as:

$$\begin{pmatrix} \psi_1(x,z,t) \\ \psi_2(x,z,t) \end{pmatrix} = \begin{pmatrix} 1 \\ se^{i\theta_{\vec{k}_c}} \end{pmatrix} \Psi_g(x,z,t), \tag{A10}$$

where $\Psi_g(x,z,t)$ is a Gaussian function with central momentum $\vec{k}_c = (k_{x,c}, k_{z,c})$, $s = 1$ ($s = -1$) if the electron is in the conduction band (valence band) and $\theta_{\vec{k}_c} = atan(k_{z,c}/k_{x,c})$. The wave packet can be considered as a Bohmian conditional wavefunction for the electron, a unique tool of Bohmian mechanics that allows to tackle the many-body and measurement problems in a computationally efficient way [25,62]. The two components are solution of the mentioned Dirac equation:

$$i\hbar \frac{\partial}{\partial t} \begin{pmatrix} \psi_1 \\ \psi_2 \end{pmatrix} = \begin{pmatrix} V(x,z,t) & -i\hbar v_f \frac{\partial}{\partial x} - \hbar v_f \frac{\partial}{\partial z} \\ -i\hbar v_f \frac{\partial}{\partial x} + \hbar v_f \frac{\partial}{\partial z} & V(x,z,t) \end{pmatrix} \begin{pmatrix} \psi_1 \\ \psi_2 \end{pmatrix} = -i\hbar v_f \left(\vec{\sigma} \cdot \vec{\nabla} + V \right) \begin{pmatrix} \psi_1 \\ \psi_2 \end{pmatrix}, \tag{A11}$$

where $v_f = 10^6\ m/s$ is the mentioned Fermi velocity and $V(x,z,t)$ is the electrostatic potential. $\vec{\sigma}$ are the Pauli matrices:

$$\vec{\sigma} = (\sigma_x, \sigma_z) = \left(\begin{pmatrix} 0 & 1 \\ 1 & 0 \end{pmatrix}, \begin{pmatrix} 0 & -i \\ i & 0 \end{pmatrix} \right). \tag{A12}$$

Usually, in the literature, one finds σ_z as σ_y, however, since we defined the graphene plane as the XZ one, the notation here is different. Then, we can obtain a continuity equation for the Dirac equation and then we can easily identify the Bohmian velocities of electrons as [44]

$$\vec{v}(\vec{r},t) = \frac{v_f \psi(\vec{r},t)^\dagger \vec{\sigma} \psi(\vec{r},t)}{|\psi(\vec{r},t)|^2}. \tag{A13}$$

By time integrating (A13) we can obtain the quantum Bohmian trajectories. The initial positions of the trajectories must be distributed according to the modulus square of the initial wavefunction, i.e., satisfying the quantum equilibrium hypothesis and thus certifying the same empirical results as the orthodox theory [44]. All this formalism was introduced in the BITLLES simulator in order to correctly model graphene and other linear band structure materials.

References

1. Jacoboni, C.; Reggiani, L. The Monte Carlo method for the solution of charge transport in semiconductors with applications to covalent materials. *Rev. Mod. Phys.* **1983**, *55*, 645. [CrossRef]
2. Available online: http://www.nextnano.de (accessed on 22 November 2019).
3. Available online: http://www.tibercad.org (accessed on 22 November 2019).
4. Available online: http://vides.nanotcad.com/vides/ (accessed on 22 November 2019).
5. Albareda, G.; Jiménez, D.; Oriols, X. Intrinsic noise in aggressively scaled field-effect transistors. *J. Stat. Mech. Theory Exp.* **2009**, *2009*, P01044. [CrossRef]
6. Breuer, H.P.; Petruccione, F. *The Theory of Open Quantum Systems*; Oxford University Press: Oxford, UK, 2002.
7. Smirne, A.; Breuer, H.P.; Piilo, J.; Vacchini, B. Initial correlations in open-systems dynamics: The Jaynes-Cummings model. *Phys. Rev. A* **2010**, *82*, 062114. [CrossRef]

8. De Vega, I.; Alonso, D. Dynamics of non-Markovian open quantum systems. *Rev. Mod. Phys.* **2017**, *89*, 015001. [CrossRef]
9. Vacchini, B. Non-Markovian dynamics for bipartite systems. *Phys. Rev. A* **2008**, *78*, 022112. [CrossRef]
10. Gisin, N. Stochastic quantum dynamics and relativity. *Helv. Phys. Acta* **1989**, *62*, 363–371.
11. Pearle, P. Combining stochastic dynamical state-vector reduction with spontaneous localization. *Phys. Rev. A* **1989**, *39*, 2277. [CrossRef]
12. Carmichael, H. *An Open Systems Approach to Quantum Optics: Lectures Presented at the Université Libre de Bruxelles, October 28 to November 4 1991*; Springer Science & Business Media: Berlin/Heidelberg, Germany, 2009; Volume 18.
13. Van Kampen, N.G. *Stochastic Processes in Physics and Chemistry*; Elsevier: Radarweg/Amsterdam, The Netherlands 1992; Volume 1.
14. De Vega, I. Non-Markovian stochastic Schrödinger description of transport in quantum networks. *J. Phys. B At. Mol. Opt. Phys.* **2011**, *44*, 245501. [CrossRef]
15. Goetsch, P.; Graham, R. Linear stochastic wave equations for continuously measured quantum systems. *Phys. Rev. A* **1994**, *50*, 5242. [CrossRef]
16. Gatarek, D.; Gisin, N. Continuous quantum jumps and infinite-dimensional stochastic equations. *J. Math. Phys.* **1991**, *32*, 2152–2157. [CrossRef]
17. Gambetta, J.; Wiseman, H. Non-Markovian stochastic Schrödinger equations: Generalization to real-valued noise using quantum-measurement theory. *Phys. Rev. A* **2002**, *66*, 012108. [CrossRef]
18. Rivas, A.; Huelga, S.F.; Plenio, M.B. Quantum non-Markovianity: Characterization, quantification and detection. *Rep. Prog. Phys.* **2014**, *77*, 094001. [CrossRef] [PubMed]
19. Diósi, L. Non-Markovian continuous quantum measurement of retarded observables. *Phys. Rev. Lett.* **2008**, *100*, 080401. [CrossRef] [PubMed]
20. Wiseman, H.M.; Gambetta, J.M. Pure-state quantum trajectories for general non-Markovian systems do not exist. *Phys. Rev. Lett.* **2008**, *101*, 140401. [CrossRef] [PubMed]
21. Eisenberg, B.; Oriols, X.; Ferry, D. Dynamics of current, charge and mass. *Comput. Math. Biophys.* **2017**, *5*, 78–115. [CrossRef]
22. Oriols, X.; Ferry, D. Quantum transport beyond DC. *J. Comput. Electron.* **2013**, *12*, 317–330. [CrossRef]
23. Gambetta, J.; Wiseman, H. Interpretation of non-Markovian stochastic Schrödinger equations as a hidden-variable theory. *Phys. Rev. A* **2003**, *68*, 062104. [CrossRef]
24. Gambetta, J.; Wiseman, H. Modal dynamics for non-orthogonal decompositions. *Found. Phys.* **2003**, *34*, 419–448. [CrossRef]
25. Colomés, E.; Zhan, Z.; Marian, D.; Oriols, X. Quantum dissipation with conditional wave functions: Application to the realistic simulation of nanoscale electron devices. *Phys. Rev. B* **2017**, *96*, 075135. [CrossRef]
26. Oriols, X. Quantum-Trajectory Approach to Time-Dependent Transport in Mesoscopic Systems with Electron-Electron Interactions. *Phys. Rev. Lett.* **2007**, *98*, 066803. [CrossRef]
27. Alarcón, A.; Yaro, S.; Cartoixa, X.; Oriols, X. Computation of many-particle quantum trajectories with exchange interaction: Application to the simulation of nanoelectronic devices. *J. Phys. Condens. Matter* **2013**, *25*, 325601. [CrossRef] [PubMed]
28. Albareda, G.; López, H.; Cartoixa, X.; Suné, J.; Oriols, X. Time-dependent boundary conditions with lead-sample Coulomb correlations: Application to classical and quantum nanoscale electron device simulators. *Phys. Rev. B* **2010**, *82*, 085301. [CrossRef]
29. Albareda, G.; Suñé, J.; Oriols, X. Many-particle hamiltonian for open systems with full coulomb interaction: Application to classical and quantum time-dependent simulations of nanoscale electron devices. *Phys. Rev. B* **2009**, *79*, 075315. [CrossRef]
30. Nakajima, S. On quantum theory of transport phenomena: Steady diffusion. *Prog. Theor. Phys.* **1958**, *20*, 948–959. [CrossRef]
31. Zwanzig, R. Ensemble method in the theory of irreversibility. *J. Chem. Phys.* **1960**, *33*, 1338–1341. [CrossRef]
32. Dalibard, J.; Castin, Y.; Mølmer, K. Wave-function approach to dissipative processes in quantum optics. *Phys. Rev. Lett.* **1992**, *68*, 580. [CrossRef]
33. Strunz, W.T.; Diósi, L.; Gisin, N. Open system dynamics with non-Markovian quantum trajectories. *Phys. Rev. Lett.* **1999**, *82*, 1801. [CrossRef]

34. Barchielli, A.; Gregoratti, M. Quantum measurements in continuous time, non-Markovian evolutions and feedback. *Philos. Trans. R. Soc. A Math. Phys. Eng. Sci.* **2012**, *370*, 5364–5385. [CrossRef]
35. Wiseman, H.M.; Milburn, G.J. *Quantum Measurement and Control*; Cambridge University Press: Cambridge, UK, 2009.
36. Kraus, K. *States, Effects and Operations: Fundamental Notions of Quantum Theory*; Springer: Berlin/Heidelberg, Germany, 1983.
37. Diósi, L.; Gisin, N.; Strunz, W.T. Non-Markovian quantum state diffusion. *Phys. Rev. A* **1998**, *58*, 1699. [CrossRef]
38. Gambetta, J.; Wiseman, H. Perturbative approach to non-Markovian stochastic Schrödinger equations. *Phys. Rev. A* **2002**, *66*, 052105. [CrossRef]
39. Budini, A.A. Non-Markovian Gaussian dissipative stochastic wave vector. *Phys. Rev. A* **2000**, *63*, 012106. [CrossRef]
40. Bassi, A.; Ghirardi, G. Dynamical reduction models with general Gaussian noises. *Phys. Rev. A* **2002**, *65*, 042114. [CrossRef]
41. Bassi, A. Stochastic Schrödinger equations with general complex Gaussian noises. *Phys. Rev. A* **2003**, *67*, 062101. [CrossRef]
42. d'Espagnat, B. *Conceptual Foundations of Quantum Mechanics*; CRC Press: Boca Raton, FL, USA, 2018.
43. Benseny, A.; Albareda, G.; Sanz, Á.S.; Mompart, J.; Oriols, X. Applied bohmian mechanics. *Eur. Phys. J. D* **2014**, *68*, 286. [CrossRef]
44. Pladevall, X.O.; Mompart, J. *Applied Bohmian Mechanics: From Nanoscale Systems to Cosmology*; CRC Press: Boca Raton, FL, USA, 2019.
45. Holland, P.R. *The Quantum Theory of Motion: An Account of the De Broglie-Bohm Causal Interpretation of Quantum Mechanics*; Cambridge University Press: Cambridge, UK, 1995.
46. Bohm, D. A suggested interpretation of the quantum theory in terms of "hidden" variables. I. *Phys. Rev.* **1952**, *85*, 166. [CrossRef]
47. Dürr, D.; Goldstein, S.; Tumulka, R.; Zanghi, N. Bohmian mechanics and quantum field theory. *Phys. Rev. Lett.* **2004**, *93*, 090402. [CrossRef]
48. Dürr, D.; Goldstein, S.; Zanghi, N. Quantum equilibrium and the origin of absolute uncertainty. *J. Stat. Phys.* **1992**, *67*, 843–907. [CrossRef]
49. Pandey, D.; Sampaio, R.; Ala-Nissila, T.; Albareda, G.; Oriols, X. Unmeasured Bohmian properties and their measurement through local-in-position weak values for assessing non-contextual quantum dynamics. 2019, submitted.
50. Alarcón, A.; Albareda, G.; Traversa, F.L.; Benali, A.; Oriols, X. Nanoelectronics: Quantum electron transport. In *Applied Bohmian Mechanics: From Nanoscale Systems to Cosmology*; Pan Standford Publishing: Singapore, 2012; pp. 365–424.
51. Albareda, G.; Marian, D.; Benali, A.; Yaro, S.; Zanghì, N.; Oriols, X. Time-resolved electron transport with quantum trajectories. *J. Comput. Electron.* **2013**, *12*, 405–419. [CrossRef]
52. Albareda, G.; Marian, D.; Benali, A.; Alarcón, A.; Moises, S.; Oriols, X., Electron Devices Simulation with Bohmian Trajectories. In *Simulation of Transport in Nanodevices*; John Wiley and Sons, Ltd.: Hoboken, NJ, USA, 2016; Chapter 7, pp. 261–318. [CrossRef]
53. Marian, D.; Colomés, E.; Oriols, X. Time-dependent exchange and tunneling: Detection at the same place of two electrons emitted simultaneously from different sources. *J. Phys. Condens. Matter* **2015**, *27*, 245302. [CrossRef]
54. Marian, D.; Colomés, E.; Zhan, Z.; Oriols, X. Quantum noise from a Bohmian perspective: Fundamental understanding and practical computation in electron devices. *J. Comput. Electron.* **2015**, *14*, 114–128. [CrossRef]
55. Alarcón, A.; Oriols, X. Computation of quantum electron transport with local current conservation using quantum trajectories. *J. Stat. Mech. Theory Exp.* **2009**, *2009*, P01051. [CrossRef]
56. López, H.; Albareda, G.; Cartoixà, X.; Suñé, J.; Oriols, X. Boundary conditions with Pauli exclusion and charge neutrality: application to the Monte Carlo simulation of ballistic nanoscale devices. *J. Comput. Electron.* **2008**, *7*, 213–216. [CrossRef]
57. Albareda, G.; Appel, H.; Franco, I.; Abedi, A.; Rubio, A. Correlated electron-nuclear dynamics with conditional wave functions. *Phys. Rev. Lett.* **2014**, *113*, 083003. [CrossRef] [PubMed]

58. Norsen, T.; Marian, D.; Oriols, X. Can the wave function in configuration space be replaced by single-particle wave functions in physical space? *Synthese* **2015**, *192*, 3125–3151. [CrossRef]
59. Albareda, G.; Kelly, A.; Rubio, A. Nonadiabatic quantum dynamics without potential energy surfaces. *Phys. Rev. Mater.* **2019**, *3*, 023803. [CrossRef]
60. Zhan, Z.; Kuang, X.; Colomés, E.; Pandey, D.; Yuan, S.; Oriols, X. Time-dependent quantum Monte Carlo simulation of electron devices with two-dimensional Dirac materials: A genuine terahertz signature for graphene. *Phys. Rev. B* **2019**, *99*, 155412. [CrossRef]
61. Albareda, G.; Benali, A.; Oriols, X. Self-consistent time-dependent boundary conditions for static and dynamic simulations of small electron devices. *J. Comput. Electron.* **2013**, *12*, 730–742. [CrossRef]
62. Marian, D.; Zanghì, N.; Oriols, X. Weak values from displacement currents in multiterminal electron devices. *Phys. Rev. Lett.* **2016**, *116*, 110404. [CrossRef]
63. Albareda, G.; Traversa, F.; Benali, A.; Oriols, X. Computation of quantum electrical currents through the Ramo–Shockley–Pellegrini theorem with trajectories. *Fluct. Noise Lett.* **2012**, *11*, 1242008. [CrossRef]
64. Pandey, D.; Bellentani, L.; Villani, M.; Albareda, G.; Bordone, P.; Bertoni, A.; Oriols, X. A Proposal for Evading the Measurement Uncertainty in Classical and Quantum Computing: Application to a Resonant Tunneling Diode and a Mach-Zehnder Interferometer. *Appl. Sci.* **2019**, *9*, 2300. [CrossRef]
65. Misra, B.; Sudarshan, E.G. The Zeno's paradox in quantum theory. *J. Math. Phys.* **1977**, *18*, 756–763. [CrossRef]
66. Home, D.; Whitaker, M. A conceptual analysis of quantum Zeno; paradox, measurement, and experiment. *Ann. Phys.* **1997**, *258*, 237–285. [CrossRef]
67. Colodny, R.G. *Paradigms and Paradoxes: The Philosophical Challenge of The Quantum Domain*; University of Pittsburgh Press: London, UK, 1972; Volume 5.
68. Cabello, A.; Gu, M.; Gühne, O.; Larsson, J.Å.; Wiesner, K. Thermodynamical cost of some interpretations of quantum theory. *Phys. Rev. A* **2016**, *94*, 052127. [CrossRef]

Publication C

Devashish Pandey, Xavier Oriols, and Guillermo Albareda. Effective 1D Time-Dependent Schrödinger Equations for 3D Geometrically Correlated Systems. *Materials*, 13(13), 2020

materials

MDPI

Article

Effective 1D Time-Dependent Schrödinger Equations for 3D Geometrically Correlated Systems

Devashish Pandey [1,*], Xavier Oriols [1,*] and Guillermo Albareda [2,3,*]

[1] Departament d'Enginyeria Electrònica, Universitat Autònoma de Barcelona, Edifici Q, 08193 Bellaterra, Spain
[2] Max Planck Institute for the Structure and Dynamics of Matter and Center for Free-Electron Laser Science, Luruper Chaussee 149, 22761 Hamburg, Germany
[3] Institut de Química Teòrica i Computacional (IQTCUB), Universitat de Barcelona, Martí i Franquès 1, 08028 Barcelona, Spain
* Correspondence: devashish.pandey@uab.cat (D.P.); xavier.oriols@uab.cat (X.O.); guillermo.albareda@mpsd.mpg.de (G.A.)

Received: 10 May 2020; Accepted: 1 July 2020; Published: 7 July 2020

Abstract: The so-called Born–Huang ansatz is a fundamental tool in the context of ab-initio molecular dynamics, viz., it allows effectively separating fast and slow degrees of freedom and thus treating electrons and nuclei with different mathematical footings. Here, we consider the use of a Born–Huang-like expansion of the three-dimensional time-dependent Schrödinger equation to separate transport and confinement degrees of freedom in electron transport problems that involve geometrical constrictions. The resulting scheme consists of an eigenstate problem for the confinement degrees of freedom (in the transverse direction) whose solution constitutes the input for the propagation of a set of coupled one-dimensional equations of motion for the transport degree of freedom (in the longitudinal direction). This technique achieves quantitative accuracy using an order less computational resources than the full dimensional simulation for a typical two-dimensional geometrical constriction and upto three orders for three-dimensional constriction.

Keywords: nanojunction; constriction; quantum electron transport; quantum confinement; dimensionality reduction; stochastic Schrödinger equations; geometric correlations

1. Introduction

Nanoscale constrictions (sometimes referred to as point contacts or nanojunctions) are unique objects for the generation and investigation of ballistic electron transport in solids. Studies of such systems have been inspired by the pioneering investigations of Sharvin in the mid-1960s [1]. Today, advances in fabrication techniques like direct growth of branched nanostructures [2], electron beam irradiation [3], thermal and electrical welding [4], or atomic force microscope [5] have allowed controlling the size and composition of nanojunctions for creating devices with desired functionalities. In this respect, a number of nanodevices based on nanojunctions like single electron transistors [6,7], field effect transistors [8,9], and heterostructure nanowires [10,11] have been recently reported, which promise great performance in terms of miniaturization and power consumption.

In the design of these nanostructures, simulation tools constitute a valuable alternative to the expensive and time-consuming test-and-error experimental procedure. A number of quantum electron transport simulators are available to the scientific community [12–16]. The amount of information that these simulators can provide, however, is mainly restricted to the stationary regime, and therefore, their predicting capabilities are still far from those of the traditional Monte Carlo solution of the semi-classical Boltzmann transport equation [17]. This limitation poses a serious problem in the near

future as electron devices are foreseen to operate in the terahertz (THz) regime. At these frequencies, the discrete nature of electrons in the active region is expected to generate unavoidable fluctuations of the current that could interfere with the correct operation of such devices both for analog and digital applications [18].

A formally exact approach to electron transport beyond the quasi-stationary regime relies in the modeling of the active region of electron devices as an open quantum system [19,20]. As such, one can then borrow any state-of-the-art mathematical tool developed to study open quantum systems [21,22]. A preferred technique has been the stochastic Schrödinger equation (SSE) approach [23–30]. Instead of directly solving equations of motion for the reduced density matrix, the SSE approach exploits the state vector nature of the so-called conditional states to alleviate some computational burden [31].

As an example of the practical utility of the SSE, a Monte Carlo simulation scheme to describe quantum electron transport in open systems that is valid both for Markovian or non-Markovian regimes guaranteeing a dynamical map that preserves complete positivity has been recently proposed [32]. The resulting algorithm for quantum transport simulations reformulates the traditional "curse of dimensionality" that plagues all state-of-the-art techniques for solving the time-dependent Schrödinger equation (TDSE). Specifically, the algorithm consists of the solution of an ensemble of single-particle SSEs that are coupled, one to each other, through effective Coulombic potentials [33–35]. Furthermore, the simulation technique accounts for dissipation [36] and guarantees charge and current conservation through the use of self-consistent time-dependent boundary conditions [37–39] that partially incorporate exchange correlation [39,40]. Solving a large number of three-dimensional (3D) single-particle TDSEs, however, may still be a very time-consuming task. Therefore, the above technique would greatly benefit from the possibility of further reducing the dimensionality of the associated numerical problem.

It is the purpose of this work to derive and discuss a method that allows solving the 3D TDSE in terms of an ensemble of one-dimensional (1D) TDSEs. The technique is inspired by the so-called Born–Huang ansatz [41], which is a fundamental tool in the context of ab-initio molecular dynamics that allows separating fast and slow degrees of freedom in an effective way [42]. Here, we consider an analogous ansatz to separate transport and confinement directions. As it will be shown, the resulting technique allows to describe arbitrary geometric correlations in terms of a coupled set of 1D TDSEs. Therefore, while we have motivated the development of this method in the context of the simulation of (non-Markovian) quantum transport in open systems, the method presented here could be of great utility in many research fields where the reduction of the computational cost associated with the solution of an ensemble of SSEs may be advantageous. This includes, for example, the description of spin thermal transport [43,44], thermal relaxation dynamics [19,45], ionic motion [46,47], or Bose–Einstein condensates [48–50] in terms of SSEs.

The manuscript is structured as follows. In Section 2, we introduce a Born–Huang-like ansatz that allows expanding the 3D single-particle TDSE in terms of an infinite set of (transverse) eigenstates weighted by (longitudinal) complex coefficients. The equations of motion for the coefficients are found to be coupled and obey a non-unitary partial differential equation. In Section 3, we apply the method to a typical 2D constriction. Section 3.1 is devoted to finding analytical expressions for the effective potentials that appear in the equation of motion of the coefficients. A discussion on the geometrical dependence of these effective potentials is provided. In Section 3.2, we illustrate the performance of the method to describe the dynamics of an electron across a 2D nanojunction. In Section 4, we provide a thorough discussion on the advantages and potential drawbacks of the method. We conclude in Section 5.

2. Single-Electron Time-Dependent Schrödinger Equation in a Born–Huang-Like Basis Expansion

As we explained in the Introduction, it is our goal to reduce the computational burden associated with the solution of an ensemble of effective single-electron 3D SSE [32]. We consider our starting point to be the 3D TDSE of a single (spin-less) electron in the position basis, i.e.,

$$i\frac{\partial}{\partial t}\Psi(x,y,z,t) = H(x,y,z)\Psi(x,y,z,t), \tag{1}$$

where we have used atomic units, x, y, and z represent the three spatial coordinates, and $\Psi(x,y,z,t)$ is a well normalized wavefunction, i.e., $\iiint dx\ dy\ dz\ |\Psi(x,y,z,t)|^2 = 1\ \ \forall t$. In Equation (1), $H(x,y,z)$ is the full Hamiltonian of the system:

$$H(x,y,z) \quad = \quad T_x + T_y + T_z + V(x) + W(x,y,z), \tag{2}$$

which has been assumed to be time-independent for simplicity. The time-dependence of the scalar potentials $V(x)$ and $W(x,y,z)$ will be discussed in later sections. In Equation (2), $T_x = -\frac{1}{2}\frac{\partial^2}{\partial x^2}$ and $V(x)$ are, respectively, the kinetic energy and the scalar potential associated with the longitudinal degree of freedom x, while $T_y = -\frac{1}{2}\frac{\partial^2}{\partial y^2}$ and $T_z = -\frac{1}{2}\frac{\partial^2}{\partial z^2}$ are the kinetic energies associated with the transversal degrees of freedom y and z. The scalar potential $W(x,y,z)$ includes any other scalar potential that is not purely longitudinal, which is responsible for making the solution of Equation (1) non-separable.

It is convenient at this point to rewrite the Hamiltonian in Equation (2) in terms of longitudinal and transverse components as:

$$H(x,y,z) = T_x + V(x) + H_x^{\perp}(y,z), \tag{3}$$

where $H_x^{\perp}(y,z)$ is the transverse Hamiltonian defined as:

$$H_x^{\perp}(y,z) = T_y + T_z + W(x,y,z). \tag{4}$$

An eigenvalue equation associated with the transverse Hamiltonian can now be introduced as follows:

$$H_x^{\perp}(y,z)\phi_x^k(y,z) = \mathcal{E}_x^k\phi_x^k(y,z), \tag{5}$$

where $\mathcal{E}_x^k$ and $\phi_x^k(y,z)$ are the corresponding eigenvalues and eigenstates respectively, and $k \in \mathbb{Z}$. The eigenstates $\phi_x^k(y,z)$ form a complete orthonormal basis in which to expand the Hilbert space spanned by the variables x, y, and z. Therefore, the 3D wavefunction in Equation (1) can be expressed in terms of transverse eigenstates $\phi_x^k(y,z)$ as:

$$\Psi(x,y,z,t) = \sum_{k=1}^{\infty}\chi^k(x,t)\phi_x^k(y,z), \tag{6}$$

where $\chi^k(x,t) = \iint dydz\phi_x^k(y,z)\Psi(x,y,z,t)$ are complex longitudinal coefficients associated with the transverse eigenstate $\phi_x^k(y,z)$. Unless otherwise stated, all integrals are evaluated from $-\infty$ to ∞. It is important to note that since the longitudinal variable x appears as a parameter in Equation (5), the transverse eigenstates obey the following normalization condition:

$$\iint dydz\phi_x^l(y,z)\phi_x^k(y,z) = \delta_{lk}, \ \ \forall x. \tag{7}$$

In addition, since the full wavefunction $\Psi(x,y,z,t)$ is well normalized, then the longitudinal complex coefficients $\chi^k(x,t)$ in Equation (6) fulfill the condition:

$$\sum_{k=1}^{\infty} \int dx |\chi^k(x,t)|^2 = 1. \tag{8}$$

The wavefunction expansion in Equation (6) can now be introduced into Equation (1) to obtain an equation of motion for the coefficients $\chi^k(x,t)$ (see Appendix A):

$$i\frac{\partial}{\partial t}\chi^k(x,t) = \left(T_x + \mathcal{E}_x^k + V(x)\right)\chi^k(x,t) - \sum_{l=1}^{\infty}\left(S^{kl}(x) + F^{kl}(x)\frac{\partial}{\partial x}\right)\chi^l(x,t), \tag{9}$$

where $\mathcal{E}_x^k$ are effective potential energies (that correspond to the eigenvalues in Equation (5)) and $F^{kl}(x)$ and $S^{kl}(x)$ are geometric (first and second order) coupling terms, which read:

$$F^{kl}(x) = \iint dydz\phi_x^{*l}(y,z)\frac{\partial}{\partial x}\phi_x^k(y,z), \tag{10a}$$

$$S^{kl}(x) = \frac{1}{2}\iint dydz\phi_x^{*l}(y,z)\frac{\partial^2}{\partial x^2}\phi_x^k(y,z). \tag{10b}$$

Since the transverse eigenstates $\phi_x^k(y,z)$ are the energy eigenstates of a bounded system and can always be chosen to be real, the term F^{kk} is zero by construction. The other terms in Equation (10) dictate the transfer of the probability presence between different longitudinal coefficients $\chi^k(x,t)$ and, therefore, will be called geometric non-adiabatic couplings (GNACs). Accordingly, one can distinguish between two different dynamic regimes in Equation (9):

(i) Geometric adiabatic regime: This is the regime where F^{kl} and S^{kl} are both negligible. Thus, the solution of Equation (9) can be greatly simplified because it involves only one transverse eigenstate.

(ii) Geometric non-adiabatic regime: This is the regime where either or both F^{kl} and S^{kl} are important. Thus, the solution of Equation (9) involves the coupling between different longitudinal coefficients and hence more than one transverse eigenstate.

Interestingly, the prevalence of either the regimes (i) or (ii) can be estimated by rewriting the first order coupling terms $F^{kl}(x)$ as (see Appendix B for an explicit derivation):

$$F^{kl}(x) = \frac{\int dy \int dz \phi_x^{*l}(y,z)\left(\frac{\partial}{\partial x}W(x,y,z)\right)\phi_x^k(y,z)}{\mathcal{E}_x^l - \mathcal{E}_x^k} \quad \forall k \neq l. \tag{11}$$

That is, the importance of non-adiabatic transitions between transverse eigenstates depends on the interplay between the transverse potential-energy differences $\mathcal{E}_x^l - \mathcal{E}_x^k$ and the magnitude of the classical force field, which is proportional to $\frac{\partial}{\partial x}W(x,y,z)$. The geometric adiabatic regime (i) is reached either when the classical force field is very small or the energy differences $\mathcal{E}_x^l - \mathcal{E}_x^k$ are large enough. In the adiabatic regime, only the diagonal terms, S^{kk}, are retained, which induce a global shift of the potential-energies $\mathcal{E}_x^k$ felt by the longitudinal coefficients $\chi^k(x,t)$. In this approximation, the longitudinal degree of freedom moves in the potential-energy of a single transverse state, i.e., $\mathcal{E}_x^k$. This regime is analogous to the so-called Born–Oppenheimer approximation in the context of molecular dynamics [51], where the term S^{kk} is often called the Born–Oppenheimer diagonal correction [52]. As will be shown in our numerical example, the evolution of the system can be governed either by the geometric adiabatic or nonadiabatic regime depending on the particular spatial region where the dynamics occurs.

Let us notice at this point that the time-dependence of the Hamiltonian in Equation (2) may arise either due to a purely longitudinal time-dependent scalar potential $V(x,t)$ or through the time-dependence of the non-separable potential $W(x,y,z,t)$. If the time-dependence is added only through

$V(x,t)$, then nothing changes in the above development. On the contrary, if a time-dependence is included in $W(x,y,z,t)$, then the eigenstate problem in Equation (5) changes with time and so do the effective potential-energies $\mathcal{E}_x^k$ and the first and second order GNACs $F^{kl}(x,t)$ and $S^{kl}(x,t)$. As it will be shown later, in this circumstance, Equation (5) should be solved self-consistently with Equation (9).

Before we move to a practical example implementing the above reformulation of the 3D TDSE, let us emphasize that it is the main goal of the set of coupled equations in Equation (9) to allow the evaluation of relevant observables in terms of 1D wavefunctions only. In this respect, let us take, for example, the case of the reduced probability density $\rho(x,t) = \iint dydz\Psi^*(x,y,z,t)\Psi(x,y,z,t)$. Using the basis expansion in Equation (6), $\rho(x,t)$ can be written as:

$$\rho(x,t) = \sum_{k,l}^{\infty} \chi^{*l}(x,t)\chi^k(x,t) \iint dydz\phi_x^{*l}(y,z)\phi_x^k(y,z), \tag{12}$$

and using the condition in Equation (7), the above expression reduces to:

$$\rho(x,t) = \sum_{k=1}^{\infty} |\chi^k(x,t)|^2. \tag{13}$$

Therefore, according to Equation (13), the reduced (longitudinal) density is simply the sum of the absolute squared value of the longitudinal coefficients $\chi^k(x,t)$, which is in accordance with Equation (8), i.e., $\int dx\rho(x,t) = \sum_{k=1}^{\infty} \int dx|\chi^k(x,t)|^2 = 1$. Similarly, other relevant observables, such as the energy can easily be derived using the expansion in Equation (6) (see Appendix C).

3. Application of the Method to a Typical Constriction

The above formulation can be cast in the form of a numerical scheme to solve the 3D TDSE, which we will call, hereafter, geometrically correlated 1D TDSE (GC-TDSE). The scheme can be divided into two different parts corresponding to their distinct mathematical nature. The first part involves the solution of the eigenvalue problem in Equation (5), which allows evaluating the transverse eigenstates $\phi_x^k(y,z)$ and eigenvalues $\mathcal{E}_x^k$, as well as geometric non-adiabatic couplings $F^{kl}(x)$ and $S^{kl}(x)$ in Equation (10). These quantities are required in the second part of the algorithm to solve the equation of motion of the longitudinal coefficients $\chi^k(x,t)$ in Equation (9), which ultimately allow us to evaluate the observables of interest.

In what follows, we discuss these two aspects of the algorithm for a typical 2D geometric constriction whose geometry does not change in time. We consider one degree of freedom in the transport direction and one degree of freedom in the transverse (or confinement) direction. The generalization to a 3D system, i.e., with two transverse degrees of freedom, is straightforward and does not add any physical insight with respect to the 2D case. As will be shown, the transverse eigenstates and eigenvalues, as well as the geometric non-adiabatic couplings are, for a time-independent constriction, functions that are computed only once. That is, the effective potential-energies $\mathcal{E}_x^k$ and the non-adiabatic couplings F^{kl} and S^{kl} are computed only at the very beginning of the GC-TDSE propagation scheme. For more general time-dependent constrictions, possibly with no analytical form of $W(x,y,z,t)$, the only change in the algorithm is that Equation (5) has to be solved, self-consistently, together with Equation (9) at each time step.

3.1. Evaluation of Transverse Eigenstates (and Values) and Geometric Non-Adiabatic Couplings

Let us consider the case of a 2D nanojunction represented by the scalar potential:

$$V(x,y) = \begin{cases} 0, & \text{if } L_2(x) < y < L_1(x) \\ \infty, & \text{otherwise} \end{cases} \tag{14}$$

where $L_1(x)$ and $L_2(x)$ define the shape of the constriction. The corresponding 2D Hamiltonian reads

$$H(x,y) = T_x + V(x) + H_x^{\perp}(y), \tag{15}$$

where $H_x^{\perp}(y) = T_y + W(x,y)$. The wavefunction for a 2D constriction in terms of the Born–Huang expansion can be written as $\Psi(x,y,t) = \sum_k \chi^k(x,t)\phi_x^k(y)$, and the transverse states $\phi_x^k(y)$ are solutions of a free particle in a 1D box whose width depends on the longitudinal variable x, i.e.,

$$\phi_x^k(y) = \begin{cases} \sqrt{\frac{2}{L(x)}} \sin\left(\frac{k\pi(y-L_2(x))}{L(x)}\right), & \text{if } L_2(x) < y < L_1(x) \\ 0, & \text{otherwise.} \end{cases} \tag{16}$$

The associated eigenvalues are given by:

$$\mathcal{E}_x^k = \frac{k^2\pi^2}{2L^2(x)}, \tag{17}$$

where we have defined $L(x) = L_1(x) - L_2(x)$. These energies, parametrically dependent on the longitudinal variable x, define the effective potential-energies on which the coefficients $\chi^k(x,t)$ evolve.

To evaluate the first and second order coupling terms $F^{kl}(x)$ and $S^{kl}(x)$, we need to rely on a particular form of the constriction. Depending on the specific form of $L_1(x)$ and $L_2(x)$, different constrictions can be conceived (see for example panels (a) and (c) of Figure 1). Given the states in Equation (16) and a particular shape of the constriction (defined in Equation (A18a,b) of Appendix D), it is then easy to evaluate the non-adiabatic coupling terms F^{kl} and S^{kl} (see panels (b) and (d) of Figure 1).

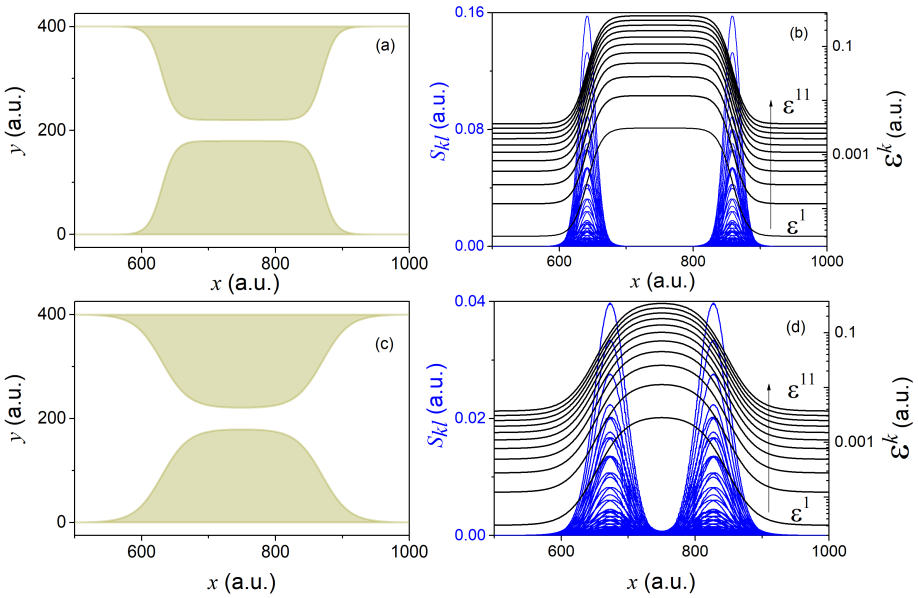

Figure 1. Two different nanojunctions, viz., (**a**,**c**), defined by Equation (A18a,b) in Appendix D and using $\mathcal{A} = 180$, $\mathcal{B} = 220$, $a_1 = 630$, $a_2 = 870$, with $\gamma = 10$ in (**a**) and $\gamma = 20$ in (**c**). Panels (**b**,**d**) show the associated second order (non-adiabatic) couplings S^{kl} (solid blue lines) and the associated potential-energies $\mathcal{E}_x^k$ (solid black lines) for the geometries in (**a**,**c**), respectively. Note that, due to the symmetry of the states defined in Equation (16), the coupling between odd and even states is zero, i.e., $F^{kl}(x) = S^{kl}(x) = 0$, $\forall k + l =$ odd.

The two different constrictions in Figure 1 serve well to gain some insight into the general form and dependence of the effective potential-energies $\mathcal{E}_x^k$, as well as of the GNACs in Equation (10). Geometries changing more abruptly lead to sharper effective potential-energies $\mathcal{E}_x^k$ and more peaked non-adiabatic coupling terms $F^{kl}(x)$ and $S^{kl}(x)$. Sharper constrictions are thus expected to cause larger non-adiabatic transitions and hence to involve a larger number of transverse eigenstates requiring a

larger number of longitudinal coefficients in order to reconstruct the reduced (longitudinal) density in Equation (12). On the contrary, smoother constrictions should yield softer non-adiabatic transitions and hence involve a smaller number of transverse eigenstates.

3.2. Time-Dependent Propagation of the Longitudinal Coefficients

Given the effective potential-energies $\mathcal{E}_x^k$ and the non-adiabatic couplings $F^{kl}(x)$ and $S^{kl}(x)$, one can then easily find a solution for the longitudinal coefficients in Equation (9). Here, we consider the dynamics of an electron that impinges upon a constriction defined by Equations (14) and (A18a,b) in Appendix D using the particular set of parameters, $\{\mathcal{A}, \mathcal{B}, a_1, a_2, \gamma\} = \{180, 220, 630, 870, 20\}$, which corresponds to panel (c) of Figure 1. Due to the symmetry of the states defined in Equation (16), transitions between odd and even states are forbidden, i.e.,

$$F^{kl}(x) = S^{kl}(x) = 0 \quad \forall k + l = \text{odd}. \tag{18}$$

We will consider two different initial states. On the one hand, the initial wavefunction $\Psi(x, y, 0)$ will be described by:

$$\Psi(x, y, 0) = \phi_x^1(y)\psi(x), \tag{19}$$

where $\phi_x^1(y)$ is the transverse ground state defined in Equation (16), and $\psi(x) = \mathcal{N} \exp\Big(ik_0(x - x_0)\Big) \exp\left(\frac{-(x-x_0)^2}{2\sigma_x^2}\right)$ is a minimum uncertainty (Gaussian) wave packet with initial momentum and dispersion $k_0 = 0.086$ a.u. and $\sigma_x = 80$ a.u., respectively, and centered at $x_0 = 300$ a.u. (while $\mathcal{N}$ is a normalization constant). On the other hand, we will consider the initial state to be defined by:

$$\Psi(x, y, 0) = \xi(y)\psi(x), \tag{20}$$

where now both $\xi(y)$ and $\psi(x)$ (defined above) are Gaussian wave packets. In particular, $\xi(y) = \mathcal{M} \exp\left(\frac{-(y-y_0)^2}{2\sigma^2}\right)$ with $y_0 = 200$ a.u., $\sigma_y = 20$ a.u. (and $\mathcal{M}$ a normalization constant). The probability densities $|\Psi(x, y, 0)|^2$ associated with the above two initial states can be seen, respectively, in panels (a) and (b) of Figure 2. Given the initial states in Equations (19) and (20), we can then evaluate the corresponding longitudinal coefficients as follows:

$$\chi^k(x, 0) = \int dy \phi_x^k(y)\Psi(x, y, 0). \tag{21}$$

While the initial state in Equation (19) corresponds to $\chi^k(x, 0) = \delta_{k1}\psi(x)$, the state in Equation (20) involves a number of transverse eigenstates. Note that this second initial condition may be more realistic in practical situations, as large enough reservoirs may imply a quasi-continuum of transverse states according to Equation (17).

Starting either from Equation (19) or (20), we then propagate the resulting longitudinal coefficients at the initial time according to Equation (9). Specifically, we used a fourth order Runge–Kutta method with a time-step size of $\Delta t = 0.1$ a.u. and a spatial grid of 1500 points with a grid spacing $\Delta x = 1$ a.u. In the left panels of Figures 3 and 4, we show the time-dependent reduced density of Equation (13) evaluated from the full 2D wavefunction (dashed green line), as well as the reduced density $\rho(x, t)$ evaluated using the GC-TDSE scheme for a finite number of transversal states N_e, i.e.,

$$\rho(x, t) = \sum_{k=1}^{N_e} |\chi^k(x, t)|^2. \tag{22}$$

In addition, we also show the absolute squared value of the longitudinal coefficients, i.e., $|\chi^k(x,t)|^2$, evaluated using the GC-TDSE. Alternatively, in the right panels of Figures 3 and 4, we plot the population of each transverse state,

$$P^k(t) = \int dx |\chi^k(x,t)|^2, \tag{23}$$

as a function of time using the GC-TDSE.

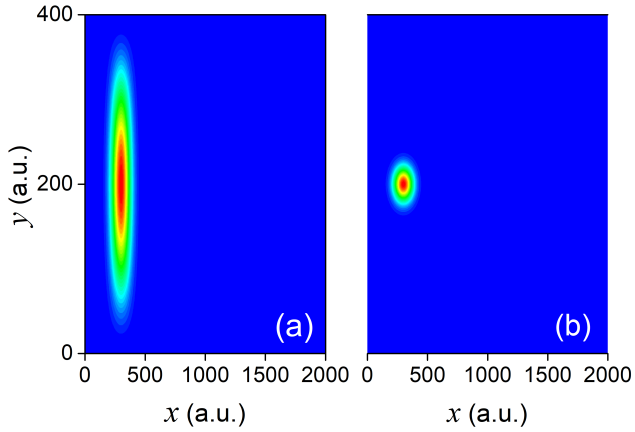

Figure 2. Panels (**a**,**b**) represent the probability density $|\Psi(x,y,0)|^2$ associated with the wavefunctions in Equations (19) and (20) respectively. Red regions in the plots correspond to higher probability densities, while blue regions correspond to lower probabilities.

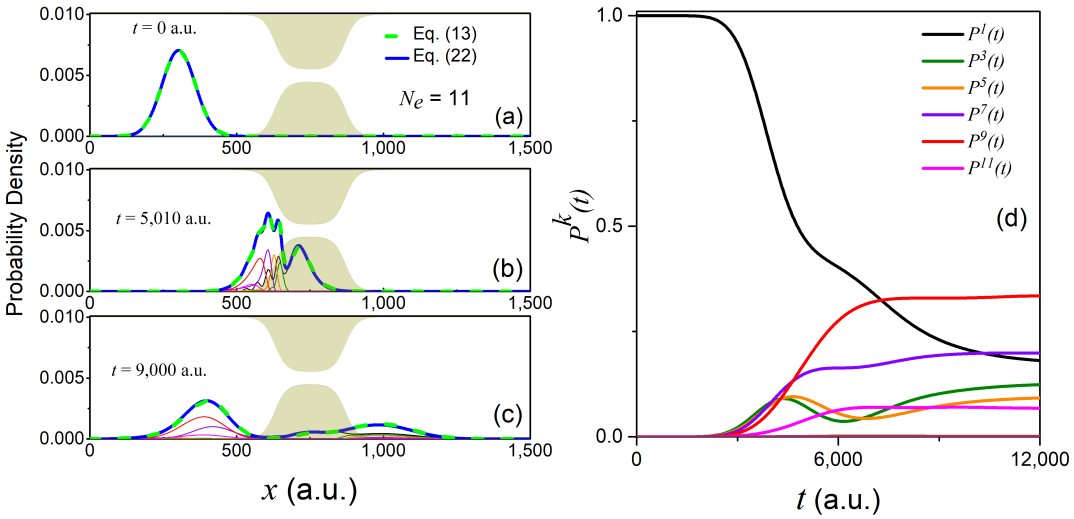

Figure 3. Time-evolution of the initial wavefunction in Equation (19). The reduced density in Equation (13) (dashed green line), as well as the reduced density in Equation (22) for $N_e = 11$ (solid dark blue) are shown at times $t = 300$ a.u., $t = 5010$ a.u., and $t = 9000$ a.u. in panels (**a**), (**b**), and (**c**), respectively. The rest of the lines correspond to the absolute squared value of the longitudinal coefficients $\chi^k(x,t)$. The evolution of the adiabatic populations in Equation (23) can be found in panel (**d**), using the same color code as in panels (**a**–**c**).

The initial state in Equation (19) yields $P^k(0) = \delta_{k1}$. This can be seen in the right-hand panel of Figure 3. This value stays constant until the wave packet hits the constriction at around $t = 2500$ a.u. At this moment, non-adiabatic transitions between different transverse states start to occur that lead to complicated interference patterns at later times (see, e.g., the reduced density $\rho(x,t)$ at $t = 5010$ a.u.). The number of significantly populated transverse states increases up to six (while up to eleven states

are required to reproduce the exact reduced density up to a 0.1% error). Among these states, only odd transverse states are accessible due to the symmetry of the initial state (as we noted in Equation (18)). Since the mean energy of the initial state in Equation (19) ($\langle\hat{\mathcal{E}}\rangle = 0.0037$ a.u.) is higher than the barrier height of the first effective potential-energy in Figure 1d ($\max(\mathcal{E}_x^1) = 0.0028$ a.u.), one could naively expect a complete transmission of the wave packet $\chi^1(x,t)$. However, due to the effect of the non-adiabatic coupling terms $F^{kl}(x)$ and $S^{kl}(x)$, $\chi^1(x,t)$ loses a major part of its population in favor of higher energy transverse components that are reflected by much higher effective potential-energy barriers.

Starting with the second initial state in Equation (20), there are up to seven transverse states populated at the initial time, all of which are again odd states due to the symmetry of the initial conditions (see Figure 4d). Once the wave packet hits the constriction at $t = 3000$ a.u, States 3, 7, and 9 become more dominant than the previously dominant States 1, 3, and 5. Overall, up to 15 states become important to reproduce the exact reduced longitudinal density within a 0.1% error. Given the above two examples, it seems clear that the specific form of the impinging wavefunction does play a significant role in the scaling of the number of relevant transverse states N_e required to evaluate Equation (9) numerically.

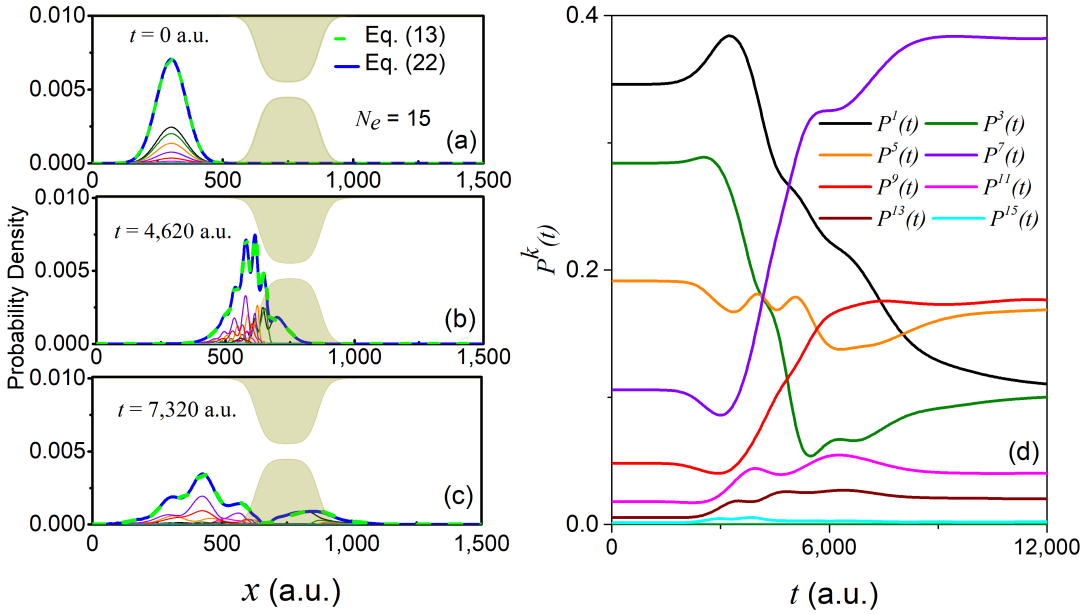

Figure 4. Time-evolution of the initial wavefunction in Equation (20). The reduced density in Equation (13) (dashed green line), as well as the reduced density in Equation (22) for $N_e = 15$ (solid dark blue line) are shown at times $t = 0$ a.u., $t = 4620$ a.u., and $t = 7320$ a.u. in panels (**a**), (**b**), and (**c**), respectively. The rest of the lines correspond to the absolute squared value of the longitudinal coefficients $\chi^k(x,t)$. The evolution of the adiabatic populations in Equation (23) can be found in panel (**d**), using the same color code as in panels (**a**–**c**).

Let us finally consider the effect that an external bias along the longitudinal direction might have on the number N_e of transverse eigenstates required to reproduce the solution of the full 2D TDSE. For that, starting with the state in Equation (20), we consider the transmission coefficient $T = \int_{-\infty}^{\infty} dy \int_{x_m}^{\infty} dx |\Psi(x,y,t_f)|^2$ for different values of the external potential $V_{ext} = V(x)$ in Equation (15). Written in terms of the Born–Huang expansion in Equation (6), the transmission coefficient T reads:

$$T = \sum_{k=1}^{N_e} \int_{x_m}^{\infty} dx |\chi^k(x,t_f)|^2, \tag{24}$$

where x_m is the center of the nanojunction in the longitudinal direction (i.e., with numerical value 750 a.u.) and t_f is the time at which no probability density (i.e., less than 0.1%) remains inside the constriction. In Figure 5, we show results for applied bias 0.0075 a.u. $\leq V_{ext} \leq$ 0.045 a.u. and two different number of states $N_e = 15$ and $N_e = 25$. As expected, a higher applied bias leads to a more vigorous collision of the wave packet against the constriction due to a higher longitudinal momentum/energy, which allows higher energy transverse states to be populated.

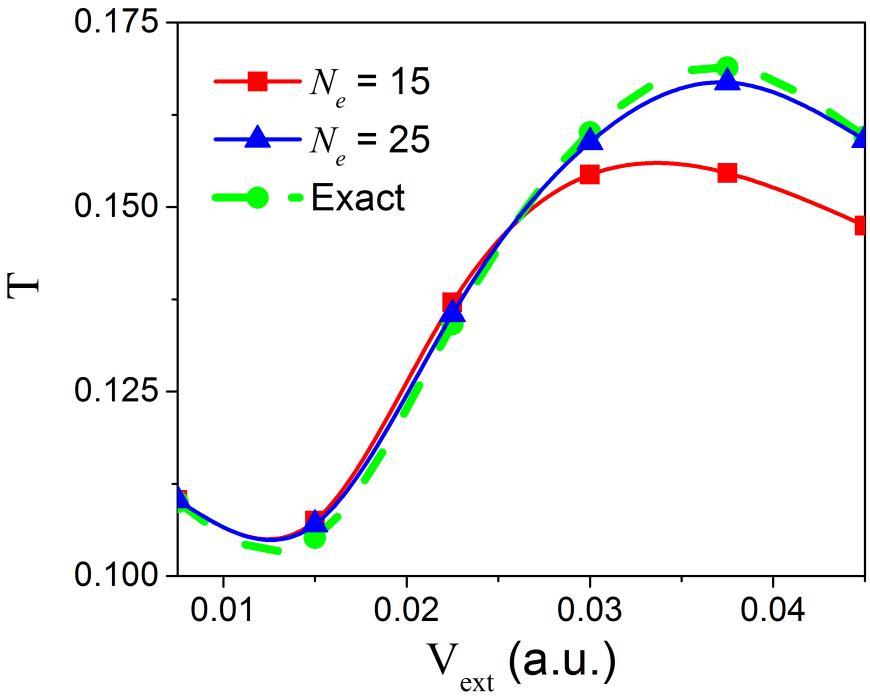

Figure 5. Figure depicting the transmission coefficient, T, under different bias voltages applied along the longitudinal direction. This plot provides a comparison for T between the exact 2D simulation (shown in dashed green line) and the 1D simulation (shown in solid red line for $N_e = 15$ states and in the solid blue line for $N_e = 25$ states). For a voltage range of 0.0075 a.u. $\leq V_{ext} \leq$ 0.045 a.u., $N_e = 25$ states are enough to capture the exact 2D case. For $\max[V_{ext}] = 0.027$ a.u., $N_e = 15$ states sufficiently capture the exact 2D case.

4. General Discussion

The GC-TDSE algorithm discussed in the previous sections has a clear computational advantage over the solution of the full 2D TDSE. This is particularly so when the quantities $\mathcal{E}_x^k$, $F^{kl}(x)$, and $S^{kl}(x)$, involved in the equation of motion of the longitudinal coefficients $\chi^k(x,t)$, are time-independent functions. For a time-independent transverse Hamiltonian, the quantities $\mathcal{E}_x^k$, $F^{kl}(x)$, and $S^{kl}(x)$ are computed only once before the propagation of the longitudinal coefficients, and thus, the computational cost of the GC-TDSE resides, mainly, on the propagation of the 1D longitudinal coefficients.

Let us provide some numbers to estimate the numerical efficiency of the GC-TDSE algorithm. Consider the numerical solution of the full 2D TDSE in a grid. For a number of grid points $\{n_x, n_y\} = \{1500, 400\}$, the resulting Hamiltonian has a dimension $(n_x \times n_y)^2$. Alternatively, the size of the Hamiltonian involved in the propagation of the longitudinal coefficients of the GC-TDSE algorithm is $(n_x \times N_e)^2$, where N_e is the number of transverse eigenstates. One can then estimate the numerical efficiency of one method over the other by simply evaluating the ratio $(n_x \times n_y)^2/(n_x \times N_e)^2$. Thus, for time-independent transverse potentials $W(x,y,z)$, the computational reduction associated with the GC-TDSE is n_y^2/N_e^2. Note that the benefits of the GC-TDSE would be even more noticeable when applied to a 3D problem, for which the above ratio would become $(n_y^2 \times n_z^2)/N_e^2$.

As we have seen in the above section, the number of required transverse states N_e is a function of the abruptness/smoothness of the constriction, but also of the energy of the impinging wave packet. Therefore, the computational advantage of the GC-TDSE method over the full dimensional TDSE is clearly system-dependent. Slow wave packets impinging upon smooth constrictions would maximize the benefits of the GC-TDSE. Contrarily, very energetic electrons colliding against abrupt constrictions would certainly minimize its benefits. In this respect, we must note that the GNACs have a clear dependence on the profile of the constriction. In particular, the second order coupling terms $S^{kl}(x)$ will be sharply peaked for very abrupt constrictions (see the important differences in the size and sharpness of the $S^{kl}(x)$ in Figure 1 for two different constrictions). Therefore, due to the non-unitary character of the equations of motion of the longitudinal coefficients, very abrupt constrictions may demand very fine grids in practice.

Finally, let us mention that whenever the transverse Hamiltonian in Equation (4) is time-dependent, the advantage of the GC-TDSE method compared to the solution of the full dimensional TDSE is not so obvious. As we have already noticed, for a time-dependent transverse potential $W(x, y, z, t)$, the eigenvalue problem in Equation (5) must be solved self-consistently with Equation (9), i.e., at each time step. Then, a comparison of the GC-TDSE and the full dimensional TDSE in terms of numerical efficiency will depend on the specific performance of the eigensolver utilized to evaluate the transverse eigenvalues, $\mathcal{E}_x^k$, and eigenstates $\phi_x^k(y, z)$.

5. Conclusions

In this work, we proposed a new method, named GC-TDSE, that allows including arbitrary 3D geometric correlations between traversal and longitudinal degrees of freedom into a coupled set of 1D TDSE. Our motivation for the development of this method was, initially, the reduction of the dimensionality of the 3D Schrödinger-like equations that result from an SSE (Monte Carlo) approach to quantum electron transport in open systems (valid for Markovian and non-Markovian regimes) that we recently proposed [32]. Nevertheless, the method presented here is general and allows reducing the dimensionality of quantum systems with geometrical correlations among different degrees of freedom, which could be of utility also in different research fields such as for example spin thermal transport [43,44], thermal relaxation dynamics [19,45], ionic motion [46,47], or Bose–Einstein condensates [48–50].

For smooth time-independent constriction profiles under low applied bias, our GC-TDSE method implies up to three orders of magnitude less computational resources than solving the full 3D TDSE directly. For very high applied bias or time-dependent constriction profiles, the GC-TDSE may still be significantly less expensive than the solution of the full 3D TDSE, but would require introducing approximations to the solution of the potential-energies $\mathcal{E}_x^k$ and the GNACs ($F^{kl}(x, t)$ and $S^{kl}(x, t)$). We thus expect the GC-TDSE presented here to trigger future investigation for making it robust against stronger geometrical correlations among different spatial directions.

Author Contributions: Conceptualization, D.P., X.O. and G.A.; methodology, D.P., X.O. and G.A.; software, D.P. and G.A.; validation, D.P., G.A. and X.O.; formal analysis, D.P., X.O. and G.A.; investigation, D.P., X.O. and G.A.; resources, D.P., X.O. and G.A.; data curation, D.P., G.A. and X.O.; writing, original draft preparation, D.P., X.O. and G.A.; writing, review and editing, D.P., X.O. and G.A.; visualization, D.P., X.O. and G.A.; supervision, X.O. and G.A.; project administration, X.O. and G.A.; funding acquisition, X.O. All authors read and agreed to the published version of the manuscript.

Funding: We acknowledge financial support from Spain's Ministerio de Ciencia, Innovación y Universidades under Grant No. RTI2018-097876-B-C21 (MCIU/AEI/FEDER, UE), the European Union's Horizon 2020 research and innovation program under Grant Agreement No. Graphene Core2 785219 and under the Marie Sklodowska-Curie Grant Agreement No. 765426 (TeraApps), and the Generalitat de Catalunya under Grant No. 001-P-001644 (QUANTUM CAT). G.A. also acknowledges financial support from the European Unions Horizon 2020 research and innovation program under the Marie Skodowska-Curie Grant Agreement No. 752822, the Spanish Ministerio de Economa y Competitividad (Project No. CTQ2016-76423-P), and the Generalitat de Catalunya (Project No. 2017 SGR 348).

Conflicts of Interest: The authors declare no conflict of interest.

Appendix A. Derivation of Equation (9)

In order to derive Equation (9), we start by introducing Equation (6) into Equation (1) to get:

$$i\frac{\partial}{\partial t}\sum_k \chi^k(x,t)\phi_x^k(y,z) = T_x\sum_k \chi^k(x)\phi_x^k(y,z) + H(y,z)\sum_k \chi^k(x)\phi_x^k(y,z) + V(x)\sum_k \chi^k(x)\phi_x^k(y,z). \quad \text{(A1)}$$

Making use of Equation (5), the above equation can be written as:

$$i\frac{\partial}{\partial t}\sum_k \chi^k(x,t)\phi_x^k(y,z) = T_x\sum_k \chi^k(x)\phi_x^k(y,z) + \mathcal{E}_x^k\sum_k \chi^k(x)\phi_x^k(y,z) + V(x)\sum_k \chi^k(x)\phi_x^k(y,z). \quad \text{(A2)}$$

By simply realizing that $T_x = -\frac{1}{2}\frac{\partial^2}{\partial x^2}$ is the kinetic energy operator in the position basis, we expand the term $T_x\sum_k \chi^k(x)\phi_x^k(y,z)$ as:

$$\begin{aligned} -\tfrac{1}{2}\tfrac{\partial^2}{\partial x^2}\textstyle\sum_k\left(\chi^k(x,t)\phi_x^k(y,z)\right) &= -\tfrac{1}{2}\tfrac{\partial}{\partial x}\textstyle\sum_k\left(\tfrac{\partial\chi^k(x,t)}{\partial x}\phi_x^k(y,z) + \chi^k(x,t)\tfrac{\partial}{\partial x}\phi_x^k(y,z)\right) \\ &= -\tfrac{1}{2}\textstyle\sum_k\left(\tfrac{\partial^2}{\partial x^2}(\chi^k(x,t))\phi_x^k(y,z) + 2\tfrac{\partial}{\partial x}\chi^k(x,t)\tfrac{\partial}{\partial x}\phi_x^k(y,z) + \chi^k(x,t)\tfrac{\partial^2}{\partial x^2}\phi_x^k(y,z)\right), \end{aligned} \quad \text{(A3)}$$

which can be written in a more compact way as:

$$T_x\textstyle\sum_k \chi^k(x,t)\phi_x^k(y,z) = \sum_k\left[(T_x\chi^k(x,t))\phi_x^k(y,z) - \frac{1}{2}\chi^k(x,t)\frac{\partial^2}{\partial x^2}\phi_x^k(y,z) - \frac{\partial}{\partial x}\chi^k(x,t)\frac{\partial}{\partial x}\phi_x^k(y,z)\right]. \quad \text{(A4)}$$

Now, introducing Equation (A4) back into Equation (A2), we get:

$$\begin{aligned} i\frac{\partial}{\partial t}\sum_k \chi^k(x,t)\phi_x^k(y,z) &= \sum_k\left[T_x + \mathcal{E}_x^k(y,z) + V(x)\right]\chi^k(x,t))\phi_x^k(y,z) \\ &- \frac{1}{2}\sum_k\left[\chi^k(x,t)\frac{\partial^2}{\partial x^2}\phi_x^k(y,z) + 2\frac{\partial}{\partial x}\chi^k(x,t)\frac{\partial}{\partial x}\phi_x^k(y,z)\right] \end{aligned} \quad \text{(A5)}$$

Multiplying both sides of Equation (A5) by $\int dy\int dz\phi_x^{*l}(y,z)$ and using the orthogonality condition, $\int dy\int dz\phi_x^{*l}(y,z)\phi_x^k(y,z) = \delta_{k,l}$, we finally obtain:

$$i\frac{\partial}{\partial t}\chi^k(x,t) = \left(T_x + \mathcal{E}_x^k + V(x)\right)\chi^k(x,t) - \sum_{l=1}^{\infty}\left(S^{kl}(x) + F^{kl}(x)\frac{\partial}{\partial x}\right)\chi^l(x,t), \quad \text{(A6)}$$

where we have defined $S^{kl} = \frac{1}{2}\int dy\int dz\phi_x^{*l}(y,z)\frac{\partial^2}{\partial x^2}\phi_x^k(y,z)$ and $F^{kl} = \int dy\int dz\phi_x^{*l}(y,z)\frac{\partial}{\partial x}\phi_x^k(y,z)$ as the first and second order coupling terms, respectively.

Appendix B. Derivation of Equation (11)

Let us define the wavefunctions $|\phi_l\rangle$ and $|\phi_k\rangle$. Now, evaluate the derivative of their inner product as follows,

$$\langle\phi_l|\phi_k\rangle' = \langle\phi_l'|\phi_k\rangle + \langle\phi_l|\phi_k'\rangle = \delta_{l.k} = 0, \quad k \neq l \quad \text{(A7)}$$

This implies,

$$\langle\phi_l'|\phi_k\rangle = -\langle\phi_l|\phi_k'\rangle \quad \text{(A8)}$$

Evaluating the expression given below,

$$\langle\phi_l|H^{\perp}|\phi_k\rangle' = \langle\phi_l'|H^{\perp}|\phi_k\rangle + \langle\phi_l|(H^{\perp})'|\phi_k\rangle + \langle\phi_l|H^{\perp}|\phi_k'\rangle \quad \text{(A9)}$$

where we have used the chain rule of differentiation. Using the eigenstate-eigenvalue relation from Equation (5), we get,

$$\langle\phi_l|H_x^{\perp}|\phi_k\rangle' = \mathcal{E}^k\langle\phi_l'|\phi_k\rangle + \langle\phi_l|(H^{\perp})'|\phi_k\rangle + \mathcal{E}^l\langle\phi_l|\phi_k'\rangle \quad \text{(A10)}$$

Using the relation in Equation (A8) in Equation (A10), we get,

$$\langle\phi_l|H^{\perp}|\phi_k\rangle' = (\mathcal{E}^l - \mathcal{E}^k)\langle\phi_l|\phi_k'\rangle + \langle\phi_l|(H^{\perp})'|\phi_k\rangle = 0 \tag{A11}$$

In the above equation, we have made use of the fact that $\langle\phi_l|H^{\perp}|\phi_k\rangle' = (\mathcal{E}^k\langle\phi_l|\phi_k\rangle)' = 0$, when $k \neq l$ Therefore,

$$F^{kl} = \langle\phi_l|(\phi_k\rangle)' \quad = \quad \frac{\langle\phi_l|(H^{\perp})'|\phi_k\rangle}{\mathcal{E}^k - \mathcal{E}^l} \tag{A12}$$

which can be written in the position representation and using the same nomenclature as used in the main text as follows,

$$F^{kl}(x) = \int dy \int dz \phi_x^{*l}(y,z)\frac{\partial}{\partial x}\phi_x^k(y,z) = \frac{\int dy \int dz \phi_x^{*l}(y,z)\left(\frac{\partial}{\partial x}H_x^{\perp}(y,z)\right)\phi_x^k(y,z)}{\mathcal{E}_x^l - \mathcal{E}_x^k} \tag{A13}$$

Using Equation (4), it is easy to see that only the potential function $W(x,y,z)$ will survive after the partial derivative with respect to the variable x. Therefore, we can equivalently write Equation (A13) as,

$$F^{kl}(x) = \frac{\int dy \int dz \phi_x^{*l}(y,z)\left(\frac{\partial}{\partial x}W(x,y,z)\right)\phi_k(y,z)}{\mathcal{E}_x^l - \mathcal{E}_x^k} \tag{A14}$$

Appendix C. Mean Energy in a Born–Huang-Like Basis

The mean energy of a 3D system with a Hamiltonian $H(x,y,z)$ is given by,

$$\langle\hat{\mathcal{E}}\rangle = \iiint dxdydz\Psi^*(x,y,z)H(x,y,z)\Psi(x,y,z), \tag{A15}$$

which in terms of the Hamiltonian in Equation (3) and the wavefunction expansion in Equation (6) can be written as:

$$\begin{aligned}\langle\hat{\mathcal{E}}\rangle \quad &= \quad \sum_{k,l}^{\infty}\int dx\chi^{*k}(x,t)\int dy\int dz\phi_x^{*k}(y,z)(T_x + V(x))\phi_x^l(y,z)\chi^l(x,t) \\ &+ \quad \sum_{k,l}^{\infty}\int dx\chi^{*k}(x,t)\int dy\int dz\phi_x^{*k}(y,z)H(y,z)\phi_x^l(y,z)\chi^l(x,t).\end{aligned} \tag{A16}$$

Introducing now Equation (5) and Equation (A2) into Equation (A16), we finally get:

$$\begin{aligned}\langle\hat{\mathcal{E}}\rangle \quad &= \quad \sum_{k,l}^{\infty}\int dx\chi^{*k}(x,t)\int dy\int dz\phi_x^{*k}(y,z)\Big(T_x\chi^l(x,t)\phi_x^l(y,z) - \frac{1}{2}\chi^l(x,t)\frac{\partial^2}{\partial x^2}\phi_x^l(y,z) \\ &- \quad \frac{\partial}{\partial x}\chi^l(x,t)\frac{\partial}{\partial x}\phi_x^l(y,z) + V(x)\chi^l(x,t)\phi_x^l(y,z)\Big) + \sum_k\int dx\chi^{*k}(x,t)\mathcal{E}_x^k(y,z)\chi^k(x,t) \\ &= \quad \sum_k^{\infty}\int dx\chi^{*k}(x,t)T_x\chi^k(x,t) + \sum_k\int dx\chi^{*k}(x,t)\mathcal{E}_x^k(y,z)\chi^k(x,t) + \sum_k^{\infty}\int dx\chi^{*k}(x,t)V(x)\chi^k(x,t) \\ &+ \quad \sum_{k,l}^{\infty}\Big[-\frac{1}{2}\chi^{*k}(x,t)\int dy\int dz\phi_x^{*k}(y,z)\frac{\partial^2}{\partial x^2}\phi_x^l(y,z) \\ &- \quad \chi^{*k}(x,t)\int dy\int dz\phi_x^{*k}(y,z)\frac{\partial}{\partial x}\phi_x^l(y,z)\frac{\partial}{\partial x}\Big]\chi^l(x,t) \\ &= \quad \sum_k^{\infty}\int dx\chi^{*k}(x,t)\Big[(T_x + \mathcal{E}_x^k(y,z) + V(x))\chi^k(x,t) + \sum_l^{\infty}\Big(-\frac{1}{2}\int dy\int dz\phi_x^{*k}(y,z)\frac{\partial^2}{\partial x^2}\phi_x^l(y,z) \\ &- \quad \int dy\int dz\phi_x^{*k}(y,z)\frac{\partial}{\partial x}\phi_x^l(y,z)\frac{\partial}{\partial x}\Big)\chi^l(x,t)\Big] \\ &= \quad \sum_{k=1}^{\infty}\int dx\chi^{*k}(x,t)\left[\left(T_x + \mathcal{E}_x^k + V(x)\right)\chi^k(x,t) - \sum_{l=1}^{\infty}\left(S^{kl}(x) + F^{kl}(x)\frac{\partial}{\partial x}\right)\chi^l(x,t)\right].\end{aligned} \tag{A17}$$

Appendix D. Definition of the Nano-Constriction in Figure 1

For our numerical simulations in Section 3, we considered a typical constriction where $L_1(x)$ and $L_2(x)$ in Equation (14) are defined as:

$$L_1(x) = \mathcal{A}\left[\left(1+\exp\left(\frac{x-a_1}{\gamma}\right)\right)^{-1} + \left(1+\exp\left(\frac{-x+a_2}{\gamma}\right)\right)^{-1}\right] + \mathcal{B}, \tag{A18a}$$

$$L_2(x) = \mathcal{A}\left[\left(1+\exp\left(\frac{-x+a_1}{\gamma}\right)\right)^{-1} + \left(1+\exp\left(\frac{x-a_2}{\gamma}\right)\right)^{-1}\right] - \mathcal{A}, \tag{A18b}$$

where γ defines the sharpness of the constriction, $\mathcal{A}$ and $\mathcal{B}$ define the maximum and the minimum width of the constriction, respectively $\max[L(x)] = \mathcal{B}+\mathcal{A}$ and $\min[L(x)] = \mathcal{B}-\mathcal{A}$, and a_1 and a_2 define the length of the constriction $\mathcal{L}_c = a_2 - a_1$.

References

1. Sharvin, Y.V. On the possible method for studying fermi surfaces. *Zh. Eksperim. I Teor. Fiz.* **1965**, *48*, 984.
2. Jin, Z.; Li, X.; Zhou, W.; Han, Z.; Zhang, Y.; Li, Y. Direct growth of carbon nanotube junctions by a two-step chemical vapor deposition. *Chem. Phys. Lett.* **2006**, *432*, 177–183. [CrossRef]
3. Terrones, M.; Banhart, F.; Grobert, N.; Charlier, J.C.; Terrones, H.; Ajayan, P. Molecular junctions by joining single-walled carbon nanotubes. *Phys. Rev. Lett.* **2002**, *89*, 075505. [CrossRef] [PubMed]
4. Peng, Y.; Cullis, T.; Inkson, B. Bottom-up nanoconstruction by the welding of individual metallic nanoobjects using nanoscale solder. *Nano Lett.* **2009**, *9*, 91–96. [CrossRef] [PubMed]
5. Shen, G.; Lu, Y.; Shen, L.; Zhang, Y.; Guo, S. Nondestructively Creating Nanojunctions by Combined-Dynamic-Mode Dip-Pen Nanolithography. *ChemPhysChem* **2009**, *10*, 2226–2229. [CrossRef]
6. Takahashi, Y.; Nagase, M.; Namatsu, H.; Kurihara, K.; Iwdate, K.; Nakajima, Y.; Horiguchi, S.; Murase, K.; Tabe, M. Fabrication technique for Si single-electron transistor operating at room temperature. *Electron. Lett.* **1995**, *31*, 136–137. [CrossRef]
7. Maeda, K.; Okabayashi, N.; Kano, S.; Takeshita, S.; Tanaka, D.; Sakamoto, M.; Teranishi, T.; Majima, Y. Logic operations of chemically assembled single-electron transistor. *ACS Nano* **2012**, *6*, 2798–2803. [CrossRef]
8. Tans, S.J.; Verschueren, A.R.; Dekker, C. Room-temperature transistor based on a single carbon nanotube. *Nature* **1998**, *393*, 49–52. [CrossRef]
9. Zhang, L.; Zaric, S.; Tu, X.; Wang, X.; Zhao, W.; Dai, H. Assessment of chemically separated carbon nanotubes for nanoelectronics. *J. Am. Chem. Soc.* **2008**, *130*, 2686–2691. [CrossRef]
10. Nah, J.; Liu, E.S.; Varahramyan, K.M.; Tutuc, E. Ge-S_xGe_{1-x} Core–Shell Nanowire Tunneling Field-Effect Transistors. *IEEE Trans. Electron. Devices* **2010**, *57*, 1883–1888. [CrossRef]
11. Hu, Y.; Churchill, H.O.; Reilly, D.J.; Xiang, J.; Lieber, C.M.; Marcus, C.M. A Ge/Si heterostructure nanowire-based double quantum dot with integrated charge sensor. *Nat. Nanotechnol.* **2007**, *2*, 622–625. [CrossRef]
12. Available online: https://engineering.purdue.edu/gekcogrp/software-projects/nemo/ (accessed on 2 July 2020).
13. Available online: http://www.nextnano.de (accessed on 2 July 2020).
14. Available online: http://www.tibercad.org (accessed on 2 July 2020).
15. Available online: http://vides.nanotcad.com/vides/ (accessed on 2 July 2020).
16. Available online: http://dipc.ehu.es/frederiksen/tstutorial/index.php/Fast (accessed on 2 July 2020).
17. Jacoboni, C.; Reggiani, L. The Monte Carlo method for the solution of charge transport in semiconductors with applications to covalent materials. *Rev. Mod. Phys.* **1983**, *55*, 645. [CrossRef]
18. Albareda, G.; Jiménez, D.; Oriols, X. Intrinsic noise in aggressively scaled field-effect transistors. *J. Stat. Mech. Theory Exp.* **2009**, *2009*, P01044. [CrossRef]
19. Breuer, H.P.; Petruccione, F. *The Theory of Open Quantum Systems*; Oxford University Press on Demand: Oxford, UK, 2002.
20. Smirne, A.; Breuer, H.P.; Piilo, J.; Vacchini, B. Initial correlations in open-systems dynamics: The Jaynes-Cummings model. *Phys. Rev. A* **2010**, *82*, 062114. [CrossRef]

21. De Vega, I.; Alonso, D. Dynamics of non-Markovian open quantum systems. *Rev. Mod. Phys.* **2017**, *89*, 015001. [CrossRef]
22. Vacchini, B. Non-Markovian dynamics for bipartite systems. *Phys. Rev. A* **2008**, *78*, 022112. [CrossRef]
23. Gisin, N. Stochastic quantum dynamics and relativity. *Helv. Phys. Acta* **1989**, *62*, 363–371.
24. Pearle, P. Combining stochastic dynamical state-vector reduction with spontaneous localization. *Phys. Rev. A* **1989**, *39*, 2277. [CrossRef]
25. Carmichael, H. *An Open Systems Approach to Quantum Optics: Lectures Presented at the Université Libre de Bruxelles, October 28 to November 4, 1991*; Springer Science & Business Media: Berlin/Heidelberg, Germany, 2009; Volume 18.
26. Van Kampen, N.G. *Stochastic Processes in Physics and Chemistry*; Elsevier: Amsterdam, The Netherlands, 1992; Volume 1.
27. De Vega, I. Non-Markovian stochastic Schrödinger description of transport in quantum networks. *J. Phys. B At. Mol. Opt. Phys.* **2011**, *44*, 245501. [CrossRef]
28. Goetsch, P.; Graham, R. Linear stochastic wave equations for continuously measured quantum systems. *Phys. Rev. A* **1994**, *50*, 5242. [CrossRef]
29. Gatarek, D.; Gisin, N. Continuous quantum jumps and infinite-dimensional stochastic equations. *J. Math. Phys.* **1991**, *32*, 2152–2157. [CrossRef]
30. Gambetta, J.; Wiseman, H. Non-Markovian stochastic Schrödinger equations: Generalization to real-valued noise using quantum-measurement theory. *Phys. Rev. A* **2002**, *66*, 012108. [CrossRef]
31. Rivas, A.; Huelga, S.F.; Plenio, M.B. Quantum non-Markovianity: Characterization, quantification and detection. *Rep. Prog. Phys.* **2014**, *77*, 094001. [CrossRef] [PubMed]
32. Pandey, D.; Colomés, E.; Albareda, G.; Oriols, X. Stochastic Schrödinger Equations and Conditional States: A General Non-Markovian Quantum Electron Transport Simulator for THz Electronics. *Entropy* **2019**, *21*, 1148. [CrossRef]
33. Oriols, X. Quantum-Trajectory Approach to Time-Dependent Transport in Mesoscopic Systems with Electron-Electron Interactions. *Phys. Rev. Lett.* **2007**, *98*, 066803. [CrossRef] [PubMed]
34. Albareda, G.; Suñé, J.; Oriols, X. Many-particle hamiltonian for open systems with full coulomb interaction: Application to classical and quantum time-dependent simulations of nanoscale electron devices. *Phys. Rev. B* **2009**, *79*, 075315. [CrossRef]
35. Albareda, G.; Saura, X.; Oriols, X.; Suné, J. Many-particle transport in the channel of quantum wire double-gate field-effect transistors with charged atomistic impurities. *J. Appl. Phys.* **2010**, *108*, 043706. [CrossRef]
36. Colomés, E.; Zhan, Z.; Marian, D.; Oriols, X. Quantum dissipation with conditional wave functions: Application to the realistic simulation of nanoscale electron devices. *Phys. Rev. B* **2017**, *96*, 075135. [CrossRef]
37. Albareda, G.; López, H.; Cartoixa, X.; Suné, J.; Oriols, X. Time-dependent boundary conditions with lead-sample Coulomb correlations: Application to classical and quantum nanoscale electron device simulators. *Phys. Rev. B* **2010**, *82*, 085301. [CrossRef]
38. Albareda, G.; Benali, A.; Oriols, X. Self-consistent time-dependent boundary conditions for static and dynamic simulations of small electron devices. *J. Comput. Electron.* **2013**, *12*, 730–742. [CrossRef]
39. Albareda, G.; Marian, D.; Benali, A.; Alarcón, A.; Moises, S.; Oriols, X. Electron Devices Simulation with Bohmian Trajectories. In *Simulation of Transport in Nanodevices*; John Wiley and Sons, Ltd.: Hoboken, NJ, USA, 2016; Chapter 7, pp. 261–318. [CrossRef]
40. López, H.; Albareda, G.; Cartoixà, X.; Suñé, J.; Oriols, X. Boundary conditions with Pauli exclusion and charge neutrality: Application to the Monte Carlo simulation of ballistic nanoscale devices. *J. Comput. Electron.* **2008**, *7*, 213–216. [CrossRef]
41. Born, M.; Huang, K. *Dynamical Theory of Crystal Lattices*; Clarendon Press: Oxford, UK, 1954.
42. Albareda, G.; Abedi, A.; Tavernelli, I.; Rubio, A. Universal steps in quantum dynamics with time-dependent potential-energy surfaces: Beyond the Born-Oppenheimer picture. *Phys. Rev. A* **2016**, *94*, 062511. [CrossRef]
43. Mejia-Monasterio, C.; Wichterich, H. Heat transport in quantum spin chains. *Eur. Phys. J. Spec. Top.* **2007**, *151*, 113–125. [CrossRef]
44. Wichterich, H.; Henrich, M.J.; Breuer, H.P.; Gemmer, J.; Michel, M. Modeling heat transport through completely positive maps. *Phys. Rev. E* **2007**, *76*, 031115. [CrossRef] [PubMed]
45. Biele, R.; Timm, C.; D'Agosta, R. Application of a time-convolutionless stochastic Schrödinger equation to energy transport and thermal relaxation. *J. Phys. Condens. Matter* **2014**, *26*, 395303. [CrossRef]

46. Appel, H.; Di Ventra, M. Stochastic quantum molecular dynamics. *Phys. Rev. B* **2009**, *80*, 212303. [CrossRef]
47. Biele, R.; D'Agosta, R. A stochastic approach to open quantum systems. *J. Phys. Condens. Matter* **2012**, *24*, 273201. [CrossRef]
48. Gardiner, C.; Anglin, J.; Fudge, T. The stochastic gross-pitaevskii equation. *J. Phys. B At. Mol. Opt. Phys.* **2002**, *35*, 1555. [CrossRef]
49. Gardiner, C.; Davis, M. The stochastic Gross–Pitaevskii equation: II. *J. Phys. B At. Mol. Opt. Phys.* **2003**, *36*, 4731. [CrossRef]
50. Weiler, C.N.; Neely, T.W.; Scherer, D.R.; Bradley, A.S.; Davis, M.J.; Anderson, B.P. Spontaneous vortices in the formation of Bose–Einstein condensates. *Nature* **2008**, *455*, 948–951. [CrossRef]
51. González, L.; Lindh, R. *Quantum Chemistry and Dynamics of Excited States: Methods and Applications*; Wiley: Hoboken, NJ, USA, 2020.
52. Handy, N.; Yamaguchi, Y.; Schaefer, H., III. The diagonal correction to the Born–Oppenheimer approximation: Its effect on the singlet–triplet splitting of CH and other molecular effects. *J. Chem. Phys.* **1986**, *84*, 4481. [CrossRef]

Publication D

Devashish Pandey, Matteo Villani, Enrique Colomés, Zhen Zhan, and Xavier Oriols. Implications of the Klein tunneling times on high frequency graphene devices using Bohmian trajectories. *Semiconductor Science and Technology*, 2018

Implications of the Klein tunneling times on high frequency graphene devices using Bohmian trajectories

Implications of the Klein tunneling times on high frequency graphene devices using Bohmian trajectories

Devashish Pandey[1], Matteo Villani[1], Enrique Colomés[1], Zhen Zhan[2] and Xavier Oriols[1]

[1] Departament d'Enginyeria Electrònica, Universitat Autònoma de Barcelona, Spain.
[2] School of Physics and Technology, Wuhan University, Wuhan 430072, China

E-mail: xavier.oriols@uab.es

17 September 2018

Abstract. Because of its large Fermi velocity, leading to a great mobility, graphene is expected to play an important role in (small signal) radio frequency electronics. Among other, graphene devices based on Klein tunneling phenomena are already envisioned. The connection between the Klein tunneling times of electrons and cut-off frequencies of graphene devices is not obvious. We argue in this paper that the trajectory-based Bohmian approach gives a very natural framework to quantify Klein tunneling times in linear band graphene devices because of its ability to distinguish, not only between transmitted and reflected electrons, but also between reflected electrons that spend time in the barrier and those that do not. Without such distinction, typical expressions found in the literature to compute dwell times can give unphysical results when applied to predict cut-off frequencies. In particular, we study Klein tunneling times for electrons in a two-terminal graphene device constituted by a potential barrier between two metallic contacts. We show that for a zero incident angle (and positive or negative kinetic energy), the transmission coefficient is equal to one, and the dwell time is roughly equal to the barrier distance divided by the Fermi velocity. For electrons incident with a non-zero angle smaller than the critical angle, the transmission coefficient decreases and dwell time can still be easily predicted in the Bohmian framework. The main conclusion of this work is that, contrary to tunneling devices with parabolic bands, the high graphene mobility is roughly independent of the presence of Klein tunneling phenomena in the active device region.

Keywords: Tunneling times, Bohmian mechanics, graphene, Dirac equation

1. Introduction

Because of its extraordinary properties, graphene has been studied as a new and promising material for electronics during the last fifteen years [1]. Although the lack of bandgap makes its use difficult for digital applications, its high mobility is expected to provide very well suited devices for (small signal) radio frequency applications [2]. For electrons in graphene, modeled by the Dirac equation (with linear bands), an exotic tunneling phenomena, known as Klein tunneling [3, 4], is predicted resulting in a perfect transmission of electrons perpendicular to a potential barrier. This result is in contradiction with traditional semiconductors with parabolic bands where the transmission strongly depends on the height and width of the barrier. Several prototypes have already been studied in the literature for developing graphene field effect transistors for high-frequency applications based on Klein tunneling phenomena [5–8]. The natural question arises: what is the mobility of electrons in graphene when undergoing Klein tunneling? This question is directly related to the time spent by the electrons in the region where they suffer Klein tunneling. For the sake of simplicity, hereafter, we assume the device active region to be equal to the potential barrier in graphene, meaning that transit and tunneling times are equivalent. The mobility determines the electron transit time that, in turn, determines the cut-off frequency which is an important figure of merit of high-frequency electron devices [9]. Surprisingly, the connection between these Klein tunneling times and cut-off frequencies of graphene devices remains mainly unstudied in the literature.

The accurate prediction of tunneling times has been a fascinating problem for the scientific community during the last century. In (non-relativistic) quantum mechanics, time enters as a parameter rather than an observable. Thus, there is no direct way to calculate tunneling times in the orthodox quantum mechanics, where measurements are directly linked to operators of the measured property [10]. The tunneling times can be indirectly determined by measuring other operators. In the literature, there exists at least three different orthodox protocols to compute the tunneling time [11]. First, one studies the evolution of the wave packets through the barrier and gets the phase time which involves the phase sensitivity of the tunneling amplitude to the energy of the incident particle [12]. The second approach makes use of a physical clock to measure the time elapsed during the tunneling [13–17]. Larmor precession, as one of physical clocks, was first introduced long time ago to measure the time associated with scattering events [14, 16]. Recently, tunneling times of 2D massless pseudo-spin Dirac particles have been analyzed, mainly within the second protocol [18–25]. Finally, the third definition of tunnel time is based on the determination of a set of dynamic paths. We will refer to such type of tunneling time as the dwell time. However, a dynamic path is an ill-defined concept in orthodox quantum mechanics [26].

In this paper, we will show that the Bohmian explanation of quantum phenomena provides a very appropriate formalism for discussing tunneling times that are later linked to cut-off frequencies. The Bohmian theory allows an accurate definition of dynamic paths (in terms of Bohmian trajectories) and the third alternative mentioned above for computing tunneling times becomes very natural. The most important advantage of the Bohmian computation of the dwell time for high-frequency electronics is its ability to distinguish, not only between transmitted and reflected electrons in the barrier [27], but also between those reflected particles that spend some time in the barrier and other reflected particles that do not spend time in the barrier.

The structure of the paper is the following. In section 2 we present how the transit (tunneling) time is related to the cut-off frequency of an electron device, specifically in graphene devices. In section 3 we define the dwell time from an orthodox perspective and from the Bohmian theory. In section 4, we explain how the different dwell times can be computed. For that purpose, the Klein tunneling effect is presented and analyzed. Numerical results are shown and discussed in section 5. Finally, we conclude in section 6.

2. Cut-off frequency and tunneling times

Along the paper we will consider a graphene two-dimensional (2D) sheet, with x as the transport direction, from the left contact to the right contact, and z as the direction perpendicular to the transport direction. The y direction contains the thickness of the graphene sheet (plus top and bottom dielectric layers). We discuss in this section how the high mobility of graphene devices can be determined from the transit times. To simplify the discussion, we focus on a two terminal device. The length of the device active region is $L_x = b - a$ with $x = a$ the position of the left metallic contact and $x = b$ the right metallic contact.

At very high frequencies, not only the particle current due to movements of particles is relevant, but also the displacement current given by the time-derivative of the electric field generated by electrons moving inside the device region becomes important. If we consider that the lateral surfaces of the metallic contacts ($L_y \times L_z$) are much larger than the length of the device, $L_x << L_y, L_z$, then, the Ramo-Shockley-Pellegrini theorem [28–30], allows us to write the total

(particle plus displacement) current at each time t as:

$$I(t) = \frac{q}{L_x} \sum_{i=1}^{N_e} v_x^i(t) \Theta[x^i(t) - a] \Theta[b - x^i(t)] \quad (1)$$

where N_e is the number of electrons inside the active region at time t, q is the electron charge and $v_x^i(t)$ the $i-th$ electron instantaneous velocity in the transport direction x. Finally, $\Theta[x]$ is the Heaviside function. Notice that the trajectories in the metals are not included in (1). This result assumes that the density of electrons in the metal and their mobility are so high that the electrical field generated by one moving electron in the metal (outside the active region) is rapidly screened by the other (free) electrons in the metal.

Now, we consider the transient of the current $I(t)$ defined in (1) after a sudden perturbation of the external bias in the contacts. We assume that before $t = 0$, the device has fixed external voltages in the contacts (V_L in the left and V_R in the right) with a stationary current value ‡. Then, we apply a new (small signal) external bias $V_R + \Delta V$ at time $t = 0$ at the right contacts of the device. This new external voltage generates a new internal potential in the graphene sheet $V(x, z)$ which perturbs the current given by (1) because the dynamics of the electrons traversing the device need to be adapted to the new scenario. After some time, the current reaches a new stationary value when all electrons inside the system have already moved along the active region $a < x < b$, all the time, with the new internal potential profile associated to $V_R + \Delta V$. This transient time can be related to the dynamics of electrons. Let us consider one electron, labeled by i, that has entered inside the active region just before $t = 0$. The electron gives a current $I(t) = q\ v_x^i(t)/L_x$ during the time $\tau_i = \int_0^\infty dt\ \Theta[x^i(t) - a]\Theta[b - x^i(t)]$ that it spent in the active region. After this time interval, we are sure that a new electron (with identical properties except the entering time) entering inside the region $a < x < b$ at time $t > \tau_i$ will be only influenced by the new scenario created by the external bias $V_R + \Delta V$. Notice that the time τ_i we have to wait is not related to the fact that the electron is transmitted of reflected. The only relevant point is that the electron spends some time in the active region $a < x < b$.

In a real device, there are more than one electron with some uncertainties in their properties. We only have access to the probability distribution of these uncertainties. Therefore, we compute an average value of the time spent by electrons over all these uncertainties to get the (average) transit time τ. In this work, as already indicated, we will simplify our discussion by considering an active region built from a graphene potential barrier between two metallic contacts. Then, the transit time along the device and the tunneling time can be considered equivalent. Finally, the previous relationship between transient of the current and dynamics of electrons can be formally established in the following expression between the ensemble transit (tunneling) time τ and the cut-off frequency of the device f_T as§:

$$f_T = \frac{1}{\tau} \quad (2)$$

The language used above in terms of trajectories, which is natural for classical systems, can also be rigorously extended to quantum systems by using Bohmian trajectories [35].

3. Definition of dwell times in graphene

The dynamics of electrons in graphene devices (as well as for other linear band structures materials) are given by the Dirac equation, and not by the usual Schrödinger equation for parabolic bands. The wave function associated to the electron is no longer a scalar, but a bispinor:

$$\psi(\vec{r}, t) \equiv \begin{pmatrix} \psi_1 \\ \psi_2 \end{pmatrix} \equiv \begin{pmatrix} \psi_1(x, z, t) \\ \psi_2(x, z, t) \end{pmatrix} \quad (3)$$

The two components are solution of the mentioned Dirac equation:

$$i\hbar \frac{\partial \psi(\vec{r}, t)}{\partial t} = -i\hbar v_f (\vec{\sigma} \cdot \vec{\nabla} + V(\vec{r}))\psi(\vec{r}, t) \quad (4)$$

where $\vec{r} = \{x, z\}$ and $\vec{\nabla} = (\frac{\partial}{\partial x}, \frac{\partial}{\partial z})$ and the Pauli matrices ‖ are:

$$\vec{\sigma} = (\sigma_x, \sigma_z) = \left(\begin{pmatrix} 0 & 1 \\ 1 & 0 \end{pmatrix}, \begin{pmatrix} 0 & -i \\ i & 0 \end{pmatrix} \right) \quad (5)$$

We remind that $v_f = 10^6 m/s$ is the graphene Fermi velocity and $V(\vec{r}) \equiv V(x, z)$ the electrostatic potential.

As discussed in the introduction, from the different orthodox definitions of the tunneling times, we will use in this paper the third definition related to dynamic paths [31]. It is the most accepted one, usually referred to as the dwell time, and it is not contaminated by the measurement procedure. By writing the modulus of the bispinor as $|\Psi(x, z, t)|^2 = |\psi_1(x, z, t)|^2 + |\psi_2(x, z, t)|^2$, the typical expression for the orthodox dwell time to quantify how much time

‡ We neglect the fluctuations of the stationary value of the current because they are not relevant in our discussion.

§ Typically, the clock frequency of a real CPU is usually 1/3 of the cut-off frequency. In any case, such factor is not relevant at all in the discussion presented here.

‖ In the literature, usually, our Pauli matrix σ_z in (5) is defined as the σ_y. However, since in this discussion the sheet of graphene is defined in the plane XZ, our notation is different.

a particle spends in a 2D spatial region limited by the boundaries $a < x < b$ and $-\infty < z < \infty$ is traditionally given by,

$$\tau_D = \int_0^\infty dt \int_a^b dx \int_{-\infty}^\infty dz |\Psi(x,z,t)|^2 \qquad (6)$$

At this point, let us briefly mention what is the tunneling time problem. A classical measurement of the dwell time can be simply defined from the measurement of the time when the particle reaches the position $x = a$, plus a final measurement of the time when the particle reaches $x = b$. The time spent between the initial and final detection of the particle position will quantify the dwell time. However, since quantum mechanics is a contextual theory, the first (strong) measurement of the position will transform the initial wave function into an eigenstate of the position measurement. Then, the posterior evolution of such delta function can be quite different from the unmeasured function used in (6). The tunneling time problem is related with the difficulties of computing the dwell time without paying the price of dealing with a perturbed wave function because of the measurement. In the orthodox theory, such attempt is quite difficult because only measured properties can be obtained from the theory.

However, there are other quantum theories which can tackle such problem in a different way. By construction, the Bohmian theory [32] has the ability of providing measured and unmeasured properties (for example, particle positions) for a quantum system. If we know how to relate measured and unmeasured properties in one experimental set-up (for example, a high-frequency measurement set-up defined in [33]) then the computation of the unmeasured properties of the Bohmian trajectories can be very useful. In this work, we will use unmeasured Bohmian trajectories to discuss Klein tunneling times. As discussed in [33], the measured Bohmian trajectories will only provide a noisier description of the total current (associated with a weak measurement process).

In the Bohmian theory for the Dirac equation [34], each electron has a well-defined position at any time that is guided by the same orthodox bispinor given by (3). Each experiment labeled by the super index $i = 1, .., N$ uses the same bispinor, but different trajectories $x^i(t)$ and $z^i(t)$. Such Bohmian trajectories are computed by time-integrating the velocity given by the bispinor:

$$\vec{v}(\vec{r},t) = \frac{v_f\ \Psi(\vec{r},t)^\dagger \vec{\sigma} \Psi(\vec{r},t)}{|\Psi(\vec{r},t)|^2} \qquad (7)$$

where $\vec{\sigma}$ is defined in (5) and $v_f = 10^6 m/s$ is the graphene Fermi velocity. See Appendix A for the explicit computation of (7). The initial position of such trajectories at time t are empirically inaccessible and given by the probability distribution [35]:

$$|\Psi(x,z,t)|^2 = \lim_{N\to\infty} \frac{1}{N} \sum_{i=1}^N \delta[x - x^i(t)]\delta[z - z^i(t)] \quad (8)$$

where N is the number of experiments that we assume infinite (or large enough to correctly get the ensemble values). In fact, due to equivariant property of the bispinor and the associated trajectories, if Eq.(8) is satisfied at the initial time, then it is true at any other time. For a review on Bohmian mechanics, you can see [32–36].

Rewriting the orthodox expression of the dwell time in Eq.(6) within the Bohmian language provide us more insights into the dwell time and its unmeasured definition [35]. Using (8) in (6) we get:

$$\tau_D = \lim_{N\to\infty} \frac{1}{N} \sum_{i=1}^N \left(\int_0^\infty dt \Theta[x^i(t) - a]\Theta[b - x^i(t)] \right) \qquad (9)$$

Now, we can rewrite Eq.(9) as an average over Bohmian dwell times τ^i associated to the different trajectories:

$$\tau_D = \lim_{N\to\infty} \frac{1}{N} \sum_{i=1}^N \tau^i \qquad (10)$$

where τ^i is defined as:

$$\tau^i = \int_0^\infty dt \Theta[x^i(t) - a]\Theta[b - x^i(t)] \qquad (11)$$

This is the dwell time associated to the i-th Bohmian trajectory inside the region $a < x < b$. Notice that the spatial integral in the z direction from $-\infty$ to ∞ in (6) implies that we do not care about which is the z position of the particle.

Up to now, our Bohmian discussion is just another way to exactly compute the orthodox dwell time in (6). We can now further develop the Bohmian expression to realize about its ability to discuss the high-frequency performance of electron devices discussed in section 2. We divide the trajectories appearing in τ_D in Eq.(10) into the three types of trajectories:

- (T-trajectories) Those Bohmian trajectories that enter into the barrier region through $x = a$ and leave through $x = b$ being finally transmitted. We define N_T as the number of such trajectories. By construction, their τ^i is different from zero.
- (R-trajectories) Those Bohmian trajectories that enter into the barrier region through $x = a$ and leave through the same point $x = a$ because they are finally reflected. We define N_R as the number of such trajectories. Again, their τ^i is different from zero.

- (R^*-trajectories) Those Bohmian trajectories that do not enter into the barrier region at any time. We define N_{R^*} as the number of such trajectories. These trajectories are reflected trajectories, but different from the R-trajectories. Here, by construction, we have $\tau^i = 0$.

By construction, with the new definitions, we have $N = N_T + N_R + N_{R^*}$. Then, the dwell time τ_D in Eq.(10) can be rewritten as:

$$\tau_D = \lim_{N\to\infty} \frac{1}{N} \left(\sum_{l=1}^{N_T} \tau^l + \sum_{m=1}^{N_R} \tau^m \right) \tag{12}$$

From the above equation we can define the transmission time, τ_T and the reflection time, τ_R as follows:

$$\tau_T = \frac{1}{N_T} \sum_{l=1}^{N_T} \tau^l \quad \text{and} \quad \tau_R = \frac{1}{N_R} \sum_{m=1}^{N_R} \tau^m \tag{13}$$

So the overall expression of the dwell time can be written as follows,

$$\tau_D = P_T\, \tau_T + P_R\, \tau_R \tag{14}$$

where we have defined the probabilities:

$$T \equiv P_T = \lim_{N\to\infty} \frac{N_T}{N} \tag{15}$$

The computation of the transmission coefficient T do not require the distinction between N_R and N_R^* since only the transmitted trajectories N_T are relevant here. Identically,

$$P_R = \lim_{N\to\infty} \frac{N_R}{N} \tag{16}$$

Notice that the reflected probability P_R is different from the reflection coefficient R, $P_R \neq R$, because the reflection coefficient requires including N_R and N_R^* in the numerator of (16).

We further discuss the role of the R^*-trajectories. Because of these trajectories the previous probability definitions give $P_T + P_R \leq 1$. We require to add the additional probability $P_{R^*} = N_{R^*}/N$ to satisfy $P_T + P_R + P_{R^*} = 1$. However, if we remember that the R^*-trajectories have a transit time equal to zero, $\tau_i = 0$, then, the transit (tunneling) time of expression (6) can be extremely misleading. If we get a scenario where $N_{R^*} \approx N$ then we get the unphysical result $\tau_D \approx 0$ in (12), that implies a cut-off frequency going to infinite from (2). This result is unphysical. The mistake appears because we have to eliminate the trajectories N_{R^*} from the computations of the dwell times when such times want to be related to predict the high-frequency behavior of electron devices as discussed in section 2. The fundamental problem is that the identification of the particles N_T, N_R and N_{R^*} is not possible within the orthodox theory. This is just a different way of realizing about the controversial tunneling time in orthodox quantum mechanics. On the contrary, the Bohmian theory provides a transparent procedure to eliminate N_{R^*} from the computations. Thus, the Bohmian dwell time (for deducing properly high-frequency performances) needs to be defined as:

$$\tau_{D_B} = \lim_{N_B\to\infty} \frac{1}{N_B} \left(\sum_{l=1}^{N_T} \tau^l + \sum_{m=1}^{N_R} \tau^m \right) \tag{17}$$

where $N_B = N_T + N_R$ are the number of trajectories entering into the barrier. Notice that now the scenario $N_{R^*} \approx N$ does not imply the unphysical result $\tau_{D_B} \approx 0$ in (17) because the particles N_{R^*} have no role. We will elaborate this point in the subsequent sections where numerical results are shown.

4. Klein tunneling and the simulation set-up

Now we detail the quantum simulation of dwell times in graphene devices. All simulation results are done with the BITLLES simulator [37]. For the simulation, we consider a two terminal device whose band structure (energy of the Dirac point as a function of the x position) is plotted in figure 1. We consider that the active region of the device is formed by the region with a barrier of $V_0 = 0.15$ eV that starts at the position $x = a = 150$ nm and ends at $x = b = 304$ nm. The simulation box in the x direction is enlarged to be able to accommodate the central position of the initial wave packet at $x = 0$ nm. The total simulation box in the x direction is 1μm, while, the one in the z direction is 600 nm. The spatial step for the computation of Dirac equation are $\Delta x = \Delta z = 1$ nm, while the time step is $\Delta t = 10^{-5}$ ps. To simplify the discussion, the contact is assumed to have the same properties as the graphene channel, but with a very fast screening time so that the only electron relevant for the total current in (1) are the ones inside the box $a < x < b$. This scenario corresponds to the idealized two-terminal device described in section 2.

As we mentioned, the wave nature of the electrons¶ is given by the Dirac equation using the bispinor in (3). The initial electron wave function is a Gaussian bispinor wave packet:

$$\begin{pmatrix} \psi_1(x,z,t) \\ \psi_2(x,z,t) \end{pmatrix} = \begin{pmatrix} 1 \\ s e^{i\theta_{\vec{k}_c}} \end{pmatrix} \Psi_g(x,z,t) \tag{18}$$

¶ The time-evolution of this wave packet can be considered as a Bohmian conditional wave function for the electron. The conditional wave packet is a unique tool of Bohmian mechanics that allows to tackle the many-body and measurement problems in a computationally very efficient way [38, 39].

where $\Psi_g(x,z,t)$ is a Gaussian function with central momentum $\vec{k_c} = (k_{x,c}, k_{z,c})$. We consider $s = 1$ for wave functions with positive kinetic energies (conduction band) and $s = -1$ for negatives kinetic energies (valence band). We define $\theta_{\vec{k_c}} = arctan(k_{z,c}/k_{x,c})$ as the incident angle. The wavepacket spatial dispersions along the x and z directions are equal to $\sigma = 40$ nm. Unless we indicate the contrary, the central energy of the electron will be 0.1 eV above the Fermi point in the left contact.

We are interested in computing the time spent by an electron while traversing the potential barrier depicted in figure 1 by Klein tunneling [40]. For this purpose we simulated different scenarios where an electron (represented by its conditional wave function) impinges a barrier. In figure 2, we see two different examples of such conditional wave function and its associated trajectories[+]. Let us notice that, in our opinion, the word tunneling is misleading here. As plotted in the cones of figure 1(a), electrons in the contact have kinetic energies available above and below the Dirac point. Identically, electrons inside the potential barrier have energies available above and below the new Dirac point. Therefore, strictly speaking, even if we consider an electron with an incident kinetic energy below the potential energy in the barrier, $E < V_0$, the electron will not find a region of forbidden energies as it happens in typical tunneling barriers built from materials with parabolic bands and with an energy gap. In this sense, the electron transport in the graphene linear band structure is quite unusual and unique. Rather than a tunneling phenomena is a interference phenomena. We will see these differences in next section and we will comment their implications in the conclusions.

We deduce here some features of the dynamics of the electrons traversing the barrier region. By construction, the total energy of the wave packet is conserved. Such energy can be divided between kinetic and potential energy. If we locate the zero of potential energy at the Dirac point in the left contact, then the electron has a positive kinetic energy of E. Once inside the barrier, the potential energy V_0 is higher than the total energy E, so that the kinetic energy in the barrier is negative $E - V_0$. These negative kinetic energies are unproblematic and perfectly well defined in the linear band structure of graphene. If the initial kinetic energy of the incident electron is $E = V_0$, then, a quite exotic situation appears because there is almost no energy eigenstates available in the barrier region to accommodate the energy eigenestates that build the wave packet outside the barrier. See figure 1(b). The previous arguments are strictly valid for wave functions that contain just one energy eigenstate, for wave packets built from a set of energies around the central value, as in our case, the time evolution is more complex.

When electrons are incident at a particular angle $\theta_{\vec{k_c}} = arctan(k_{z,c}/k_{x,c})$ with momentum $\vec{k_c} = (k_{x,c}, k_{z,c})$, due to the translational invariance of the potential $V(x,z)$ in the z direction, the momentum in that direction should be conserved. This means that, for example, the transport process depicted in figure 3(a) is not possible because the $k_{z,c}$ is not conserved. The k_z in the left contact is much larger than the k_{lim} value at the barrier region. The argument of conservation of z-momentum leads to scenarios where electrons change its direction in the interfaces contact-barrier and barrier-contact resulting in a Snell's law-like expression [4]:

$$E \sin(\theta_{\vec{k_c}}) = (E - V_0) \sin(\theta_{\vec{k_b}}) \tag{19}$$

where $\theta_{\vec{k_c}}$ is the angle before the barrier (incident angle) and $\theta_{\vec{k_b}}$ the angle in the barrier (refracted angle). See figure 3(b) for a definition of the angles in the contact-barrier interface. In the barrier region, we have $E - V_0 < 0$ so that the angle of transmission of the trajectory is negative. From (19), we conclude [4] that the angle of incidence $\theta_{\vec{k_c}}$ in graphene has to satisfy $\theta_{\vec{k_c}} > \theta_C$ to have a completely reflected wavefunction, where

$$\theta_C = \sin^{-1}\left(\frac{E - V_0}{E}\right) \tag{20}$$

is the critical angle. Again, the previous arguments are strictly valid for just one energy eigenstate. For wave packets built from a set of energies around the central value, as in our case, there can also be a small transmission above the critical angle.

The most surprising result for the dynamics of electrons in graphene, as already indicated, appears when considering an incident angle $\theta_{\vec{k_c}} = 0$ meaning that the momentum in the z direction is zero, $k_{z,c} = 0$. Then, the conservation of the z momentum does not provide any restriction on the dynamics of the electron and, in fact, the transmission coefficient is equal to one ($T = 1$) for any positive or negative kinetic energy of the electron incident on the barrier with $\theta_{\vec{k_c}} = 0$. This is known as the Klein tunneling paradox [3, 40] because it is surprising for typical tunneling (parabolic band) scenarios with forbidden energy regions. But, this is not the case in graphene, and the paradox just disappears. In our study, since the injected wave function is a wave packet, it will have some wave vectors with some dispersion in the injecting angle around $\theta_{\vec{k_c}} = 0$, and therefore $T \leq 1$.

[+] We observe in figure 2 (b) trajectories which are crossing in the $\{x,z\}$ space. We remind that different Bohmian trajectories cannot cross at the space $\{x,z,t\}$ at the same time. The trajectories plotted here satisfy this requirement.

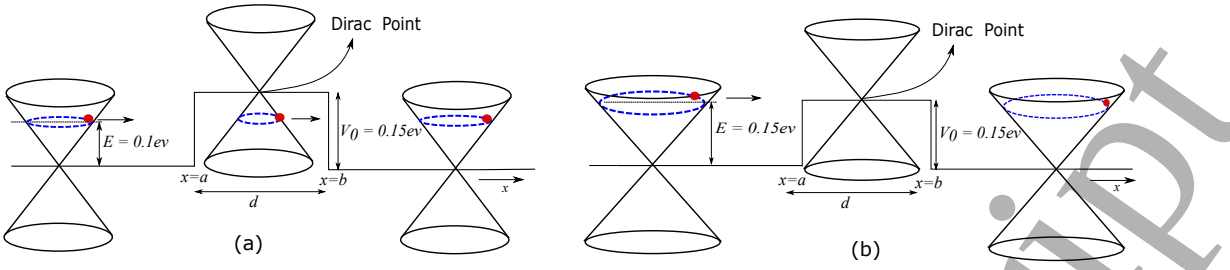

Figure 1: (a) Klein tunneling barrier region where the electron, which impinges perpendicularly to the barrier, has an energy E lower than the barrier height V_0. The cones represents the linear energy momentum dispersion at different positions. The electron has available states in the valence band of the barrier region which allows them to tunnel freely. The transmission coefficient in such cases is close to unity. (b) The same plot for an electron with energy similar to the barrier height $E = V_0$. In this case the electron has to occupy the Dirac point in the barrier region which has almost no available energy states. In these scenarios the transmission probability almost vanishes. This decrease can also be explained through a momentum conversation argument, as depicted in figure 3.

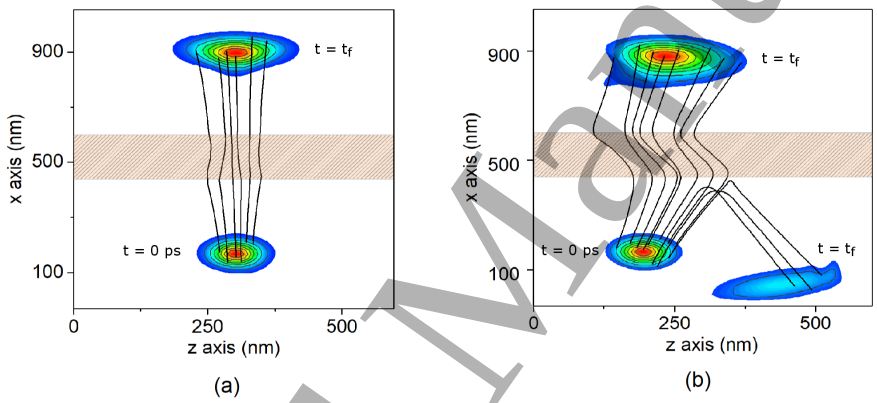

Figure 2: (a) Conditional wavefunction of the electron that impinges perpendicularly ($\theta_{\vec{k_c}} = 0$ degrees) to a barrier (in the shaded orange region) in the initial ($t = 0$ ps) and final ($t_f = 0.746$ ps) times. A set of the associated Bohmian trajectories are also plotted. As it can be seen, from both the wave packet and the set of trajectories, the electron exhibits Klein tunneling and all trajectories traverse the barrier. (b) The same plot for an electron that does not impinge perpendicular to the barrier ($\theta_{\vec{k_c}} = 15$ degrees). Now, there is no complete Klein tunneling and part of the wave packet and some trajectories are reflected. The transmitted part of the wave packet and transmitted trajectories suffered refraction according to Snell's law-like expression (19).

5. Numerical results and discussion

We consider here a wave packet in (18) with a kinetic energy given by $E = 0.1$ eV located initially at the left side, $x = 0$ nm, far from the barrier region. We will consider different incident angles $\theta_{\vec{k_c}}$ that determine different propagation directions, meaning different x and z momenta $\{k_{x,c}, k_{z,c}\}$. The time evolution of such bispinor, while traversing the barrier, is given by (4). From the knowledge of the bispinor at any time and position, we compute the velocity of the Bohmian trajectories from (7). By time integrating these velocities, we compute the Bohmian trajectories $\{x^i(t), z^i(t)\}$ where the super index i specifies different experiments that imply different initial positions of the particles selected according to (8).

First, we discuss the transmission coefficient that can be computed from the bispinor easily as:

$$T = \int_b^\infty dx \int_{-\infty}^\infty dz |\Psi(x, z, t_f)|^2 \qquad (21)$$

where t_f is a time large enough so that there is no probability presence in the barrier region. Identically, by putting (8) into (21), the transmission coefficient

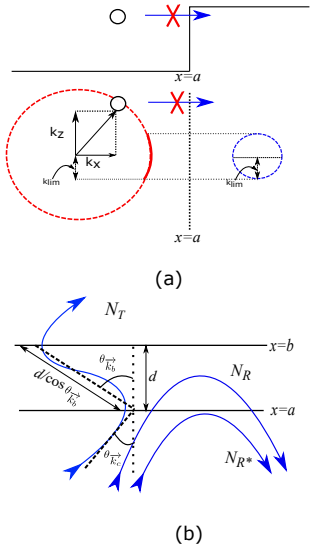

Figure 3: (a) Scheme of an electron that cannot tunnel through the barrier region because of conservation of the total energy and the z momentum forbids it. The electron is reflected before entering into the barrier, contributing to the N_R^* particles, because there are no available z-momentum for the the corresponding kinetic energy in the barrier region. (b) Scheme depicting the three possible types of trajectories considered in this work: transmitted particles, N_T, particles entering into the barrier but eventually reflected, N_R and particles that are reflected before entering the barrier N_R^*.

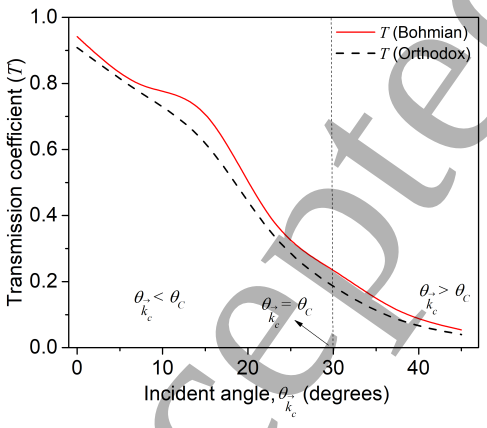

Figure 4: Transmission coefficient as a function of the incident angle computed from the square modulus of the wave function in (21) and the Bohmian trajectories in (15). Bohmian and orthodox computations show an excellent agreement.

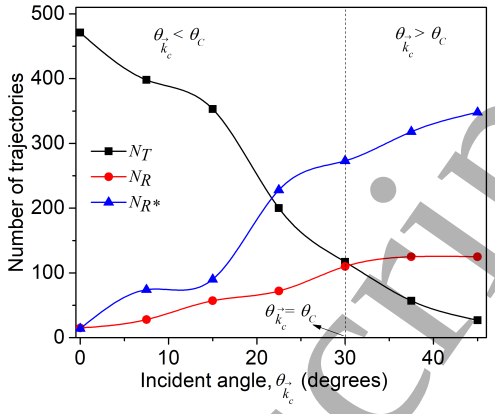

Figure 5: Number of transmitted particles, N_T, particles entering into the barrier but eventually reflected, N_R and particles that are reflected before entering the barrier N_{R^*} as a function of the incident angle.

can be computed from the Bohmian trajectories as in (15). The plot in figure 4 confirms that the results computed from the Bohmian trajectories in (15) (with N=500 experiments) reproduce accurately the orthodox results in (21). Following the discussion about the Klein tunneling in section 4, for $\theta_{\vec{k}_c} = 0$ we get $T \approx 1$, while T tends to zero as we increase the angle. We have a small transmission probability for $\theta_{\vec{k}_c} = \theta_C$.

As we discussed in section 3, the correct computation of the dwell time requires the distinction among N_T, N_R and N_R^*. With Bohmian mechanics it is possible to distinguish among the transmitted trajectories, N_T , reflected after entering in the barrier, N_R and those that are reflected before entering the barrier, N_R^*. The schematic representation of these trajectories is plotted in figure 3(b). In Figure 5 we show how the number of these trajectories vary with the angle of incidence $\theta_{\vec{k}_c}$. The simulations show that for $\theta_{\vec{k}_c} = 0$ almost all the particles are transmitted. Increasing $\theta_{\vec{k}_c}$ leads to an increase in the reflected particles. By construction, the behavior of N_T in figure 5 just reproduces the transmission coefficient T in figure 4. We divide these reflected Bohmian trajectories into two sets: N_R and N_{R^*}. The estimation of the current delay in (1) does only take into account particles entering in the barrier, either N_T or N_R. In the orthodox computation, just with the bispinor (without trajectories), N_R, N_T and N_{R^*} cannot be treated separately. This fact represents an important limitation of the orthodox theory in the proper description of tunneling times and, subsequently, high-frequency response of graphene

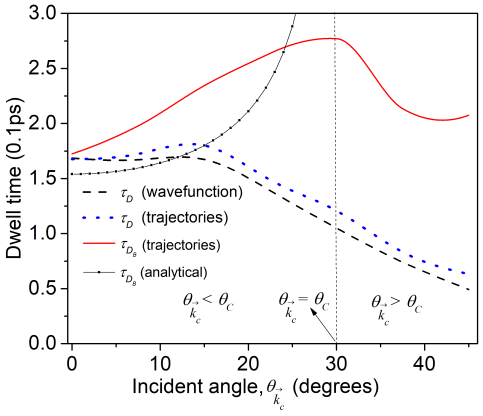

Figure 6: Dwell time as a function of the incident angle computed from Eq.(6) (black dashed line), Eq.(12) (blue dotted line), Eq.(17) (red solid line) and Eq.(23) (black solid line with square symbols).

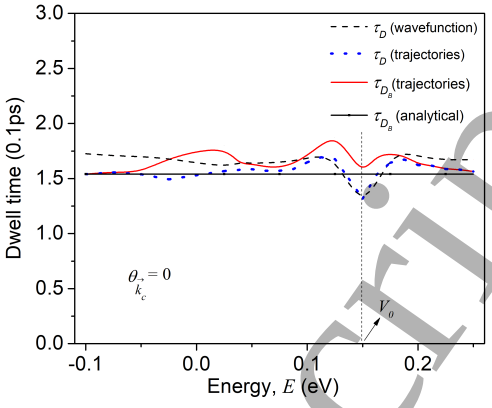

Figure 7: Dwell time as a function of the positive and negative energy of electrons that impinge perpendicularly to the barrier computed from Eq.(6) (black dashed line), Eq.(12) (blue dotted line), Eq.(17) (red solid line) and Eq.(23) (black solid line with square symbols).

devices.

In figure 6, we plot with dashed lines the orthodox dwell time τ_D given by (6). We find that it decreases monotonically with the increase of the incidence angle $\theta_{\vec{k}_c}$. These results are compatible with the decrease of the transmission coefficient T in figure 4 because particles have less and less probability to enter into the barrier region and, therefore, τ_D decreases. For an incident angle larger than the critical angle, $\theta_{\vec{k}_c} > \theta_C$, we expect $T \to 0$ and $\tau_D \to 0$. Then, using (2) for the computation of the cut-off frequency, we get an unphysical result of an infinite cut-off frequency $f_T \to \infty$. This unphysical result is also present in (9) computed with trajectories. The problem appears because of the large number of N_{R^*} while $N_T, N_R \to 0$, at high incident angles (see figure 4). A physical computation of the dwell time can be obtained using the Bohmian trajectories in (17), that ignores N_{R*}, as seen in figure 6 with solid line. This is one of the main results of this work.

For $\theta_{\vec{k}_c} = 0$, the situation is much more simple because $N_{R*} \to 0$ and then the dwell time (either with the orthodox or Bohmian expression) is roughly equal to:

$$\tau_D \approx \tau_{D_B} \approx \frac{d}{v_f} \tag{22}$$

Numerically, we get in figure 6 the value $\tau_{D_B} \approx 0.17$ ps for $\theta_{\vec{k}_c} = 0$. The expected value would be $\tau_{D_B} \approx 0.15$ ps with $v_f = 10^6$ m/s and $d = 154$ nm. The difference occurs since there are electrons described by the wave packet with a velocity slower than the Fermi velocity.

The Bohmian dwell time τ_{D_B} increases with the increase in the angle of incidence until the critical angle θ_C. This occurs because when increasing the incident angle, the angle at which the trajectory enters into the barrier also increases following the condition (19). The effective distance that the electron has to traverse under the barrier is $d_{eff} = d/\cos(\theta_{\vec{k}_b})$. See figure 3(b) for a definition of such a distance. The Bohmian dwell time can be written as:

$$\tau_{D_B} = \frac{d\sqrt{E^2 + V_0^2 - 2V_0E}}{v_f\sqrt{E^2\cos^2(\theta_{\vec{k}_c}) + V_0^2 - 2V_0E}} \tag{23}$$

We notice that (23) reproduces (22) for $\theta_{\vec{k}_c} = 0$. For the critical angle $\theta_{\vec{k}_c} = \theta_C$, the value of (23) gives infinite which means that the electron travels in the perpendicular direction z inside the barrier, never reaching $x = b$. On the other hand, when $\theta_{\vec{k}_c} > \theta_C$ the number of transmitted electrons decreases, so most of the trajectories are either reflected from the barrier boundary, $x = a$, or are reflected after spending some time in the barrier and the estimation of the tunneling time then is more complex. In any case, there are very few electrons with $\theta_{\vec{k}_c} > \theta_C$.

Once we have analyzed the dependence of the orthodox and Bohmian dwell times on the incident angle, $\theta_{\vec{k}_c}$, let us discuss its dependence on the positive or negative kinetic energy E for a zero incident angle $\theta_{\vec{k}_c} = 0$. The main feature present in figure 7 is that all electrons have similar Bohmian dwell time, roughly given by (22), meaning that all electrons are moving with the Fermi velocity, $v_f = 10^6$ m/s.

These results of the Klein tunneling in figure 7 are in a great contradiction with what is usually found in semiconductor structures with parabolic band

energies, where the dwell times strongly depends on the difference between the barrier and the electron energies, $V_0 - E$. Here, even for negative kinetic energies, for example $E = -0.1$ eV, or positive energies above the barrier, for example, $E = 0.2$ eV, the predicted value of the dwell time given by the Fermi velocity is not greatly modified. In figure 8 we have plotted the transmission coefficient given by (21) (dashed line) and by (15) (solid line), with great agreement. In figure 9 we plot the number of particles N_T, N_R and N_{R*} discussed in section 4. The low number of reflected particles without even reaching the barrier region, $N_{R*} \approx 0$, explains why the dwell times in figure 7 are all almost identical. Only, small deviations are seen around $E \approx V_0 = 0.15$ eV and around $E \approx 0$. The first deviations around $E \approx V_0 = 0.15$ eV are explained by the effects of the conservation of the z momentum shown in figure 3(a). The later deviations in both figures around $E \approx 0$ are mainly related to the difficulties of defining an initial wave packet around the Dirac Point. Because of the momentum uncertainty, such initial wave packet have positive and negative energies simultaneously.

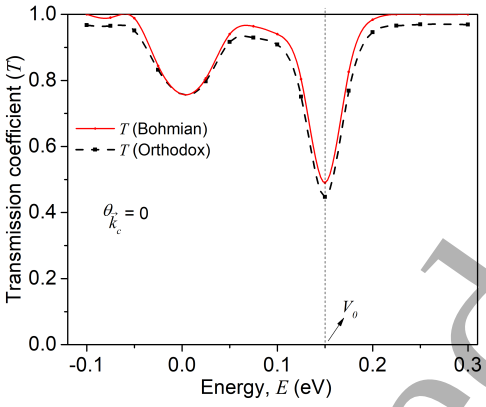

Figure 8: Transmission coefficient for electrons that impinge perpendicularly to the barrier as a function of their initial energy.

6. Conclusion

Motivated by the expected ability of graphene transistors to work at THz frequencies and the development of prototypes of graphene field effect transistors for high-frequency applications based on Klein tunneling phenomena [5–8], an analysis on the Klein tunneling times in graphene structures has been presented in this work. In particular, we study dwell times for electrons in a two-terminal graphene barrier using the BITLLES simulator [37]. We show that

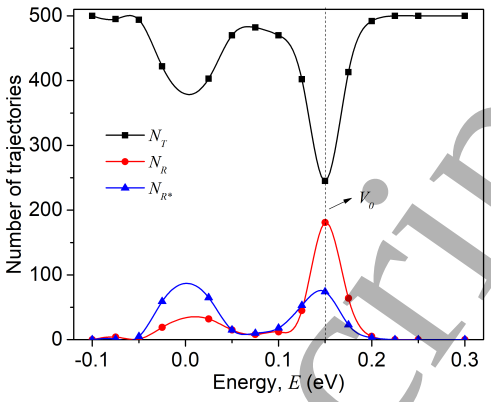

Figure 9: Number of trajectories belonging to each of the three cases (N_T, N_R and N_{R*}) for electrons that impinge perpendicularly to the barrier as a function of their initial energy.

Bohmian trajectories are well suited formalism to discuss transit (tunneling) times and its relation to the cut-off frequencies of electron devices.

We have shown that Klein tunneling time (in gapless graphene with linear band structure) is not like the typical tunneling time (in materials with parabolic bands and with an energy gap). Such differences directly imply completely opposite features in the transit (tunneling) times of graphene structures in comparison to what is expected from traditional semiconductor structures with parabolic bands.

The main conclusions plotted in the figures of the text are next summarized. Because of the well known Klein paradox [3, 40], for an incident angle equal to zero, $\theta_{\vec{k}_c} = 0$, the transmission coefficient is roughly equal to the unity, $T = 1$, with $N_R \approx 0$ and $N_{R^*} \approx 0$. Then, the velocity of particles in the barrier region and outside is roughly equal to the Fermi velocity, $v_f = 10^6$ m/s. This is true for all incident kinetic energy (with positive or negative kinetic energy). Then, the dwell time in the barrier region can be identically computed from the orthodox expression τ_D or the Bohmian one τ_{D_B}, roughly estimated as $\tau_D \approx \tau_{D_B} \approx d/v_f$.

For incident angles different from zero and smaller than the critical angle, $0 < \theta_{\vec{k}_c} < \theta_C$, the transmission coefficient decreases because $N_{R^*} > 0$, but $N_R \approx 0$. Under these scenarios, the dwell time of the electrons has to be estimated only for the trajectories that spend some time in the barrier (what we name N_T and N_R in the text) but not by the trajectories N_{R^*} that do not spend time in the barrier. Then, the orthodox expression τ_D in (6) is not adequate and it has to be substituted by the Bohmian dwell time expression τ_{D_B}. The dwell time can be roughly estimated as

$\tau_{D_B} \approx d/cos(\theta_{\vec{k_c}})/v_f$ where $d/cos(\theta_{\vec{k_c}})$ is the distance traversed by an electron in the barrier because of the Snell's law-like equation in (19). Notice that τ_{D_B} is not a transmitted time, because it is not related with the transmitted particles N_T only, but with N_T and N_R, excluding N_{R^*}.

Finally, for incident angles larger than the critical angle, $0 < \theta_{\vec{k_c}} > \theta_C$, the Bohmian dwell time can be computed numerically from τ_{D_B}, but there is no simple expression for its evaluation because $N_R > N_T$ and it is not obvious what is the dwell time for the N_R particles. Again, the Bohmian dwell time is different from the orthodox τ_D because the latter includes particles that do not enter into the barrier region ($N_{R^*} > 0$). In any case, there are few electrons traversing the barrier with such angles.

The main conclusion of this work, regarding the high-frequency capabilities of graphene devices based on Klein tunneling is that the high graphene mobility is roughly independent of the presence of Klein tunneling phenomena in the active device region. The reason is a direct consequence of the graphene band structure. All electrons, at all positive or negative kinetic energies, move roughly with the Fermi velocity above or below the potential barrier.

At this point we want to notice that the relation between cut-off frequencies and tunneling time has been analyzed in section 2 for an idealized two terminal device under the assumption that $L_x < L_z, L_y$. In more general scenarios, for example in a three terminal device, like a graphene transistor, the expression (1) for the current is no longer valid. This means that the cut-off frequencies cannot be directly linked to the inverse of the transit (tunneling) time. Further discussion of this issue can be found in [41].

Apart from the previous conclusions devoted to graphene devices for high-frequency applications we have a final remark on the type of simulators required for predicting high-frequency features of nanoelectronic devices. There are several quantum theories empirically equivalent to discuss the quantum behavior of nanoelectronic devices at high-frequency. By construction, the Bohmian theory [42] has the ability to provide measured and unmeasured properties (for example, particle positions or the total current) for quantum systems. Such ability is very convenient because it allows to get information of the system that are not contaminated by the measurement. This is specially relevant in the two consecutive measurements required to get transit (tunneling) times. Later, if we know how to relate measured and unmeasured properties in one experimental set-up (such as the high-frequency measurement set-up defined in [33]), the unmeasured properties provided by the Bohmian theory become very useful for computations of high-frequency applications of electronic devices. The BITLLES simulator used in this work is a clear example of this computing strategy.

Acknowledgment

We are grateful to Dmitry Sokolovski for enlightening discussions on tunneling times. We acknowledge funding from Fondo Europeo de Desarrollo Regional (FEDER), the "Ministerio de Ciencia e Innovación" through the Spanish Project TEC2015-67462-C2-1-R, the Generalitat de Catalunya (2014 SGR-384), the European Union's Horizon 2020 research and innovation programme under grant agreement No Graphene Core2 785219 and under the Marie Skodowska-Curie grant agreement No 765426 (TearApps).

Appendix A. Graphene electron trajectories

Here we demonstrate how the Bohmian velocity (7) can be obtained from the Dirac equation (4). The typical procedure to deduce the Bohmian velocity from the Schrödinger equation gives:

$$\vec{v}(\vec{r},t) = \frac{d\vec{r}}{dt} = \frac{\hbar}{m}\,\mathrm{Im}\left(\frac{\nabla\psi(\vec{r})}{\psi(\vec{r})}\right) \tag{A.1}$$

We adapt here the previous procedure to deduce the Bohmian velocity associated to the Dirac equation (for details see [43]). To obtain the current density, we find out first the continuity equation from the Dirac equation (4) rewritten here as:

$$i\hbar\frac{\partial\psi(\vec{r},t)}{\partial t} = -i\hbar v_f(\vec{\sigma}\cdot\vec{\nabla})\psi(\vec{r},t) \tag{A.2}$$

with $\vec{r} = \{x, z\}$. Now, multiply the Hamiltonian by the conjugated wave function:

$$\psi(\vec{r},t)^\dagger i\hbar\frac{\partial\psi(\vec{r},t)}{\partial t} = -i\psi(\vec{r},t)^\dagger\hbar v_f(\vec{\sigma}\cdot\vec{\nabla})\psi(\vec{r},t) \tag{A.3}$$

and conjugate and transpose the above equation (A.3):

$$\psi(\vec{r},t)\frac{\partial\psi(\vec{r},t)^\dagger}{\partial t} = -\psi(\vec{r},t)v_f(\vec{\sigma}\cdot\vec{\nabla})\psi(\vec{r},t)^\dagger \tag{A.4}$$

The above expression (A.4) implies that the Pauli matrices are hermitian. If we now add (A.3) and (A.4) we get:

$$\psi(\vec{r},t)^\dagger\frac{\partial\psi(\vec{r},t)}{\partial t} + \psi(\vec{r},t)\frac{\partial\psi(\vec{r},t)^\dagger}{\partial t} \tag{A.5}$$
$$= -\left[\psi(\vec{r},t)^\dagger v_f(\vec{\sigma}\cdot\vec{\nabla})\psi(\vec{r},t) + \psi(\vec{r},t)v_f(\vec{\sigma}\cdot\vec{\nabla})\psi(\vec{r},t)^\dagger\right]$$

which leads directly to the continuity equation:

$$\frac{\partial|\psi(\vec{r},t)|^2}{\partial t} + \vec{\nabla}\cdot\left(v_f\psi(\vec{r},t)^\dagger\vec{\sigma}\psi(\vec{r},t)\right) = 0 \tag{A.6}$$

where we can easily identify the probability current density (of the Dirac equation) as:

$$\vec{J}(\vec{r},t) = v_f \psi(\vec{r},t)^\dagger \vec{\sigma} \psi(\vec{r},t) \qquad \text{(A.7)}$$

From here, we can also identify the Bohmian velocities by using the general expression $\vec{J}(r,\vec{t}) = \rho\vec{v} = |\psi(\vec{r},t)|^2\vec{v}$ in (A.6) so that ,

$$\vec{v}(\vec{r},t) = \frac{J(\vec{r},t)}{|\psi(\vec{r},t)|^2} = \frac{v_f \psi(\vec{r},t)^\dagger \vec{\sigma} \psi(\vec{r},t)}{|\psi(\vec{r},t)|^2} \qquad \text{(A.8)}$$

And from the above equation the bohmian velocity in the x and z directions can be given as :

$$v_x(\vec{r},t) = \frac{J_x(\vec{r},t)}{|\psi(\vec{r},t)|^2} = \frac{v_f \psi(\vec{r},t)^\dagger \sigma_x \psi(\vec{r},t)}{|\psi(\vec{r},t)|^2} \qquad \text{(A.9)}$$

and,

$$v_z(\vec{r},t) = \frac{J_z(\vec{r},t)}{|\psi(\vec{r},t)|^2} = \frac{v_f \psi(\vec{r},t)^\dagger \sigma_z \psi(\vec{r},t)}{|\psi(\vec{r},t)|^2} \qquad \text{(A.10)}$$

Since (A.9) and (A.10) are independent of s (see (18) in the text), it is evident that independently of whether the electrons are in the conduction or valence band, they move in the same direction. It is important to emphasize that the identity $\vec{J}(r,\vec{t}) = \rho\vec{v} = |\psi(\vec{r},t)|^2\vec{v}$ in (A.6) used above guarantees the empirical equivalence between orthodox and Bohmian mechanics.

References

[1] A. K. Geim and K. S. Novoselov, *Nat. Mater.* **63**, 183 (2007)
[2] G. Fiori et al. *Nat. Nanotech.* **9** 768 (2014)
[3] O. Klein, Z. Phys. **53**, 157 (1929).
[4] P.E. Allain and J.N. Fuchs, *Eur. Phys. J. B* **83**, 301 (2011)
[5] Q. Wilmart et al. *Nat. Sci. Rep.* **6** 21085 (2016)
[6] Y. M. Lin et al., *IEDM 2009* **10** 237 (2009)
[7] Q. Wilmart et al., *2D Mat.* **1** 011006 (2014)
[8] Y. Tan et al., *Nat. Sci. Rep.* **7** 9714 (2017)
[9] Y. Taur and T. H. Ning, *Fundamentals of Modern VLSI Devices, 2nd ed., 290, New York: Cambridge University Press (2009)*
[10] E. H. Hauge and J. A. Stovneng, *Rev. Mod. Phys.* **61**, 917 (1989)
[11] R. Landauer and T. Martin, *Rev. Mod. Phys.* **66**, 217 (1994).
[12] E. P. Wigner, *Phys. Rev.* **98**, 145 (1955)
[13] A. I. Baz, Sov. *J. Nucl. Phys.* **4**, 182 (1967)
[14] V. F. Rybachenko, Sov. J. Nucl. Phys. **5**, 635 (1967)
[15] M. Büttiker and R. Landauer, *Phys. Rev. Lett* **49**, 1739 (1982)
[16] M. Büttiker, *Phys. Rev. B* **27**, 6178 (1983).
[17] Z. J. Li, J. Q. Liang and D. H. Kobe,*Phys. Rev. A* **64**, 042112 (2001); Z. J. Li, J. Q. Liang and D. H. Kobe, *Phys. Rev. A* **65**, 024101 (2002)
[18] F. Sattari *Physica B Condens Matter* **454**, 240 (2014)
[19] X. Chen, Z. Y. Deng and Y. Ban, *J. Appl. Phys.*, **115**, 173703 (2014)
[20] Z. J. Lia, H. Zhao, Y. H. Nie and J.-Q. Liang, *J. Appl. Phys.* **113**, 043714 (2013)
[21] Z. Wu, K. Chang, J. T. Liu, X. J. Li and K. S. Chan, *J. Appl. Phys.* **105**, 043702 (2009)
[22] Y. Gong and Y. Guo, *J. Appl. Phys.* **106**, 064317 (2009)
[23] E. Faizabadi and F. Sattari, *J. Appl. Phys.* **111**, 093724 (2012)
[24] R. A. Sepkhanov, M. V. Medvedyeva and C. W. J. Beenakker, *Phys. Rev. B* **80**, 245433 (2009)
[25] T. E. Hartman, *J. Appl. Phys.* **33**, 3427 (1962)
[26] D. Sokolovski and L. M. Baskin, *Phys. Rev. A* **36**, 4604 (1987)
[27] C. R. Leavens, *Solid State Commun.* **74**, 923 (1990)
[28] W. Shockley, *J. Appl.Phys.* **9**, 635 (1938)
[29] S. Ramo, *Proceedings of the I. R. E.* **27**, 584 (1939)
[30] B. Pellegrini, *Phys. Rev. B* **34** 5921 (1986)
[31] H. Aoyama and T. Harano, *Nucl. Phys. B* **446**, 315 (1995)
[32] D. Bohm, *Phys. Rev.* **85**, 166 (1952)
[33] D. Marian, N. Zanghì and X. Oriols, *Phys. Rev. Lett.* **116**, 110404, (2016)
[34] P. R. Holland, *The Quantum Theory of Motion*, Cambridge University Press, Cambridge (1993)
[35] X. Oriols and J. Mompart (eds.), *Applied Bohmian Mechanics: From Nanoscale Systems to Cosmology*, Pan Stanford, Singapore (2012)
[36] J. S. Bell, *Rev. Mod. Phys.* **38**, 447 (1966)
[37] The BITLLES simulator is free available at: http://europe.uab.es/bitlles
[38] X. Oriols, *Phys. Rev. Lett.* **98**, 066803 (2007)
[39] E. Colomés, Z. Zhan, D. Marian and X. Oriols, *Phys. Rev. B* **96**, 075135 (2017)
[40] M. I. Katsnelson, K. S.Novoselov and A. K. Geim, *Nat. Phys.* **2**, 620 (2006)
[41] Z. Zhan, E. Colomés and X. Oriols *IEEE Trans Electron Devices* **64**, 6 2617 (2017)
[42] K. J. Bostrm, *arXiv:1503.00201 [quant-ph]*
[43] E. Colomés, Doctoral Thesis, Universidad Autónoma de Barcelona

Publication E

Devashish Pandey, Laura Bellentani, Matteo Villani, Guillermo Albareda, Paolo Bordone, Andrea Bertoni, and Xavier Oriols. A Proposal for Evading the Measurement Uncertainty in Classical and Quantum Computing: Application to a Resonant Tunneling Diode and a Mach-Zehnder Interferometer. *Applied Sciences*, 9(11):2300, 2019

applied sciences

MDPI

Article

A Proposal for Evading the Measurement Uncertainty in Classical and Quantum Computing: Application to a Resonant Tunneling Diode and a Mach-Zehnder Interferometer

Devashish Pandey [1,*], Laura Bellentani [2], Matteo Villani [1], Guillermo Albareda [3], Paolo Bordone [2,4], Andrea Bertoni [4] and Xavier Oriols [1]

1 Departament d'Enginyeria Electrònica, Universitat Autònoma de Barcelona, 08193-Bellaterra (Barcelona), Spain; matteo.villani@uab.cat (M.V.); xavier.oriols@uab.cat (X.O.)
2 Dipartimento di Scienze Fisiche, Informatiche e Matematiche, Università degli Studi di Modena e Reggio Emilia, Via Campi 213/A, I-41125 Modena, Italy; laura.bellentani@unimore.it (L.B.); paolo.bordone@unimore.it (P.B.)
3 Max Planck Institute for the Structure and Dynamics of Matter and Center for Free-Electron Laser Science, Luruper Chaussee 149, 22761 Hamburg, Germany; guillermo.albareda@mpsd.mpg.de
4 S3, Istituto Nanoscienze-CNR, Via Campi 213/A, 41125 Modena, Italy; andrea.bertoni@unimore.it
* Correspondence: devashish.pandey@uab.cat

Received: 8 April 2019; Accepted: 29 May 2019; Published: 4 June 2019

Abstract: Measuring properties of quantum systems is governed by a stochastic (collapse or state-reduction) law that unavoidably yields an uncertainty (variance) associated with the corresponding mean values. This non-classical source of uncertainty is known to be manifested as noise in the electrical current of nanoscale electron devices, and hence it can flaw the good performance of more complex quantum gates. We propose a protocol to alleviate this quantum uncertainty that consists of (i) redesigning the device to accommodate a large number of electrons inside the active region, either by enlarging the lateral or longitudinal areas of the device and (ii) re-normalizing the total current to the number of electrons. How the above two steps can be accommodated using the present semiconductor technology has been discussed and numerically studied for a resonant tunneling diode and a Mach-Zehnder interferometer, for classical and quantum computations, respectively. It is shown that the resulting protocol formally resembles the so-called collective measurements, although, its practical implementation is substantially different.

Keywords: quantum computing; classical computing; Mach-Zehnder Interferometer; resonant tunneling diode; quantum uncertainty; measurement

1. Introduction

Assessing the future of emergent technologies is not an easy task. Today there is a lively debate in the scientific community about whether classical or quantum computing will offer better performance in the coming future. At present, the field effect transistor is still the most efficient device to perform classical computations. The electronic industry is able to fit 10^{10} transistors all together in a single chip, working at frequencies of a few GHz [1]. State-of-the-art transistors, with nanoscale dimensions, are quantum devices in the sense that their ability to convert the input into output information is based on quantum laws governing electron transport [2]. In digital binary classical computing, the logical state '1' is encoded into a value of a well-defined measurable physical property of the transistor, while the logic state '0' corresponds to a different value of such property. Usually the physical properties used in

electron devices for classical computing are the electrical current or the voltage in different (input and output) terminals. It is important to notice that although the transistor is a quantum device whose performance is determined by the evolution of quantum states, these quantum states are not directly used to encode information in classical computing.

In quantum computing [3], contrarily, the logical state '1' is directly encoded in a quantum state of the physical system, namely $|1\rangle \rightarrow \psi_1(\vec{r}, t)$ where $\vec{r}$ represents the degrees of freedom of the system. Similarly, the logical state '0' corresponds to another quantum state $|0\rangle \rightarrow \psi_0(\vec{r}, t)$. Because of the quantum superposition principle, a sum of the two physical states, $a|1\rangle + b|0\rangle$ where a and b are complex numbers, is also a valid physical state of the system. As a consequence, quantum mechanics offers the possibility of operating simultaneously on the logical states '1' and '0'. This opens classically inaccessible computing possibilities.

Many companies and researchers are advocating for quantum computing. Among many others, for example, Google has said that its state-of-the-art quantum chip will be the first to perform calculations beyond the best existing classical supercomputers [4]. Other companies and researchers, on the contrary, understand quantum computing as an exciting discipline, with an unquestionable scientific interest, but argue that quantum technologies will not substitute our classical computing machines at home (because quantum computers are complex, expensive and built using a more immature technology) [5,6]. In any case, without making any risky prediction, what seems clear today is that classical and quantum computing are both valuable research avenues.

Any classical or quantum computation using quantum devices is implemented following three main steps: (i) initial preparation of the quantum state, (ii) unitary evolution of the state and (iii) the final measurement of the state. In this paper, we will focus on the last step for both classical and quantum computations. The measurement step is linked to the quantum uncertainty [7] that implies a practical inconvenience since it gives rise to quantum noise at the output of the device (The reader can argue that the uncertainty disappears when the quantum state is prepared as an eignestate of the projective (measuring) operator. However, typically, the *preparation* of the state of an electron being injected into the active device region from the contact (reservoir) is done by the contacts itself, which do not provide such eigenstates). Solid-sate quantum electron devices are unquestionably the best technology to implement classical computing. It is, however, not clear today which will be the best technology for quantum computing. In any case, it seems clear that the possibility of implementing quantum computing algorithms with solid-sate devices would benefit from the maturity of the existing technology and offers the possibility of making quantum computing platforms compatible with classical ones.

The paper is structured as follows. In Section 2, we will propose a simple protocol that allows evading the quantum uncertainty associated with the measurement process in quantum electron devices, for either classical or quantum computing applications. This is the main result of this work. In Section 3, we will first investigate the measurement of the electrical current under this protocol for a resonant tunneling diode (RTD) understood as a quantum electron device useful for classical computing. Later, in Section 4, we will analyze the measurement of the electrical current in a Mach-Zehnder interferometer (MZI) which is tailored to design the logic gates suitable for implementing quantum computing. We will conclude in Section 5. More technical details are presented in the appendices.

2. Quantum Uncertainty: The Problem and the Solution

In this section, in order to simplify the discussion and better understand the problem and the solution explained here, we made the following simplifying assumptions. First, we will focus on a quantum electron device with just one degree of freedom indicated by $\vec{r}$. The consideration of more realistic situations, with many degrees of freedom in a quantum device, would not modify the conclusions drawn here and would only complicate the notations and understanding of the results.

See Appendix A for the straightforward generalization of the present results to an unmodified (original) quantum device with many degrees of freedom in the active region.

Second, we will assume that the measurement of the electrical current of the quantum electron device is done through a projective (strong) operator and that the state of the system after the measurement is just an eigenstate of this operator. In other words, we will assume that the measurement process is done with a projective value measure (PVM), while it has been argued that the realistic type of measurement of the electrical current is better described by a positive operator valued measure (POVM) [8,9]. In any case, the explicit consideration of a POVM to describe the measurement process will not add any relevant point in the discussion. In Appendix C, we explain with more detail the measurement of the electrical current in a realistic quantum electron device as a POVM.

2.1. The Problem

The first step to implement a classical or quantum computing algorithm using quantum devices is the initial preparation of the quantum state associated with the quantum electron device $\psi_{in}(\vec{r},0)$. In quantum computing, the initial state is directly linked to a combination of two states, $\psi_1(\vec{r},0)$ and $\psi_0(\vec{r},0)$, respectively associated with the logical values '1' and '0', whereas in classical computing, the link between logical information and initial quantum state is not direct. Typically, a quantum device for classical computation is connected to the external world through the contacts (also know as reservoirs) that determine the electron wave function depending on temperature and doping conditions. The input logical information is then linked to a value of an observable I, not directly to the quantum state. We have used the symbol I to remind readers that hereafter, we will consider the electrical current as the physical magnitude where information is encoded.

The second step is the manipulation of the initial quantum state through the quantum electron device (also known as gate in the literature). Typically, such manipulation, whether in classical or quantum computing is done through a (usually unitary) operator $\hat{U}(t,0)$. In quantum computing, the final state $\psi_{out}(\vec{r},t) = \hat{U}(t,0)\psi_{in}(\vec{r},0)$ is directly linked to the output logical information, while in classical computing the output logical information is linked to an observable I associated with this final state through a measurement process that we describe below. See Figure 1a where different gates of an RTD which are connected to exemplify a classical computation gate connected through output values of the electrical current (or voltage), while the connection among different gates of the quantum computing device is done through the wave function itself as depicted in Figure 1b.

The third and last step, both in classical or quantum computing algorithms, is the measurement step. To get the final observable value I in classical computing, the quantum electron device has to be measured through a (non-unitary) process. Such non-unitary process is depicted as an ammeter in Figure 1. The evolution from the final state to the measured state, $\psi_{out}(\vec{r},t) \rightarrow \psi_I(\vec{r},t)$, is called collapse or reduction of the wave function. The subindex I here refers to the measured state of the current which corresponds to an eigenvalue I of the eigenfunction $\psi_I(\vec{r},t)$ associated with the operator $\hat{I}$. In quantum computing, the final wave function $\psi_{out}(\vec{r},t)$ is not directly measurable in a single shot measurement. Instead, the logical information assigned to this final quantum state has to be indirectly deduced from the measurement of an observable assigned to such final state. See Figure 1b. Notice that the measurement in quantum computing has to be done only once, at the end of the gate, because each measurement collapses the wave function, destroying the required superpositions of different states in the quantum computing algorithms.

The process of measurement involves a quantum uncertainty which is a consequence of the fact that each time a quantum measurement is done, the wave function collapses into an eigenstate of the operator $\hat{I}$ associated with the measuring apparatus. The observable output I_{out} is a random value equal to the eigenvalue associated with the mentioned eigenstate. In general, and this is true for the measurement of the electrical current, the final state before measurement $\psi_{out}(\vec{r},t)$ is not an eigenstate of the current $\psi_I(\vec{r},t) \neq \psi_{out}(\vec{r},t)$. In fact, the final state can be written as a superposition of many different current eigenstates. Thus, each time we repeat an experiment to obtain information about

the output current, we get different values. This randomness in the output values can be quantified through the probability distribution $P(I) = |\langle \psi_I(\vec{r})|\psi_{out}(\vec{r},t)\rangle|^2$ given by Born's law. From a quantum engineering point of view, this quantum uncertainty (seen as noise in the current) is inconvenient for efficiently processing logical (either classical or quantum) information.

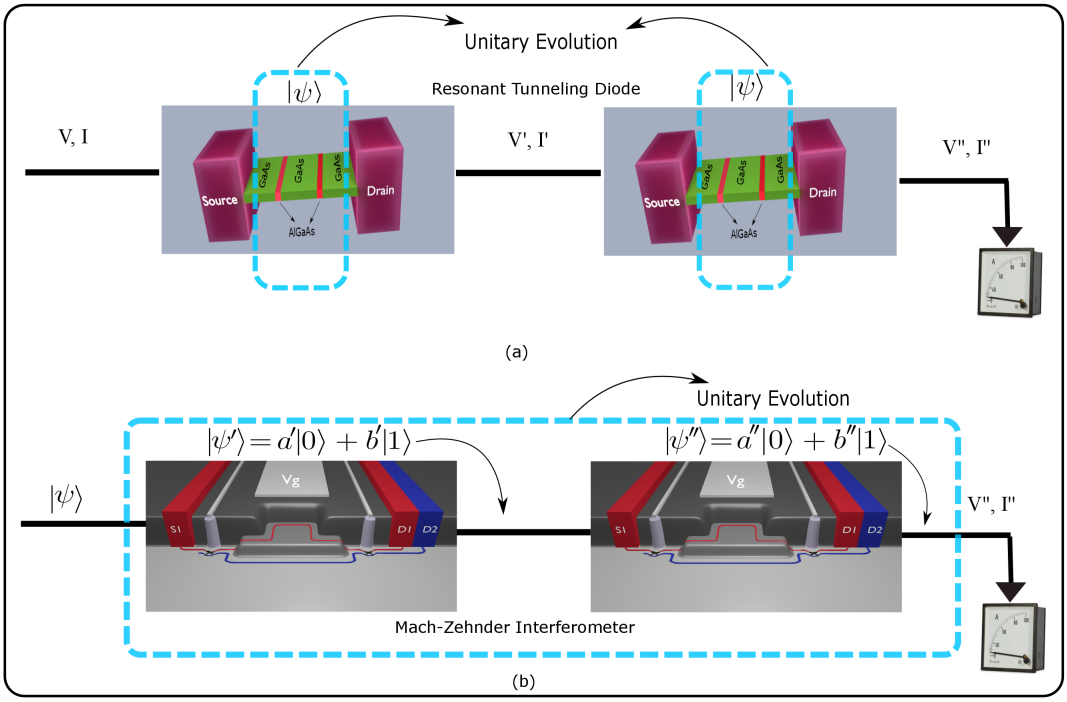

Figure 1. (**a**) Schematic of classical computing exemplified with RTD where only the active device is governed by unitary quantum evolutions (enclosed in the cyan color dashed line), while the contacts and the cable leads to quantum decoherence which provides a fixed value of the current obtained in the measuring apparatus (shown at the right end). (**b**) Schematic of quantum computing exemplified with an MZI where the quantum wholeness require that a coherent unitary evolution appears in all the gates (enclosed in the cyan color dashed line). Only at the end, when the wave function is measured, decoherence can be accepted.

In classical computations, the uncertainty on the electrical current can be eliminated by using the ensemble value of the current $\langle I \rangle$ computed from a large number of identical experiments, each one giving I^i, with the subindex i identifying the experiment. The ensemble value is defined as $\langle I \rangle = (\sum_{i=1}^{N_{exp}} I^i)/N_{exp}$, where $N_{exp} \to \infty$ is the number of experiments. In principle, this ensemble value would require repeating the same experiment for a large set of N_{exp} identical quantum electron devices. In practice, by invoking ergodic arguments, the repetition of the experiment is substituted by measuring at different times in the same quantum electron device. Thus, instead of defining the signal of the output logical value as the instantaneous current I^1 (which has noise) one defines it as the DC value of the electrical current $\langle I \rangle$ computed during a large time interval (which has no noise). This solution is efficient for reducing the noise, but it requires a large measuring time. (In our simulation example with an RTD with a device active region length of 10 nm, the injection time of 0.05 ps and the velocity of electrons as 10^4 m/s, the time after which we get the non-fluctuating value of the current is around 50 ps. In any case, the measuring time is again a parameter that depends on many factors, like injection time, velocity of electrons, electron density, level of tolerable uncertainty. etc., and that can be enlarged or reduced as desired by manipulating these parameters.)

The quantum uncertainty described above represents also a problem for quantum computing. In fact, although the logical output information in quantum computing is encoded in the final wave function $\psi_{out}(\vec{r},t)$ (not in an observable I^i), the quantum state $\psi_{out}(\vec{r},t)$ is not itself an observable

(i.e., it cannot be measured in a single shot measurement). Thus, the quantum state of the system needs to be deduced from the expectation value $\langle I \rangle$. Again, the measurement process of such observable $\langle I \rangle$ has the same inconveniences mentioned above for classical computing, due to the quantum uncertainty. We notice that in a quantum computing algorithm, with many interconnected quantum gates, the measurement of the observable is done only at the last gate. In fact, trying to measure at an intermediate gate would be understood as a type of decoherent phenomena that would dramatically perturb the unitary evolution required in typical quantum algorithms. In Figure 1 we encircle the regions of the connected gates where the dynamics of electrons are supposed to be governed by unitary quantum evolutions. From Figure 1, one can understand why decoherence is a serious problem for quantum computing, but not for classical computing. In an array of interconnected classical computing devices, the decoherence that can appear at the output of each particular device due to the measurement does not affect the performance of the algorithm because the interconnection between devices is done in terms of observables (not in terms of wave functions).

In summary, the electrical current in nanoscale devices, for classical or quantum computing, has an inherent quantum uncertainty, seen as noise in the measured value of the electrical current. Since the information is usually encoded in the average value $\langle I \rangle$ of the electrical current, we require an effort to wash out the noise from the measured current to get valid information. The typical solution in the literature to wash out the noise is repeating the experiment many times (or using the ergodic theorem to get $\langle I \rangle$ after a large time).

2.2. The Solution

In this work, we explain a novel solution to the problem discussed above about reducing the quantum noise induced by the measurement process. We argue in this paper that such noise can be eliminated by modifying the quantum device to accommodate $N \to \infty$ electrons, simultaneously. We will show that the dispersion of a random distribution of the (normalized) electrical current of $N \to \infty$ electrons tends to zero, which implies eliminating the quantum noise.

Let us consider an original or unmodified quantum electron device (before applying our protocol) that has only one transport electron, at each time, responsible for the measured current. Such electron at time t_{in} is described by a single particle quantum state $|\psi^1(t_{in})\rangle$ where the superindex 1 refers to this first electron. We are measuring the current through a single particle operator $\hat{I}^1$. If the state $|\psi^1(t_{in})\rangle$ is not an eigenstate of the operator $\hat{I}$, then, the measurement of the I gives rise to the quantum noise discussed in the previous subsection (we notice again that the generalization to more electrons is done in Appendix A).

The solution that we propose to minimize the quantum noise requires designing a new quantum device (that we will refer to as the modified quantum device or just the quantum device) so that this new device satisfies the following two conditions:

- **Condition 1:** We enlarge the original quantum electron device in order to accommodate a large number of electrons $N \to \infty$ simultaneously. Then, the many-particle wave function $\Psi_T(t_{in})$ that defines this N electrons at time t_{in} is:

$$|\Psi_T(t_{in})\rangle = |\psi^1(t_{in})\rangle \otimes |\psi^2(t_{in})\rangle \otimes .... \otimes |\psi^N(t_{in})\rangle, \quad (1)$$

  where the wave function $|\psi^i(t_{in})\rangle$ is the single electron wave function that corresponds to the i-th electron prepared under the same conditions that we have used to prepare the wave function $|\psi^1(t_{in})\rangle$ in the original quantum electron device.

  Strictly speaking, the condition $N \to \infty$ is inaccessible in a practical scenario. We will see numerically in the following sections that a finite number of electrons is enough to drastically reduce the quantum noise. Identically, if the number of transport electrons in the original (unmodified) quantum electron device is already larger than one, the solution proposed here is still perfectly valid. See Appendix A for a generalization of the present protocol to more than one

electron in the unmodified electron device. Finally, as can be seen in Equation (1), we assume a many-particle wave function of non-interacting electrons. This is obviously an approximation in realistic quantum devices since these electrons will suffer exchange and Coulomb interactions. In Appendix D, we test our protocol under the exchange symmetry for two electrons. Under the assumption of an initial negligible overlap of the wavepackets our protocol does not deviate from the actual result. These issues will be further elaborated in the practical implementation of this protocol in next two section.

We mention that some (small) variation in the preparation of the state $|\psi^1(t_{in})\rangle$, $|\psi^2(t_{in})\rangle$,... forming $\Psi_T(t_{in})$ is allowed. For example, the time delay between the injection of different single electron wave packets can vary. Also the central position of the wave packets along the lateral dimension of the device can be different. Similarities between different wave packets have to be enough to justify that the probability distribution of the values of the current is identical for all single electron wave packets.

- **Condition 2:** We substitute the measuring apparatus associated with the single particle operator $\hat{I}^1$ with a new measuring apparatus whose associated many-body operator $\hat{I}_T$ is:

$$\hat{I}_T = \frac{\hat{\mathcal{I}}^1 + \hat{\mathcal{I}}^2 + ... + \hat{\mathcal{I}}^N}{N}, \tag{2}$$

where $\hat{\mathcal{I}}^i = \hat{\mathbb{I}} \otimes .... \otimes \hat{I}^i \otimes ... \otimes \hat{\mathbb{I}}$ acts only on the quantum state $|\psi^i(t_{in})\rangle$ and $\hat{\mathbb{I}}$ is the identity operator in the small Hilbert space of each degree of freedom. Notice the presence of the factor $N \to \infty$ in the denominator of the operator $\hat{I}_T$.

In next section, we will show the physical soundness of the many-particle operator in Equation (2) for typical semiconductor electron device technology.

Now let us formally demonstrate that the dispersion of the electrical current of the modified quantum device (satisfying **condition 1** and **condition 2**) is zero. For the operator $\hat{I}_T$ defined in Equation (2), we calculate the variance of the $\langle I_T^2 \rangle$ as the mean square value of the operator $\hat{I}_T$ as:

$$\langle \Psi_T | (\hat{I}_T)^2 | \Psi_T \rangle = \frac{1}{N^2} \sum_i^N \langle \psi^i | \hat{I}^i \hat{I}^i | \psi^i \rangle + \sum_{i,j \neq i}^N \frac{1}{N^2} \langle \psi^i | \hat{I}^i | \psi^i \rangle \langle \psi^j | \hat{I}^j | \psi^j \rangle. \tag{3}$$

By construction of the wave function in Equation (1), we know that the mean values $\langle \psi^j | \hat{I}^j | \psi^j \rangle$ are all identical for any j. Therefore, we can consider $\langle \psi^j | \hat{I}^j | \psi^j \rangle = \langle \psi^1 | \hat{I}^1 | \psi^1 \rangle$ because all electrons are described by the same wave function and we can rewrite Equation (3) as follows,

$$\langle \Psi_T | (\hat{I}_T)^2 | \Psi_T \rangle = \frac{N}{N^2} \langle \psi^1 | (\hat{I}^1)^2 | \psi^1 \rangle + \frac{N(N-1)}{N^2} \langle \psi | \hat{I}^1 | \psi^1 \rangle \langle \psi^1 | \hat{I}^1 | \psi \rangle. \tag{4}$$

Therefore, when $N \to \infty$, we get:

$$\langle \hat{I}_T^2 \rangle = \langle \Psi_T | (\hat{I}_T)^2 | \Psi_T \rangle = \langle \psi^1 | \hat{I}^1 | \psi^1 \rangle \langle \psi^1 | \hat{I}^1 | \psi^1 \rangle = \langle \hat{I}^1 \rangle^2. \tag{5}$$

Now, we have to demonstrate that the logical information provided by the modified quantum device dealing with I_T is the same as the one that one gets from the original quantum device. As we discussed, the logical information of the original quantum device was represented by the mean value of the current $\langle \hat{I}^1 \rangle$ and not by the instantaneous value I^1 (which was too noisy due to quantum uncertainty). It is quite simple to demonstrate that $I_T = \langle \hat{I}^1 \rangle$ for $N \to \infty$. By construction, we know $\langle \hat{I}^1 \rangle = \langle \hat{I}^j \rangle$, from Equation (2) we get $\langle \hat{I}_T \rangle = N \langle I^1 \rangle / N = \langle \hat{I}^1 \rangle$ and with Equation (5), we conclude that the dispersion σ_{I_T} of the distribution of the total current I_T is zero:

$$\sigma_{I_T}^2 = \langle \hat{I}_T^2 \rangle - \langle \hat{I}_T \rangle^2 = 0. \tag{6}$$

The result $\sigma_{I_T} = 0$ in Equation (6) implies that the distribution of I_T is a delta function around $\langle \hat{I}^1 \rangle$. This implies that in every measurement one gets the mean value of the single particle average current $I_T = \langle I^1 \rangle$.

It can be easily checked that the state in Equation (1) in the limit $N \to \infty$ is, in fact, an eigenstate of any operator of the type of Equation (2) at any time. This state, with this unusual property, has been used by one of the co-authors to study the quantum-to-classical transition [10]. In addition, a similar state and operator as the ones invoked in our **condition 1** and **condition 2** has been used to develop the new concept of collective measurements [11,12]. Such collective measurements do really invoke multiple physical repetitions of the quantum system, while in our paper we make use of this idea in the same many-particle state and operator and in a single (modified) quantum device. In other words, the demonstration provided above is mathematically equivalent to the one that appears in the theory of collective measurements, but their physical implementation in the laboratory is radically different. In the rest of the paper, we will show how these two conditions can be effectively implemented with the semiconductor electron device technology in a single device for classical and quantum computing.

3. Application to Classical Computing Device: Resonant Tunneling Diode

As an example for the application of the discussed protocol in a classical computing device, we consider the computation of the electrical current in an RTD. This type of electron device is a pure quantum device, whose performance is based on tunneling, and has been successfully implemented in some particular high frequency applications particularly to explore the missing THz gap for various analog and digital applications [13–16]. The main element that defines an RTD is a double barrier potential created, for example, by alternating Gallium Arsenide (GaAs) and Aluminum Gallium Arsenide (AlGaAs) III-V semiconductors with different energy gaps, as shown in Figure 2. The combination of low band gap and high band gap semiconductors leads to the formation of a well in the potential energy profile, which gives rise to discrete set of energies inside, known as resonant energies.

As depicted in Figure 2, two reservoirs or contacts emit or collect the electrons through the RTD structure. We name the left contact as source (also known as emitter in the literature) and the right contact as drain (also known as collector in the literature). These contacts are responsible for the first step of classical computing algorithm: the preparation of the initial quantum states. The energy of the injected electrons is determined by the Fermi-Dirac statistics (depending on the doping conditions of the contacts). A regular injection of electrons is assumed according to the discussion of the Appendix B. The second step of the classical computing algorithm is carried out by the barrier structure that determines whether the injected electrons are effectively transmitted or not. An electron incident on the double barrier with an energy equal to one of the resonant energies tunnels through the barrier, being transmitted with a transmission coefficient T close to one, while electrons with other energies have a transmission coefficient close to zero. An external potential between the drain and source potentials, modifies the double barrier potential energy profile, controlling the ON and OFF currents. One value of the current can be assigned to the logical output information '1' and the other to the '0'.

The last step of the classical computing algorithm is the measurement of the ON or OFF current which implies the measurements (collapse) of the quantum wave function assigned to electrons inside the RTD, which provides the undesired quantum uncertainty in the output values of the current. We discuss next how the conditions of Section 2.2 can be implemented.

3.1. Implementation of Condition 1 and Condition 2

We consider that the RTD depicted in Figure 2 corresponds to the modified design of the device that accommodates a large number of N electrons simultaneously inside. In this particular device, enlarging the lateral area A is enough to enlarge the number of electrons inside the RTD. We can reasonable assume that the contact *prepares* the wave packets of each electron in a similar way so that the **condition 1** of our protocol in Equation (1) is easily satisfied. Certainly, a point that requires

further discussion is how to ensure that the many-body wave function of electrons in the active region of this modified device can be approximated by the non-interacting wave function in Equation (1). In the Appendices A and B some qualitative indications are mentioned. A different solution for minimizing the undesired Coulomb and exchange interactions will be discussed in next section, for quantum computing.

To satisfy the second condition we have to ensure that all electrons inside the device contribute equivalently to the measured value of the electrical current. A detailed discussion of the conditions that have to be satisfied by the quantum device to ensure this point is provided in the Appendix C. We anticipate here that such discussion is greatly simplified by associating to each electrons a quantum (Bohmian) trajectories, whose positions and velocities are well-defined even in absence of a measurement, in addition to the orthodox wave function. Then, the electrical current due to the simultaneous contribution of all electron leads to the following expression,

$$I_{exp}(t) = \sum_{i=1}^{N(t)} I^i(t) = \sum_{i=1}^{N(t)} q\frac{v_x^i(t)}{L}, \tag{7}$$

As discussed in the Appendix C the above expression assumes that the lateral dimensions of the (two terminal) electron device are much larger than the longitudinal one, and that the contacts are formed by metals with a fast screening time in comparison with that on the active region. The **condition 2** of our protocol to define the current operator as in Equation (2), requires to define the output instantaneous value of the current as,

$$I_T(t) = \frac{I_{exp}(t)}{N(t)}, \tag{8}$$

The value of $N(t) \approx N$ can be assumed to be proportional to the enlarged lateral area, and the value $I_T(t)$ computed from $I_{exp}(t)$ after knowing the ratio of the modified/unmodified areas. The detailed discussion on the definition of the current and the implications of **condition 2** is given in Appendix C.

3.2. Numerical Results

In this subsection, to show how the quantum uncertainty of the values of the measured electrical currents can be controlled, we compute the autocorrelation function of the current I_T defined as:

$$\langle I_T(t_2) I_T(t_1) \rangle = \int dI_T^k \int dI_T^\omega \; I_T^k I_T^\omega P(I_T^k, I_T^\omega), \tag{9}$$

where $P(I_T^k, I_T^\omega)$ is the probability associated with the subsequent measurement of the multiparticle state $|\Psi_T\rangle$ at two times t_1 and $t_2 > t_1$, with I_T^ω and I_T^k defined as the output values of the current at times t_1 and t_2, respectively.

As indicated in the previous section, for practical reasons in the computation of the particle and displacement components of the current, we will use a wave function plus a Bohmian trajectory for each electron in the computation of the dispersion of I_T in the modified quantum device through expressions in Equations (7) and (8). The measurement of the current in an electrical device is a weak measurement process [8] in the sense that the perturbation of the wave function due to the measurement process is not very dramatic. This type of measurement is mathematically represented by three subsystems: the quantum system, the measuring apparatus plus an intermediate system or *ancilla*. In fact, the system interacts with the *ancilla* during the measurement (not with the apparatus) and the apparatus measures the ancilla (not the system). This indirect way of getting information of the system by measuring the *ancilla* implying that the output value of the total current has the quantum noise of the system plus the quantum noise of the *ancilla*. In our particular example, the *ancilla* is just the cable (in fact there are a very large number of electrons) connecting the RTD with the ammeter [8]. As indicated in the previous section, for practical reasons in the computation of the particle and

displacement components, in addition to the wave function, each electron will be described by a Bohmian trajectory.

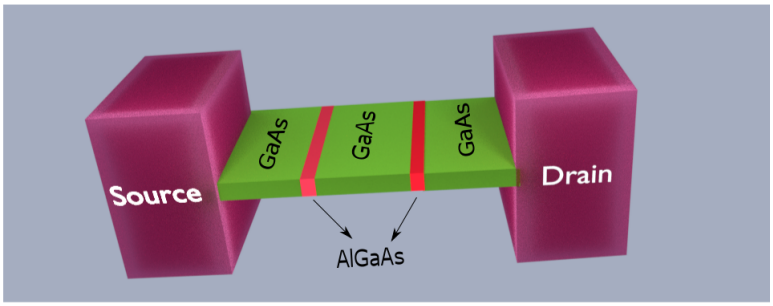

Figure 2. A 3D schematic of the RTD where the green material represents GaAs while the red represents AlGaAs. The alternating AlGaAs-GaAs-AlGaAs structure results in a potential well with discrete resonant energies.

As we have mentioned, the elimination of the quantum uncertainty in the measured current implies that the total wave function in Equation (1) is an eigenstate of the many-particle operator in Equation (2). Then, the first measured value of the current $I_T(t_1)$ at time t_1 has no influence on the output of a second measurement $I_T(t_2)$ at time t_2, and it can be shown [17] that the two time probability of the autocorrelation given in Equation (9) can be written as the product of two independent probabilities, which leads to the following expression of the two time correlation in Equation (9),

$$\begin{aligned} \langle I_T(t_2) I_T(t_1) \rangle &= \int dI_T^k \int dI_T^\omega \; I_T^k I_T^\omega P(I_T^k) P(I_T^\omega) \\ &= \int dI_T^k I_T^k P(I_T^k) \int dI_T^\omega I_T^\omega P(I_T^\omega) \qquad (10) \\ &= \langle I_T(t_2) \rangle \langle I_T(t_1) \rangle \qquad (11) \end{aligned}$$

The condition in Equation (11) is a test of the fact that the quantum uncertainty has disappeared in the measurement process of the modified device. Please note that from a pure engineering point of view, the autocorrelation mentioned above contains rich information on the high frequency response of the quantum device. In order to get the frequency response of the device we compute the power spectral density which is just the Fourier transform of the autocorrelation function (since the current signal has a constant mean, it is in a wide sense a stationary process, hence the auto-correlation depends only on the time difference $t = t_2 - t_1$. Therefore the auto-correlation function and the PSD form a Fourier transform pair). We therefore define the power spectral density due to the unmodified system, i.e., the system where the protocol is not applied, as $\mathbb{P}_{unmodified} = \mathcal{F}\{\langle I_T(t_2) I_T(t_1) \rangle\}$ while $\mathbb{P}_{modified} = \mathcal{F}\{\langle I_T(t_2) \rangle \langle I_T(t_1) \rangle\}$ for the modified system where the protocol is implemented. Here $\mathcal{F}$ represents the Fourier transform operator. Finally we can define the relative error (RE) as:

$$\text{RE} = \frac{\mathbb{P}_{modified} - \mathbb{P}_{unmodified}}{\mathbb{P}_{modified}}, \qquad (12)$$

which is plotted in Figure 3. The RE in Equation (12) contains quantum noise at all frequencies. Since all electrical devices are, in fact, a low pass filter, it is interesting for engineering purposes to quantify the error as a function of the frequency. A value of the RE equal to zero indicates that the quantum uncertainty (of the system and *ancilla*) has been eliminated which has a direct correspondence with the increase in the transport electrons in the device that can be further attributed to a large transmission or a large average current. Besides this it is also easy to see that to arrive at a zero quantum uncertainty we do not need an infinite number of electrons.

In our simulation the total number of electrons injected is given by $N = t/\tau_{in}$ where t is the total simulation time (the time after which the mean current reaches a constant value) and τ_{in} is the injection time of electrons. Now we know that $\langle I_T \rangle = \frac{qTf_e}{\tau_{in}}$ where T is the transmission coefficient and f_e is the Fermi function which we assume to be unity. So it is straightforward to see that $N = \frac{t\langle I_T \rangle}{qTf_e}$. We used the total time of simulation as 50 ps , $T = 0.7$, $f_e = 1$ and $\langle I_T \rangle = 5$ μA . These values correspond to a point in graph where the uncertainty starts to disappear which gives us the value of $N \approx 2232$. Which is a large value but not infinite.

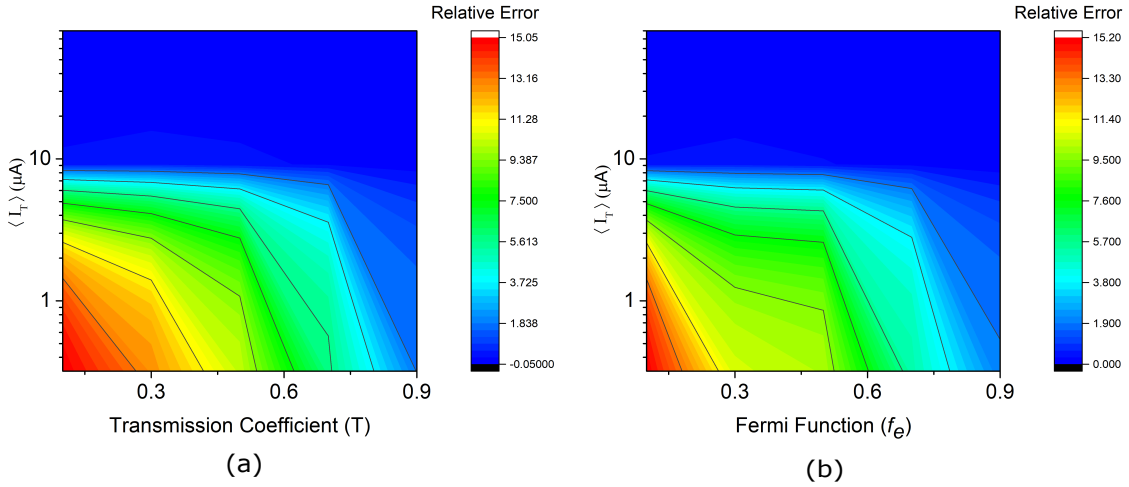

Figure 3. (**a**) Plot between the relative error, the transmission coefficient and the average current with the Fermi function fixed to unity. The relative error which is an indicator of quantum randomness, goes to zero, when the number of electrons in the device quantified by transmission coefficient and the mean current becomes very large (blue shaded region) while the relative probability of error is greater (in the red region) when the number of particles in the device is very small. In the green region the uncertainty already starts to disappear. (**b**) The same plot but with a constant transmission probability as unity and varying Fermi function also demonstrate the same outcome.

4. Application to Quantum Computing Devices: Mach-Zehnder Interferometer

We provide now an example of our protocol for reducing the quantum uncertainty in a quantum computing device. Quantum computing algorithms require a suitable set of quantum gates to reproduce logical operations [18–20]. With respect to most recent implementations, mainly based on superconducting [21] or single-ion qubits [22], solid-state devices are promising candidates because of their scalability and potential to be integrated into classical circuitry. In this section we will study how the quantum uncertainty can be eliminated in a solid-state MZI acting as quantum gate.

It is important to notice that any practical implementation of a quantum gate tends to have a non-negligible interaction between the quantum system and the environment (in terms of scattering with photons, background charges, impurities etc.) even when no measurement is designed. This interaction affects the expected unitary evolution of the state of the quantum system and produces loss of the logical information encoded in the state (decoherence). In solid-state MZI proposal, decoherence can be successfully minimized by injected electrons in *edge states*, chiral conductive channels generated in the Integer Quantum Hall regime [23]. Then, a strong enough magnetic field B is applied perpendicularly to a 2DEG, so that the band structure is discretized into Landau levels. In proximity to the confining potential of the device, the system eigenstates form chiral channels where an electron propagates coherently for large distances [24]. The chirality of such *edge states* prevents the electron to be back-reflected by eventual impurities on its path, unless it is scattered to the counterpropagating edge channel by a narrow quantum point contact [25,26]. Coherent transport

of electrons in *edge states* has been tested in a large variety of semiconductor devices, as Fabry-Perot interferometers [27], Hanbury-Brown-Twiss [28] and Hong-Ou-Mandel interferometers [29], thus validating the Integer Quantum Hall regime as an ideal framework to implement solid-state quantum logic gates [30].

Our MZI is schematically depicted in Figure 4. To simplify the discussion, as done along the whole paper, only one degree of freedom (one qubit) is considered for the unmodified quantum device. The generalization of the present protocol to a realistic quantum computing gate with more qubits, is explained in Appendix A. We consider that a contact or reservoir (as elaborated in Appendix B) is connected to the source contact (S1) in Figure 4a filling only one Landau level and all injected electrons have the same wave function $|0\rangle$, but displaced in time by the distance $\tau_{in} v_x$, as depicted in Figure 4b. At this point, we have not yet constructed the superposition of states to get our initial qubit. In our device setup, a potential dip or a quantum point contact acts as a half-reflecting beam splitter by randomly scattering the electron in one of the two available edge channels [31–33] so that the description of the quantum electron in the central region of our MZI is given by the quantum bit $a|0\rangle + b|1\rangle$. This conclude the first step of the preparation of the quantum state. Then, a tunable potential mesa generated by top gates further separates the two quantum rails, so that the traveling electron accumulates a different phase according to its path [34] as shown in Figure 4a. The two electron beams are then recollected at the second beam splitter to produce the electron interference which is the second step in a quantum device for the (unitary) manipulation of our initial quantum logical information. The final step is the measuring of the observable associated with the final qubit $a'|0\rangle + b'|1\rangle$ by the detectors $D1$ and $D2$ in Figure 4. As in the case of the RTD, typically the electrical current (which is proportional to the transmission probability from source $i = 1$ to detector $j = 1, 2$) is used to indirectly identify the final qubit [35].

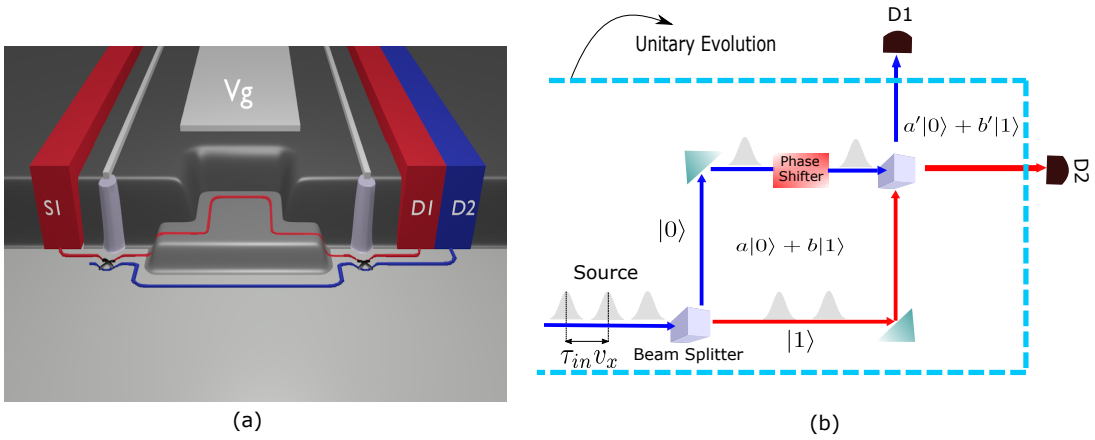

Figure 4. (**a**) 3D view of the potential landscape felt by the electrons in the MZI at bulk filling factor 2 in the Integer Quantum Hall regime, in presence of a perpendicular magnetic field [34]. Electrons are injected in the first edge channel by the source S_1, and collected at the end of the device by the drain $D_1(D_2)$. The paths of the electrons in the interferometer is defined by the red (blue) line for the first (second) Landau level. (**b**) Schematic diagram and functioning of the MZI. Electron injection with non-interacting and non-overlapping wavepackets is shown in gray, while the region encapsulated by the cyan color dashed line box defines the region where the unitary evolution of the quantum states is preserved.

The magnetically dependent transmission probability $T_{21}(B)$ for an electron in the input channel S1 to be detected at D2 can be analytically computed by means of a simplified 1D model based on the scattering matrix approach, as in Ref. [34] and reads:

$$T_{21}(B) = 2T(1-T)(1+\cos(\Phi)), \tag{13}$$

where T is the transmission coefficient of the single beam splitter and Φ is the total phase difference accumulated in the MZI:

$$\Phi = \frac{qB\mathcal{A}}{\hbar} + \varphi. \tag{14}$$

Aharonov-Bohm oscillations in the transmission amplitude [36] are then driven by a variation of the magnetic field B or the loop area $\mathcal{A}$, affecting the phase Φ. This platform can be used to implement other electron interferometry schemes for single electrons, e.g., Fabry-Perot geometries [27], or two interacting electrons [31,37,38]. Let us notice that the consideration of more qubits in the unmodified quantum device will just require occupying different Landau levels, but the basic understanding of how the uncertainty in the measurement can be controlled will not be modified by the presence of more qubits.

4.1. Implementation of Condition 1 and Condition 2

As with Section 3, here too we ensure that our modified quantum device satisfies the conditions mentioned in Section 2.2. Here **condition 1** can be obtained with a different strategy than the one used for the RTD since electrons are entering in the MZI one by one (as in a quantum wire). The strategy is enlarging the length L of the arms of the active region of the device (between $S1$ and $D1, D2$) to increase the number of simultaneous single particle wave packets that fit inside the device. We argue in the Appendix B that a *natural* way in the injection of electrons from the contacts in the device is at time intervals τ_{in}, as defined in Equation (A8) in Appendix B. Neglecting the thermal noise of the contacts the spatial separation between electrons is therefore given by $\tau_{in} v_x$ as plotted in Figure 4. Notice that such spatial separation ensures that the consideration of non-interacting electrons required in Equation (1) is more accurate for our modified MZI than for the RTD mentioned before.

As indicated in Appendix C, the consideration of metallic contacts with a lateral area A satisfying $\sqrt{A} \gg L$ is necessary condition to be able to successfully use Equation (7) in the computation of the experimental current. Notice that enlarging the lateral area A does not imply an increment of the number N of electrons here since electrons can only enter inside the device, one by one, in the 1D edge channels. Besides this **condition 2** can again be obtained by post-processing the experimental current I_{exp} as indicated in Section 3, by fixing the total time T that we allow the electrons to enter inside the enlarged active device region, $N = T/\tau_{in}$.

4.2. Numerical Results

To prove the discussions in the previous sections numerically we implemented the Mach-Zehnder like behaviour in the simulations. We were able to attain the Aharonov-Bohm oscillations where the maximum and the minimum value of the current obtained in one of the drains of the MZI oscillates with the change in the magnetic field (see Figure 5a). These oscillations are a signature of the correct working of our simulations. As expected, we observe that the instantaneous current $I_T(t)$ computed in the quantum device with a large number of electrons is much less noisy than the ones with fewer electrons, as plotted in Figure 5b. The noise in the current value due to fewer electrons results in very high fluctuations in the instantaneous value (black line in Figure 5b) which forces the experimenter to record the values in several experiments to finally get an ensemble value which is non-fluctuating. However, with the successful application of our protocol the fluctuation of the instantaneous value of the current almost disappears (cyan line in Figure 5b) as a result one needs to make just one measurement to get the correct value of the current. The final step of this protocol is determining the value of N which as discussed above can be given by $N = T/\tau_{in}$.

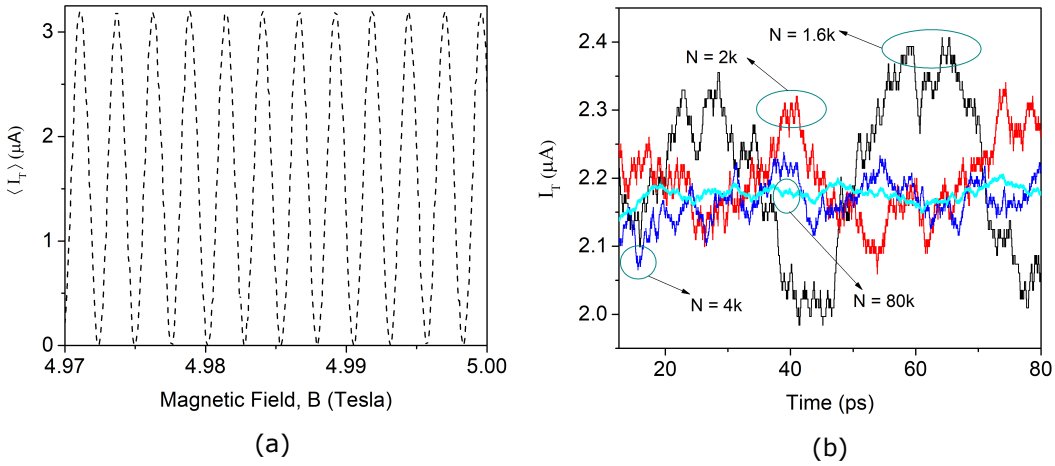

Figure 5. (**a**) The Aharonov-Bohm oscillations of the mean current resulting due to the interference of the wavepackets at the output of the Detector 2 oscillating between the maximum and minimum limit of the mean current. (**b**) The instantaneous current normalized to the number of particles is plotted at the output of the detector 2 of the MZI with respect to the simulation time, for different number of electrons N. As expected, the noise in the current reduces with the increase in the number of transport electrons due to the elimination of quantum uncertainty demonstrating the successful implementation of the protocol discussed in the text.

5. Conclusions

The measured current associated with a quantum device with few electrons has a quantum uncertainty due to the intrinsic stochastic process of the quantum measurement of the electrical current. From an engineering point of view, this quantum uncertainty becomes an undesired quantum noise that makes the discrimination of the final state in classical or quantum gates more difficult. To avoid the quantum uncertainty in the evaluation of the output value, one usually repeats the measurement at different time (using ergodic arguments) to compute a time-averaged value free from uncertainties. We have presented in this paper a new protocol that modifies the original quantum electron device to accommodate a larger number of electrons inside, so that the total electrical current of the modified device (when normalized to the number of electrons inside) gives the value of the output current without quantum uncertainty. We provide numerical examples for classical and quantum computing, with an RTD and MZI, respectively. We demonstrate that the many-particle wave function associated with the modified device is, in fact, an eigenstate of the many-particle electrical current operator. The similitude and differences of our protocol with the collective measurements is mentioned in the text. The results of our protocol can be alternatively understood as a consequence of the central limit theorem (see Appendix E). Although the assumption of non-interacting quasi-particles can seem reasonable in nanoscale electron devices, further work is needed to check whether or not the presence of strong Coulomb and exchange correlations among electrons located inside the device can affect the present predictions. In addition, the discussion on the advantages of the protocol presented here needs to be explored for the quantum measurements of transient currents and delay time of classical and quantum gates.

Author Contributions: Conceptualization, D.P., L.B., M.V., G.A., P.B., A.B. and X.O.; Formal analysis, D.P., L.B., M.V., G.A., P.B., A.B. and X.O.; Investigation, D.P., L.B., M.V., G.A., P.B., A.B. and X.O.; Methodology, D.P., L.B., G.A., P.B., A.B. and X.O.; Software, D.P., L.B., M.V., G.A., P.B., A.B. and X.O.; Supervision, G.A. and X.O.; Validation, D.P., L.B., M.V., G.A., P.B., A.B. and X.O.; Visualization, D.P., L.B., M.V. and X.O.; Writing—original draft, D.P., L.B., M.V., G.A., P.B., A.B. and X.O.; Writing—review and editing, D.P., L.B., M.V., G.A., P.B., A.B. and X.O.

Acknowledgments: The authors acknowledge funding from Fondo Europeo de Desarrollo Regional (FEDER), the "Ministerio de Ciencia e Innovación" through the Spanish Project TEC2015-67462-C2-1-R, the European Union's Horizon 2020 research and innovation programme under grant agreement No Graphene Core2 785219 and under the Marie Skłodowska-Curie grant agreement No 765426 (TeraApps), and the EC Research Innovation Action under the H2020 for the Project HPC-EUROPA3 (INFRAIA-2016-1-730897), together with the support provided by Barcelona Supercomputing Center (project HPC17D8XLY).

Conflicts of Interest: The authors declare no conflict of interest.The funders had no role in the design of the study; in the collection, analyses, or interpretation of data; in the writing of the manuscript, or in the decision to publish the results'.

Appendix A. Generalization to an Unmodified Quantum Device with Many Electrons

In the text, to simplify the notation and the discussion of our protocol, we have assumed that the unmodified (original) quantum device has only one electron in the active region.This assumption is obviously unrealistic in many scenarios for either classical or quantum computing. For example, in quantum computing, we need a nanoscale devices with, at least, the number of electrons equal to the number of qubits we want to deal with. We show in this appendix that the very same protocol described in the text for one electron can be straightforwardly generalized to deal with an unmodified (original) quantum device with many electrons present in the active region of the nanoscale device.

We consider an unmodified (original) quantum device with M electrons in the active region. To simplify the discussion, we will write the quantum state in the position representation. Then, each electron is described by the degree of freedom x_j with $j = 1, 2, ..., M$. Such quantum system is described by the M-particle wave function:

$$\psi(x_1, x_2, ..., x_M, t_{in}) \tag{A1}$$

Notice that we do not assume any particular shape of this M-particle wave function so that exchange and Coulomb interaction among the M electrons is taken into account in the definition of this M-particle system (without any restriction).

Now, we consider N set of M electrons which are prepared under the same conditions as the ones in Equation (A1). In other words, the quantum dynamics of each set of these M electrons can be described by the same wave function in Equation (A1). Thus, we define $N \times M$ degrees of freedom for the modified quantum device as x_j^i with $i = 1, 2, ..., N$ counting the repetitions and $j = 1, 2, ..., M$ counting the number of electrons in each repetition. We define N wave function identical to Equation (A1), but with a superindex $i = 1, 2, ..., N$ indicating which is the repetition we are dealing with:

$$\psi^i(x_1^i, x_2^i, ..., x_M^i, t_{in}) \tag{A2}$$

Introducing the wave function in Equation (A2) into the quantum state of the modified quantum device written in Equation (1), in the position representation, we have:

$$\Psi_T(x_1^1, ...x_M^N, t_{in}) = \psi^1(x_1^1, ..., x_M^1, t_{in}) \cdot \psi^2(x_1^2, ..., x_M^2, t_{in}) \cdot .... \cdot \psi^N(x_1^N, ..., x_M^N, t_{in}) \tag{A3}$$

Clearly, we have assumed in our definition of $\Psi_T(x_1^1, ...x_M^N, t_{in})$ in Equation (A3) that there is no Coulomb or exchange interaction between the subset of electrons $\{x_1^k, ..., x_M^k\}$ (for a treatment of the effect of exchange interaction see Appendix D) and the subset of electrons $\{x_1^l, ..., x_M^l\}$ for any $j \neq k$, but no restriction is imposed on the interaction among the M electrons of each subset. The rest of the demonstration till the final result in Equation (6) with $\sigma_{I_T}^2 = 0$ are basically the same that we wrote in Equations (3)–(5) for the evaluation of mean values.

A relevant point in our discussion is that even with our best technological means to exactly reproduce the same wave function in Equation (A1) with another set of M electrons, the quantum dynamics of these new set of electrons is not exactly identical to the previous one because of the inherent quantum uncertainty. The key element in our demonstration is that all these N different uncertainties of the set of M electrons have to follow an identical probability distribution given by the same wave function ψ in Equation (A1).

We notice that we have discussed in this appendix that if a system of $N \times M$ electrons are described by Equation (A3) (what we call **condition 1** in the text) and if we use a (center-of-mass-type) operator in Equation (2) (what we called **condition 2** in the text), then, the uncertainty in the measurement disappears in the $\lim N \to \infty$. A different question is how to ensure that a modified quantum device is effectively described by Equation (A3) and the measurement by the operator in Equation (2). This last point is what we discussed in detail in the implementations of our protocol with a RTD and a MZI in the text.

Finally, let us notice that the results in this appendix can be understood in a quite different way. It can be used to justify that some amount of Coulomb interaction (between nearest neighbors) can be accepted between the different N subsets. Let us consider again an unmodified system with only one electron described by the wave function $\psi(x_1, t_{in})$. Let us consider that some of the electrons of the N subsets (not all) do have interaction among them. We define M as the number of electrons that have interaction among them (for example we can consider two-electron interaction, but neglect three-electron interaction). Then, the wave function that define these interacting electrons is $\psi^i(x_1^i, x_2^i, ..., x_M^i, t_{in})$. If we assume that the (normalized to the number of electrons) probability distribution of the electrical current assigned to $\psi^i(x_1^i, x_2^i, ..., x_M^i, t_{in})$ is not much different than the probability distribution of the electrical current assigned to $\psi(x_1, t_{in})$, then, the demonstration in this appendix can be used to justify that our protocol can be reasonably valid when some interaction is accepted between nearest neighbors $\{x_1^k, ..., x_M^k\}$ and $\{x_1^l, ..., x_M^l\}$.

Appendix B. The Injection Time

The phase space density of electrons in a reservoir can be anticipated by assuming that each degree of freedom of an electron needs a phase space area equal to 2π, which is usually derived by using the single particle wavefunction of electrons as the Bloch states and then introducing the Born-von Karman boundary conditions. The interpretation of this result for two wave packets with spatial dispersion σ_x and wave vector dispersion $\sigma_k = 1/\sigma_x$, center positions x_{01} and x_{02}, and center wave packets k_{01} and k_{02} is simple. When they are far away from each other in the phase space, i.e., $|x_{o1} - x_{o2}| >> \sigma_x$ or $|k_{o1} - k_{o2}| >> \sigma_k$, the norm of the two-electron wave function is equal to the unity. However, when the wave packets are approaching each other, the probability decreases. In particular, for $x_{o1} = x_{o2}$ and $k_{o1} = k_{o2}$, we get $\psi_1(x) = \psi_2(x)$ and $\Phi(x_1, x_2) = \psi_1(x_1)\psi_1(x_2) - \psi_1(x_2)\psi_1(x_1) = 0$. This is the time-dependent wave packet version of the Pauli exclusion principle (or exchange interaction) mentioned for time-independent Hamiltonian eigenstates.

For example, for electrons in a 2D space (with the position $\vec{r} = \{x, y\}$ and wave vector $\vec{k} = \{k_x, k_y\}$), we consider a volume of the phase space equal to $\Delta x \Delta z \Delta k_x \Delta k_z$, with the degrees of freedom $\{x_0, z_0, k_x, k_z\}$ satisfying $x_0 < x < x_0 + \Delta x$, $z_0 < z < z_0 + \Delta z$, $k_{x0} < k_x < k_{x0} + \Delta k_x$ and $k_{z0} < k_z < k_{z0} + \Delta k_z$. The total number of electrons in this phase space cell taking into account the properties of a fermion are,

$$n_p = \frac{\Delta x \Delta z \Delta k_x \Delta k_z}{(2\pi)^2}, \tag{A4}$$

where $(2\pi)^2$ is the volume occupied by a single electron in the 2D phase space. Then, the time of injection of an electrons in the x direction from this volume of the phase space will be given by:

$$\tau_{in} = \frac{\Delta x}{v_x n_p} = (2\pi)^2 \frac{1}{v_x \Delta z \Delta k_x \Delta k_z}, \tag{A5}$$

where v_x is the electron velocity in the phase space volume. It can be demonstrated [39] that interpretation of Δx and Δk_x in terms of the wave packets mentioned above implies:

$$\Delta x = \sigma_x \sqrt{2\pi}, \tag{A6}$$

$$\Delta k_x = \sigma_k \sqrt{2\pi}. \tag{A7}$$

We notice that the condition $\sigma_x \cdot \sigma_k = 1$ implies the desired condition $\Delta x \cdot \Delta k_x = 2\pi$. Then, the injection time in Equation (A5) is just:

$$\tau_{in} = \frac{\sigma_x}{v_x}, \tag{A8}$$

which only depends on the properties of the reservoir.

Appendix C. Description of the Current Signal and Condition 2

We discuss here which are the necessary considerations to design the modified (new) quantum device that allows us to assume that all electrons inside it have identical simultaneous contribution to the total current I_T.

The first step is identifying the proper single particle operator $\hat{I}^1$. Then, once we identify $\hat{I}^1$, we can compute the eigenstates $|\psi^1(t_{in})\rangle$ and the eigenvalues I^1 that will correspond to the measured output results. However, identifying the electrical current operator is not so simple for several reasons. First, the measured current in an ammeter at time t_{in} is not just the particle current, defined as the number of particles crossing a particular surface of the device, but it also includes the displacement current. The latter component of the electrical current is proportional to the time-dependent variations of the electric field on a particular surface of the device. Typically, such component is not relevant at low frequencies, but at larger frequencies no instantaneous current conservation at time t_{in} can be guaranteed without it. What is the operator associated with the measurement of the total, particle plus displacement, current? The answer is not trivial at all. In fact, the measurement of the electrical current in quantum electron devices has an additional difficulty. The measurement of the electrical current corresponds to a generalized or weak measurement, which are mathematically described by a POVM. So, the proper question is even more complicated now: What is the POVM associated with the measurement of the total, particle plus displacement, current ?

Fortunately, we can describe the measurement of the total electrical current in a quantum electron device without having to anticipate the POVM. We will use in this appendix an explanation of the measurement process of the total electrical current using the Bohmian quantum theory. Such theory is formally equivalent to the orthodox quantum theory, it gives the same empirical results, but it does not require to identify *a priori* the measurement operator. Such theory defines a quantum system assigned to one electron by the orthodox wave function $\psi^1(\vec{r},t)$ plus a quantum trajectory $\vec{r}^1(t) = \{x^1(t), y^1(t), z^1(t)\}$ constructed from a velocity field given by the wave function itself. Such trajectory allows the definition of the properties of a quantum system, like the instantaneous electrical current $I^1(t)$, independently of the fact of being measured or not. An identically prepared state for a second experiment will be described by the same wave function $\psi^2(\vec{r},t) = \psi^1(\vec{r},t)$, but with a different trajectory $\vec{r}^2(t) = \{x^2(t), y^2(t), z^2(t)\}$. The quantum uncertainty in the output value of the electrical current is due to the different initial positions of the trajectories, which describe an ensemble of identical experiments. The selection of the initial positions of the i-th trajectories is selected according to the quantum equilibrium [40].

According to the Bohmian theory, for the electron with trajectory $\vec{r}^1(t) = \{x^1(t), y^1(t), z^1(t)\}$ and velocity $\vec{v}^1(t) = \{v_x^1(t), v_y^1(t), v_z^1(t)\}$, the electrical (particle plus displacement) current $I^1(t)$ generated in a surface of the quantum device is given by the Ramo-Shockley-Pellegrini theorem [41]. If we assume that each dimension of the lateral contact area A of the quantum device is much larger than the length L between contacts (from source to drain), i.e., $\sqrt{A} \gg L$, and this contacts are ideal metals (with an instantaneous screening time), then the total current generated by an electron crossing the device between the metals is given by the expression:

$$I^1(t) = q\frac{v_x^1(t)}{L}[\Theta(t - t_{in}^1)\Theta(t_{out}^1 - t)], \tag{A9}$$

where $\Theta(t)$ is the Heaviside function representing the time dependence of the single electron current pulse with t_{in}^1 and $t_{out}^1 = t_{in}^1 + t_r$ being the entering and leaving times, respectively, and t_r is the

electron transit time. The pulse starts when the electron enters the device and ends when the electron leaves it. We notice that the integration in time of Equation (A9), during the time interval L/v_x, gives the fundamental electron charge $\int_{t_{in}^1}^{t_{out}^1} I(t)dt = q$.

As discussed in the Appendix B, we do not have a perfect control on the preparation of the electrons leaving the contacts and entering inside the device but, assuming the contact to be in (quasi) thermodynamic equilibrium we can anticipate the energy distribution of the injected electrons (Fermi-Dirac distribution) and the interval time between consecutive injection of electrons. The total (particle plus displacement) instantaneous current I_{exp} of the device is then given by:

$$I_{exp}(t) = \sum_{i=1}^{N(t)} I^i(t) = \sum_{i=1}^{N(t)} q\frac{v_x^i(t)}{L}, \tag{A10}$$

where $N(t)$ is the number of electrons inside the device at time t. Expression (A10) has the desired property that the current due to all electrons inside the device is just the sum of currents due to individual electrons. Notice, however, that I_{exp} in terms of Bohmian currents is not exactly equal to the I_T defined in Equation (2) reinterpreted in terms of Bohmian currents, because a factor N in the denominator of Equation (2) is missing in Equation (A10).

Finally, we emphasize that the Bohmian trajectories have been introduced in this last part just to simplify our practical discussion about the measurement of the total (particle plus displacement) current in quantum electron devices, but it has no fundamental role in the demonstration of the proposed protocol. In other words, the validity of the main result in Equation (6) can be equivalently demonstrated with orthodox quantum mechanics (as we have done) or with Bohmian quantum mechanics. The knowledge that we gain from the Bohmian development done here is that the total (particle plus displacement) current measured in experiments do satisfy the required superposition of currents associated with individual electrons and that a factor $N(t)$ has to be added into the experimentally measured current of the modified quantum device I_{exp} to properly define I_T as $I_T(t) = \frac{I_{exp}(t)}{N(t)}$ where two proper ways of computing $N(t)$ are explained in the RTD and MZI applications mentioned in th text.

Appendix C.1. On the Assumption of a Large Lateral Area in the Active Region

The size of the lateral area A is a very important point in our protocol since we want that each electron inside the device active region contribute to the measured electrical current. If the electrical current were only due to the particle (conduction) current component, then, only the electrons crossing the drain (or source) surface, would have contributed to the current. However, it is well known that the electrical current is due to both particle and displacement currents. In fact, an electron far from the drain surface can still affect the current if its dynamics generates a significant perturbation in the electric field. If the lateral area is large compared to the longitudinal ones i.e., $\sqrt{A} \gg L$, then, effectively all electrons inside the active device region can contribute to the measured current, as required by the operator in Equation (2). The formal derivation of this issue is presented in Ref. [8]. Thus, the large lateral area is an important point of our protocol.

Only when $L \ll W, H$, then, one can ensure that all electrons are equally contributing (through the displacement current) to the total current and hence condition 2 in the main text is satisfied.

Appendix C.2. On the Assumption of an Instantaneous Screening Time in the Metallic Contacts

Next we discuss the motivation behind approximating the screening time in the metalic contacts to be instantaneous. The fact that we assume a screening time in the contacts (metals) much smaller than in the active region is something usual in electron semiconductor devices. Typically, the screening time in metals is considered to be negligible in comparison with the screening time in a semiconductor. The implications of this condition is that we do not need to simulate the electrons deep inside

the source/drain contact (without entering in the device) generating displacement current in the drain (or source) contact. This is possible only if we assume the screening time in the metals to be (almost) instantaneous.

Appendix D. Effects of Exchange Symmetry on the Total Current Many Body Operator

In the text, we have assumed that the many-particle wave function in Equation (1) has no exchange symmetry. Here, we discuss the physical soundness of such approximation. Let us evaluate the effects of exchange symmetry on the squared total current of Equation (2) for two particle case, which can be rewritten as:

$$\langle \hat{I}_T^2 \rangle = \frac{1}{4}\sum_{i=1}^{2}\langle I_i I_i\rangle + \frac{1}{4}\sum_{i=1,j\neq i}^{2}\langle I_i I_j\rangle, \tag{A11}$$

where indexes i, j refers to the particle with coordinate x^i in the phase space. We assume the system wave function described by the two-fermion state with exchange symmetry

$$\Psi(x_1, x_2) = \frac{1}{\sqrt{2}}(\psi^1(x^1)\psi^2(x^2) - \psi^2(x^1)\psi^1(x^2)), \tag{A12}$$

where the superindex k of the state ψ^k refers to the injection time (e.g., ψ^1 is injected at t_{in}, while ψ^2 is injected at $t_{in} + \tau_{in}$). Within this definition of the state, the diagonal average values of the first value in Equation (A11) read:

$$\begin{aligned}\langle I^1 I^1\rangle &= \frac{1}{4}(\langle\psi^1|(I^1)^2|\psi^1\rangle\langle\psi^2|\psi^2\rangle + \langle\psi^2|\psi^2\rangle\langle\psi^1|(I^1)^2|\psi^1\rangle \\ &- \langle\psi^1|(I^1)^2|\psi^2\rangle\langle\psi^2|\psi^1\rangle - \langle\psi^2|(I^1)^2|\psi^1\rangle\langle\psi^1|\psi^2\rangle),\end{aligned} \tag{A13}$$

for $i = 1, 2$. We reasonably assume an initial negligible overlap of the wave packets,

$$\langle\psi^\alpha|\psi^\beta\rangle \approx \delta_{\alpha,\beta}, \tag{A14}$$

which is conserved during the evolution of the two electrons, carrying out the same procedure for the second diagonal element we get:

$$\langle I^1 I^1\rangle + \langle I^2 I^2\rangle = \frac{1}{2}(\langle\psi^1|(I^1)^2|\psi^1\rangle + \langle\psi^2|(I^2)^2|\psi^1\rangle), \tag{A15}$$

as for distinguishable particles. Similarly, the first non-diagonal term of Equation (A11) is computed:

$$\begin{aligned}\langle I^1 I^2\rangle &= \frac{1}{4}(\langle\psi^1|I^1|\psi^1\rangle\langle\psi^2|I^2|\psi^2\rangle + \langle\psi^2|I^1|\psi^2\rangle\langle\psi^1|I^2|\psi^1\rangle \\ &- \langle\psi^1|I^1|\psi^2\rangle\langle\psi^2|I^2|\psi^1\rangle - \langle\psi^2|I^1|\psi^1\rangle\langle\psi^1|I^2|\psi^2\rangle),\end{aligned} \tag{A16}$$

Computing the same for the second non-diagonal element we get,

$$\langle I^1 I^2\rangle + \langle I^2 I^1\rangle = \frac{1}{2}\langle\psi^1|I^1|\psi^1\rangle\langle\psi^2|I^2|\psi^2\rangle. \tag{A17}$$

So using Equations (A15) and (A17) in Equation (A11) we get,

$$\begin{aligned}\langle \hat{I}_T^2\rangle &= \frac{1}{4}\sum_{i=1}^{2}\langle I_i I_i\rangle + \frac{1}{4}\sum_{i=1,j\neq i}^{2}\langle I_i I_j\rangle \\ &= \frac{1}{4}\sum_{i=1}^{2}(\langle\psi^i|(I^i)^2|\psi^i\rangle + \frac{1}{4}\sum_{i=1,j\neq i}^{2}\langle\psi^i|I^i|\psi^i\rangle\langle\psi^j|I^j|\psi^j\rangle,\end{aligned} \tag{A18}$$

The mean value of the squared of the total current for distinguishable particles is therefore recovered by assuming $\langle \psi^i | I | \psi^j \rangle \approx \delta_{i,j}$. This constraint is fulfilled by Equation (A14), together with the definition of the current operator, which is related to momentum (proportional to a spatial derivative in the real space) and position operators. Indeed, we expect that for a weak measurement of the current discussed in the text, the state $|\psi^j\rangle'$ produced by its application to a wave packet ($|\psi^j\rangle' = I|\psi^j\rangle$) is characterized by a spatial localization that does not significantly differ from the unperturbed state $|\psi^j\rangle$, so that $\langle \psi^i | I | \psi^j \rangle \approx 0$ is valid.

Appendix E. The Ontological Meaning of the Total Measured Current $\hat{I}_T$ and the Classical Central Limit Theorem

We discuss here a simple interpretation of the main result given in Section 2.2. The ammeter mentioned in the text does only measure the value of the total current $\hat{I}_T$. Therefore, strictly speaking, the currents $\hat{\mathcal{I}}^1$, $\hat{\mathcal{I}}^2$, etc. contributed by the single electrons, have not been measured, so the electrons have no (orthodox) definite value of their current. We are invoking here the well known eigenvalue-eigenstate link. The i-th electron has a well-defined value of the current when its wavefunction is an eigenstate of the single particle current operator $\hat{\mathcal{I}}^i$. However as explained in Section 2.1, the single particle state describing the i-th electron is not a current eigenstate. Therefore there is no orthodox value for the current assigned to the i-th electron.

In any case, let us assume that we can assign (unmeasured) values of the current of each electron (for $i = 1, .., N$) at any time (The physical correctness of this assumption will be provided below). Thus, the definition of the total current in Equation (2) in terms of operators can be translated into an expression in terms of variables which takes well-defined values:

$$I_T = \frac{\mathcal{I}^1 + \mathcal{I}^2 + ... + \mathcal{I}^N}{N}, \tag{A19}$$

We eliminate the "hat" in Equation (A19) to clarify that now $\mathcal{I}^i$ is not an operator, but a variable. Then, assuming again the independence among the variables $\mathcal{I}^i$ and that the total current can be given by the above sum, the simple application of the classical central limit theorem will be enough to certify that the variance of I_T goes to zero when N is large enough.

However, the reader can argue that such simple understanding is not appropriate because, as we emphasized at the beginning of this appendix, the current of each electron has no well-defined value. Such values are not measured by the ammeter and, strictly speaking, the values associated with the current operators $\hat{\mathcal{I}}^1$, $\hat{\mathcal{I}}^2$ are undefined in the orthodox theory.

In any case, the simple understanding based on the central limit theorem, can be invoked by using a quantum theory with a definition of the reality of the properties of electrons independent of the measurement process. This understanding is supported for example from modal interpretation of the quantum world where the reality of some properties of electrons (like its electrical current) has a well-defined value independently of the fact that they are measured or not. This understanding is consistent with our paper where the Bohmian theory [40], which is the most famous modal interpretation today, is invoked for the computation of the currents. At the end of the day, the discussion about the (hidden) reality of the values of the current of each electron are not relevant for the empirical results presented along the work. Bohmian and orthodox theories are empirically equivalent for all known experiments. The above discussion provides a simple and intuitive understanding of the physical soundness of providing a many-body quantum state in Equation (1) with no quantum uncertainty.

References

1. Le, H.Q.; Van Norstrand, J.A.; Thompto, B.W.; Moreira, J.E.; Nguyen, D.Q.; Hrusecky, D.; Kroener, M. IBM POWER9 processor core. *IBM J. Res. Dev.* **2018**, *62*, 2:1–2:12. [CrossRef]
2. Cory, C.D.; Datta, S. Nanoscale transistors—Just around the gate? *Science* **2013**, *341*, 140–141.

3. Nielsen, M.A.; Chuang, I.L. Quantum computation. In *Quantum Information*; Cambridge University Press: Cambridge, UK, 2000.
4. Boixo, S.; Isakov, S.V.; Smelyanskiy, V.N.; Babbush, R.; Ding, N.; Jiang, Z.; Neven, H. Characterizing quantum supremacy in near-term devices. *Nat. Phys.* **2018**, *14*, 595. [CrossRef]
5. Classical and quantum computers are vying for superiority. *Nature* **2018**, *564*, 302. [CrossRef] [PubMed]
6. Tang, A.E. Quantum-inspired classical algorithm for recommendation systems. *arXiv* **2018**, arXiv:1807.04271.
7. Deutsch, D. Uncertainty in quantum measurements. *Phys. Rev. Lett.* **1983**, *50*, 631. [CrossRef]
8. Marian, D.; Zanghì, N.; Oriols, X. Weak values from displacement currents in multiterminal electron devices. *Phys. Rev. Lett.* **2016**, *116*, 110404. [CrossRef] [PubMed]
9. Zhan, Z.; Kuang, X.; Colomés, E.; Pandey, D.; Yuam, S.; Oriols, X. Time-dependent quantum Monte Carlo simulation of electron devices with two-dimensional Dirac materials: A genuine terahertz signature for graphene. *Phys. Rev. B* **2019**, *99*, 155412. [CrossRef]
10. Oriols, X.; Benseny, A. Conditions for the classicality of the center of mass of many-particle quantum states. *New J. Phys.* **2017**, *19*, 063031 . [CrossRef]
11. Lloyd, S.; Slotine, J.J.E. Quantum feedback with weak measurements. *Phys. Rev. A* **2000**, *62*, 012307. [CrossRef]
12. Hou, Z.; Tang, J.F.; Shang, J.; Zhu, H.; Li, J.; Yuan, Y.; Wu, K.D.; Xiang, G.Y.; Li, C.F.; Guo, G.C. Deterministic realization of collective measurements via photonic quantum walks. *Nat. Commun.* **2018**, *9*, 1414 [CrossRef] [PubMed]
13. Encomendero, J.; Faria, F.A.; Islam, S.M.; Protasenko, V.; Rouvimov, S.; Sensale-Rodriguez, B.; Xing, H.G. New tunneling features in polar III-nitride resonant tunneling diodes. *Phys. Rev. X* **2017**, *7*, 041017. [CrossRef]
14. Gaskell, J.; Eaves, L.; Novoselov, K.S.; Mishchenko, A.; Geim, A.K.; Fromhold, T.M.; Greenaway, M.T. Graphene-hexagonal boron nitride resonant tunneling diodes as high-frequency oscillators. *Appl. Phys. Lett.* **2015**, *107*, 103105. [CrossRef]
15. Avedillo, M.J.; Quintana, J.M.; Roldán, H.P. Increased Logic Functionality of Clocked Series-Connected RTDS. *IEEE Trans. Nanotechnol.* **2006**, *5*, 606–611. [CrossRef]
16. Park, J.; Lee, J.; Yang, K. A 24-GHz Low-Power RTD-Based ON-OFF Keying Oscillator with an RTD Pair Configuration. *IEEE Microwave Wirel. Comp. Lett.* **2018**, *28*, 521–523. [CrossRef]
17. Pandey, D.; Albareda, G.; Oriols, X. Measured and unmeasured properties of quantum systems. *arXiv* **2018**, arXiv:1812.10257.
18. Bertoni, A.; Bordone, P.; Brunetti, R.; Jacoboni, C.; Reggiani, S. Quantum Logic Gates based on Coherent Electron Transport in Quantum Wires. *Phys. Rev. Lett.* **2000**, *84*, 5912. [CrossRef] [PubMed]
19. Buscemi, F.; Bordone, P.; Bertoni, A. Carrier-carrier entanglement and transport resonances in semiconductor quantum dots. *Phys. Rev. B* **2007**, *76*, 195317. [CrossRef]
20. Buscemi, F.; Bordone, P.; Bertoni, A. Quantum teleportation of electrons in quantum wires with surface acoustic waves. *Phys. Rev. B* **2010**, *81*, 045312. [CrossRef]
21. Lanting, T.; Przybysz, A.J.; Smirnov, A.Y.; Spedalieri, F.M.; Amin, M.H.; Berkley, A.J.; Dickson, N. Entanglement in a Quantum Annealing Processor. *Phys. Rev. X* **2014**, *4*, 021041. [CrossRef]
22. Debnath, S.; Linke, N.M.; Figgatt, C.; Landsman, K.A.; Wright, K.; Monroe, C. Demonstration of a small programmable quantum computer with atomic qubits. *Nature* **2016**, *536*, 63–66. [CrossRef] [PubMed]
23. Büttiker, M. Absence of backscattering in the quantum Hall effect in multiprobe conductors. *Phys. Rev. B* **1988**, *38*, 9375. [CrossRef]
24. Roulleau, P.; Portier, F.; Roche, P.; Cavanna, A.; Faini, G.; Gennser, U.; Mailly, D. Direct Measurement of the Coherence Length of Edge States in the Integer Quantum Hall Regime. *Phys. Rev. Lett.* **2008**, *100*, 126802. [CrossRef] [PubMed]
25. Venturelli, D.; Giovannetti, V.; Taddei, F.; Fazio, R.; Feinberg, D.; Usaj, G.; Balseiro, C.A. Edge channel mixing induced by potential steps in an integer quantum Hall system. *Phys. Rev. B* **2011**, *83*, 075315. [CrossRef]
26. Beggi, A.; Bordone, P.; Buscemi, F.; Bertoni, A. Time-dependent simulation and analytical modelling of electronic Mach–Zehnder interferometry with edge-states wave packets. *J. Phys.: Condens. Matter* **2015**, *27*, 475301. [CrossRef] [PubMed]
27. Deviatov, E.V.; Lorke, A. Experimental realization of a Fabry-Perot-type interferometer by copropagating edge states in the quantum Hall regime. *Phys. Rev. B* **2008**, *77*, 161302. [CrossRef]

28. Neder, I.; Ofek, N.; Chung, Y.; Heiblum, M.; Mahalu, D.; Umansky, V. Interference between two indistinguishable electrons from independent sources. *Nature* **2007**, *448*, 333–337. [CrossRef]
29. Bocquillon, E.; Freulon, V.; Berroir, J.M.; Degiovanni, P.; Plaçais, B.; Cavanna, A.; Jin, Y.; Fève, G. Coherence and Indistinguishability of Single Electrons Emitted by Independent Sources. *Science* **2013**, *339*, 1054–1057. [CrossRef]
30. Weisz, E.; Choi, H.K.; Sivan, I.; Heiblum, M.; Gefen, Y.; Mahalu, D.; Umansky, V. An electronic quantum eraser. *Science* **2014**, *3444*, 1363–1366, 10.1126/science.1248459. [CrossRef]
31. Giovannetti, V.; Taddei, F.; Frustaglia, D.; Fazio, R. Multichannel architecture for electronic quantum Hall interferometry. *Phys. Rev. B* **2008**, *77*, 155320. [CrossRef]
32. Karmakar, B.; Venturelli, D.; Chirolli, L.; Giovannetti, V.; Fazio, R.; Roddaro, S.; Pellegrini, V. Nanoscale Mach-Zehnder interferometer with spin-resolved quantum Hall edge states. *Phys. Rev. B* **2015**, *92*, 195303. [CrossRef]
33. Bellentani, L.; Beggi, A.; Bordone, P.; Bertoni, A. Dynamics of copropagating edge states in a multichannel Mach-Zender interferometer. *J. Phys.: Conf. Ser.* **2017**, *906*, 012027. [CrossRef]
34. Bellentani, L.; Beggi, A.; Bordone, P.; Bertoni, A. Dynamics and Hall-edge-state mixing of localized electrons in a two-channel Mach-Zehnder interferometer. *Phys. Rev. B* **2018**, *97*, 205419. [CrossRef]
35. Ji, Y.; Chung, Y.; Sprinzak, D.; Heiblum, M.; Mahalu, D.; Shtrikman, H. An electronic Mach–Zehnder interferometer. *Nature* **2003**, *422*, 415. [CrossRef] [PubMed]
36. Bird, J.P.; Ishibashi, K.; Stopa, M., Aoyagi, Y.; Sugano, T. Coulomb blockade of the Aharonov-Bohm effect in GaAs/Al_x Ga_{1-x} As quantum dots. *Phys. Rev. B* **1994**, *50*, 14983–14990, 10.1103/PhysRevB.50.14983. [CrossRef]
37. Marian, D.; Colomés, E.; Oriols, X. Time-dependent exchange and tunneling: Detection at the same place of two electrons emitted simultaneously from different sources. *J. Phys.: Condens. Matter* **2015**, *27*, 245302. [CrossRef]
38. Bellentani, L.; Bordone, P.; Oriols, X.; Bertoni, A. Coulomb and exchange interaction effects on the exact two-electron dynamics in the Hong-Ou-Mandel interferometer based on Hall edge states. *arXiv* **2019**, arXiv:1903.02581.
39. Oriols, X. Non-universal conductance quantization for long quantum wires: The role of the exchange interaction. *Nanotechnology* **2004**, *15*, S167. [CrossRef]
40. Oriols, X.; Mompart, J. *Applied Bohmian Mechanics: From Nanoscale Systems to Cosmology*; CRC Press: Boca Raton, FL, USA, 2012.
41. Albareda, G.; Traversa, F.L.; Benali, A.; Oriols, X. Computation of quantum electrical currents through the Ramo–Shockley–Pellegrini theorem with trajectories. *Fluctuat. Noise Lett.* **2012**, *11*, 1242008 [CrossRef]

Bibliography

[1] nemo, (accessed November 8, 2020). https://engineering.purdue.edu/gekcogrp/software-projects/nemo3D/. 2

[2] nextnano, (accessed November 8, 2020). http://www.nextnano.de.

[3] tibercad, (accessed November 8, 2020). http://www.tibercad.org.

[4] nanocad, (accessed November 8, 2020). http://vides.nanotcad.com/vides/.

[5] transiesta, (accessed November 8, 2020). https://departments.icmab.es/leem/siesta/. 2

[6] Gianluca Fiori, Francesco Bonaccorso, Giuseppe Iannaccone, Tomás Palacios, Daniel Neumaier, Alan Seabaugh, Sanjay K Banerjee, and Luigi Colombo. Electronics based on two-dimensional materials. *Nature nanotechnology*, 9(10):768–779, 2014. 3

[7] Fengnian Xia, Vasili Perebeinos, Yu-ming Lin, Yanqing Wu, and Phaedon Avouris. The origins and limits of metal–graphene junction resistance. *Nature nanotechnology*, 6(3):179–184, 2011. 3

[8] Carlo Jacoboni and Lino Reggiani. The monte carlo method for the so-

lution of charge transport in semiconductors with applications to covalent materials. *Reviews of modern Physics*, 55(3):645, 1983. 3

[9] Simon Ramo. Currents induced by electron motion. *Proceedings of the IRE*, 27(9):584–585, 1939. 5, 44, 45

[10] William Shockley. Currents to conductors induced by a moving point charge. *Journal of applied physics*, 9(10):635–636, 1938. 5, 44, 45

[11] G Cavalleri, E Gatti, G Fabri, and V Svelto. Extension of ramo's theorem as applied to induced charge in semiconductor detectors. *Nuclear Instruments and Methods*, 92(1):137–140, 1971. 5

[12] Peter O Lauritzen. Noise due to generation and recombination of carriers in pn junction transition regions. *IEEE Transactions on Electron Devices*, 15(10):770–776, 1968.

[13] Bruno Pellegrini. Electric charge motion, induced current, energy balance, and noise. *Physical Review B*, 34(8):5921, 1986. 5, 45

[14] Travis Norsen. *Foundations of quantum mechanics*. Springer, 2017. 12, 97, 99

[15] Claude Cohen-Tannoudji, Bernard Diu, and Franck Laloë. *Claude Cohen-Tannoudji; Bernard Diu; Franck Laloë: Quantenmechanik*, volume 1. Walter de Gruyter, 2013. 99, 102

[16] Peter R Holland. *The quantum theory of motion: an account of the de Broglie-Bohm causal interpretation of quantum mechanics*. Cambridge university press, 1995. 12, 35, 39, 97

[17] Ramamurti Shankar. *Principles of quantum mechanics*. Springer Science & Business Media, 2012. 12

[18] Gian Carlo Ghirardi, Alberto Rimini, and Tullio Weber. A model for a unified quantum description of macroscopic and microscopic systems. In *Quantum Probability and Applications II*, pages 223–232. Springer, 1985. 12

[19] David Bohm. A suggested interpretation of the quantum theory in terms of" hidden" variables. i. *Physical review*, 85(2):166, 1952. 12, 13, 83

[20] Detlef Dürr, Sheldon Goldstein, Roderich Tumulka, and Nino Zanghi. Bohmian mechanics and quantum field theory. *Physical Review Letters*, 93(9):090402, 2004.

[21] Xavier Oriols Pladevall and Jordi Mompart. *Applied Bohmian mechanics: From nanoscale systems to cosmology*. CRC Press, 2019. 12, 13, 35, 39, 40, 55, 83, 114, 117, 122, 125

[22] Hugh Everett III. " relative state" formulation of quantum mechanics. *Reviews of modern physics*, 29(3):454, 1957. 12

[23] John S. Bell. *Speakable and Unspeakable in Quantum Mechanics*. Cambridge University Press, Cambridge, 1987. 13, 27, 28, 82

[24] J. S. Bell. Beables for quantum field theory. In Basil J. Hiley and D. Peat, editors, *Quantum Implications: Essays in Honour of David Bohm*, pages 227–234. Methuen, 1987.

[25] Travis Norsen. The theory of (exclusively) local beables. *Foundations of Physics*, 40(12):1858–1884, 2010. 13, 55

[26] Detlef Dürr, Sheldon Goldstein, and Nino Zanghì. *Quantum physics without quantum philosophy*. Springer Science & Business Media, 2012. 13, 83

[27] JOHN S. BELL. On the problem of hidden variables in quantum mechanics. *Rev. Mod. Phys.*, 38:447–452, Jul 1966. doi: 10.1103/RevModPhys.38.447. 13

[28] Simon Kochen and E. P. Specker. The problem of hidden variables in quantum mechanics. *Journal of Mathematics and Mechanics*, 17:59–87, 1967. 13

[29] H. D. Zeh. On the interpretation of measurement in quantum theory. *Foundations of Physics*, 1(1):69–76, Mar 1970. ISSN 1572-9516. doi: 10.1007/BF00708656. 14

[30] Tim Maudlin. Three measurement problems. *Topoi*, 14(1):7–15, Mar 1995. ISSN 1572-8749. doi: 10.1007/BF00763473. 14

[31] John Von Neumann. *Mathematical foundations of quantum mechanics: New edition*. Princeton university press, 2018. 14

[32] Heinz-Peter Breuer, Francesco Petruccione, et al. *The theory of open quantum systems*. Oxford University Press on Demand, 2002. 14

[33] John S Bell. Against" measurement" physics world, 1990. 25

[34] Paul Adrien Maurice Dirac. *The principles of quantum mechanics*. Number 27. Oxford university press, 1981. 26

[35] D Bohm. On interpretation of quantum mechanics on the basis of the" hidden" variable conception. *Phys. Rev*, 85(166):180, 1952. 28

[36] Harry JD Miller and Janet Anders. Time-reversal symmetric work distributions for closed quantum dynamics in the histories framework. *New Journal of Physics*, 19(6):062001, 2017.

[37] B Prasanna Venkatesh, Gentaro Watanabe, and Peter Talkner. Quantum fluctuation theorems and power measurements. *New Journal of Physics*, 17 (7):075018, aug 2015. doi: 10.1088/1367-2630/17/7/075018. 28

[38] Anthony J Leggett and Anupam Garg. Quantum mechanics versus macroscopic realism: Is the flux there when nobody looks? *Physical Review Letters*, 54(9):857, 1985. 28

[39] Clive Emary, Neill Lambert, and Franco Nori. Leggett–garg inequalities. *Reports on Progress in Physics*, 77(1):016001, 2013. 29

[40] Agustin Palacios-Laloy, François Mallet, François Nguyen, Patrice Bertet, Denis Vion, Daniel Esteve, and Alexander N Korotkov. Experimental violation of a bell's inequality in time with weak measurement. *Nature Physics*, 6(6):442, 2010. 29

[41] ME Goggin, MP Almeida, Marco Barbieri, BP Lanyon, JL O'brien, AG White, and GJ Pryde. Violation of the leggett–garg inequality with weak measurements of photons. *Proceedings of the National Academy of Sciences*, 108(4):1256–1261, 2011.

[42] George C Knee, Stephanie Simmons, Erik M Gauger, John JL Morton, Helge Riemann, Nikolai V Abrosimov, Peter Becker, Hans-Joachim Pohl, Kohei M Itoh, Mike LW Thewalt, et al. Violation of a leggett–garg inequality with ideal non-invasive measurements. *Nature communications*, 3:606, 2012. 29

[43] Fabio Benatti, GianCarlo Ghirardi, and Renata Grassi. On some recent proposals for testing macrorealism versus quantum mechanics. *Foundations of Physics Letters*, 7(2):105–126, 1994. 29

[44] Christopher Timpson and Owen Maroney. Quantum-vs. macro-realism: what does the leggett-garg inequality actually test? *The British Journal for the Philosophy of Science*, 2013. 29

[45] Eugene P Wigner. On the quantum correction for thermodynamic equilibrium. In *Part I: Physical Chemistry. Part II: Solid State Physics*, pages 110–120. Springer, 1997. 31

[46] Bas C van Fraassen. A modal interpretation of quantum mechanics. In *Current issues in quantum logic*, pages 229–258. Springer, 1981. 33

[47] Jeffrey Bub. Modal interpretations and bohmian mechanics. In *Bohmian Mechanics and Quantum Theory: An Appraisal*, pages 331–341. Springer, 1996. 33, 39

[48] Jeffrey Bub. *Interpreting the quantum world*. Cambridge University Press, 1999. 33

[49] Devashish Pandey, Xavier Oriols, and Guillermo Albareda. From micro-to macrorealism: addressing experimental clumsiness with semi-weak measurements. *New Journal of Physics*, 2020. 34

[50] Yakir Aharonov, David Z Albert, and Lev Vaidman. How the result of a measurement of a component of the spin of a spin-1/2 particle can turn out to be 100. *Physical review letters*, 60(14):1351, 1988. 36, 40, 43, 83

[51] Xavier Oriols and Jordi Mompart. Overview of bohmian mechanics. *arXiv preprint arXiv:1206.1084*, page 76, 2012. 38

[52] HM Wiseman. Grounding bohmian mechanics in weak values and bayesianism. *New Journal of Physics*, 9(6):165, 2007. 40, 47, 125

[53] A. Matzkin. Weak values from path integrals. *Phys. Rev. Research*, 2: 032048, Aug 2020. doi: 10.1103/PhysRevResearch.2.032048. URL `https://link.aps.org/doi/10.1103/PhysRevResearch.2.032048`. 40

[54] Detlef Dürr, Sheldon Goldstein, and Nino Zanghì. On the weak measurement of velocity in bohmian mechanics. *Journal of Statistical Physics*, 134 (5-6):1023–1032, 2009. 40

[55] Sacha Kocsis, Boris Braverman, Sylvain Ravets, Martin J Stevens, Richard P Mirin, L Krister Shalm, and Aephraim M Steinberg. Observing the average trajectories of single photons in a two-slit interferometer. *Science*, 332(6034):1170–1173, 2011. 40, 43

[56] Dylan H Mahler, Lee Rozema, Kent Fisher, Lydia Vermeyden, Kevin J Resch, Howard M Wiseman, and Aephraim Steinberg. Experimental nonlocal and surreal bohmian trajectories. *Science advances*, 2(2):e1501466, 2016.

[57] Ya Xiao, Yaron Kedem, Jin-Shi Xu, Chuan-Feng Li, and Guang-Can Guo. Experimental nonlocal steering of bohmian trajectories. *Optics Express*, 25 (13):14463–14472, 2017.

[58] Ya Xiao, Howard M Wiseman, Jin-Shi Xu, Yaron Kedem, Chuan-Feng Li, and Guang-Can Guo. Observing momentum disturbance in double-slit "which-way" measurements. *Science Advances*, 5(6):eaav9547, 2019.

[59] Lev Vaidman, Alon Ben-Israel, Jan Dziewior, Lukas Knips, Mira Weißl, Jasmin Meinecke, Christian Schwemmer, Ran Ber, and Harald Weinfurter. Weak value beyond conditional expectation value of the pointer readings. *Physical Review A*, 96(3):032114, 2017. 40

[60] Yakir Aharonov, Peter G Bergmann, and Joel L Lebowitz. Time symmetry in the quantum process of measurement. *Physical Review*, 134(6B):B1410, 1964. 42

[61] Yakir Aharonov and Lev Vaidman. Properties of a quantum system during the time interval between two measurements. *Physical Review A*, 41(1):11, 1990. 42

[62] Ramón Ramos, David Spierings, Isabelle Racicot, and Aephraim M Steinberg. Measurement of the time spent by a tunnelling atom within the barrier region. *Nature*, 583(7817):529–532, 2020. 43

[63] Ming-Cheng Chen, Chang Liu, Yi-Han Luo, He-Liang Huang, Bi-Ying Wang, Xi-Lin Wang, Li Li, Nai-Le Liu, Chao-Yang Lu, and Jian-Wei Pan. Experimental demonstration of quantum pigeonhole paradox. *Proceedings of the National Academy of Sciences*, 116(5):1549–1552, 2019.

[64] Tobias Denkmayr, Hermann Geppert, Stephan Sponar, Hartmut Lemmel, Alexandre Matzkin, Jeff Tollaksen, and Yuji Hasegawa. Observation of a quantum cheshire cat in a matter-wave interferometer experiment. *Nature communications*, 5(1):1–7, 2014.

[65] Justin Dressel, CJ Broadbent, JC Howell, and Andrew N Jordan. Experimental violation of two-party leggett-garg inequalities with semiweak measurements. *Physical review letters*, 106(4):040402, 2011.

[66] Jeff S Lundeen and Aephraim M Steinberg. Experimental joint weak measurement on a photon pair as a probe of hardy's paradox. *Physical review letters*, 102(2):020404, 2009.

[67] Yakir Aharonov, Alonso Botero, Sandu Popescu, Benni Reznik, and Jeff Tollaksen. Revisiting hardy's paradox: counterfactual statements, real mea-

surements, entanglement and weak values. *Physics Letters A*, 301(3-4): 130–138, 2002. 43

[68] Anthony J Leggett. Comment on "how the result of a measurement of a component of the spin of a spin-(1/2 particle can turn out to be 100". *Physical review letters*, 62(19):2325, 1989. 43

[69] IM Duck, Paul M Stevenson, and ECG Sudarshan. The sense in which a" weak measurement" of a spin-1/2 particle's spin component yields a value 100. *Physical Review D*, 40(6):2112, 1989.

[70] Xuanmin Zhu, Yuxiang Zhang, Shengshi Pang, Chang Qiao, Quanhui Liu, and Shengjun Wu. Quantum measurements with preselection and postselection. *Physical Review A*, 84(5):052111, 2011.

[71] Christopher Ferrie and Joshua Combes. How the result of a single coin toss can turn out to be 100 heads. *Physical review letters*, 113(12):120404, 2014.

[72] Aharon Brodutch. Comment on "how the result of a single coin toss can turn out to be 100 heads". *Physical Review Letters*, 114(11):118901, 2015.

[73] Fabrizio Piacentini, Alessio Avella, Enrico Rebufello, Rudi Lussana, Federica Villa, Alberto Tosi, Marco Gramegna, Giorgio Brida, Eliahu Cohen, Lev Vaidman, et al. Determining the quantum expectation value by measuring a single photon. *Nature Physics*, 13(12):1191–1194, 2017.

[74] Josiah Sinclair, David Spierings, Aharon Brodutch, and Aephraim M Steinberg. Interpreting weak value amplification with a toy realist model. *Physics Letters A*, 383(24):2839–2845, 2019. 43

[75] A Matzkin. Weak values and quantum properties. *Foundations of Physics*, 49(3):298–316, 2019. 43

[76] Zhen Zhan, Enrique Colomes, and Xavier Oriols. Limitations of the intrinsic cutoff frequency to correctly quantify the speed of nanoscale transistors. *IEEE Transactions on Electron Devices*, 64(6):2617–2624, 2017. 44, 124

[77] Zhen Zhan, Xueheng Kuang, Enrique Colomés, Devashish Pandey, Shengjun Yuan, and Xavier Oriols. Time-dependent quantum monte carlo simulation of electron devices with two-dimensional dirac materials: A genuine terahertz signature for graphene. *Physical Review B*, 99(15):155412, 2019. 44

[78] G. Alabreda, H. López, X. Cartoixà, J. Suñé, and X. Oriols. Time-dependent boundary conditions with lead-sample coulomb correlations: Application to classical and quantum nanoscale electron device simulators. *Phys. Rev. B*, 82:085301, Aug 2010. doi: 10.1103/PhysRevB.82.085301. URL `https://link.aps.org/doi/10.1103/PhysRevB.82.085301`. 47, 59

[79] G. Albareda, J. Suñé, and X. Oriols. Many-particle hamiltonian for systems with full coulomb interaction: Application to classical and quantum time-dependent simulations of nanoscale electron devices. *Phys. Rev. B*, 79: 075315, Feb 2009. doi: 10.1103/PhysRevB.79.075315. URL `https://link.aps.org/doi/10.1103/PhysRevB.79.075315`.

[80] D Marian, E Colomés, and X Oriols. Time-dependent exchange and tunneling: detection at the same place of two electrons emitted simultaneously from different sources. *Journal of Physics: Condensed Matter*, 27 (24):245302, 2015. URL `http://stacks.iop.org/0953-8984/27/i=24/a=245302`.

[81] Damiano Marian, Enrique Colomés, Zhen Zhan, and Xavier Oriols. Quantum noise from a bohmian perspective: fundamental understanding and practical computation in electron devices. *Journal of Computational Electronics*, 14(1):114–128, 2015.

[82] A Alarcón and X Oriols. Computation of quantum electron transport with local current conservation using quantum trajectories. *Journal of Statistical Mechanics: Theory and Experiment*, 2009(01):P01051, 2009.

[83] H. López, G. Albareda, X. Cartoixà, J. Suñé, and X. Oriols. Boundary conditions with pauli exclusion and charge neutrality: application to the monte carlo simulation of ballistic nanoscale devices. *Journal of Computational Electronics*, 7(3):213–216, Sep 2008. ISSN 1572-8137. doi: 10.1007/s10825-008-0193-7. URL `https://doi.org/10.1007/s10825-008-0193-7`. 61

[84] Guillermo Albareda, Damiano Marian, Abdelilah Benali, Alfonso Alarcón, Simeon Moises, and Xavier Oriols. *Electron Devices Simulation with Bohmian Trajectories*, chapter 7, pages 261–318. John Wiley and Sons, Ltd, 2016. ISBN 9781118761793. doi: 10.1002/9781118761793.ch7. 47, 59, 61

[85] Heinz-Peter Breuer, Francesco Petruccione, et al. *The theory of open quantum systems*. Oxford University Press on Demand, 2002. 50, 53, 61

[86] Andrea Smirne, Heinz-Peter Breuer, Jyrki Piilo, and Bassano Vacchini. Initial correlations in open-systems dynamics: the jaynes-cummings model. *Physical Review A*, 82(6):062114, 2010. 50

[87] Inés De Vega and Daniel Alonso. Dynamics of non-markovian open quantum systems. *Reviews of Modern Physics*, 89(1):015001, 2017. 50

[88] Bassano Vacchini. Non-markovian dynamics for bipartite systems. *Phys. Rev. A*, 78:022112, Aug 2008. doi: 10.1103/PhysRevA.78.022112. URL `https://link.aps.org/doi/10.1103/PhysRevA.78.022112`. 50

[89] Nicolas Gisin. Stochastic quantum dynamics and relativity. *Helv. Phys. Acta*, 62(4):363–371, 1989. 50

[90] Philip Pearle. Combining stochastic dynamical state-vector reduction with spontaneous localization. *Physical Review A*, 39(5):2277, 1989.

[91] Howard Carmichael. *An open systems approach to quantum optics: lectures presented at the Université Libre de Bruxelles, October 28 to November 4, 1991*, volume 18. Springer Science & Business Media, 2009. 53

[92] Nicolaas Godfried Van Kampen. *Stochastic processes in physics and chemistry*, volume 1. Elsevier, 1992.

[93] Inés De Vega. Non-markovian stochastic schrödinger description of transport in quantum networks. *Journal of Physics B: Atomic, Molecular and Optical Physics*, 44(24):245501, 2011.

[94] Peter Goetsch and Robert Graham. Linear stochastic wave equations for continuously measured quantum systems. *Physical review A*, 50(6):5242, 1994.

[95] Dariusz Gatarek and Nicolas Gisin. Continuous quantum jumps and infinite-dimensional stochastic equations. *Journal of mathematical physics*, 32(8):2152–2157, 1991.

[96] Jay Gambetta and HM Wiseman. Non-markovian stochastic schrödinger equations: Generalization to real-valued noise using quantum-measurement theory. *Physical Review A*, 66(1):012108, 2002. 50

[97] Angel Rivas, Susana F Huelga, and Martin B Plenio. Quantum non-markovianity: characterization, quantification and detection. *Reports on Progress in Physics*, 77(9):094001, 2014. 50

[98] Lajos Diósi. Non-markovian continuous quantum measurement of retarded observables. *Physical review letters*, 100(8):080401, 2008. 50

[99] Howard M Wiseman and Jay M Gambetta. Pure-state quantum trajectories for general non-markovian systems do not exist. *Physical review letters*, 101 (14):140401, 2008. 50

[100] Jay Gambetta and HM Wiseman. Interpretation of non-markovian stochastic schrödinger equations as a hidden-variable theory. *Physical Review A*, 68(6):062104, 2003. 50

[101] Jay Gambetta and HM Wiseman. Modal dynamics for non-orthogonal decompositions. *Found. Phys.*, 34(quant-ph/0306145):419–448, 2003. 50

[102] Karl Kraus. *States, effects and operations: fundamental notions of quantum theory*. Springer, 1983. 53

[103] Howard M Wiseman and Gerard J Milburn. *Quantum measurement and control*. Cambridge university press, 2009. 53

[104] Travis Norsen, Damiano Marian, and Xavier Oriols. Can the wave function in configuration space be replaced by single-particle wave functions in physical space? *Synthese*, 192(10):3125–3151, 2015. 55

[105] X. Oriols. Quantum-trajectory approach to time-dependent transport in mesoscopic systems with electron-electron interactions. *Phys. Rev. Lett.*, 98:066803, Feb 2007. doi: 10.1103/PhysRevLett.98.066803. URL `https://link.aps.org/doi/10.1103/PhysRevLett.98.066803`. 57, 58, 61

[106] Guillermo Albareda, Heiko Appel, Ignacio Franco, Ali Abedi, and Angel Rubio. Correlated electron-nuclear dynamics with conditional wave functions. *Physical review letters*, 113(8):083003, 2014. 57, 58

[107] Alfonso Alarcón, Guillem Albareda, Fabio Lorenzo Traversa, A Benali, and X Oriols. Nanoelectronics: quantum electron transport. *Applied Bohmian Mechanics: From Nanoscale Systems to Cosmology*, pages 365–424, 2012. 59

[108] G Albareda, D Marian, A Benali, S Yaro, N Zanghì, and X Oriols. Time-resolved electron transport with quantum trajectories. *Journal of Computational Electronics*, 12(3):405–419, 2013.

[109] Guillermo Albareda, Damiano Marian, Abdelilah Benali, Alfonso Alarcón, Simeon Moises, and Xavier Oriols. Electron devices simulation with bohmian trajectories. *Simulation of Transport in Nanodevices*, pages 261–318, 2016. 59

[110] Max Born and Kun Huang. *Dynamical theory of crystal lattices*. Clarendon press, 1954. 60

[111] Guillermo Albareda, Ali Abedi, Ivano Tavernelli, and Angel Rubio. Universal steps in quantum dynamics with time-dependent potential-energy surfaces: Beyond the born-oppenheimer picture. *Phys. Rev. A*, 94:062511, Dec 2016. doi: 10.1103/PhysRevA.94.062511. URL `https://link.aps.org/doi/10.1103/PhysRevA.94.062511`. 60

[112] G Albareda, Jordi Suñé, and X Oriols. Many-particle hamiltonian for open systems with full coulomb interaction: Application to classical and quantum time-dependent simulations of nanoscale electron devices. *Physical Review B*, 79(7):075315, 2009. 61

[113] G Albareda, X Saura, X Oriols, and J Suné. Many-particle transport in the channel of quantum wire double-gate field-effect transistors with charged atomistic impurities. *Journal of Applied Physics*, 108(4):043706, 2010. 61

[114] E Colomés, Z Zhan, D Marian, and X Oriols. Quantum dissipation with conditional wave functions: Application to the realistic simulation of nanoscale electron devices. *Physical Review B*, 96(7):075135, 2017. 61

[115] G Albareda, H López, X Cartoixa, J Suné, and X Oriols. Time-dependent boundary conditions with lead-sample coulomb correlations: Application to classical and quantum nanoscale electron device simulators. *Physical Review B*, 82(8):085301, 2010. 61

[116] G Albareda, A Benali, and X Oriols. Self-consistent time-dependent boundary conditions for static and dynamic simulations of small electron devices. *Journal of Computational Electronics*, 12(4):730–742, 2013. 61

[117] Carlos Mejia-Monasterio and Hannu Wichterich. Heat transport in quantum spin chains. *The European Physical Journal Special Topics*, 151(1): 113–125, 2007. 61

[118] Hannu Wichterich, Markus J Henrich, Heinz-Peter Breuer, Jochen Gemmer, and Mathias Michel. Modeling heat transport through completely positive maps. *Physical Review E*, 76(3):031115, 2007. 61

[119] R Biele, C Timm, and R D'Agosta. Application of a time-convolutionless stochastic schrödinger equation to energy transport and thermal relaxation. *Journal of Physics: Condensed Matter*, 26(39):395303, sep 2014. doi: 10.1088/0953-8984/26/39/395303. URL `https://doi.org/10.1088%2F0953-8984%2F26%2F39%2F395303`. 61

[120] Heiko Appel and Massimiliano Di Ventra. Stochastic quantum molecular dynamics. *Physical Review B*, 80(21):212303, 2009. 61

[121] Robert Biele and Roberto D'Agosta. A stochastic approach to open quantum systems. *Journal of Physics: Condensed Matter*, 24(27):273201, 2012. 61

[122] CW Gardiner, JR Anglin, and TIA Fudge. The stochastic gross-pitaevskii equation. *Journal of Physics B: Atomic, Molecular and Optical Physics*, 35 (6):1555, 2002. 61

[123] CW Gardiner and MJ Davis. The stochastic gross–pitaevskii equation: Ii. *Journal of Physics B: Atomic, Molecular and Optical Physics*, 36(23):4731, 2003.

[124] Chad N Weiler, Tyler W Neely, David R Scherer, Ashton S Bradley, Matthew J Davis, and Brian P Anderson. Spontaneous vortices in the formation of bose–einstein condensates. *Nature*, 455(7215):948–951, 2008. 61

[125] Oskar Klein. Die reflexion von elektronen an einem potentialsprung nach der relativistischen dynamik von dirac. *Zeitschrift für Physik*, 53(3-4):157–165, 1929. 66

[126] Pierre E Allain and Jean-Noel Fuchs. Klein tunneling in graphene: optics with massless electrons. *The European Physical Journal B*, 83(3):301–317, 2011. 66

[127] Hartmut Häffner, Wolfgang Hänsel, CF Roos, Jan Benhelm, Michael Chwalla, Timo Körber, UD Rapol, Mark Riebe, PO Schmidt, Christoph Becher, et al. Scalable multiparticle entanglement of trapped ions. *Nature*, 438(7068):643–646, 2005. 76

[128] E. H. Hauge and J. A. Støvneng. Tunneling times: a critical review. *Rev. Mod. Phys.*, 61:917–936, Oct 1989. doi: 10.1103/RevModPhys.61.917. 83, 124

[129] Leslie E Ballentine. *Quantum Mechanics*. WORLD SCIENTIFIC, 1998. doi: 10.1142/3142. URL `https://www.worldscientific.com/doi/abs/10.1142/3142`. 101

[130] Jose MG Vilar and J Miguel Rubi. Failure of the work-hamiltonian connection for free-energy calculations. *Physical review letters*, 100(2):020601, 2008. 119

[131] David Gelbwaser-Klimovsky and Alán Aspuru-Guzik. On thermodynamic inconsistencies in several photosynthetic and solar cell models and how to fix them. *Chemical science*, 8(2):1008–1014, 2017.

[132] Wolfgang Niedenzu, Marcus Huber, and Erez Boukobza. Concepts of work in autonomous quantum heat engines. *Quantum*, 3:195, 2019. 119

[133] Martí Perarnau-Llobet, Elisa Bäumer, Karen V. Hovhannisyan, Marcus Huber, and Antonio Acin. No-go theorem for the characterization of work fluctuations in coherent quantum systems. *Phys. Rev. Lett.*, 118:070601, Feb 2017. doi: 10.1103/PhysRevLett.118.070601. 120, 123, 124

[134] Augusto J. Roncaglia, Federico Cerisola, and Juan Pablo Paz. Work measurement as a generalized quantum measurement. *Phys. Rev. Lett.*, 113: 250601, Dec 2014. doi: 10.1103/PhysRevLett.113.250601. 120

[135] Gabriele De Chiara, Augusto J Roncaglia, and Juan Pablo Paz. Measuring work and heat in ultracold quantum gases. *New Journal of Physics*, 17(3): 035004, 2015. 120

[136] A. E. Allahverdyan. Nonequilibrium quantum fluctuations of work. *Phys. Rev. E*, 90:032137, Sep 2014. doi: 10.1103/PhysRevE.90.032137. 120

[137] Patrick P. Hofer. Quasi-probability distributions for observables in dynamic systems. *Quantum*, 1:32, October 2017. ISSN 2521-327X. doi: 10.22331/q-2017-10-12-32. 120

[138] Donald H Kobe. Quantum power in de broglie–bohm theory. *Journal of Physics A: Mathematical and Theoretical*, 40(19):5155, 2007. 121

[139] Rui Sampaio, Samu Suomela, Tapio Ala-Nissila, Janet Anders, and TG Philbin. Quantum work in the bohmian framework. *Physical Review A*, 97(1):012131, 2018. 121

[140] G Orlando, C R McDonald, N H Protik, G Vampa, and T Brabec. Tunnelling time, what does it mean? *Journal of Physics B: Atomic, Molecular and Optical Physics*, 47(20):204002, 2014. 124

[141] R Landauer and Th Martin. Barrier interaction time in tunneling. *Reviews of Modern Physics*, 66(1):217, 1994. 127

[142] Eugene P Wigner. Lower limit for the energy derivative of the scattering phase shift. *Physical Review*, 98(1):145, 1955.

[143] AI Baz. Ai baz', sov. j. nucl. phys. 4, 182 (1967). *Sov. J. Nucl. Phys.*, 4: 182, 1967. 127

[144] VF Rybachenko. Vf rybachenko, sov. j. nucl. phys. 5, 635 (1967). *Sov. J. Nucl. Phys.*, 5:635, 1967. 127

[145] M. Büttiker and R. Landauer. Traversal time for tunneling. *Phys. Rev. Lett.*, 49:1739–1742, Dec 1982. doi: 10.1103/PhysRevLett.49.1739.

[146] M Büttiker. Larmor precession and the traversal time for tunneling. *Physical Review B*, 27(10):6178, 1983. 127